SUPPLEMENTO
AL VOLUME IV, SERIE X, DEL
NUOVO CIMENTO
A CURA DELLA SOCIETÀ ITALIANA DI FISICA

1956 — 2° Semestre — N. 3

RENDICONTI
DEL
III CORSO CHE NELLA VILLA MONASTERO A VARENNA
DAL 17 LUGLIO AL 6 AGOSTO, 1955
FU TENUTO A CURA
DELLA SCUOLA INTERNAZIONALE DI FISICA
DELLA SOCIETÀ ITALIANA DI FISICA

INDICE

INTRODUZIONE.

G. POLVANI – Discorso inaugurale . . . . . pag. 1081
C. SALVETTI – Prolusione . . . . . » 1085

PARTE PRIMA. – **Struttura del nucleo e modelli nucleari.**

A. BOHR – Problems of Nuclear Structure . . . . . » 1091
D. M. BRINK and S. YOSHIDA – The Inelastic Scattering of Protons and Neutrons by Deformed Nuclei . . . . . » 1121
L. N. COOPER – The Nuclear Radius . . . . . » 1125
J. HOROWITZ – Théorie des réactions de « stripping » . . . . . » 1137

H. J. Lipkin – On the Description of Collective Motion by the Use of Superfluous Co-ordinates . . . . . pag. 1147
J. O. Newton – Coulomb Excitation of Heavy Nuclei . . . . . » 1156
C. G. Schuhl – Les réactions photonucléaires avec émission de neutrons » 1162
M. Cini and S. Fubini – A Theoretical Investigation of Nuclear Reactions with Neutrons . . . . . » 1172
A. Kind – The Low Energy Nuclear Mechanics and the Independent Particle Model . . . . . » 1173

Parte seconda. – **Momenti nucleari.**

I. I. Rabi – Atomic and Molecular Beam Experiments . . . . . » 1174
A. de Shalit – Magnetic Moments of Nuclei . . . . . » 1195
C. H. Townes – On the Interpretation of H.F.S. in Molecules in Terms of Molecular Structure and Nuclear Moments . . . . . » 1201

Parte terza. – **Nuove specie d'atomi: il positronio e gli atomi mesici.**

S. De Benedetti – New Atoms (Positronium and Mesonic Atoms) . » 1209
L. N. Cooper – μ-Mesonic Atoms . . . . . » 1271

Parte quarta. – **Fisica dei reattori.**

A. Weinberg – Nuclear Reactor Physics . . . . . » 1278
T. M. Fry – « Zephir » - Zero Energy Fast Reactor . . . . . » 1324
T. M. Fry – The Displacement of Atoms in Solids by Radiation . . » 1329
J. Horowitz – Différentes méthodes de mesure du libre parcours moyen de transport des neutrons thermiques . . . . . » 1335

La Direzione del Corso ringrazia vivamente i dott. U. L. Businaro, G. Cristiani, G. Ghilardotti e E. Montaldi per la collaborazione prestata nella redazione di alcuni gruppi di lezioni, e il dott. S. de Petris per l'aiuto dato nella sistemazione e revisione dell'intero fascicolo.

INTRODUZIONE

Discorso inaugurale

DI

G. POLVANI

Presidente della Società Italiana di Fisica

Questo III Corso estivo della Scuola Internazionale di Fisica istituita dalla nostra Società, si apre quest'anno purtroppo sotto il segno del lutto; e la soddisfazione e il piacere di qui trovarsi o ritrovarsi sono tristemente angustiati da un pensiero che in questo stesso momento pesa nella mente e sul cuore di tutti noi e che, per quanto cerchiamo di scacciarlo, tenacemente rimane presente e lista di nero questa inaugurazione: il pensiero cioè, che un anno fa ENRICO FERMI era qui con noi e oggi è tra i morti.

Altri, il Prof. RABI, con la sua alta competenza parlerà diffusamente di lui; qui io desidero solo dire che a noi che volemmo questa Scuola, rimane come sprone alla nostra opera e conforto al nostro dolore, l'avere egli dato pienamente il suo assenso a questa nostra istituzione ed esortandoci a mantenerla in vita e a consolidarla, avere aggiunto consigli e suggerimenti.

Ai quali ci siamo strettamente attenuti nella organizzazione di questo III Corso, che si aggiunge ai due precedenti per lo studio della Fisica delle particelle elementari e dei processi nucleari, trattanto ora quelli di bassa energia e la loro maggiore applicazione, quale è il reattore nucleare, cioè la pila di Fermi; la sorgente di energia verso la quale oggi si appuntano le speranze di un migliore benessere umano.

Ma, come le altre volte, la possibilità di passare dal progetto all'attuazione, è legata alla premura e alla comprensione di molti enti e persone che, convinti dagli ammaestramenti che la storia porge e sapendo di quanto pregio non solo filosofico, ma anche economico, si rivesta la nostra scienza, la Fisica, hanno voluto venirci generosamente incontro.

Di fronte a questa sperimentata e commovente comprensione, vi dirò che,

contrariamente a quanto si potrebbe pensare e a quanto — giustamente del resto — qualcuno mi ha suggerito (trovare cioè modo di costituire stabilmente i cespiti che assicurino il funzionamento della Scuola senza più doversi preoccupare anno per anno di andarli a trovare), io quasi quasi propendo per la forma, finora necessariamente seguita, della questua, perchè essa è testimonianza e metro sia della nostra sia dell'altrui volontà; e soprattutto perchè, vietando a noi di cullarci nella comoda certezza del domani e agli altri di abbandonarsi alla indifferenza verso le cose che non riguardano immediatamente la propria attività, spinge e gli uni e gli altri verso un comune ideale.

Il procedimento della questua — scusate se mi esprimo con termini dirò così francescani — rompe le barriere, unisce e collega persone e istituzioni cosicchè chi vuole può dire: «anch'io ho collaborato a questa Scuola», «essa è un po' anche mia»; e dir questo — si badi — non per la falsa esteriore vanità di un'etichetta, ma per l'interna, muta sodisfazione di avere operato per il bene comune senza distinzione dell'altrui o del proprio.

E pertanto più che mai la Società Italiana di Fisica è riconoscente e grata a coloro, enti e persone, che in questo stile e con questo spirito di reciproca comprensione, si sono accompagnati a noi: il Ministro della Pubblica Istruzione, per il quale desidero soprattutto ricordare il Direttore generale all'Istruzione Superiore, dott. Mario Di Domizio; il Consiglio Nazionale delle Ricerche e per esso il Presidente prof. Gustavo Colonnetti; il Comitato Nazionale per la Fisica e per esso il Presidente prof. Eligio Perucca; il Comitato Nazionale per le Ricerche Nucleari e per esso il prof. Francesco Giordani; la Prefettura di Como e per essa l'Eccellenza il Prefetto, dott. Giulio Bianchi, al quale, assente, all'ultimo minuto, per indisposizione inviamo i migliori auguri; l'Università di Milano e per essa il Rettore Magnifico prof. Giuseppe Menotti De Francesco; la Società Condor di Milano e il suo Consigliere Delegato ing. Mario Mortara; la Società Moto Guzzi di Mandello sul Lario e il suo Presidente rag. Enrico Parodi; la Società Badoni di Lecco e il suo Presidente ing. Giuseppe Badoni; la Società Caleotto di Lecco e il suo Presidente comm. Ernesto Bonaiti; la Società Serpentino Italiana di Lecco e il suo Presidente ing. sen. Piero Amigoni; la Società Fabbrica Italiana Lampadine Elettriche di Lecco e il suo Presidente comm. Luigi Butti; la Società Metalgraf di Lecco e il suo Presidente cav. Egisto Biffi; la Società Orobia e il Direttore della Sezione di Lecco ing. Vasco Zoccolini; l'ing. Eugenio Somaini, immancabile amico dei fisici italiani.

A tutti quanti ho ricordato giungano per l'aiuto dato, l'espressione della più viva riconoscenza della Società Italiana di Fisica, del Consiglio della Società e mio personale.

Una particolare parola di gratitudine desidero aggiungere poi sia verso l'Ente Villa Monastero e per il suo Presidente, avv. Giberto Bosisio, per tutto quello che ha fatto e fa per il funzionamento dell'Ente Villa Mona-

stero e per il riordinamento della Villa; sia verso il Sindaco di Varenna che tanto si adopera per offrire ai partecipanti ai vari corsi che si svolgono nella Villa un'ospitalità sempre più scelta e cordiale, sia infine verso il dott. BACCARINI, già Commissario dell'Istituto Nazionale d'Idrobiologia, largo di consigli e di aiuti, sia infine il prof. VITTORIO TONOLLI, Direttore del detto Istituto. Nè voglio dimenticare i proprietari degli Alberghi Vittoria e Royal, signori VITALI e REBUSCHINI, per l'impegno messo nel riordinamento di essi.

* * *

Ma non si chiude qui il nostro debito di gratitudine; esso con altra forma si stende a tutti coloro che hanno accettato di partecipare come docenti a questo Corso: il prof. ISIDORO RABI della Columbia University di New York; il prof. AAGE BOHR dell'Università di Copenhagen; il prof. ALVIN WEINBERG dell'Oak Ridge National Laboratory; il prof. SERGIO DE BENEDETTI del Carnegie Institut of Technology di Pittsburg; il prof. C. H. TOWNES della Columbia University; il prof. J. HOROWITZ del Centro di Studi Nucleari di Saclay; il prof. T. M. FRY del Centro di Harwell; il prof. A. DE SHALIT dell'Università di Rehovoth e il dott. L. N. COOPER dell'Istitute for Advanced Study di Princeton.

È verosimile che durante il Corso altri docenti si aggiungeranno a questi che ho nominato: a tutti giunga gradito il ringraziamento più vivo della Scuola e della Società.

Una particolare menzione deve essere fatta e un particolare ringraziamento deve essere rivolto al prof. CARLO SALVETTI, allievo, amico e collega carissimo della Facoltà di Scienze dell'Università di Milano, il quale ha voluto sobbarcarsi alla non indifferente fatica di organizzare tutto il Corso e ora si accinge a quella, non meno grave, di dirigerlo.

Come vi ho presentato i maestri, permettete che ora vi presenti anche gli allievi che, scelti tra i molti che hanno domandato di partecipare al Corso, qui rappresentano ben sedici paesi diversi di tutte le parti del mondo. Alcuni di loro sono appena esordienti, altri già provetti nelle ricerche, tutti desiderosi di ulteriormente accrescere la propria conoscenza delle cose fisiche: R. AMADO proveniente da Oxford, R. BALLINI da Saclay, R. BARJON da Parigi, M. BLOOM da Leiden, D. M. BRINK da Oxford, P. J. BRUSSAARD da Leiden, R. JOLY da Saclay, H. J. LIPKIN da Rehovoth, V. MIDDELBOE da Copenhagen, A. MIJATOVIC da Belgrado, D. MORGAN da Cambridge, J. O. NEWTON da Harwell, L. PAPINEAU da Saclay; J. M. POOLE da Harwell, H. ROBL da Vienna, K. SAHAI da Bombay, J. SCHMOUKER da Parigi, C. G. SCHUHL da Parigi, E. SOKOLOWSKI da Upsala, I. TANAKA da Parigi, P. TEITELBAUM da Jerusalem, S. YOSHIDA da Birmingham, B. L. YOUTZ da Beirut, e ancora G. BERTOLINI, U. L. BUSINARO, G. CAGLIOTI, G. CORTELLESSA, N. D'ANGELO, U. FARINELLI, F. FERRARI, S. GALLONE, A. KIND, A. ROSSI, S. SCIUTI, P. VERONESI, V.

WATAGHIN dall'Italia; e ancora gli uditori F. CAP di Innsbruck, M. RENÉ da Bruxelles, M. AGENO da Roma, G. C. GHILARDOTTI da Milano, P. MITTNER da Padova.

A tutti coloro che ho nominato e che costituiscono da oggi per tre settimane il piccolo mondo del III Corso della Scuola Internazionale di Fisica della nostra Società il « benvenuto » più cordiale di questa e mio personale.

* * *

Il Corso si chiuderà il 6 Agosto, anniversario dell'ultima lezione qui tenuta da FERMI e segnata da un così vivo, affettuoso e interminabile applauso che giunse a commuoverlo. Il 6 Agosto verrà scoperta in questa stessa aula una lapide in sua memoria, e poi a Como, nel Tempio Voltiano, sarà dal prof. RABI pronunciato il discorso commemorativo (*). Anche per questa sua collaborazione vogliamo esprimere a lui la nostra più profonda gratitudine.

* * *

Ed ora, concludendo queste brevi parole di apertura del Corso, desidero porgere a tutti l'augurio migliore per il più proficuo lavoro, sicuro che a questo risultato scientifico si aggiungerà — direi all'insaputa di tutti — un risultato umano non meno importante: quello cioè della formazione, tra le varie persone partecipanti al Corso, di vincoli di amicizia e di simpatia promossi sia dalla tranquilla bellezza del luogo che rende inclini gli animi alla comprensione, sia dalla affettuosa cordiale ospitalità italiana che non conosce differenze, sia infine dal comune desiderio di spingersi sempre più a fondo nella conoscenza del mondo fisico che ci circonda: nobile maniera, questa, per sodisfare l'aspirazione sempre più ampia e sempre più profonda di migliorare noi stessi.

Con questi sentimenti dichiaro aperto il 3° Corso della Scuola Internazionale di Fisica della Società Italiana di Fisica.

(*) Vedi *Supplemento* No. 2 al Vol. 2, Serie X, del *Nuovo Cimento*, 1955, 2° Semestre.

SUPPLEMENTO AL VOLUME IV, SERIE X
DEL NUOVO CIMENTO

N. 3, 1956
2° Semestre

Prolusione

DI

C. SALVETTI

Direttore del Corso

Per la terza volta nel giro di due anni ha luogo questa riunione che segna l'inizio di un corso di Fisica: anche quest'anno, grazie al generoso contributo di Enti e di privati, e soprattutto grazie all'Ente Villa Monastero, la nostra Società ha potuto organizzare il suo Corso estivo di Fisica, il terzo della serie.

Quest'anno, come avrete visto dal programma e dal bando, si parlerà essenzialmente di due argomenti riguardanti rispettivamente la Fisica nucleare delle basse energie e le basi scientifiche e le applicazioni fisiche dei reattori nucleari.

L'accostamento dei due argomenti, proposto e voluto sia dal Consiglio della nostra Società sia dalla Direzione del Corso, può a tutta prima sorprendere. Ma quando si mediti sui profondi legami che esistono tra la Fisica nucleare e le sue applicazioni si comprende come questi due argomenti si completino e si integrino a vicenda.

Già in altre occasioni si sono rilevati la complessità e il numero dei problemi fisici connessi con le applicazioni dell'energia nucleare, per cui ora ben poco resta da aggiungere. L'idea di includere nel Corso di quest'anno, sostanzialmente dedicato alla Fisica nucleare delle basse energie, anche un gruppo di lezioni interamente dedicato ai reattori nucleari, ha trovato fin dall'inizio un completo ed unanime appoggio. D'altronde è evidente l'interesse puramente scientifico connesso con gli studi sui reattori; ma a me sembra che vi sia anche un'altra considerazione da tener presente, e cioè che la nostra Scuola Internazionale di Fisica debba non solo trattare questioni strettamente teoriche, che interessano una più o meno limitata cerchia di cultori, ma anche questioni che pur essendo di natura rigorosamente scientifica, abbiano anche un certo interesse applicativo.

Del resto è in questo modo che l'Ente Villa Monastero intende svolgere la sua funzione, che non è quella di una pura accademia, ma di inserirsi profondamente in quelle branche della cultura e della scienza che per la loro portata e vastità interessino la vita di tutte le nazioni. E pertanto l'Ente crede di assolvere il suo principale compito accogliendo qui in Varenna, in questa meravigliosa cornice di bellezze naturali, scienziati italiani e stranieri, che sono così chiamati non solo ad infondere ad altri le loro conoscenze e i risultati delle loro ricerche, ma anche a portare il loro contributo e la loro esperienza a problemi che, come dicevo, interessano larga parte della vita nazionale di tutti i paesi e particolarmente del nostro. Questo modo di intendere le proprie funzioni, l'Ente lo dimostra del resto con i corsi internazionali di alta cultura che si tengono in campi assai diversi dal nostro: in alta Matematica, in Biometria, in Scienza delle Finanze, ecc. ecc.

* * *

Ma torniamo al nostro Corso e lasciatemi in primo luogo ringraziare gli illustri docenti che hanno gentilmente acconsentito a tenere le lezioni sui diversi argomenti: il prof. ISIDOR RABI, della Columbia University, premio Nobel per la Fisica e presidente dell'Advisory Committee dell'Atomic Energy Commission americana; il prof. AAGE BOHR, dell'Università di Copenhagen; il prof. SERGIO DE BENEDETTI, del Carnegie Institute of Technology di Pittsburgh; il prof. GEORGE PLACZEK dell'Institute for Advanced Studies di Princeton, il quale purtroppo, con suo vivo rincrescimento, non potrà intervenire al Corso a causa delle sue condizioni di salute (*); e infine il dott. ALVIN WEINBERG, direttore delle ricerche dell'Oak Ridge National Laboratory.

Il nostro ringraziamento va inoltre a quei numerosi scienziati che hanno accettato di tenere lezioni e seminari su vari argomenti, fra i quali desidero ricordare i professori: CINI, COOPER, DE SHALIT, FRY, FUBINI, HOROWITZ, TOWNES e diversi altri che ci parleranno su questioni varie di Fisica nucleare.

* * *

Ed ora vorrei, se me lo permettete, illustrare brevemente i diversi argomenti che fanno oggetto del Corso di quest'anno. Come ho detto essi riguardano sostanzialmente la Fisica nucleare e le questioni fisiche dei reattori.

Per quanto concerne la Fisica nucleare il *leit-motif* è stato quello dei modelli nucleari; si è cercato cioè di costituire vari gruppi di lezioni più o meno direttamente connessi col problema della struttura e dei modelli del nucleo:

(*) Il prof. PLACZEK doveva, purtroppo, mancare ai vivi qualche mese dopo. La Direzione del Corso si unisce all'unanime cordoglio per l'immatura perdita dell'illustre Fisico. [*Nota aggiunta sulle bozze*].

problema questo di preminente e singolare importanza, che ha assunto negli ultimi anni una posizione sempre più notevole nel campo delle ricerche della Fisica nucleare.

È nota la storia dei tentativi di fornire un'immagine, un modello del nucleo atomico che renda conto del maggior numero possibile di fenomeni.

Si è così giunti in primo luogo, per merito soprattutto di NIELS BOHR, al cosiddetto modello a goccia del nucleo il quale rende conto assai bene di numerosi fenomeni.

In questo modello il nucleo è visto come una goccia liquida dotata di carica e di una energia di superficie: alla repulsione elettrostatica dovuta ai protoni si oppongono le forze nucleari che tengono uniti nel loro insieme i costituenti nucleari. Il successo di tale modello si è avuto soprattutto, come è ben noto, nella interpretazione di quel singolare fenomeno che è la fissione dei nuclei pesanti. Altri successi il modello a goccia ha avuto nell'interpretare il problema del nucleo composto, la distribuzione dei livelli eccitati e diversi altri fenomeni. Alla visione del nucleo a goccia in cui sostanzialmente i nucleoni perdono la loro individualità, fa contrasto quella di un modello, elaborato soprattutto per opera di MARIA GOEPPERT MAYER, in cui i nucleoni conservano invece la loro individualità e che viene detto appunto modello a particelle indipendenti. In tale modello, detto anche modello a shell, i nucleoni vengono trattati secondo le regole della meccanica quantistica come particelle indipendenti immerse in un campo di forze centrali: si ottengono così gli stati quantici in cui si trovano i nucleoni e si ha del nucleo una rappresentazione di tipo quasi atomico. Se pure le basi di questo modello sono quanto mai deboli, in quanto non si vede come si possano trascurare le interazioni individuali dei nucleoni e pensare quest'ultime sostituite da un campo di forza derivante da un potenziale, i successi di questo modello sono innegabili: esso rende conto in maniera molto soddisfacente dei momenti angolari, i cosiddetti spin nucleari, e permette di giustificare a posteriori il successo del modello a particella singola, introdotto da SCHMIDT per interpretare i momenti magnetici nucleari.

È chiaro dunque che il modello a goccia e il modello a shell rappresentano due casi estremi, vorremmo dire due casi-limite, di una medesima realtà. E ancora più chiaro è che i successivi tentativi effettuati dai fisici in questi ultimi anni dovessero volgere verso una visione unitaria della quale il modello a goccia e quello a particelle individuali apparissero come casi estremi e fossero, per così dire, in esso contenuti.

In questo modo è nato lo studio dei modelli collettivi in cui si cerca di fondere concetti apparentemente contrastanti dei due modelli estremi sopra ricordati.

I modelli collettivi al cui sviluppo tanto ha contribuito AAGE BOHR, che come ho detto sarà qui fra noi, si fondano sulla ammissione che gli stati individuali

dei nucleoni siano sensibili alla deformabilità della materia nucleare. Di questi modelli collettivi vi sono diverse formulazioni: dalla prima, di più immediata intuizione, dovuta a RAINWATER a quella di WHEELER fino a quella più raffinata dovuta a BOHR. In tutti però è presente il concetto che i nucleoni interagiscono più o meno fortemente con la materia nucleare tramite la superficie del nucleo, concepito quest'ultimo come un aggregato deformabile di particelle. Mentre da un lato si conservano così i concetti di stato individuale, che sono caratteristici dei modelli a shell, e quelli della deformabilità dei nuclei, caratteristici del modello a goccia, in modo che si possono inquadrare tutti i fenomeni già in precedenza interpretati dagli altri due modelli, si possono spiegare con i modelli collettivi nuovi ed importantissimi risultati fra cui, in primo luogo, l'esistenza dei momenti elettrici di quadrupolo e degli stati rotazionali dei nuclei, risultati questi che non trovavano alcuna interpretazione soddisfacente nei precedenti modelli. Di qui l'importanza dei modelli collettivi.

Ma come è caratteristico della Fisica fin d'ora si vede che anche i modelli collettivi potranno probabilmente essere inquadrati in una forma più generale e più soddisfacente nel senso che sembra possibile, partendo dal problema quantummeccanico esatto dei nucleoni fra loro interagenti, dedurre, con appropriati metodi di calcolo, questo o quel modello nucleare: secondo questo modo di vedere i precedenti tentativi sui modelli nucleari apparirebbero semplicemente come rappresentazioni adatte ciascheduna a illustrare e interpretare questa o quella particolare proprietà.

E già si parla di una teoria generale dei modelli nucleari e non sembra lontano il giorno in cui sarà possibile dedurre dalle sole interazioni fra nucleoni le proprietà di insieme del nucleo atomico: sembra anzi che i primi tentativi in questa direzione siano già coronati da successo.

Sui modelli nucleari — vogliate perdonare la lunga digressione — è impostata, dicevo, gran parte della materia che verrà trattata quest'anno; in primo luogo i gruppi delle lezioni di BOHR e di RABI: dedicato, il primo gruppo ai modelli nucleari e alle loro conseguenze, l'altro ai momenti nucleari— argomento, questo, che costituisce, in un certo senso, un banco di prova molto sensibile, vorrei dire quasi un campanello d'allarme, per la verifica delle teorie nucleari —. Anche il gruppo delle lezioni di DE BENEDETTI, dedicato alle nuove specie di atomi, positronio e atomo mesico, si collega, attraverso l'atomo mesico, ai due precedenti: quest'ultimo gruppo sarà di particolare interesse anche perchè tratterà in larga misura di quelle tecniche di rivelazione ultrarapida che tanta parte hanno oggi nella sperimentazione nucleare.

Un altro gruppo di lezioni riguarda, come dicevo, la Fisica dei reattori nucleari. Per esso abbiamo avuto la ventura di avere fra noi uno dei più noti specialisti mondiali sull'argomento, il prof. WEINBERG di Oak-Ridge. Egli ci intratterrà sui problemi fondamentali e sulle costanti fisiche relative alla teoria dei reattori nucleari e in particolare ci illustrerà, con la sua

alta competenza, le più significative realizzazioni acquisite in questo campo negli Stati Uniti d'America. Altre lezioni sulla teoria dei reattori ci terrà il dr. FRY dell'Atomic Energy Research Establishment di Harwell, il quale ci parlerà di un reattore sperimentale veloce e del problema estremamente attuale ed avvincente degli effetti delle radiazioni nei solidi.

Quest'ultimo gruppo di lezioni connesse con le applicazioni della Fisica nucleare mi sembra rivesta un particolare significato sia perchè, come si è detto, esso interessa una parte delle attività scientifiche nazionali di primaria importanza, sia perchè esso si riallaccia direttamente con gli argomenti che verranno trattati, su ben più vasta scala alla prossima Conferenza di Ginevra la quale apre i battenti l'8 Agosto, all'indomani, cioè, della chiusura della nostra Scuola. Molti dei docenti e degli allievi lasceranno Varenna per recarsi direttamente a Ginevra: vorrei aggiungere che questa circostanza, non del tutto casuale del resto, dimostra una volta di più, se pur ve ne fosse bisogno, quanto viva e vitale sia la nostra Scuola e come essa si inserisca profondamente nella vita scientifica mondiale.

* * *

Potrei qui chiudere queste mie brevi parole d'illustrazione del Corso che oggi s'inaugura; ma mi sembrerebbe che il mio discorso rimarrebbe monco, proprio in questa sua parte d'impostazione didattico-scientifica, se non ricordassi ENRICO FERMI che l'anno passato tenne qui le sue ultime indimenticabili lezioni. Altri, assai più degnamente di me, parlerà di Lui e della sua opera, e così chiuderà il Corso (*). Ma oggi all'inizio del Corso stesso vorrei far notare che gli argomenti che verranno trattati nei prossimi giorni ci faranno amaramente rimpiangere che Fermi non possa più essere fra noi. La Fisica nucleare e la pila atomica sono, si può dire, sue creature, e noi nel sentire le lezioni che seguiranno in questi due campi che Egli predilesse e nei quali fu grande, sentiremo aleggiare il suo spirito e parlarci con quella stessa voce che viva qui già udimmo.

* * *

And now a few words to the students. First of all, I wish to thank you all for having come here and welcome you. Since most of you will attend this Course for the first time, please let me explain and summarize in a few words what is the aim and the characteristics of our School.

The Course organization may be far off from being perfect, but I hope that the interesting lectures and the beautiful place will help you in overcoming all the difficulties that may arise.

(*) Vedi *Supplemento* No. 2 al Vol. 2, Serie X, del *Nuovo Cimento*, 1955, 2° Semestre.

The lectures that are to be held, will be seminars more than mere lectures according to the academic meaning of this word: they require your complete collaboration and I will appreciate very much any discussion held at the end of every lecture; I am sure that most of you, scientists who have been working for many years in the field of nuclear physics, have many interesting things to tell us all. Moreover, it is my purpose to organize, in addition to discussions, special seminars held by you yourselves.

And now, last but not least, a few requests of mine: not everything which is going to be done here will be completely amusing. There are, of course, some necessities for the good success of the School and in this field your collaboration is essential. In particular I am referring to the necessity of recording and collecting the lectures which will later be published in the *Supplemento al Nuovo Cimento*.

So I am compelled to ask your collaboration in accomplishing this task; all of you will be requested to collect, write and submit the lectures to their respective lecturers.

And, lastly, let me express the wish that this Summer School of Varenna may not only contribute to the development of your future research activities, but also allow the arising of new and deep friendships among the scientists from the various countries, attending it.

I thank you again for your participation and I wish you all the most profitable stay with us. Welcome to everybody.

1. I. Tanaka
2. De Shalit
3. A. M. Weinberg
4. S. Yoshida
5. H. J. Lipkin
6. I. I. Rabi
7. V. Middelboe
8. P. J. Brussard
9. A. Mijatovic
10. J. O. Newton
11. S. De Benedetti
12. M. Bloom
13. S. Sciuti
14. G. C. Bertolini
15. B. L. Voutz
16. D. M. Brink
17. G. Caglioti
18. R. Amado
19. V. Middelboe
20. K. Sahai
21. H. Robb
22. U. Farinelli
23. D. Morgan
24. G. C. Ghilardotti
25. J. Schmonker
26. S. Gallone
27. A. Rossi
28. M. René
29. L. Papineau
30. R. Ballini
31. E. Sokolowsky
32. R. Bargion
33. J. M. Poole
34. G. Cortellessa
35. C. H. Townes
36. U. L. Businaro
37. L. Peli
38. P. Veronesi
39. P. Teitelbaum
40. C. Salvetti
41. F. Ferrari
42. A. Kind
43. L. N. Cooper
44. C. G. Schuhl
45. P. Mittner
46. C. Coceva
47. A. Bohr
48. P. Giacometti

SCUOLA INTERNAZIONALE DI FISICA

3º CORSO ESTIVO - VARENNA SUL LAGO DI COMO - VILLA MONASTERO - 17 Luglio - 6 Agosto 1955

PARTE PRIMA

Struttura del nucleo e modelli nucleari.

Problems of Nuclear Structure (*).

A. Bohr

Universiteets Institut for Teoretisk Fysik - Copenhagen

1. – Introduction.

These lectures are concerned mainly with low energy nuclear spectra. Two limiting approaches have been used in the theoretical studies of nuclear structure, viz., firstly, a model analogous to that of the atom, in which the nucleons are considered to move approximately independently in a self-consistent field; this leads to the shell model with strong spin-orbit coupling; and, secondly, a model in which the nucleus is treated as a liquid drop and only collective modes of motion are considered. These two limiting approaches are combined in the unified model, in which the nuclear dynamics is described in terms of a superposition of independent particles and collective types of motion.

2. – The Shell Model.

The features of the shell model have been described in great detail in the literature (+); therefore only a brief summary is given here.

The basic evidence for the shell structure is the special stability of nuclei having certain numbers of neutrons and protons. These so-called « magic numbers » are 2, 8, 20, 28, 50, 82, and 126. This special stability has been shown by 1) the high relative abundance of stable nuclei containing magic numbers of neutrons or protons; 2) discontinuities at the magic numbers in the curves of binding energy; 3) alpha and beta decay energies as functions of the number of neutrons or the number of protons.

(*) Based on Lecture Notes, prepared by a group of participants in the Course.

(+) Cf. especially M. Goeppert Mayer and H. J. Jensen: *Elementary Theory of Nuclear Shell Structure* (New York, 1955).

A nuclear shell model has been proposed in which shells are closed at all the experimentally determined magic numbers. This model differs from the atomic shell model because of the difference between the average nuclear potential and the Coulomb potential. If the nucleons are assumed to move in a potential approximated by a harmonic oscillator or a square well, a sequence of levels is obtained which is not in agreement with the experimental magic numbers. Agreement can be obtained by the addition of a spin-orbit coupling which lowers the state having higher angular momentum. The resultant potential can then be written

$$V = V(r) - D(\mathbf{l}\cdot\mathbf{s}) ,$$

where D is a function of the orbital angular momentum l and the mass number A.

Independent evidence for the existence of this spin-orbit force has been found in scattering experiments at low and high energies using polarized beams

The simplest application of the shell model is to a nucleus consisting of closed shells of both neutrons and protons, plus one additional particle. The nuclear properties are then considered simply in terms of the state of the last odd particle. Shell model predictions for ground state spins and parities are in complete agreement with experiment. Magnetic moments show good agreement in some cases; in others, discrepancies are found, indicating that the particles in the closed shells must also be considered. The low-lying energy levels can also be well accounted for, but certain discrepancies are observed in the lifetimes of the excited states.

For the case where there are several particles outside of the closed shells, these particles can be coupled together in different ways to states having different values of the total angular momentum, but having the same energy. This degeneracy is not observed experimentally and the inter-particle interaction required to give agreement with observed splittings must often be so strong as to produce appreciable configuration mixing.

Even-even nuclei all have zero spin in the ground state. This is an experimental fact which has been explained theoretically in various models and special cases. The excitation energies for the low-lying excited states of even-even nuclei show pronounced maxima at the magic numbers. In the regions far from magic numbers, states of low excitation energy are found which exhibit regularities unexplained by the shell model. These are shown later to have a simple interpretation using a collective model.

The fact that all even-even nuclei have spin zero in the ground state suggests the use of an extreme single-particle model to describe the ground states of odd-even nuclei. The odd-even nucleus is assumed to consist of an inert even-even core plus a single particle which is responsible for the nuclear pro-

perties. This extremely simplified model gives ground state spins and parities in agreement with experiment in about 90% of the cases. Good qualitative agreement is obtained for magnetic moments (Schmidt lines). This model also predicts long-lived isomeric states which are experimentally observed in regions where the spin-orbit interaction brings together single-particle levels differing greatly in angular momentum. Orders of forbiddenness of beta transitions are given reasonably well by this model, although there are great discrepancies in lifetime values.

3. – Rotational States in Nuclei [1].

In the usual shell model, the field in which the nucleons move is considered to be spherically symmetric. RAINWATER first pointed out the necessity for taking into account possible deformations of this field. In cases where there are particles outside of closed shells, the distribution of nuclear matter is not spherically symmetric; therefore a spherically symmetric field is not self-consistent. As more particles are added outside of the closed shells, the deformation increases until the middle of the shell is reached, after which it again decreases. This behaviour is in accord with the large nuclear quadrupole moments which have been observed experimentally in the regions between closed shells. These moments are much greater than those predicted by a single-particle model, in some case by more than a factor of ten.

If a nucleus is deformed, it defines a direction in space which can change as a function of time. A rotational motion of the nucleus is therefore possible. If this rotation is slow in comparison with the intrinsic particle motions, it only slightly disturbs the intrinsic structure. The energy of this collective motion is then given by

$$E_{\text{kin}} = \tfrac{1}{2}\Im\omega^2 , \tag{1}$$

where ω is the angular velocity of the rotation and $\Im$ is an effective moment of inertia, which depends upon the type of motion. Rotational spectra have been observed, but the experimental value for the moment of inertia is much smaller than the value $\Im_{\text{rig}} = \sum_p mr_p^2$ corresponding to a rigid rotation. A somewhat better description of the motion is given by an irrotational flow

---

[1] For a survey of the theory and experimental data concerning rotational states, cf. A. BOHR: *Rotational States in Atomic Nuclei* (Copenhagen, 1954) and a forthcoming article on Coulomb excitation by K. ALDER, A. BOHR, T. HUUS, B. R. MOTTELSON, and A. WINTHER (to appear in *The Reviews of Modern Physics*).

in a liquid drop. This can be pictured as a surface wave travelling around the nucleus, as is illustrated in Fig. 1. The kinetic energy of such a motion is proportional to the square of the wave amplitude, i.e. the magnitude of the deformation. The effective moment of inertia is approximately given by

Fig. 1.

$$\Im \approx \Im_{\mathrm{rig}} \left(\frac{\Delta R}{R}\right)^2 , \tag{2}$$

where ΔR is the difference between the major and minor semi-axes of the nucleus, R is the mean radius, and $\Im_{\mathrm{rig}}$ is the moment of inertia of a rigid rotation. Most nuclei possess a shape of axial symmetry. Since the moment of inertia about a nuclear symmetry axis is zero, the rotation is always about an axis perpendicular to the symmetry axis. If the rotational angular momentum vector is $\hbar \boldsymbol{Q}$, the rotational kinetic energy is given by

$$E_{\mathrm{rot}} = \frac{\hbar^2}{2\Im} Q^2 . \tag{3}$$

The motion of the individual particles in the deformed nuclear field may be characterized by their component of angular momentum Ω_p along the symmetry axis (the total angular momentum of a particle is in general not a constant of the motion for non-spherical fields). The quantum numbers Ω_p take on half integer values, positive or negative. States differing only in the sign of Ω_p are degenerate. The Ω_p of the individual particles add up to a total component K of particle angular momentum along the nuclear symmetry axis.

The ground state of a nucleus is obtained by filling the particles pairwise in states of opposite Ω_p. Thus, in an even-even nucleus, one obtains a total $K = 0$, while in an odd-A nucleus the total K is equal to the Ω_p of the last odd particle.

The rotations of such a symmetric nucleus are characterized by the three quantum numbers I, K, M, where K and M are the components of the total angular momentum I along the symmetry axis and a space fixed axis, respectively (Fig. 2).

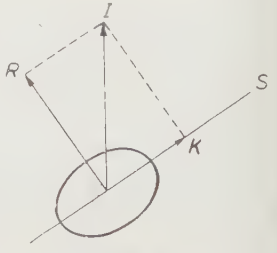

Fig. 2.

The possible quantum states of the nucleus are restricted by the reflection symmetry of the deformations, which implies that states labelled by (K) must be combined in a definite way with those labelled by $(-K)$. Moreover, the reflection symmetry implies that the collective motion has even parity, and

the parity of a nuclear state is, therefore, determined by that of the particle structure.

For an even-even nucleus, in which the ground state is $K = 0$, the lowest rotational band is given by

$$E_{\mathrm{rot}} = \frac{\hbar^2}{2\Im} I(I+1)\,, \tag{4}$$

with the total angular momentum

$$I = 0,\ 2,\ 4,\ 6,\ \ldots$$

and even parity. In this case, the wave function is

$$\Psi = \Phi_{K=0} Y_{IM}(\vartheta, \varphi)\,, \tag{5}$$

where Φ_K represents the intrinsic structure characterized by K, and Y_{IM} is the rotational wave function: ϑ and φ are angles describing the orientation of the nucleus.

The above treatment is a first order approximation in which it is assumed that the deformation and therefore the moment of inertia are not affected by the rotation. Actually, the deformation increases with the rotational angular momentum because of the effect of the centrifugal force. If this effect is small, it gives rise to a correction analogous to the rotation-vibration interaction in molecular spectra, and is given by

$$\Delta E = -\,\mathrm{const}\, I^2(I+1)^2\,. \tag{6}$$

The condition which must be satisfied in order to have a rotational spectrum is that the rotational energy must be small compared to the vibrational energy. We shall later consider as well the perturbation of the motion of individual particles by the rotation.

Rotational states have been found experimentally in a large number of nuclei. One finds the series of states having $I = 0, 2, 4$, etc., in even-even nuclei far removed from closed shells. The energies decrease as the deformation increases, and the energy ratios within a given spectrum agree with striking precision with the theoretically predicted values $E_4/E_2 = 10/3$ and $E_6/E_2 = 7$.

The collective character of these states is characterized by the strong electric quadrupole transitions between them, which in some cases are more than 100 times faster than single-particle transitions.

Rotational states are observed primarily in the regions $A > 225$ and

$150 < A < 185$. This is because both neutron and proton shells close at $A = 208$; in the regions on either side both neutron and proton structures thus favour large deformations. For lighter nuclei, the neutron and proton shells are out of phase and the large deformations only appear to occur again in the region around ^{24}Mg and ^{8}Be.

In odd-A or odd-even nuclei and in even-even nuclei with excited particle structures, the lowest rotational state has an angular momentum $I_0 = K \neq 0$. The rotational angular momentum Q is then given by

$$Q^2 = I(I+1) - K^2 . \tag{7}$$

Since K is a constant in a rotational band, the rotational level spacings are still given by (4). However, the values of I which occur are now I_0, I_0+1, I_0+2, etc.

A special situation occurs in the case of $K=\frac{1}{2}$, where there is a partial decoupling of the intrinsic spin of the last odd particle. The rotational energy for this case assumes the form

$$E_{\mathrm{rot}} = \frac{\hbar^2}{2\Im}[I(I+1) + a(-1)^{I+\frac{1}{2}}(I+\tfrac{1}{2})] , \tag{8}$$

where a is a constant depending upon the intrinsic state.

In an experimental spectrum with $K = \frac{1}{2}$, two energy levels are required to determine the constants $\Im$ and a. The rotational character of the spectrum is verified by the location of the higher states.

4. – Transition Probabilities for Deformed Nuclei.

It is convenient to characterize a β- or γ-transition by its multipolarity L and parity Π, these being the angular momentum and parity of the emitted radiation.

For γ-transitions, this corresponds to the usual classification in terms of electric and magnetic multipole order (EL and ML). The parity is

$$\Pi = \begin{cases} (-1)^L & \text{for} \quad EL \\ (-1)^{L+1} & \text{for} \quad ML . \end{cases} \tag{9}$$

The rigorous selection rules on L and Π for a transition from a state with quantum numbers (K_i, I_i, Π_i) to a state with (K_f, I_f, Π_f) are

1) Conservation of total angular momentum

$$|I_i - I_f| \leqslant L \leqslant |I_i + I_f| ; \tag{10}$$

2) Conservation of parity

$$\Pi = \Pi_i \Pi_f . \tag{11}$$

There is a further selection rule involving K, corresponding to conservation of angular momentum along the symmetry axis. The rigour of this rule depends on how good a quantum number K is. In general, the effect will be to reduce considerably the probability of the process rather than to forbid it completely. This rule is

$$K_i - K_f \leqslant L . \tag{12}$$

A transition which disobeys this rule is known as a K-forbidden transition.

A simple example of this is given by the decay of $^{180}_{72}\mathrm{Hf}$. In this case, a 5.5 hour metastable level of high spin and $K = 1$ decays to the $(0, 8+)$ rotational state. This transition should be highly forbidden; it may, for instance, be associated with a small admixture of $K = 8$ in the $8+$ state (2).

The transition probability $T(L)$ for emission of γ-radiation of multipolarity L and frequency ω is given by

$$T(L) = C_L \omega^{2L+1} B(L) , \tag{13}$$

where $B(L)$ is the reduced transition probability for γ-ray emission between an initial state i and a final state f

$$B(L) = \sum_{\mu, M_f} |\langle i | \mathcal{M}(L, \mu) | f \rangle|^2 . \tag{14}$$

The electric multipole operator of order L and magnetic component μ is given by

$$\mathcal{M}(L, \mu) = \sum_p e_p r_p^L Y_{L\mu}(\theta_p, \varphi_p) , \tag{15}$$

the sum being taken over all the protons. A similar expression can be given for the magnetic multipole operator.

---

(2) Added March 1956: The isomeric transition has now been established to be of $E1$ type with a forbiddenness factor of about 10^{15} (G. Scharff-Goldhaber, M. McKeown, and J. W. Mihelich: *Bull. Am. Phys. Soc.*, in press).

The quantity $B(L)$ can be determined from the lifetime of the state or from cross-section σ for Coulomb excitation. This is given by a relation of the form

$$\sigma = f(Z, M, \Delta E)\cdot B(L)\,, \tag{16}$$

where f can be calculated from the charge and mass of the bombarding and target nuclei, from the energy of the bombarding nuclei, and from the excitation ΔE of the state.

The quantity $B(L)$ for β-transitions can be derived from the comparative lifetime ft by a relation of the form

$$ft = \frac{\text{constant}}{B(L)}\,. \tag{17}$$

It is convenient to consider the quantity $\mathcal{M}$ in the nuclear co-ordinate system x' rather than in the laboratory system x. The relation between the two is given by

$$\mathcal{M}(L, \mu, x) = \sum_{\nu} \mathcal{M}(L, \nu, x')\mathcal{D}^{L}_{\mu\nu}(\theta, \varphi)\,. \tag{18}$$

Since $\nu = K_i - K_f$, there is only a single term in the expansion, and we get

$$B(L) = |\langle K_i|\mathcal{M}(L, \nu, x')|K_f\rangle|^2\langle I_i L K_i \nu | I_i L I_f K_f\rangle\,, \tag{19}$$

where $\langle I_i L K_i \nu | I_i L I_f K_f\rangle$ is the vector addition coefficient for compounding the angular momenta I_i and L to give the final angular momentum I_f. The other quantity $\langle K_i|\mathcal{M}|K_f\rangle$ depends on the nuclear structure. It will be the same for all states in a given rotational band.

5. – Transitions Between States of a Rotational Band.

For $E2$ transitions between states in a rotational band we have

$$B(E2) = \frac{5}{16\pi}\, e^2 Q_0^2 \langle I_i L K_i \nu | I_i L I_f K_f\rangle^2\,. \tag{20}$$

The intrinsic quadrupole moment Q_0 is given by

$$Q_0 = \int \varrho(3z'^2 - r^2)\,\mathrm{d}\tau\,, \tag{21}$$

ϱ being the charge density in the nucleus at the point (z', r). The quadrupole

moment in laboratory space is given by

$$Q = Q_0 \frac{I}{I+1} \cdot \frac{2I-1}{2I+3}. \tag{22}$$

The values for Q obtained from Coulomb excitation data are in fair agreement with those derived from spectroscopic data. The accuracy of the latter type of measurement is however not large, owing to the difficulty of estimating the electric field gradient at the nucleus. Only in the more favourable cases can errors as low as $\pm 20\%$ be given. Expressions similar to the above for the $B(EL)$ of higher multipoles L can also be given. By measuring these it is possible in principle to estimate the amounts of the higher order modes in the nuclear deformation.

In an odd-A nucleus, magnetic dipole transitions can occur between the states $I+1$ and I in a rotational band. The transition probability for these is related to the magnetic properties of the particle and collective motion; if the g factors for these are g_K and g_R, respectively, we have

$$T(M1) \sim (g_K - g_R)^2 . \tag{23}$$

The magnetic moment μ of the nucleus is given by a linear function of g_K and g_R, so that, if both $T(M1)$ and μ are known, then g_K and g_R can be calculated. For rotation of uniformly charged nuclear matter

$$g_R \approx \frac{Z}{A} . \tag{24}$$

6. – Transitions Between Different Rotational Bands.

The absolute probabilities depend on the nuclear structure. However, the relative intensities of states in a given rotational band will be independent of the structure [3].

7. – Fine Structure in Alpha Decay [4].

As has been stated above, the nuclei heavier than ^{226}Ra have large deformations and exhibit the regularities characteristic of such nuclei, in par-

[3] For examples of these intensity rules, cf. A. Bohr, P. O. Fröman, and B. R. Mottelson: *Dan. Mat. Fys. Medd.*, **29**, No. 10 (1955), and G. Alaga, K. Alder, A. Bohr, and B. R. Mottelson: *Dan. Mat. Fys. Medd.*, **29**, No. 9 (1955).

[4] Most of the material presented in this section can be found in greater detail in the paper by A. Bohr, P. O. Fröman, and B. R. Mottelson: *Dan. Mat. Fys. Medd.*, **29**, No. 10 (1955). Cf. also a forthcoming, more extensive article by P. O. Fröman (to appear in *Dan. Mat. Fys. Medd.*).

ticular the rotational energy levels. An additional effect of the deformation is to introduce a selection rule for the α-decay of these nuclei, namely

$$\Delta K = 0 . \tag{25}$$

This rule results from the strong interaction of pairs of nucleons having equal and opposite values of Ω_ν (the projection of their angular momentum along the nuclear symmetry axis). An α-particle is therefore most easily formed by two such pairs within the nucleus, and the escape of such an α-particle leaves the value of K for the nucleus unchanged. As there is no reason for a selection rule on the total angular momentum of the α-particle, transitions can occur to several states in the same rotational band, thereby producing a fine structure showing simple regularities.

8. – Alpha Decay in Even-Even Nuclei.

The decay of $^{238}_{94}$Pu to $^{234}_{92}$U is a typical example of α-decay in even-even nuclei. The ground states both give $I = K = 0$, and the strongest transition is to the ground state of the daughter nucleus. All the populated excited states show the characteristics of a rotational band: they have the proper spins and energy ratios, and the transitions between them are electric quadrupole.

The energies and lifetimes for decay to the ground state are given very well by the Geiger-Nuttall law

$$\log_{10} P_0 = C - \frac{D}{\sqrt{E}} , \tag{26}$$

where P_0 is the transition probability, E is the energy, and C and D are constants depending upon the nuclear charge Z in a systematic manner. Fluctuations by about a factor of two are observed from the values predicted by (26); this is not very much since P_0 varies by a factor of 10^{10}.

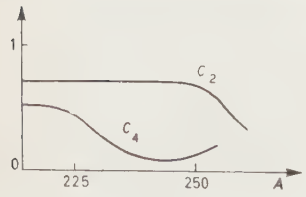

Fig. 3.

9. – Intensities of the Fine Structure Components.

The branching ratios of the transitions to the different rotational states vary systematically with A. This is shown schematically by the curves in Fig. 3 for the coefficient C_l which is defined by the relation

$$C_l = P_l(E)/P_0(E) \tag{27}$$

in order to normalize the energy dependence. $P_l(E)$ is the transition probability for the emission of an α-particle of angular momentum l.

An approximate estimate of the fine structure intensities may be obtained by dividing the barrier into two regions $r \gtrless R_1$. The distance R_1 may be chosen in such a manner that for $r > R_1$ the potential acting on the particle is almost isotropic, while for $r < R_1$ the nuclear rotational motion may be neglected. In the inner region one thus has a static anisotropic barrier, the penetration through which may be treated by a WKB type method discussed by CHRISTY. As a first approximation, one obtains for the α-wave function at distance R_1, neglecting the effect of the centrifugal barrier for $r > R$,

$$\psi(R_1, \theta) = \psi(R, \theta) \exp\left| - \int_R^{R_1} \varkappa \, \mathrm{d}r \right| , \tag{28}$$

where

$$\frac{\hbar^2 \varkappa^2}{2m} = V(r, \theta) - E , \tag{29}$$

and where $R = R(\theta)$ gives the nuclear surface. Expanding $\psi(R_1, \theta)$ in spherical harmonics, the penetration of each partial wave through the remaining (isotropic) part of the barrier may be treated by the usual theory.

Such calculations [5] show that the fine structure intensities do not only depend strongly on the nuclear quadrupole moment, but are also sensitive to small multipole moments of higher order in the nuclear shape. Thus, the observed variation of C_4 provides evidence for a corresponding variation of the $E4$ moment.

10. – Effects of the Admixture of Odd Multipoles in the Deformation.

In addition to the rotational band of the ground state of the daughter nucleus, a $1-$ state is often populated in the decay of even-even nuclei (cf. ^{230}Th to ^{226}Ra). This $1-$ state occurs systematically with energy increasing with A [6]. One possible interpretation of this state, that of the breakup of a pair which is then coupled to $K = 1$, does not explain the systematic occurrence of the state as the orbits change with A.

CHRISTY has suggested a collective excitation due to the presence of odd multipoles in the nuclear deformation. These odd multipoles would destroy the reflection symmetry of the nucleus about a plane perpendicular to the

---

[5] P. O. FRÖMAN, to be published.

[6] Cf. especially F. STEPHENS Jr., F. ASARO, and I. PERLMAN: *Phys. Rev.*, **96**, 1568 (1954) and **100**, 1543 (1955).

nuclear symmetry axis, thereby giving the nucleus a pear shape. Odd values of the rotational angular momentum then become allowed, and the corresponding states have odd parity. But because of the possibility of transitions between such a nucleus and its mirror image, the odd states are shifted upward with respect to the even states by the vibration frequency of the image transition.

Evidence that the $1-$ state really does have $K=0$ and does belong to the ground state rotational band is provided by the branching ratios of the electric dipole transitions to the $0+$ and $2+$ states. The ratio of the reduced transition probabilities $B(1- \to 0+)/B(1- \to 2-)$ is just 2, as is given by the theory discussed above. An important point to check experimentally would be the possible excitation of the $3-$ state by Coulomb excitation. The transition would be electric octupole and have a large matrix element.

11. – Alpha Decay in Odd-Even Nuclei.

Two types of spectra are found in the α-decay of odd-even nuclei. In some cases, the principal transition is to the ground state of the daughter nucleus, as in even-even nuclei; in other cases, the principal transition is to an excited state. This is in accord with the selection rule $\Delta K = 0$. In those cases where the ground state spins and parities of the parent and daughter nuclei are equal, a favoured transition is possible between these states; this is the case in the decay of ^{233}U to ^{229}Th, where both ground states have $I = K = \frac{5}{2}$ and even parity. In those cases where the ground state spins and parities are different, the principal transition occurs to an excited state having the proper value of K and the proper parity. An example of this is the decay of ^{241}Am to an excited state of ^{237}Np. Both these states have $I = K = \frac{5}{2}$ and even parity, whereas the ground state of ^{237}Np has odd parity. Only 0.5 % of the transitions goes to the ground state and its rotational band.

In most cases, transitions are found satisfying the Geiger-Nuttall relation. This indicates that there is no change in the state of the odd particle in the transition. Curves for the variation of α-particle energy with the mass number A for constant charge Z show that the odd-A energies are systematically smaller than even-A energies. This can be interpreted as due to the shrinkage of the nuclear radius during the transition and therefore of the potential well in which the odd particle moves. The kinetic energy of the odd particle must therefore increase slightly and this leaves less energy for the α-particle. The relative intensities of the fine structure components in the favoured odd-A transitions can also be related to those observed in the even-even nuclei.

12. – Single-Particle Motion in Ellipsoidal Nuclei.

Recently, calculations have been made by S. G. NILSSON (7) on the energy levels of a nucleon in an ellipsoidal potential.

For spherical nuclear shape, the field is taken to be of the form

$$V = \tfrac{1}{2}M(\omega^2x^2 + \omega^2y^2 + \omega^2z^2) - Cl^2 - D(\boldsymbol{l}\cdot\boldsymbol{s}) \,. \tag{30}$$

This means that two terms are added to the usual oscillator potential: a spin-orbit term $(\boldsymbol{l}\cdot\boldsymbol{s})$ and l^2 term. The l^2 term gives a correction to the oscillator potential especially at large distances and serves to depress the high angular momentum states. One might also say that this term has some of the features of the interpolation between the square well and the oscillator potential that is usually employed in the shell model. The constants C and D must be chosen in such a way that, in the case of spherically symmetric nuclei, the potential (30) gives the known sequence of the single-particle levels considered in the shell model.

When we want to take account of the deformation δ, we must substitute the quantity ω by the quantities ω_x, ω_y, ω_z (for axially symmetric nuclei $\omega_x = \omega_y$) and the potential in this case becomes

$$V = \tfrac{1}{2}M(\omega_x^2x^2 + \omega_y^2y^2 + \omega_z^2z^2) - Cl^2 - D(\boldsymbol{l}\cdot\boldsymbol{s}) \,. \tag{31}$$

The effect of the deformation of the nucleus is analogous to that which is given by the application of an external electric field. The only simple quantum numbers characterizing the single-particle orbits are the parity and the Ω. Levels with opposite sign of Ω are degenerate.

MOTTELSON and NILSSON have used this level spectrum to calculate the equilibrium nuclear deformation for a given number of protons and neutrons by minimizing the total energy of the nucleus with respect to the deformation. On the other hand, the equilibrium deformation can be deduced empirically from the observed quadrupole transition probabilities of the nuclei. In Fig. 4, the theoretical and empirical values of δ are plotted for nuclei having A ranging from 150 to 200, and one can see that the agreement is very good.

Furthermore, by using this model and a given value of δ (which can be calculated theoretically or taken from the experimental data for the quadrupole moments), one can deduce the intrinsic configurations for the different nuclei. In particular, it is possible to predict the nuclear ground state spins which, for odd-A nuclei, simply equal the Ω-value of the last odd nucleon (8).

---

(7) S. G. NILSSON: *Dan. Mat. Fys. Medd.*, **29**, no. 16 (1955).

(8) For a comparison with the empirical data, cf. B. R. MOTTELSON and S. G. NILSSON: *Phys. Rev.*, **99**, 1615 (1955) and to appear in *Dan. Mat. Fys. Medd.*

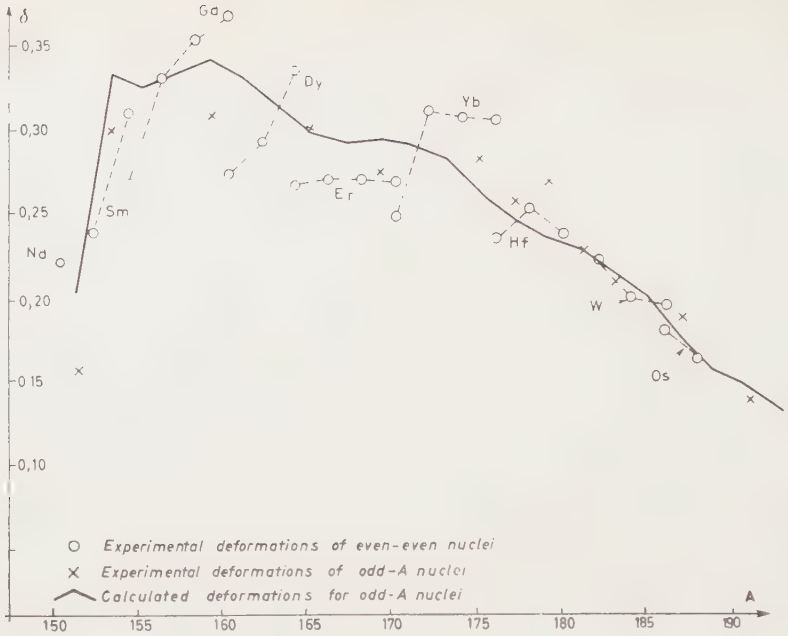

Fig. 4.

One can also classify on this basis the low-lying intrinsic excitations of the strongly deformed nuclei. As an example, Fig. 5 shows the level spectrum of $^{175}_{71}$Lu, deduced from Coulomb excitation, from the β-decay of ^{175}Yb and the K-capture of ^{175}Hf.

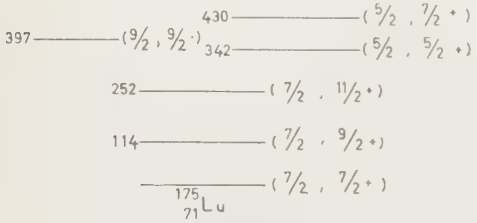

Fig. 5.

The observed levels appear to correspond to three rotational bands with the K-values 7/2+, 5/2+, and 9/2−. From the level spectrum of NILSSON, one also finds that just these three levels are available for the 71-st proton.

13. – Nuclear Moments of Inertia [9].

We shall consider a system of particles in a slowly rotating field and derive the effect of the rotation on the energy of the system, following INGLIS [10]. For simplicity, we first treat the case of a single particle.

[9] For a more detailed discussion of the contents of this section, cf. A. BOHR and B. R. MOTTELSON: *Dan. Mat. Fys. Medd.*, **30**, no. 1 (1955).

[10] D. R. INGLES: *Phys. Rev.*, **96**, 1059 (1954).

Choosing the axis of rotation as the z-axis, and denoting by φ the azimuth with respect to this axis, the Hamiltonian may be written

$$H = T + V(r, z, \varphi - \omega t) , \tag{32}$$

where ω is the angular velocity of rotation. Since V is time dependent, we have

$$ih \frac{\partial \psi}{\partial t} = H\psi . \tag{33}$$

It is convenient to transform to a system of co-ordinates fixed in the rotating nucleus. Writing the wave function in the form

$$\psi = \psi(r, z, \varphi', t) , \tag{34}$$

where

$$\varphi' = \varphi - \omega t , \tag{35}$$

we have

$$ih \frac{\partial \psi}{\partial t} - ih \frac{\partial \psi}{\partial \varphi'} \cdot \omega = H\psi \tag{36}$$

or

$$ih \frac{\partial \psi}{\partial t} = (H - \omega p_\varphi)\psi , \tag{37}$$

where p_φ is the angular momentum operator. (We have omitted the primes).

We require solutions which are stationary in the rotating system. These have the form

$$\psi = \exp[-(i/h)Et]\Phi(r, z, \varphi) , \tag{38}$$

so that

$$(H - \omega p_\varphi)\Phi = E\Phi . \tag{39}$$

If the rate of rotation is slow, ωp_φ is small and may be treated as a perturbation. The unperturbed wave functions Φ_i are given by

$$H\Phi_i = E_i\Phi_i . \tag{40}$$

The perturbed wave function Φ is then given by

$$\Phi = a_0\Phi_0 + \sum_{i\neq 0} a_i\Phi_i \,, \tag{41}$$

where $a_0 \approx 1$, and $a_i \ll 1$ ($|a_0|^2 = -\sum |a_i|^2$).

In the first order perturbation treatment, the a_i are given by the relation

$$a_i = -\omega \frac{\langle 0|p_\varphi|i\rangle}{E_0 - E_i} \,, \tag{42}$$

where $\langle 0|p_\varphi|i\rangle$ is the matrix element of the operator p_φ acting between the states 0 and i.

The expectation value of H is given by

$$\overline{H} = \int \overline{\Phi} H \Phi \, d\tau = |a_0|^2 E_0 + \sum_{i\neq 0} |a_i|^2 E_i = E_0 + \sum_i |a_i|^2 (E_i - E_0) \tag{43}$$

$$= E_0 + \omega^2 \sum_{i\neq 0} \frac{|\langle 0|p_\varphi|i\rangle|^2}{E_0 - E_i} = E_0 + \tfrac{1}{2}\Im\omega^2 \,.$$

Thus, the particle gets a small increase in its energy as a consequence of the rotation. The effective moment of inertia is given by

$$\Im = 2\sum_{i\neq 0} \frac{|\langle 0|p_\varphi|i\rangle|^2}{E_0 - E_i} \,. \tag{44}$$

If the particle possesses a spin, p_φ represents the total angular momentum ($p_\varphi = j_z = l_z + s_z$). For a system of several particles, expression (44) still holds if only p_φ is replaced by $\sum p_\varphi$.

The results which can be derived from this expression, for the case of particles moving independently in a common field, will now be considered. For one particle only in an arbitrary field, WICK showed that, for the ground state, $\Im$ can be obtained by assuming irrotational flow. If ϱ is the density of particles, we thus define a flow velocity $\boldsymbol{v}$ by the equations

$$\operatorname{curl} \boldsymbol{v} = 0 \,, \qquad \operatorname{div} \varrho\boldsymbol{v} = -\frac{\partial\varrho}{\partial t} = \omega\frac{\partial\varrho}{\partial\varphi} \,. \tag{45}$$

The rotational energy is then given by

$$E_{\text{rot}} = \tfrac{1}{2}\Im\omega^2 = \tfrac{1}{2}m\int \varrho\boldsymbol{v}^2 \, d\tau \,. \tag{46}$$

For small ellipsoidal deformations, one obtains from this irrotational flow model

$$\Im_{\text{irrot}} \approx \Im_{\text{rig}} \cdot \beta^2 , \tag{47}$$

where $\Im_{\text{rig}}$ is the moment of inertia which would be associated with a rigid rotation and where β is the deformation parameter ($\beta \approx \Delta R/R$).

For a system of several nucleons, the expression (44) in general differs from $\Im_{\text{irrot}}$; only in the special case, considered by INGLIS, of a closed shell configuration in a harmonic oscillator type of potential, is the irrotational moment obtained. However, a closed shell nucleus has spherical symmetry and, hence, $\Im = 0$, so that this case is of no practical interest. For other ground state configurations, the moment (44) is larger than that predicted by the hydrodynamical model; thus, in the limit of many particles, $\Im$ approaches the value for rigid rotation. This result is independent of the field.

It is possible to see in a simple way how this result arises for a Fermi gas. Initially each point in space has an isotropic velocity distribution. Now, set the system into rotation and look at it in the rotating system of co-ordinates. We have to consider the effect of the Coriolis forces which are equivalent to those produced by a magnetic field. These forces do not change the velocity distribution, a result which is equivalent to that of the absence of diamagnetism in an electron gas. Hence, there is no net flow when viewed in the rotating system. It therefore follows that the particles rotate with the body and that the effective moment of inertia is that of the rigid body.

The empirical moments of inertia, although larger than for irrotational flow, are smaller than those of the rigid bodies (cf. above). This indicates departures from independent motion, and therefore we must consider also the residual interactions between the particles.

We have to do with a competition between the effect of inter-particle interactions, which tend to make the nucleus spherical, and the effect of the coupling of the particles to the nuclear deformation, which tends to decouple the particles from one another. This decoupling effect of the deformation is analogous to that of a strong magnetic field applied to an atom, producing the well-known Paschen-Back effect. There will be a critical deformation β_c in the sense that, for deformations less than β_c, inter-particle forces will dominate and, for deformations larger than β_c, the particles will move approximately independently about the nuclear axis.

For $\beta \ll \beta_c$, we may treat the deformation as a small perturbation and the wave function can be expanded in powers of the deformation. For an even-even nucleus, in which the particles couple to a lowest state of $J = 0$, we have therefore

$$\psi = \psi(J = 0) + \beta\psi(J \neq 0) . \tag{48}$$

The operator P_φ has no effect on the spherically symmetric state $J = 0$, so that from (44) we obtain

$$\Im = \text{const}\, \beta^2 . \tag{49}$$

On the other hand, for β much greater than β_c, the value of $\Im$ approaches that for the rigid body. Thus, the constant in (49) is of the order of $\Im_{\text{rig}} \cdot \beta_c^{-2}$.

The value of β_c increases with the strength of the residual interactions, and the moments of inertia are thus smaller, the stronger the interactions. The model of irrotational flow is seen to correspond to $\beta_c \approx 1$, i.e. to a situation in which the residual forces are so strong that the entire shell structure breaks down.

To obtain some more information on the effect of the interactions, a simplified model has been considered. The effect of the nucleons outside of the closed shells is represented by two spinless particles in p-states, whilst the closed shells are treated collectively in terms of their resistance to deformation. One can vary the number of nucleons in the closed shells in a formal way, thus giving a series of configurations with different deformations. The interaction parameter v measures the ratio of the interaction energy to the configuration spacing $\hbar\omega$ in a harmonic oscillator potential. It is chosen to be

$$v = u/\hbar\omega , \tag{50}$$

where u is the energy between the $J = 0$ and $J = 2$ states of the two nucleons. From this model one can obtain, for every value of v, a curve of $\Im$ as a function of equilibrium deformation. The curves (Fig. 6) show that $\Im$ increases rapidly for small deformations and approaches the value for a rigid body when $\beta \quad v$. The curves are only drawn for values of β greater than 0.6 v, since the model gives no stable equilibrium deformation for nuclei nearer to closed shells.

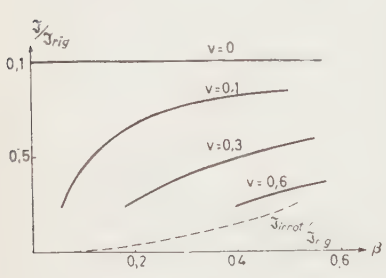

Fig. 6.

The occurrence of even-even nuclei with stable equilibrium deformations thus indicates that the coupling scheme for these nuclei is approaching that of independent particles. However, even for the largest deformations, there remain significant effects of the interactions. These are revealed by the systematic difference in the binding energies and the large difference in the intrinsic excitation spectra of the even-even and odd-A nuclei. A striking example of the latter is given by the two nuclei ^{182}W and ^{183}W. Whilst ^{182}W shows no intrinsic excited states below 1.2 MeV, ^{183}W has approximately one intrinsic level per 100 keV near the ground state. These results show that

there exists a « pairing » energy, of about 1.5 MeV for $A \sim 150$, between each pair of nucleons in a doubly degenerate orbit.

If one employs the single-particle wave functions of a deformed potential with spin-orbit coupling [11] to evaluate $\mathfrak{I}$ from equation (44), and in addition includes in the energy denominator a pairing energy of about 1.5 MeV, the moment of inertia for a deformation of $\beta = 0.3$ is reduced by a factor of about 2. Comparison with Fig. 6 suggests that this corresponds to a value of ν about 0.3. A comparison of the results, shown in Fig. 7, with the observed data also gives a value of about 0.3.

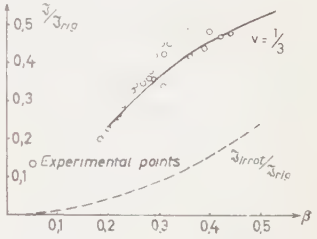

Fig. 7.

14. – Decoupling of Nucleonic Motion from Collective Rotation.

It has been shown that the moment of inertia is given by the expression (44). The evaluation of this expression for independent particle motion gives the rigid moment of inertia. If interactions are introduced, the moment of inertia is decreased. In particular, in even-even nuclei, the effect of the pairing energy is to raise the energies of the low-lying excited states which require the breaking up of a pair. This increases the energy denominators in (44) and decreases the moment of inertia. In odd-A nuclei, the odd particle can have a number of low-lying states so that the moments of inertia of odd-A nuclei are usually somewhat larger than those of neighbouring even-even nuclei.

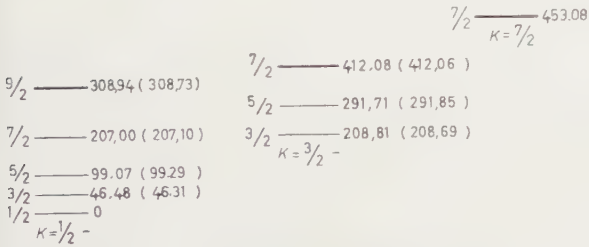

Fig. 8. – Energy level diagram of ^{183}W.

Example of ^{183}W. – A detailed study of the energy spectrum of ^{183}W has been made by A. K. KERMAN [12], using the extremely precise experimental data available for nine energy levels belonging to three different rotational bands. The level scheme is shown in Fig. 8.

The level scheme is in agreement with the model of shell structure in the deformed nuclear field [13], which gives just the three observed low-lying states

---

[11] S. G. NILSSON. loc. cit.
[12] A. K. KERMAN: *Dan. Mat. Fys. Medd.*, **30**, no. 15 (1956).
[13] S. G. NILSSON, loc. cit.

for the 109th neutron, $\frac{1}{2}$, $\frac{3}{2}$, and $\frac{7}{2}$ —. The rotational bands for two of these states are observed, but a discrepancy of 2% is found in the energy ratios. This has been explained by KERMAN as due to the interaction between states in different bands having the same angular momentum and parity. A first order perturbation treatment of this interaction simply changes the effective moment of inertia. In higher order the energy ratios are also affected. An exact calculation of the interaction between the two lowest bands gives the energy values shown in parenthesis in Fig. 8. Five parameters have been chosen to give the best fit, the two moments of inertia, the decoupling constant a for the $\frac{1}{2}$ state, the position of the $(\frac{3}{2}, \frac{3}{2})$ level, and the strength of the interaction. Seven levels have been calculated. Intensity ratios have also been calculated, giving good agreement for twelve pieces of data with the introduction of only four parameters.

15. – Effects of the Competition between Independent Particle Motion and Interactions.

As has been discussed above, the interactions between the particles tend to couple them to a state of total angular momentum zero, while the deformation of the nuclear field tends to decouple the particles. Near closed shells the interactions have a strong effect and favour a spherical symmetric shape. As more particles are added, the nucleus becomes « softer »; i.e. it requires less energy to produce a deformation. Finally a point is reached where an equilibrium deformation develops. This is shown qualitatively in Fig. 9, in which the deformation energy $V(\beta)$ is plotted against the deformation β for even even nuclei having increasing numbers of particles outside of closed shells.

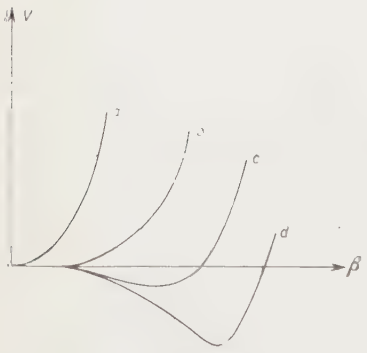

Fig. 9.

This effect has been calculated very roughly using the simple two-nucleon model discussed above. The minimum equilibrium deformation obtained is $\beta_{\min} \sim 0.6 \cdot v \sim 0.2$; this determines the minimum value of the moment of inertia and thus the maximum value of the energy of the first rotational state

$$\Im_{\min} \sim (1/4)\Im_{\text{rig}}\,, \qquad (E_2)_{\max} \sim 12\hbar^2/\Im_{\text{rig}}\,. \tag{51}$$

The experimental values for the energies of the first excited states of even-even nuclei are in agreement with (51). These energies are below $(E_2)_{\max}$ only in the regions where rotational spectra are expected and observed.

Vibrational Energy States. – For nuclei near closed shells, which possess a spherical equilibrium shape, the collective excitations are expected to be of vibrational type. The vibrational modes may be classified by their multipole order $(\lambda\mu)$, giving the total angular momentum of the excitation quanta and its z-component. Each mode corresponds in first approximation to a harmonic oscillator, characterized by a restoring force C_λ and a mass parameter B_λ. The frequency of oscillation is then $\omega_\lambda = \sqrt{C_\lambda/B_\lambda}$ and the excitation quanta have the energy $\hbar\omega_\lambda$.

The vibrations of principal importance are those of quadrupole type ($\lambda=2$). In an even-even nucleus, for which the intrinsic angular momentum vanishes for the ground state configuration, the first $\lambda = 2$ vibrational excitation is of $2-$ type, and has the energy $\hbar\omega_2$ above the ground state. The second has an energy of $2\hbar\omega_2$ and is degenerate; it includes $0+$, $2+$, and $4+$.

The experimental data show that the first excited state of even-even nuclei is indeed 2^+, and that the energy decreases as one goes away from closed shells; i.e. as the nucleus becomes more easily deformed. The second state is found to have a spin of either 0, 2 or 4, except very near closed shells. The method of populating these states in the experiment is generally such that one would not expect to observe all these states. The energy ratios agree qualitatively, which is all that is to be expected, since the harmonic oscillator model is a very rough approximation.

The transitions between these states show strong evidence for the collective character of the excitation. For the case where the second state is $2+$, while a single-particle transition would be predominantly $M1$, the decay to the first exited 2^+ state is mainly $E2$. The cross-over transition is sometimes 100 times weaker than the cascade transition; this is only understandable if there is some selection rule forbidding the cross-over, such as the rule for the harmonic oscillator, which allows only transitions between neighbouring states. The reduced transition probabilities $B(E2)$ for the transition to the first excited state, as determined from the Coulomb excitation cross-section, are an order of magnitude larger than those from single-particle transitions.

The above data give an indication of the validity of this vibrational picture, but considerably more experimental evidence is necessary before the theory can be well established [14].

As in the rotational case, the vibrational excitations must be adiabatic and not perturb excessively the intrinsic particle motions. Non-adiabatic

---

[14] The vibrational interpretation of the states in question was first suggested by G. SCHARFF-GOLDHABER and J. WENESER: *Phys. Rev.*, **98**, 212 (1955). A discussion of the available experimental evidence on the vibrational excitations is given in a review article on Coulomb excitation (K. ALDER, A. BOHR, T. HUUS, B. R. MOTTELSON, and A. WINTHER, to appear in *The Reviews of Modern Physics*).

effects can be expected to be greater than in the rotational case, because the vibrational energy spacings are greater than the rotational ones. Very near the closed shells, where a large energy is required to deform the nucleus, the lowest excited states are not of collective type.

16. – Nuclear Fission (*).

When a heavy nucleus captures a neutron or absorbs a high energy photon, a compound nucleus is formed in which the excitation energy is distributed among a large number of degrees of freedom of the nucleus ([15]). The complex state of motion thereby initiated may be described in terms of collective nuclear vibrations and rotations coupled to the motion of individual nucleons ([16,17]).

The compound nucleus lives for a relatively very long period, usually of the order of a million times longer than the fundamental nuclear periods, after which it decays by emission of radiation or of neutrons, or by fission. The latter process occurs if a sufficient amount of energy becomes concentrated on potential energy of deformation to enable the nucleus to pass over the saddle point shape, at which the repulsive Coulomb forces balance the cohesive nuclear interactions ([18,19]).

For excitation energies not too far above the fission threshold, the nucleus, in passing over the saddle point, is « cold », since the major part of its energy content is bound in potential energy of deformation. The quantum states available to the nucleus at the saddle point of the « fission channels » are then widely separated and represent relatively simple types of motion of the nucleus. These channels are expected to form a similar spectrum as the observed low-energy excitations of the nuclear ground state.

This ordered character of the motion of the nucleus at saddle point gives rise to a number of regularities in the fission phenomena. Thus, a fission process passing through a single channel may exhibit a marked anisotropy in the angular distribution of the fragments, depending on the angular mo-

(*) The contents of this lecture was similar to that subsequently delivered at the Geneva Conference, August 1955. We therefore reproduce the article from the *Proceedings of the Conference*, **2**, 151 (New York, 1956).

([15]) N. BOHR: *Nature*, **137**, 344 (1936); N. BOHR and F. KALCKAR: *Dan. Mat. Fys. Medd.*, **14**, no. 10 (1937).

([16]) A. BOHR: *Dan. Mat. Fys. Medd.*, **26**, no. 14 (1952); A. BOHR and B. R. MOTTELSON: *Dan. Mat. Fys. Medd.*, **27**, no. 16 (1953).

([17]) D. L. HILL and J. A. WHEELER: *Phys. Rev.*, **89**, 1102 (1953).

([18]) L. MEITNER and O. R. FRISCH: *Nature*, **143**, 239 (1939).

([19]) N. BOHR and J. A. WHEELER: *Phys. Rev.*, **56**, 426 (1993).

mentum quantum numbers of the channel. Moreover, the wide spacing of the channels implies that the fission threshold may depend significantly on the spin and parity of the compound nucleus. Experimental data on these aspects of the fission phenomenon may thus provide valuable information on the structure of the fissioning nuclei at a crucial stage of the process.

16·1. *Fission Channel Spectrum.* – The channel spectrum for fissioning nuclei refers to the sequence of potential energy surfaces $E(\alpha)$ considered as functions of the deformation parameter α characterizing the motion towards fission, and evaluated at the saddle point deformation.

In this section, we briefly describe the channel spectrum expected on the basis of present knowledge of the low energy spectra of the nuclei in the region of the very heavy elements. These nuclei have already in their ground state a strongly elongated shape, and the ground state excitations therefore exhibit many similarities to those of the saddle point.

We shall assume that the nuclear shape during the passing of the saddle point remains axially symmetric, as it is the preferred shape of the nuclear ground states. The channels can then be characterized by the quantum number K, representing the component of the nuclear angular momentum about the symmetry axis.

For even-even nuclei, the lowest state of the nucleonic structure has $K=0$, corresponding to a paired nucleon configuration. With this intrinsic state is associated a rotational band with energies [20]

$$E_{I,K} = E_K + \frac{\hbar^2}{2J} I(I+1)\,, \tag{52}$$

where I is the total nuclear angular momentum and J the effective moment of inertia. This latter quantity depends on the nuclear deformation. For the ground states of the very heavy elements, the value of $\hbar^2/2J$ is about 7 keV, and for the greater deformation at saddle point the value may be even smaller.

For nuclei, whose shape possesses reflection symmetry, the spectrum (52) contains, for $K=0$, only the rotational levels with even I-values: 0, 2, 4, ..., which all have positive parity. The observed mass ratio of the fission fragments indicates, however, that at the saddle point the nuclear shape in general does not possess reflection symmetry. The rotational band then also contains the odd I-values having negative parity; however, the negative parity levels will be displaced with respect to the positive parity levels by an amount of $\hbar\omega$, where

[20] For a discussion of nuclear rotational states, cf., e.g., A. Bohr and B. R. Mottelson, *Beta- and Gamma-Ray Spectroscopy*, edited by K. Siegbahn, chapter 17 (Amsterdam, 1955) and A. Bohr: *Rotational States of Atomic Nuclei* (Copenhagen, 1954).

ω is the frequency of the tunnelling motion between the mirror shapes of the preferred asymmetry. The more pronounced the asymmetry, the smaller will be ω.

In this connection it is of interest that low-lying (1) excitations of the nuclear ground states have been observed to occur systematically in the even isotopes of Ra and Th with energies in the region of 200–300 keV ([21]). The energies increase as one goes to heavier elements. The interpretation of these states as collective modes of excitation associated with an asymmetry in the nuclear shape ([22]) is suggested by the fact that the lowest intrinsic excitations in even-even nuclei appear to have energies of the order of an MeV, and by the observed branching ratios for the $E1$ decay to the ground state and first excited (2+) state, which indicate a K-value of 0 ([23]).

At the saddle point shape, one thus expects even-even nuclei to have a lowest state of $I = 0+$, and close lying collective excitations of $2+$, $4+$, ... type as well as, although with somewhat higher energies, states of $1-$, $3-$, ... type.

Apart from these collective rotational excitations, the nucleus possesses states involving the excitation of the nucleonic configuration. Since, however, these require the breaking of a nucleon pair, there will be a significant energy gap, estimated to be of the order of an MeV, between the lowest configuration (with K 0) and the first excited configuration. After this gap the spacing between intrinsic excitations is expected to be only of the order of a hundred keV, corresponding to the average spacing of individual particle orbits. With each such intrinsic excitation, characterized by a definite K, there is associated a rotational band with I K, $K+1$, K 2, ... and both parities. The rotational energies are again given by (52).

In odd-A nuclei, the lowest K-value is given by the component of angular momentum of the last odd particle in its lowest binding state. At saddle point this lowest K-value will in general differ from that of the nuclear ground state ([24]). The spacing between the states of the last odd particle is of the order of a few hundred keV, and the intrinsic excitations in odd-A nuclei in-

([21]) F. Stephens Jr., F. Asaro and I. Perlman: *Phys. Rev.*, **96**, 1568 (1954).

([22]) Such an interpretation was first suggested by R. F. Christy: private communication, October 1954.

([23]) As an alternative to the interpretation of the (1 —) states as rotational excitations of asymmetric nuclei, one may also consider the possibility of an asymmetric vibration of the nuclear shape about an equilibrium which is symmetric but very soft towards asymmetric deformations.

([24]) This circumstance has been suggested as the explanation of the slower rate of spontaneous fission in odd-A nuclei as compared to that observed in even-even nuclei (J. O. Newton: *Nuclear Properties of the Very Heavy Elements*, in *Contribution to Progress in Nuclear Physics*, vol. 4, edited by O. R. Frisch (1954)).

volve no energy gap similar to that characterizing the paired configuration in even-even nuclei. With each particle configuration is associated a rotational band with $I \geq K$, $K = 1, \ldots$ and both parities, assuming a preference for an asymmetric shape at saddle point, or a softness towards deformations of this type (cf. reference [23]). Similarly, in odd-odd nuclei, the intrinsic excitations may be closely spaced.

16·2. *Photofission.* – The case of photofission of even-even nuclei presents certain especially simple features, since in this case the compound nucleus is always produced in a (1^-) state, assuming electric dipole absorption. As mentioned above, the lowest (1^-) fission channel at saddle point corresponds to the $K = 0$ configuration, with the nuclear angular momentum taken up by rotational motion. For photon energies close to the fission threshold, the great majority of the fissioning nuclei is therefore expected to pass through this particular channel. This circumstances provides an explanation of the observed angular anisotropy of the fission fragments [25,26].

Thus for the state involved, with $I = 1$, $K = 0$, and magnetic quantum numbers $M = \pm 1$ in the direction of the incident beam of photons, the probability for the nuclear symmetry axis to form an angle θ with the photon direction is of the form

$$W(\theta) = b \sin^2 \theta. \tag{53}$$

After the saddle point has been passed, the coupling between rotational and intrinsic motion may to some extent weaken the anisotropy, but since this last stage of the fission process takes place rapidly, the angular distribution of the emitted fragments is expected to be mainly of the type expressed in equation (53).

[25] E. J. Winhold, P. T. Demos, and I. Halpern: *Phys. Rev.*, **87**, 1139 (1952).

[26] The observed anisotropy in photofission has been earlier discussed (ref. [17]) in terms of a tendency for the absorbed photon to set up an oscillation of the nucleus preferentially in a direction perpendicular to the beam. From similar arguments an opposite anisotropy in fast neutron induced fission was predicted and later verified experimentally (cf. below). It would appear, however, that any such correlation in the initial stage of the process is quickly lost in the highly complex motion of the compound nucleus, since the quantum number K, which determines the direction of the nuclear axis with respect to the total angular momentum vector, is not a constant of the motion for the compound state. Thus, the anisotropy in the photofission depends on the fact that, in the threshold region, the nucleus must pass through the saddle point in a definite channel, having $K = 0$. In the fast neutron fission the situation is somewhat different. The high angular momentum values given to the nucleus here implies a tendency even in the complex motion of the compound nucleus to concentrate a large part of this angular momentum on collective rotational motion.

With increasing photon energy, other channels of (1 —) type representing intrinsic nuclear excitations become available. Those having $K = 1$ give an anisotropy of opposite character to that in equation (53) and on the average an approximately isotropic distribution is expected for the nuclei passing through the saddle point in a state of intrinsic excitation. Thus, the total angular distribution becomes

$$W(\theta) = a + b \sin^2 \theta, \tag{54}$$

with the ratio b/a decreasing as the photon energy is increased. Assuming the first intrinsic excitations to have an energy of about one MeV (cf. above), the anisotropy would become small at an energy of a few MeV above threshold.

The experimentally observed angular distribution for photofission ([25-27]) of ^{232}Th and ^{238}U follows such a pattern. The distribution is found to be of the type in equation (54), with the $\sin^2 \theta$ term dominating close to the threshold and becoming relatively small already a few MeV above threshold.

The anisotropy is observed to be somewhat larger in ^{232}Th than in ^{238}U, which might indicate a somewhat larger gap in the former nucleus between the first collective and intrinsic (1) excitations at the saddle point. It is of interest to note in this connection that the energy of the collective (1 -) excitations of the ground state appears to increase as one goes from Th to U (cf. above).

In odd-A nuclei, several spin states may be formed by absorption of a dipole quantum, and the M-values extend from I to I. Moreover, as mentioned above, the quantum states at saddle point lie denser than in the even-even nuclei. Even rather close to threshold, therefore, the photofission may proceed through several states, and no pronounced anisotropy is expected. The experiments on the photofission of ^{235}U have also yielded an approximately isotropic distribution of the fragments ([27]).

The photofission of odd-A nuclei should be more comparable to the part of the even-even photofission which passes through intrinsic excitations, where the level density is high. It has also been noted ([27]) that the isotropic part of the even-even photofission shows a similar yield curve as for the odd-A nuclei, while the anisotropic component appears as an additional contribution to the photofission process.

The interpretation of the anisotropic component in photofission as representing the nuclei which pass through the saddle point in the (1 —) collective excitation has a further interesting consequence for the mass distribution of

([27]) E. J. Winhold: *Ph. D. Thesis*, Mass. Inst. of Technology, Sept. 1953.

the fragments. In fact, since the wave function for this state is antisymmetric in the co-ordinate describing the degree of asymmetry of the nuclear shape, a nucleus in this state cannot undergo symmetric fission. Such a discrimination against symmetric mass division has been observed experimentally in the photofission of ^{232}Th ([28]). It is found that the anisotropy vanishes for symmetric division and increases strongly with the ratio between the fragment masses.

16·3. *Slow Neutron Induced Fission.* – Slow neutron capture by an even-odd nucleus of spin I_0 leads to a compound nucleus of even-even type with spin $I = I_0 \pm \frac{1}{2}$, and with same parity π as the target nucleus.

As follows from the above discussion of the spectrum at saddle point, only one of these spin-parity combinations is contained in the rotational band associated with the lowest nucleonic configuration ($K = 0$), viz., the state with $(-1)^I = \pi$.

Therefore, the fission threshold is expected to differ appreciably, by as much as an MeV, for the two types of compound levels formed. This may imply a rather different ratio of fission to capture for the two level systems, especially if the neutron binding energy is smaller than the larger of the threshold values.

The circumstance that slow neutron fission is expected to proceed through one or a few channels also implies large fluctuations in the fission width among the levels of same I. The fluctuations should be similar to those observed for the neutron width, which likewise depends on the presence in the compound nucleus wave function of a definite component (representing the channel for elastic neutron scattering).

The parity of the target nucleus may further affect the mass distribution of the fission fragments. Thus, for the levels with $(-1)^I = \pi$, the nuclear wave function is symmetric or antisymmetric in the asymmetry co-ordinate, for $\pi = +1$ and -1, respectively. In the latter case, symmetric fission is expected to be inhibited, as in the case of the photofission (cf. above).

If slow neutron fission of aligned nuclei could be studied, large angular anisotropies of the fragments would be expected. For the states with $(-1)^I = \pi$, which pass through the saddle point with $K = 0$, the distribution is directly related to the distribution of M-values of the compound states. For the other set of levels with $(-1)^I = -\pi$, the distribution in addition depends on the K-value of the fissioning nucleus.

Some even-even target nuclei have also been observed to undergo slow neutron fission. For such targets the compound states all have $I = \frac{1}{2}$ and even

([28]) A. W. Fairhall, I. Halpern and E. J. Winhold: *Phys. Rev.*, **94**, 733 (1954).

parity, and the fission threshold depends on the energy of the lowest $K = \frac{1}{2}$ configuration at saddle point. If the intrinsic parity of this configuration is odd, symmetric fission should again be inhibited.

16·4. *Fission Produced by Fast Particles.* – In the case of fission initiated by the impact of faster particles, there may be a correlation between the direction of the incident beam and of the fragment emission. This correlation depends on the distribution of the I- and M-values with which the compound nucleus is formed, as well as on the K-values of the states available to the fissioning nucleus at the saddle point. For a fission process proceeding through a channel with quantum numbers I, M, K, the orientation of the nuclear symmetry axis, representing the direction of fission, is distributed according to the corresponding symmetric top wave function.

For relatively small energies, at which a single angular momentum state of the incident particle may play an important role, or close to the fission thresholds, specific effects may occur associated with the dominance of a single or a few fission channels.

For larger energies of the incident particle, the fissioning nuclei may pass through a great number of different states at the saddle point, with different angular momentum quantum numbers. Nevertheless, a systematic tendency for anisotropy in the fragment emission results from the fact that the M- and K-values are not distributed uniformly from $-I$ to I, but are concentrated towards numerically small values. Thus, assuming the incident particle to be a proton or a neutron, the M-values are restricted to the range $M = I_0 \pm \frac{1}{2}$, where I_0 is the spin of the target nucleus. Moreover, the channel spectrum is expected to exhibit a marked preference for small K-values; this is especially so for even-even nuclei, but also the density of K-values for additional individual nucleons decreases with increasing K [29].

The tendency towards small values of M implies that, for large I, the nuclear angular momentum vector points preferentially in a direction perpendicular to the incident direction. Moreover, for small K-values, the nuclear axis is orientated predominantly perpendicular to the angular momentum vector. Consequently, the distribution of the fission fragments per solid angle is peaked in the forward direction.

An anisotropy of this type has been found for fast neutron fission in a number of elements [30]. The dependence of the observed anisotropy on the even-odd character of the target nucleus can also be understood from the above line of argumentation. Thus, if the target is even-odd (even Z, odd N), so that the compound nucleus is even-even, the K-values at the saddle point

[29] S. G. Nilsson: *Dan. Mat. Fys. Medd.*, **29**, No. 16 (1956).
[30] J. E. Brolley Jr. and W. C. Dickinson: *Phys. Rev.*, **94**, 640 (1954).

are the smallest. On the other hand, the M-values are smallest for even-even targets, in which case the compound nucleus has $M = \pm \frac{1}{2}$. Therefore, the anisotropy should be relatively large for these two types of targets, and appreciably smaller for odd-even or odd-odd targets. The experiments ([30]) indicate comparable anisotropies in ^{233}U, ^{235}U, and ^{238}U, but only half the effect in ^{237}Np.

For even-odd targets, the anisotropy is expected to be largest for small values of the target spin I_0, since the range of M-values is then most restricted. The observed small difference between the anisotropies of ^{233}U ($I_0 = \frac{5}{2}$) and ^{235}U ($I_0 = \frac{7}{2}$) is in this direction, but may not be significant in view of the experimental uncertainties. An especially large anisotropy should result for ^{239}Pu with $I_0 = \frac{1}{2}$.

In order to obtain a theoretical estimate of the order of magnitude of the anisotropy in the fission fragment distribution, we may employ the classical approximation to the angular distribution functions, which becomes valid for high angular momenta. Considering a particle incident on an even-even target and neglecting the spin of the particle, the compound nucleus has $M = 0$ and the angular distribution of the fragments is then, in the classical approximation, given by

$$W(\theta) = \int dI \int_{|K| < I \sin\theta} dK f(K, I) \left(\sin^2\theta - \frac{K^2}{I^2}\right)^{-\frac{1}{2}}, \tag{55}$$

where $f(K, I)$ gives the distribution in K and I of the fissioning nuclei.

For simplicity, we shall represent the distribution in K at the saddle point by a constant for K less than some effective limit K_m. Moreover, in the classical approximation, the probability for formation of the compound nucleus in a state of total angular momentum I is proportional to I up to a limiting value I_m, given by

$$\hbar I_m = R_0 M V, \tag{56}$$

where R_0 is the mean nuclear radius and MV the momentum of the particle. The distribution in equation (55) then depends only on the ratio $x = I_m/K_m$. For $x \leq 1$, the distribution is isotropic, but for larger x it exhibits a forward peak which increases with x. The ratio $W(0°)/W(90°)$ takes on values of about 1.15, 1.3, and 1.8 for $x = 1.25$, 1.5, and 2, respectively.

The observed anisotropy for fast neutron fission in ^{235}U follows such a general trend increasing with the energy of the incident neutron ([31]). A max-

([31]) J. E. Brolley Jr. and R. L. Henkel: *Bull. Am. Phys. Soc.*, **30**, no. 3, pag. 16.

imum anisotropy of $W(0^o)/W(90^o) \sim 1.4$ was obtained for a neutron energy of about 7 MeV. For this energy we have $I_m \sim 5$, so that the observed anisotropy corresponds to the above estimated, if we take $K_m \sim 3$, which is of the expected order of magnitude. For still larger neutron energies, fission processes occurring after neutron emission are expected to become increasingly important ([32]) and would seem to account for the observed decrease in the anisotropy of the fragment distribution. Similar anisotropies have also been observed in the fission of Th- and U-isotopes produced by protons of about 22 MeV ([33]).

([32]) N. BOHR: *Phys. Rev.*, **58**, 864 (1940).

([33]) B. L. COHEN, W. H. JONES, G. H. MCCORMICK and B. L. FERREL: *Phys. Rev.*, **94**, 625 (1954); B. L. COHEN, B. L. FERRELL, D. J. COOMBE and H. K. HULLINGS: *Phys. Rev.*, **98**, 685 (1955).

SUPPLEMENTO AL VOLUME IV, SERIE X
DEL NUOVO CIMENTO

N. 3, 1956
2° Semestre

The Inelastic Scattering of Protons and Neutrons by Deformed Nuclei.

D. M. BRINK

Clarendon Laboratory - Oxford

S. YOSHIDA

Department of Mathematics and Physics - University of Birmingham

Many of the features of the inelastic scattering of neutrons by nuclei have been explained on the basis of N. BOHR's compound nucleus model. In this model it is assumed that when a neutron strikes the target nucleus it may be absorbed to form a compound system of some stability. Subsequently this compound system can decompose emitting a neutron and leaving the target nucleus in an excited state. The theory supposes that the formation and decay of the compound nucleus may be treated as independent processes, so that the mode of decay depends only on its energy, total angular momentum, and parity; but not specifically on the way in which it was formed. With the above assumptions the cross sections for inelastic scattering have been calculated by HAUSER and FESHBACH.

In this theory it is supposed that the cross section or compound nucleus formation σ^0 is independent of the details of nuclearf structure and depends smoothly on the atomic weight of the target nucleus. Two models have been proposed for the calculation of this cross section, both of which assume that the interaction of the incident neutron with the nucleus can be approximated by an average potential. The « black nucleus » or « strong coupling » model proposed by WEISSKOPF and others assumes that the mean free path of a neutron inside the nuclear matter is short compared with the nuclear radius so that the neutron is absorbed very soon after it enters the interior of the nucleus. On the other hand the « optical model » proposed by FESHBACH, PORTER and WEISSKOPF supposes that the interaction is such that the neutron has a finite mean free path in nuclear matter of the order of the nuclear radius.

Thus there is a finite probability that the incident neutron may enter the nucleus and escape again without being absorbed. For those values of the nuclear radius at which the neutron wave just fits inside the nucleus, the neutron will be reflected many times from the walls of the nucleus before escaping. Thus the probability of forming a compound state is increased. Thus the model predicts resonances in the total neutron cross section and in the cross section for compound nucleus formation. These resonances are observed and occur at values of the atomic weight near $A = 50$, $A = 100$, $A = 150$ and $A = 230$ for neutron energy below 1 MeV. Mathematically the absorption of the neutron to form a compound nucleus is represented by taking a complex potential, $V = V_0(r)(1 + ig)$ for the neutron-nucleus interaction.

The inelastic cross sections can be computed from the cross sections for compound nucleus formation predicted by the above models using the methods of Hauser and Feshbach.

In the region of strongly deformed nuclei there is another process which can give rise to inelastic scattering. A neutron scattered by such a deformed nucleus may be reflected from the nuclear surface in such a way that the impact causes the target nucleus to be set into rotation.

Evidently the cross section for this process will be highest for these nuclear radii at which a standing wave develops inside the nucleus thus giving rise to many reflections.

For the calculation of the cross section the interaction of the neutron with the deformed nucleus was approximated by a non-spherical potential well, with an absorption term to allow for compound nucleus formation. The calculation was made by first solving exactly the problem of scattering in a spherical potential by the methods of Feshbach, Porter and Weisskopf. The nuclear deformation was then treated as a perturbation of this spherical potential. The total cross section for the direct process was found to be

$$\sigma = \frac{M(I_0, I)(R_0K)^4}{k_0^2} \sum_{l,l_0} \left| (2l_0 + 1)(2l + 1)[G(ll_0 2.00)]^2 \frac{s_{l_0}}{M_{l_0}^2 + N_{l_0}^2} \cdot \frac{s_0}{M_l^2 + N_l^2} \right| ,$$

where $M(I_0, I)$ is a nuclear matrix element;

$$\frac{1}{(2I_0 + 1)} \sum_{MM_0} |\langle IM | \alpha_\mu | I_0 M_0 \rangle|^2 ,$$

I_0, I are the initial and final nuclear spins, $l_0 l$ are the initial and final neutron orbital angular momenta, α_μ are the nuclear deformation coordinates, k_0 is the incident neutron wave number, k is the neutron wave number inside the nucleus, R_0 is the nuclear radius, $G(ll_0 2.00)$ is a Clebsch-Gordon coefficient and s_l, M_l and N_l are constants of the well, calculated by Fehsbach, Porter and Weisskopf.

To compare the predictions of the two models the cross section for the excitation of a 2^+ state in an even-even nucleus has been calculated as a function of atomic weight A for an incident neutron energy of 1 MeV. The direct cross section is proportional to the square of the nuclear deformation, and the curve shown corresponds to a constant value $\beta = 0.3$. The calculation of the compound nucleus cross section assumes that the 2^+ state is the only excited state below 1 MeV. Its energy was taken to be 200 keV, but the general features shown are not sensitive to this energy.

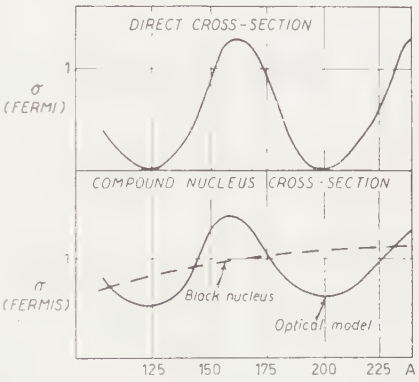

Fig. 1.

The differential cross section of inelastically scattered nucleons through the direct process were also calculated and it is interesting to compare it with experiments. The available experiments are now restricted to the case where the incident beam is proton and the target is a rather light nucleus. For the reaction $^{12}C(p, p')^{12}C^*(4.43\ \text{MeV}, I = 2^+)$ and the incident energy 9.5 MeV, the differential cross section was measured by BURCHAM *et al.* and the result is the following:

$$15.9(P_0 + 0.04P_2 - 0.38P_4)\ \text{mF}\,, \qquad (*)$$

$P_n(\cos\theta)$ is the Legendre polynomial of order n. The most characteristic feature of this curve is the symmetry about 90°. If one assumes the following optical potential

$$V_0 = (35 + 5l)\ \text{MeV}\,, \qquad r < R_0,$$

$$= 0\,, \qquad r > R_0,$$

$$R_0 = 1.45 \cdot 10^{-13} A^{\frac{1}{3}}\ \text{cm}\,,$$

which gives a good agreement to the experiment of elastic scattering of protons at same incident energy, then the S and D waves are near the resonance for both incoming and outgoing wave and the contribution to the inelastic cross section from odd partial waves is negligible. The inelastic cross section is given by

$$24.4(P_0 + 1.42P_2 + 0.04P_3 + 0.31P_4)\ \text{mF}\,.$$

(*) The symbol F is used to indicate the cross-section unit « Fermi » = 10^{-24} cm², also know as barn.

The absolute value was calculated assuming the weak coupling approximation by A. Bohr and Mottelson with the hydrodinamical constants used by them; the absolute value need not be taken seriously. But the angular distribution is symmetric about 90°, which agrees with experiment. As for the detailed values of the coefficients of the Legendre polynomial, the agreement with experiments is not good. Next we add the spin orbit interaction to the optical potential which gives a correct energy separation of the $d_{\frac{1}{2}}$ and $d_{\frac{3}{2}}$ levels of ^{17}O and has the δ-function type radial dependence $\delta(r - R_0)$. Then the result gives a better agreement with experiment as shown by

$$18.5(P_0 + 0.02P_1 + 0.80P_2 - 0.08P_3 - 0.11P_4) \text{ mF} .$$

The case of ^{20}Ne(p′, p)Ne is also calculated and result gives a symmetry about 90°, which agrees with experiment. In this case the main partial waves which contribute to the cross section are the p and f waves. But the theory gives a wrong sign for the coefficient of P_2. It may be because the intrinsic quadrupole moment Q_0 is not so large compared to the case of ^{12}C. The Q_0 of ^{24}Mg is very large and experiments are available, so it is interesting to see whether our theory based on the direct interaction gives a good agreement with experiment, but the calculation is not yet finished.

SUPPLEMENTO AL VOLUME IV, SERIE X
DEL NUOVO CIMENTO

N. 3, 1956
2° Semestre

The Nuclear Radius.

L. N. COOPER (*)

The Institute for Advanced Study - Princeton, N. J.

One of the first surprises the nucleus presented to physicists was due to a measurement of the nuclear radius. This was, of course, Rutherford's classic α scattering experiment in which he discovered that the positive charge of the gold atom must be concentrated in a sphere of very small radius. Since then the neutron and the meson have been discovered and one would say that Rutherford made the first measurement of the electromagnetic radius of the nucleus.

The reason one uses the term radius for an object like the nucleus which cannot, by the uncertainty principle, be so well defined geometrically is that one can write for the nuclear radius the following expression:

$$R = r_0 A^{\frac{1}{3}} 10^{-13} \text{ cm} . \tag{1}$$

Now r_0 is not a constant, but for very different experiments, ranging from α decay to neutron scattering and the maximum energy of the β decay electron in a mirror nuclei transition, one obtains values for r_0 which vary from $r_0 \simeq 1.2$ to $r_0 \simeq 1.5$ [1]. Eq. (1) for R is implied if one assumes that the nucleus is saturated. That is to say, the volume of the nucleus is proportional to A, the number of particles which make up the nucleus. These results were all obtained a long time ago. The fact that Eq. (1) exists and that r_0 does not fluctuate too violently from nucleus, and from experiment to experiment, make the term « nuclear radius » useful.

The recent reawakening of interest in this subject is due to the development of two experiments which are capable of measuring very precisely some

(*) National Science Foundation Postdoctoral Fellow. Now at the University of Illinois, Urbana, Illinois.

(1) J. M. BLATT and V. F. WEISSKOPF: *Theoretical Nuclear Physics* (New York, 1952), pp. 14, 15.

of the parameters which characterize the distribution of positive charge inside the nucleus. These are the electron scattering experiment ([2,3,4]) and the μ mesonic atom experiment ([5]).

The results of these experiments have been quite surprising. They have been interpreted as indicating that the positive charge inside the nucleus is concentrated into a smaller volume than thought previously ([6,7]). At the same time experiments which would be expected to be sensitive to a « nuclear potential » radius continue to give a volume of the nuclear potential much larger than that of the charge distribution ([8,9]).

I will speak in detail of these later, but first let me try to define what one means by the electromagnetic or nuclear force radius. In dealing with the nuclear electric charge distribution the ground on which one stands is fairly firm. Given a charge distribution $\varrho(r)$ a potential is uniquely determined, and the effect of this potential on a μ-meson or a fast electron can be calculated. However an experiment will generally not give $\varrho(r)$ but rather some functionals of $\varrho(r)$ such as the various moments of the charge distribution:

$$\langle r^n \rangle = \int \varrho(\boldsymbol{r}) r^n \, \mathrm{d}\boldsymbol{r} \, . \tag{2}$$

The electron scattering experiments, at the energies at which they have been run so far, give two parameters, while the μ-mesonic atom experiment, to the accuracy to which it has been carried out, gives one parameter which is related to the volume into which the charge is concentrated. For light nuclei both of these experiments provide a measurement of $\langle r^2 \rangle$ of eq. (2) above.

In the case of the nuclear force radius things are not so simple, and this is due of course to the fact that one does not know how to calculate the nuclear forces due to a distribution of nucleons. Thus if we assume a nuclear potential to explain neutron scattering we are not sure if this potential is consistent with, for example, α decay, or, what the nucleon distribution is that produces

---

([2]) E. M. Lyman, A. O. Hanson and M. B. Scott: *Phys. Rev.*, **84**, 626 (1951).

([3]) R. Hofstadter, H. R. Fechter and J. A. Mc Intyre: *Phys. Rev.*, **92**, 978 (1953); R. Hofstadter, B. Hahn, A. W. Knudsen and J. A. Mc Intyre: *Phys. Rev.*, **95**, 512 (1954); B. Hahn, D. G. Ravenhall and R. Hofstadter: *Phys. Rev.*, **101**, 1131 (1956).

([4]) R. W. Pidd, C. L. Hammer and E. C. Raka: *Phys. Rev.*, **92**, 436 (1953).

([5]) V. L. Fitch and J. Rainwater: *Phys. Rev.*, **92**, 789 (1953).

([6]) D. R. Yennie, D. G. Ravenhall and R. N. Wilson: *Phys. Rev.*, **95**, 500 (1954).

([7]) L. N. Cooper and E. M. Henley: *Phys. Rev.*, **92**, 801 (1953).

([8]) *Statistical Aspects of the Nucleus*, Brookhaven National Laboratory, Conference held Jan. 24-26, 1955.

([9]) G. P. Millburn, W. Birnbaum, W. E. Crandall and L. Schecter: *Phys. Rev.*, **95**, 1268 (1954).

this potential. Recently there has been some success in using optical models with five adjustable parameters to describe low energy elastic scattering ([8]).

The electron scattering experiments are consistent with a nuclear charge density almost constant with a small tail (Fig. 1).

For the nuclear mass distribution, no such information is available.

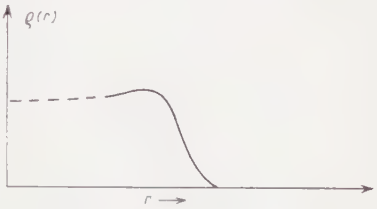

Fig. 1.

Let us use the term « radius » as follows: the electromagnetic radius R_E

$$R_E = r_e A^{\frac{1}{3}} 10^{-13} \text{ cm}, \tag{3}$$

will be the radius of a uniform sphere of nuclear charge. For the nuclear potential radius let us write R_N, where

$$R_N = r_n A_{\frac{1}{3}} 10^{-13} \text{ cm}. \tag{4}$$

In both cases the use of the above defined radii is convenient for comparison of different experiments.

I should now like to discuss some of the experimental results which yield information about the distribution of nuclear matter.

Electric Charge Distribution Measurements.

1. – Electron Scattering Experiments.

The angular distribution of fast electrons scattered from nuclei provides a very sensitive probe of the shape of the nuclear charge distribution, $\varrho(r)$. If the total cross section can also be measured one can find the density of the nuclear charge. Several fast electron experiments have been performed ([2,3,4]).

The work of HOFSTADTER *et al.* at Stanford ([3]) is the most detailed and has been analyzed very carefully by YENNIE, RAVENHALL and WILSON ([6]) and SCHIFF ([10]). There are many difficulties in analyzing this experiment and *I* shall not have the time to go into them here. One of the most interesting however revealed the inadequacy of the Born approximation in giving a reasonable estimate of the correct cross section. If one calculates the angular distribution of scattered electrons from a uniform sphere of positive charge

([10]) L. I. SCHIFF: *Phys. Rev.*, **92**, 988 (1953).

using the Born approximation one gets rather sharp diffraction minima. These are mathematically due to the fact that in the first Born approximation the scattering amplitude is real and must go through zero to change sign. It is at these zero points that one gets the diffraction minima.

Since the angular distributions obtained by the Stanford group did not show marked diffraction minima, it was at first thought that $\varrho(r)$ could not be nearly constant but perhaps was exponential. However the more complete analysis based on a phase shift calculation showed that the Born approximation was incorrect especially in the high Z cases in predicting the sharp minima. The exact calculation gives a complex number for the scattering amplitude which rotates in the complex plane without changing its magnitude violently, even when the sign of the real part of the amplitude changes. Thus the minima were filled in, to a large extent, and it was again possible to make a charge distribution, $\varrho(r) \simeq$ constant, consistent with the experimental results. The best $\varrho(r)$ given by this experiment so far have a shape approximately as shown in Fig. 1, although the experiment is not too sensitive to $\varrho(r)$ near $r = 0$ (the dotted portion of the curve).

For the heavy elements such as gold and bismuth, the electron scattering experiments give a value for r_e of $r_e \cong 1.2$. In the case of the lighter elements, however, there has been some indication recently that r_e might not remain constant. For ${}_{20}Ca^{40}$ HAHN *et al.* [3] report a value of $r_e \cong 1.32$.

2. – The μ-Mesonic Atom.

In this experiment a μ-meson is stopped in condensed material and the atom formed by the meson-nucleus system is studied through the photon emitted when the μ-meson makes transitions between the Bohr orbits. In particular, the $2P_{\frac{1}{2}}$, $2P_{\frac{3}{2}} \to 1S_{\frac{1}{2}}$ transition energies are extremely sensitive to the nuclear charge distribution. FITCH and RAINWATER [5], at Columbia, studied these transitions in elements ranging from aluminum and silicon to lead and bismuth, and found that the measured transition energies were larger than would be expected if the positive charge inside the nucleus occupied as large a volume as was previously believed to be the case (see Table I).

The results of these measurements were analyzed by COOPER and HENLEY [7] and they concluded that among the many effects which could shift the $2P$–$1S$ transition energies of the mesonic atoms, if one did not assume a large anomalous μ-nuclear interaction, only one was sufficient to explain the large transition energies; this was to reduce the value of r_e to approximately $r_e \simeq 1.2$.

Although the mesonic atom results were more accurate for the heavy elements, the transition energies for all the elements measured were consistent with an r_e of 1.2 which was consistent with the results of the electron scattering

experiments being done at approximately the same time. Since then, extensive numerical calculations by HILL and FORD [11] have shown that the charge distributions determined by the two experiments, for the heavy elements, are consistent to within 1%.

TABLE I.

Elements	Z	Calculated $2P_{\frac{3}{2}} \rightarrow 1S_{\frac{1}{2}}$ transition energies in MeV for a uniform charge distribution to $r_0 = 1.3$	Observed $2P_{\frac{3}{2}} \rightarrow 1S_{\frac{1}{2}}$ transition energies in MeV	r_0 required to give transition energy in agreement with the observed transition energies
Titanium	22	0.935	0.955	1.17
Copper	29	1.52	1.55	1.21
Antimony	51	3.41	3.50	1.22
Lead	82	5.48	6.02	1.17

These results lead to the following conclusions. For the heavy elements (lead, gold, bismuth) there is agreement between the two experiments that the positive charge of the nucleus is roughly contained in a sphere of radius $R_E \sim 1.2 \cdot A^{\frac{1}{3}} \cdot 10^{-13}$ cm. For the lighter elements the latest electron scattering results seem to indicate an increasing value for r_e with the average density of positive charge remaining constant, while the μ-meson experiment seems to indicate a value for r_e which remains constant at $r_e \sim 1.2$ down to Titanium ($Z = 22$) with the density of positive charge increasing as Z/A. Since the two experiments have not been performed on the same light elements, the possibility remains that they do not contradict one another, but that r_e begins to vary systematically in the light elements perhaps reflecting shell structure effects. This possibility will be discussed further in connection with the mirror nuclei.

These are the new experiments. It must now be seen whether the density of nuclear charge they seem to indicate is consistent with other measurements which are sensitive to the nuclear charge distribution. I will limit myself now to three other experiments of this type. They are older than the two mentioned above, and are also less accurate.

---

[11] D. L. HILL and K. W. FORD: *Phys. Rev.*, **94**, 1617, 1630 (1954).

3. – The Isotope Shift.

The change of the electron hyperfine structure when measured in an atom with nucleus (A, Z) and in an atom with nucleus $(A+1, Z)$ is called the Isotope Shift. The addition of a neutron to the nucleus (A, Z) dilates this nucleus and would be expected to reduce the nuclear electric potential, and change the hyperfine structure. The observed values of the hyperfine structure shift, however, are approximately one half those calculated on the basis of a constant mass and charge density throughout a sphere of radius $R = 1.5A^{\frac{1}{3}} \cdot 10^{-13}$ cm ([12]).

A possible explanation of this, is to assume a charge distribution which is denser than the mass distribution; in fact to assume $r_0 \simeq 1.2$([12]). However any rigidity in the charge structure which prevented the added neutron from dilating it fully would also explain this effect. Although the magnitude of the isotope shift seems to be a measure of the charge density inside the nucleus, it may just as well be a measure of the rigidity of this distribution.

4. – The Mirror Nuclei.

Mirror nuclei occur only for the lighter elements, $Z \leqslant 21$. The old calculations set the difference in Coulomb energy between the parent and daughter nucleus equal to

$$\Delta E_c = \tfrac{6}{5} Ze^2/R \,. \tag{5}$$

This assumes that it is the decay of a nucleon uniformly distributed over the nuclear sphere which produces the transition from $Z = N \pm 1$ to $Z = N \mp 1$ and that the difference in energy between the parent and daughter nuclei is due only to the Coulomb energy of the extra nucleon. This last statement follows if one assumes charge symmetry of nuclear forces.

When ΔE_c of Eq. (5) is equated to the maximum energy of the emitted electron or positron (with corrections due to the mass of the emitted particles etc.) one finds values of r_0 which fluctuate between 1.37 and 1.5. Cooper and Henley attempted to reanalyze the mirror nuclei data by using, instead of Eq. (5), the following for the change of energy due to the transformation of the i-th nucleon:

$$\Delta E_c = \sum_{j=1}^{Z} \iint \mathrm{d}\boldsymbol{R}_1 \, \mathrm{d}\boldsymbol{R}_2 \frac{e^2}{R_{12}} \Big\{ |\psi_j(\boldsymbol{R}_2)|^2 |\psi_i(\boldsymbol{R}_1)|^2 - \frac{1}{2} \psi_i(\boldsymbol{R}_1)\psi_i^*(\boldsymbol{R}_2)\psi_j^*(\boldsymbol{R}_2)\psi_j(\boldsymbol{R}_1) \Big\} , \tag{6}$$

where $R_{12} = |R_1 - R_2|$.

([12]) M. F. Crawford and A. L. Shawlow: *Phys. Rev.*, **76**, 1311 (1949).

This is the Coulomb energy of the i-th nucleon in the Hartree approximation and includes the exchange as well as the direct interaction. When one evaluates Eq. (6) for a shell structure (square well or harmonic potential) ΔE_i is decreased from the value given by Eq. (5) by the exchange term, and by the fact that in a state of high kinetic energy and angular momentum the probability of the i-th nucleon being at the perifery of the nuclear sphere, where the Coulomb potential is smaller, is increased. These considerations reduced the predicted nuclear radii to values of $r_e \simeq 1.2$ for the cases when the nucleon which makes the transition is just above a closed shell. JANCOVICI [13] making a somewhat more elaborate calculation found that the above considerations, alone, do not reduce r_e to 1.2 in the cases where the extra nucleon just completes a shell. However CARLSON and TALMI [14] by assuming a harmonic oscillator model with j-j coupling to calculate the Coulomb energy differences of mirror pairs find that r_e ranges from 1.2 to 1.35 for Z between 8 and 21.

The situation at present would seem to be the following. The mirror nuclei require an r_e smaller than that given by Eq. (5), but the value of r_e seems to vary from nucleus to nucleus in the region of very light nuclei. It would not be so surprising if r_e should become less constant in this region [3] and it would be very interesting to have evidence from some other source as to this possible variation of r_e. A systematic analysis of $r_{e,}^{2}$ for $A < 40$ could be done with the electron scattering apparatus at Stanford, and would probably be useful in revealing shell structure effects on the charge distribution, as well as revealing further the degree of agreement with the mirror nuclei.

5. – The Fine Structure Splitting in Heavy Elements.

The measurement of the shift of the $2P_{\frac{1}{2}}$ level with respect to the $2P_{\frac{3}{2}}$ level in heavy atoms ($Z \geqslant 80$) provides another measurement of the extension of the nuclear charge. The $2P_{\frac{1}{2}}$ atomic level is sensitive to the nuclear charge distribution because the small component of its wave function remains finite at the origin (Fig. 2).

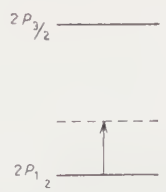

Fig. 2. – Displacement of the $2P^{\frac{1}{2}}$ level due to the finite size of the nucleus.

These level shifts have been analyzed by SCHAWLOW and TOWNES [15] to yield for r_e, $r_e \gtrsim 1.7$. This, of course, is very much larger than the value of r_e given by the

[13] B. G. JANCOVICI: *Phys. Rev.*, **95**, 389 (1954).

[14] B. C. CARLSON and I. TALMI: *Phys. Rev.*, **96**, 436 (1954).

[15] A. L. SHAWLOW and C. H. TOWNES: *Science*, **115**, 284 (1952); A. SHAWLOW and N. M. KROLL: *Phys. Rev.* **100**, 1273 (1955).

first two experiments discussed above just in the region of nuclei where they are most accurate.

There are several directions being taken in order to understand this result. It is possible, first of all, that there are important electrodynamic contributions to the level shift. However because $Z\alpha \sim .6$ for $Z \sim 80$ the usual approximation made in electrodynamic calculations, $Z\alpha \ll 1$, may no longer be valid so that, from calculations that have already been performed, it is not possible to say for certain what these effects will be. This problem is being pursued by WICHMANN and KROLL [16] at Columbia. They have already obtained an expression for the vacuum polarization making no approximation in $Z\alpha$. This yields a correction to the $2P_{\frac{3}{2}} - 2P_{\frac{1}{2}}$ fine structure splitting which has the proper dependence, but unfortunately has the wrong sign. As the effect of vacuum polarization is to *increase* the nuclear electric potential, the inclusion of this effect would require an even larger value for r_e.

However one still has left the « mass operator » correction which has not yet been obtained without the approximation, $Z\alpha \ll 1$. The lowest order term of this correction gives as one of its effects the anomalous magnetic moment of the electron. What the inclusion of this correction (without the $Z\alpha \ll 1$ assumption) would give is still unknown.

There is also work being done to attempt to improve the original calculations of CHRISTY and KELLER [17] of the screening effects of the other electrons. And some machine calculations are being done by KING at Columbia to determine the proper normalization of the $2P_{\frac{1}{2}}$ wave functions near the nucleus [18]. At present however, the results of the fine structure splitting are in disagreement with the other measurements of r_e outlined above.

To conclude the discussion of the electric charge distribution inside the nucleus it is worth mentioning also that recently a redetermination of r_1 as given by the Weizsäcker semi-empirical nuclear mass formula was made using a least squares method by A. E. S. GREEN [19].

He found a value for r_e of $r_e = 1.216$.

Now let us proceed to the experiments which give us an idea of r_n. Here the situation is quite different from that above as one does not know the connection between the nuclear mass distribution and the nuclear potential. Also different approximations are introduced to deal with different kinds of processes and each of these can determine its own radius. There have been a very large number of experiments which in some way or another give an indication of the extension of the nuclear potential. I shall deal with only a

---

[16] E. H. WICHMANN and N. M. KROLL: *Phys. Rev.*, **101**, 843 (1956).
[17] R. F. CHRISTY and J. M. KELLER: *Phys. Rev.*, **61**, 147 (1942).
[18] The Author wishes to thank Professor C. H. TOWNES for telling him of this work.
[19] A. E. S. GREEN: *Phys. Rev.*, **95**, 1006 (1954).

few of these below. What is typical of almost all of these experiments is that they seem to give values of r_n larger than the values of r_e discussed above.

First I shall mention the 90 MeV neutron scattering data which were fitted using an optical model by FERNBACH, SERBER and TAYLOR ([20]). By adjusting such parameters as the well depth, the radius etc. they obtained a fit of the total neutron scattering cross sections for elements from lithium to uranium with an r_n of 1.37.

Some recent low energy scattering data which have been fitted by using an optical model with five adjustable parameters give also values for r_n which are of the order of $r_n = 1.4$. In many cases however the calculations are not sensitive to the choice of r_n. A general discussion of this work can be found in the report of the Brookhaven Conference held in January 1955 ([*]). In all of the optical model analysis there is more uncertainty as to the degree to which the data have necessitated the parameters chosen than in the electromagnetic experiments mentioned above. However in the cases mentioned r_n comes out larger than 1.2 by a considerable amount. A very old measurement of r_n is provided by Gamow's analysis of the lifetimes for α decay. Here what one determines is the distance at which the repulsive Coulomb barrier has overcome the attractive nuclear potential. There are many uncertainties in this calculation such as the radius of the α-particle. However r_n determined in this fashion was always given to be of the order of $r_n \simeq 1.5$. Recently TOLHOEK and BRUSSAARD ([21]) have shown that it is possible to adjust the nuclear parameters in such a manner that r_n becomes $r_n = 1.13$. In particular it has been necessary for them to assume that the depth of the nuclear potential is 16 MeV for the α-particle, instead of 30 MeV. This I think is an indication of the kind of freedom one often has in adjusting the parameters of the nuclear models one chooses. Of course when more data become available the parameters will become delimited. The present status of the α-decay data in the light of the above result, is that the α-decay is not in it self evidence for any particular r_n.

Extensive inelastic scattering cross section measurements have been made recently by MILLBURN *et al.* ([9]). In these the cross section for rather high energy (of the order of 200 MeV) protons, deuterons, and α-particles scattered on nuclei ranging in weight from beryllium to uranium have been measured by attenuation. Such an experiment should certainly give one an idea of what the reaction radius of the nucleus is, and at such high energies one would

---

([20]) S. FERNBACH, R. SERBER and T. B. TAYLOR: *Phys. Rev.*, **75**, 1352 (1949); L. J. COOK, E. M. MCMILLAN, J. M. PETERSON and D. C. SEWELL: *Phys. Rev.*, **75**, 7 (1949).

([21]) H. A. TOLHOEK and P. J. BRUSSAARD: *Physica*, **21**, 449 (1955).

expect that a very small potential due perhaps to the fringe of the nuclear mass distribution would not be so important. Yet the results of this group give for r_n the value $r_n \simeq 1.6$.

The fact that these last measurements give so much larger a value for r_n than the 90 MeV neutron scattering data requires some explanation. HECKROTTE [22] has attempted to do this by employing for the nucleus an optical model with a parabolic potential instead of the usual square well. He finds that with such a potential, when one fits the 90 MeV neutron scattering data the tail extends to $r_n \simeq 1.6$ and thus perhaps can explain the reaction data [9] as being due to interactions of the incident particles with the tail. However it seems strange that the small tail of the potential should give so marked an effect at such high energies. Also the $r_n^{\frac{2}{3}}$ of this potential corresponds to an r_n of about 1.4 and thus is not concentrated enough for the charge distribution. There are other measurements of this type, but perhaps the data mentioned above give a good enough idea of what the situation with regard to r_n is. One would say that though, individually, each of the above determinations might be questioned due to the uncertainty of the analysis, taken together it becomes very difficult to understand why the scattering and particularly the reaction measurements conspire to give such large values of r_n unless it is actually so that the nuclear potential extends to $r_n \simeq 1.4$ and that it is strong enough at its edge to have a sizable effect on particles which approach it (*).

If we accept, tentatively, as the situation that $r_e = 1.2$ and $r_n \simeq 1.4$ (for the heavy elements at least), we can consider how it would be possible to explain this. There are two approaches. The first is to assert that the protons cluster in a smaller sphere than the neutrons (or the charge is more concentrated than the mass). This would make plausible the experimental results outlined above, but then of course one has to explain why, in spite of the Coulomb repulsion, the protons are inside and the neutrons are outside. An attempt to do this has been made by JOHNSON and TELLER [23] who assert that it is just the Coulomb repulsion combined with the possibility for $\beta^{\pm}$ decay which makes the protons occupy a smaller volume than the neutrons. Their argument gives a density of protons larger at the perifery of the proton sphere than at the center, as one would expect on the basis of Coulomb repulsion, but keeps

---

[22] W. HECKROTTE: *Phys. Rev.*, **95**, 1279 (1954).

(*) Recent measurements of neutron absorption cross-sections at 1.4 GeV, by T. COOR, D. A. HILL, W. F. HORNYAK, L. W. SMITH and G. SNOW: *Phys. Rev.*, **98**, 1369 (1955) have been interpreted (R. W. WILLIAMS: *Phys. Rev.*, **98**, 1387 (1955)) as indicating a decrease of r_n to $r_n \cong 1.2$ at this energy. At higher energies, however, r_n seems to increase again. (R. W. WILLIMAS: *Phys. Rev.*, **98**, 1393 (1955)).

[23] M. H. JOHNSON and E. TELLER: *Phys. Rev.*, **93**, 357 (1954).

the proton radius smaller than the neutron radius. Whether or not this argument is correct for the heavy nuclei, it certainly does not apply to the light elements where the number of protons and neutrons are the same.

The other approach is to permit the protons and neutrons to occupy essentially the same volume but to assume that the nuclear potential is strong far beyond the actual distribution of nuclear matter. This does not seem to be the case if one assumes the usual short range Yukawa-like potential, but recently DRELL [24] has tried to show that the nuclear potential might extend beyond the mass distribution if one combines long range central two body potentials with a repulsive core.

It would be of great interest to know whether the nuclear charge and mass distributions coincide. To this end, COOPER and TOBOCMAN [25] recently proposed an experiment which might resolve this question. The experiment is based on the symmetry of the deuteron with respect to the proton and the neutron, and on the fact that stripping and pickup cross sections are proportional to the probability that the stripped off (picked up) particle be at the surface of the residual (target) nucleus.

Using this fact, it is proposed that a comparison of (d, p) and (d, n) reactions could reveal the probability that a neutron or a proton is at the surface of the final nucleus. The possibility of carrying out this experiment is particularly favorable for the light elements where the residual or target nuclei can be made identical. Thus if the nuclear forces are charge symmetric, the only difference between a (d, p) and a (d, n) process leading to the same residual mirror nucleus, if the proton and neutron distributions are identical, should be the Coulomb interaction for which the theory of Tobocman [26] should be able to account (*). For the heavy elements where one cannot have complete symmetry in protons and neutrons, the situation is not so simple. However one can choose cases in which the proton and neutron shells are completed in the respective residual nuclei. An example would be ^{205}Tl(d, n)^{206}Pb and ^{207}Pb(d, p)^{208}Pb.

However even in such a case the captured neutron and proton go into different angular momentum states and so one would have to take into account the differing probabilities that the captured particles be at the surface of the residual nucleus due the angular momentum state into which they are captured.

---

[24] S. DRELL: *Phys. Rev.*, **100**, 97 (1955).

[25] L. N. COOPER and W. TOBOCMAN: *Phys. Rev.*, **97**, 243 (1955).

[26] W. TOBOCMAN: *Phys. Rev.*, **94**, 1655 (1954).

(*) J. M. CALVERT, A. A. JAFFE and E. E. MASLIN: *Phys. Rev.*, **101**, 501 (1956), have charried out such a comparison for several light elements and have found no indication of significant distribution differences.

Hess and Moyer ([27]) have also attempted to employ the symmetry of the deuteron to find ratio of protons to neutrons at the nuclear surface. At high energies they have found that the ratio of (p, d) to (n, d) for various nuclei is much larger than could be explained by the ratio N/Z. Since at high energies one does not have to worry so much about Coulomb effects, if the pickup process is confined to the surface of the nucleus, this would indicate an excess of neutrons on the surface of the heavier nuclei.

([27]) W. N. Hess and B. J. Moyer: *Phys. Rev.*, **96**, 859 (A), (1954) and W. N. Hess: *Thesis*, UCRL-2670 (1954), unpublished.

SUPPLEMENTO AL VOLUME IV, SERIE X
DEL NUOVO CIMENTO

N. 3, 1956
2° Semestre

Théorie des réactions de «stripping».

J. Horowitz

Commissariat à l'Energie Atomique - Centre d'Études de Saclay

1. – Introduction.

Les réactions (d, p) et (d, n) se distinguent de la plupart des autres réactions nucléaires (à basse ou moyenne énergie) par le fait qu'elles ne s'effectuent pas par le processus de formation de noyau composé. Il est bien connu que le neutron et le proton formant le deuton sont très faiblement liés (énergie de liaison = 2.23 MeV) et que leur distance moyenne est grande ($\sim 2.2 \cdot 10^{-13}$ cm), sensiblement supérieure à la portée de leur interaction. Dans ces conditions on conçoit que dans certaines collisions l'un des constituents du deuton, le neutron par exemple, rencontre le noyau cible $\mathcal{N}_1$ et soit capturé pendant que le proton se trouve loin de $\mathcal{N}_1$ et est libéré sans avoir pu avoir une interaction nucléaire appréciable avec $\mathcal{N}_1$. Le neutron est en quelque sorte arraché au proton d'où le nom de « stripping » donné à ce mécanisme. Nous venons de considérer la réaction

$$\mathrm{d} + \mathcal{N}_1 \rightarrow \mathcal{N}_2 + \mathrm{p} \,. \tag{1}$$

La réaction inverse

$$\mathrm{p} + \mathcal{N}_2 \rightarrow \mathcal{N}_1 + \mathrm{d} \tag{2}$$

fait intervenir un mécanisme analogue. Le proton incident peut capter un neutron superficiel du noyau $\mathcal{N}_2$ sans pénétrer dans celui-ci, d'où le nom de « pick-up » donné à ce processus.

Certaines caractéristiques des réactions (dp) et (dn) dépendent fortement de l'énergie du deuton incident. A faible énergie la répulsion coulombienne joue un role essentiel empêchant le proton de s'approcher du noyau cible, de sorte que la réaction (dp) est seule notable. A très grande énergie on ne résout pas en général les différents groupes énergétiques des neutrons et protons. Nous nous intéressons plus particulièrement aux énergies intermédiaires où

l'interprétation des distributions angulaires au moyen de le théorie de Butler (1) constitue une méthode puissante d'investigation des noyaux légers. Rappelons que d'après cette théorie la distribution angulaire du nucléon émergenti dépend de façon caractéristique du moment orbital l du nucléon capturé. Lorsque plusieurs valeurs de l sont possibles leurs contributions sont purement additives et la distribution totale est une superposition des distributions angulaires caractéristiques de chaque valeur de l. Toutes ces distributions ont un pic prononcé vers l'avant, à 0° pour $l=0$, à des angles croissants quand l augmente. Les formes sont suffisamment caractéristiques pour que la comparison avec l'expérience permette, dans de nombreux cas, la détermination des valeurs de l qui ont contribué à la réaction. On en déduit la parité relative des noyaux $\mathcal{N}_1$ et $\mathcal{N}_2$ et éventuellement leur spin.

Nous prendrons comme point de départ de ces considérations théoriques, un théorème très général (2) que nous avons jugé utile d'exposer avec quelques détails.

2. – Un théorème général.

Considérons un système régi par l'Hamiltonien H et qui, à l'énergie E, peut se séparer de plusieurs manières en deux fragments. Désignons par $\alpha, \beta, \gamma, \ldots$ ces voies ouvertes et soit k_α, ϑ_α, M_α les nombres d'onde vitesses et masses réduites correspondantes.

Une réaction initiée dans la voie α est décrite par la fonction d'onde $\Psi_\alpha(\boldsymbol{k}_\alpha)$ vérifiant l'équation $(H - E)\Psi_\alpha = 0$ et présentant les formes asymptotiques suivantes:

$$\text{Voie } \alpha: \qquad \underset{r_\alpha\to\infty}{\Psi_\alpha(\boldsymbol{k}_\alpha)} \simeq \frac{\psi_\alpha}{v_\alpha^{\frac{1}{2}}}\left|\exp[i\boldsymbol{k}_\alpha\boldsymbol{r}_\alpha] + f_\alpha(\boldsymbol{r}_\alpha)\,\frac{\exp[ik_\alpha r_\alpha]}{r_\alpha}\right|,$$

$$\text{Voie } \gamma \neq \alpha: \qquad \underset{r_\gamma\to\infty}{\Psi_\alpha(\boldsymbol{k}_\alpha)} \simeq \frac{\psi_\gamma}{v_\gamma^{\frac{1}{2}}} f_{\alpha\gamma}(\boldsymbol{r}_\gamma)\,\frac{\exp[ik_\gamma r_\gamma]}{r_\gamma}.$$

Les fonctions d'onde normalisées ψ_α, ψ_β, ψ_γ, ... représentent les états internes des fragments et l'orientation de leurs spins.

La section efficace différentielle $\sigma(\boldsymbol{k}_\alpha \to \boldsymbol{k}_\beta)$ est donnée par

$$\sigma(\boldsymbol{k}_\alpha \to \boldsymbol{k}_\beta) = |f_{\alpha\beta}(\boldsymbol{r}_\beta)|^2 .$$

(1) S. T. Butler: *Proc. Roy. Soc.*, A **208**, 559 (1951).

(2) Voir par exemple: A. Messiah: *Cours de Mécanique Quantique* (C.E.N. Saclay), chap. XIV.

A côté des fonctions d'onde Ψ_α nous devrons également considérer des fonctions propres de H qui asymptotiquement décrivent une onde plane dans une seule voie (la voie α par exemple), plus des *ondes convergentes*.

Une telle fonction d'onde $\overline{\Psi}_\alpha(\boldsymbol{k}_\alpha)$ vérifie $(H-E)\overline{\Psi}_\alpha = 0$ et l'on a:

$$\text{Voie } \alpha: \qquad \overline{\Psi}_{\substack{\alpha(\boldsymbol{k}_\alpha) \\ r_\alpha\to\infty}} \simeq \frac{\psi_\alpha}{v_\alpha^{\frac{1}{2}}} \exp[i\boldsymbol{k}_\alpha \boldsymbol{r}_\alpha] + \bar{f}_\alpha(\boldsymbol{r}_\alpha) \frac{\exp[-ik_\alpha r_\alpha]}{r_\alpha}.$$

$$\text{Voie } \gamma \neq \alpha: \qquad \Psi_{\substack{(\boldsymbol{k}_\alpha) \\ r_\gamma\to\infty}} \simeq \frac{\psi_\gamma}{v_\gamma^{\frac{1}{2}}} f_{\alpha\gamma}(\boldsymbol{r}_\gamma) \frac{\exp[-ik_\gamma r_\gamma]}{r_\gamma}.$$

L'existence des fonctions Ψ tient à l'invariance de l'Hamiltonien par renversement du sens du temps: c'est par cette opération, qui change le sens des impulsions et des moments cinétiques que les états stationnaires $\overline{\Psi}$ se déduisent des états Ψ.

On peut être amené à traiter à part certaines interactions V' et à décomposer l'Hamiltonien H en $H = H_0 - V'$. A l'Hamiltonien partiel $H_0 = T + V$ (T est l'énergie cinétique) correspondent des fonctions propres $\Psi^{(0)}$ et $\overline{\Psi}^{(0)}$ analogues aux Ψ et $\overline{\Psi}$ vérifiant l'équation $(H_0 - E)\Psi^{(0)} = (H_0 - E)\overline{\Psi}^0 = 0$.

Les formes asymptotiques sont identiques à celles données ci-dessus sauf que les fonctions f et $\bar{f}$ sont à remplacer par d'autres fonctions $f^{(0)}$ et $\bar{f}^{(0)}$.

Pour calculer la section efficace différentielle $\sigma(\boldsymbol{k}_\gamma, \boldsymbol{k}_\beta)$, donc l'amplitude $f_{\alpha\beta}(\boldsymbol{r}_\beta)$ nous considérons l'élément de matrice

$$I = \langle \overline{\Psi}_\beta^{(0)}, V'\Psi_\alpha \rangle = \langle (H-E)\overline{\Psi}_\beta^{(0)}, \Psi_\alpha \rangle - \langle \overline{\Psi}_\beta^{(0)}, (H-E)\Psi_\alpha \rangle =$$
$$= \langle T\overline{\Psi}_\beta^{(0)}, \Psi_\alpha \rangle - \langle \overline{\Psi}_\beta^{(0)}, T\Psi \rangle .$$

Le théorème de Green permet de transformer les intégrales de volume de l'énergie cinétique en intégrales de surface à l'infini dans les différentse voies, ce qui donne

$$I = -\sum_\gamma \frac{\hbar^2}{2M_\gamma} \lim_{r\gamma\to\infty} \left\langle \int \left[\frac{\partial \overline{\Psi}_\beta^{(0)*}}{\partial r_\gamma} \Psi_\alpha - \overline{\Psi}_\beta^{(0)*} \frac{\partial \Psi_\alpha}{\partial r_\gamma} \right] \mathrm{d}S_\gamma \right\rangle .$$

A cause des comportements asymptotiques de $\Psi_\beta^{(0)}$ et Ψ_α, seules les voies α et β peuvent donner une contribution. Après un calcul simple on trouve

$$\langle \overline{\Psi}_\beta^{(0)}, V'\Psi_\alpha \rangle = -\frac{2\pi\hbar^2}{M_\beta v_\beta} f_{\alpha\beta}(\boldsymbol{k}_\beta) + \frac{2\pi\hbar^2}{M_\alpha v_\alpha} \bar{f}_{\beta\alpha}^{(0)*}(-\boldsymbol{k}_\alpha).$$

Cette relation reste vraie si $V' = 0$; on en déduit:

$$\frac{2\pi\hbar^2}{M_\alpha v_\alpha} \bar{f}_{\beta\alpha}^{(0)*}(-\boldsymbol{K}_\alpha) = \frac{2\pi\hbar^2}{M_\beta v_\beta} f_{\alpha\beta}^{(0)}(\boldsymbol{K}_\beta),$$

d'où

$$f_{\alpha\beta}(\boldsymbol{k}_\beta) = f^{(0)}_{\alpha\beta}(\boldsymbol{k}_\beta) - \frac{M_\beta v_\beta}{2\pi\hbar^2} \langle \overline{\Psi}^{(0)}_\beta, V'\Psi_\alpha \rangle \quad . \tag{3}$$

Le terme $f^{(0)}_{\alpha\beta}(\boldsymbol{k}_\beta)$ n'est différent de zèro que si l'Hamiltonien réduit H_σ permet déjà un passage de la voie α à la voie β.

En écrivant ci-dessus les expressions asymptotiques des fonctions Ψ et $\overline{\Psi}$ nous n'avons pas tenu compte des interactions coulombiennes des deux fragments. En fait le raisonnement est identique si on tient compte de ces interactions; il suffit de remplacer dans les expressions asymptotiques les ondes planes et les ondes convergentes et divergentes par le fonctions coulombiennes correspondantes. On démontre ainsi la relation (3) en toute généralité.

Nous possédons une grande liberté pour le choix de V'. La relation démontrée étant rigoureuse, le résultat ne dépend pas de ce choix. Ceci est vrai tant que nous conservons les expressions exactes des fonctions Ψ et $\overline{\Psi}$. Si on remplace ces fonctions par des expressions approchées, le résultat dépendra à la fois de ces approximations et du choix de V'.

3. – Application aux réactions (d, p) et (d, n).

Considérons par exemple la réaction (d, p)

$$\mathrm{d} + \mathcal{T}_1 \to \mathrm{p} + \mathcal{T}_2 \, .$$

L'état stationnaire de collision créé par le deuton de vecteurs d'onde $\boldsymbol{K}$ tombant sur le noyau $\mathcal{T}_1$ est représenté par la fonction d'onde Ψ qui décrit le deuton incident sur le noyau $\mathcal{T}_1$, sa diffusion élastique et éventuellement inélastique, la réaction (d, p) considérée ainsi que toutes les autres réactions se produisant en même temps. $\Psi^{(0)}$ décrit une onde protonique de vecteur d'onde $\boldsymbol{k}$ tombant sur le noyau $\mathcal{T}_2$, plus des ondes convergentes dans toutes les voies que l'Hamiltonien réduit $H_0 = H - V'$ couple avec la voie (p, $\mathcal{T}_2$). Pour V' nous prenons l'interaction entre le neutron et le proton quand ces deux particules sont à l'extérieur du noyau $\mathcal{T}_1$ (r_n et $r_p > R_0$ où R_0 est le « rayon » de $\mathcal{T}_1$). Dans ces conditions H_0 ne couple pas la voie (d, $\mathcal{T}_1$) à la voie (p, $\mathcal{T}_2$) et l'élément de matrice $\langle \overline{\Psi}^{(0)}, V'\Psi \rangle$ donnera toute l'amplitude de la réaction considérée.

3·1. *Approximations.* – Nous ne connaissons pas exactement la fonction Ψ; en particulier nous ignorons son amplitude dans la voie (p, $\mathcal{T}_2$), amplitude qui fait précisément l'objet de notre calcul.

— Une première approximation consistera donc à négliger la partie de Ψ située dans la voie (p, $\mathcal{T}_2$) et même les parties correspondantes à toutes les les voies autres que (d, $\mathcal{T}_1$). Nous remplacerons ainsi Ψ par la fonction Φ qui ne représente que l'onde incidente et l'onde diffusée élastiquement.

— On remplacera de même $\overline{\Psi}^{(0)}$ par la fonction $\Phi^{(0)}$ qui ne retient de $\overline{\Psi}^{(0)}$ que la partie située dans la voie (p, $\mathcal{T}_2$).

Notations.

$\boldsymbol{r}_n$ et $\boldsymbol{r}_p$=coordonnées du neutron et de proton; $\boldsymbol{R}=(\boldsymbol{r}_n+\boldsymbol{r}_p)/2$, $\boldsymbol{r} \quad \boldsymbol{r}_p - \boldsymbol{r}_n$.

R_0 = rayon du noyau $\mathcal{T}_1$.

$\psi_{j_1}^{\mu_1}$ et $\psi_{j_2}^{\mu_2}$ fonctions d'onde dex noyaux $\mathcal{T}_1$ et $\mathcal{T}_2$. j_1 et j_2 sont leurs spins, μ_1 et μ_2 les composantes du spin sur un axe de quantification. $\chi_{\frac{1}{2}}^{\pi}$, $\chi_{\frac{1}{2}}^{\nu}$, χ_1^{δ} représentent les états des spins du proton, du neutron et de deuton.

Pour $r_n > R_0$ on a:

$$\psi_{j_2}^{\mu_2} = \sum_{\mu,\mu} \beta_j C_{j_1 j}(j_2\mu_2;\ \mu_1,\ \mu) C_{e\frac{1}{2}}(j,\ \mu;\ m,\ \nu)\chi_{\frac{1}{2}}^{\nu} g_e^{m}(\boldsymbol{r})_n \psi_{j_1}^{\mu_1} +$$

$$+ \text{termes orthogonaux à } \Psi j_1 .$$

β_j est l'amplitude de probabilité pour l'apparition du neutron à la surface du noyau avec le moment cinétique total j. A cause de la conservation de la parité, $(-1)^l$ = (parité $\mathcal{T}_1$)$\times$(parité $\mathcal{T}_2$) et à chaque valeur de j correspond une seule valeur de l. La fonction $g_e^{m}(\boldsymbol{r}_n)$ vérifie l'équation $(\Delta - t^2)g = 0$, $t^2\hbar^2/2M$ étant l'énergie de liaison du neutron et M sa masse.

$g_e^m = Y_e^m h_e^{(1)}(itr)$. Nous adoptons les notations de SCHIFF: *Quantum Mechanics* p. 66-79) pour les fonctions de Bessel sphériques j_e et $h_e^{(1)}$.

Si nous admettons que les diffusions (d, $\mathcal{T}_1$) et (p, $\mathcal{T}_2$) ne dépendent pas des orientations des spins des particules nous pouvons écrire (pour r_n et $r_p > R_0$):

$$\Phi^0_{k,\delta,\mu_1} = \chi_1^{\delta}\psi_{j_1}^{\mu_1} S(\boldsymbol{r}_n, \boldsymbol{r}_p) ,$$

$$\overline{\Phi}^0_{k,\pi,\mu_2} = \chi_{\frac{1}{2}}^{\pi}\psi_{j_2}^{\mu_2} g_p(\boldsymbol{r}_p) .$$

en nous limitant à l'état ^3S pour le deuton, c'est-à-dire en négligeant la partie tensorielle de V').

Il nous faut évaluer

$$I_{\pi\mu_2\delta\mu_1} = \langle \Phi_{k,\pi,\mu_2} | V' | \Phi_{\boldsymbol{K},\delta,\mu_1} \rangle .$$

Après quelques calculs simples on trouve que

$$\frac{1}{3(2j_1+1)}\sum_{\mu_1,\delta,\mu_2,\pi}|I_{\pi\mu_2\delta\mu_1}|^2=\frac{3(2j_2+1)}{2}\sum_{j,m}|\beta_j|^2\frac{|F_e^m|^2}{2l+1}. \tag{4}$$

La section efficace différentielle $\sigma(\boldsymbol{K}\to\boldsymbol{k})$ est proportionnelle à cette quantité où

$$F_e^m=\int_{\substack{r_n>R_0\\ r_p>R_0}} g_e^{m*}(\boldsymbol{r}_n)g_p^*(\boldsymbol{r}_p)V'S(\boldsymbol{r}_n,\boldsymbol{r}_p)\,\mathrm{d}^3r_n\,\mathrm{d}^3r_p\,. \tag{5}$$

Nous voyons qu'avec les approximations indiquées ci-dessus les contributions correspondantes aux différentes valeurs de j et de l s'ajoutent de façon incohérente.

Pour simplifier le calcul des F_e^m nous remplacerons l'interaction centrale V' par une interaction de portée nulle. Ceci revient à remplacer la fonction d'onde interne du deuton φ_d par $\varphi_d'=(\gamma/2\pi)^{\frac{1}{2}}(e^{-\gamma r}/r)$ et $V'\varphi_d$ devient égal à $(-4\pi/M)(\gamma/2\pi)^{\frac{1}{2}}\delta(\boldsymbol{r})$.

$\hbar^2\gamma^2/M$ est l'énergie de liaison du deuton.

3·2. *Formule de Butler* ([1,3]). – Une approximation extrême consiste à ne retenir dans Ψ et $\bar{\Psi}^{(0)}$ que les ondes incidentes et à négliger même les forces coulombiennes.

Dans ces conditions on a:

$$g_p(\boldsymbol{r}_p)=\exp[i\boldsymbol{k}\cdot\boldsymbol{r}_p];\qquad S(\boldsymbol{r}_n,\boldsymbol{r}_p)=\varphi'(r)\exp\left[i\boldsymbol{K}\cdot\frac{\boldsymbol{r}_n+\boldsymbol{r}_p}{2}\right],$$

$$\mathcal{F}_e^m=-\frac{4\pi}{M}\left(\frac{\gamma}{2\pi}\right)^{\frac{1}{2}}\int_{r>R_0} g_e^{m*}(\boldsymbol{r})\exp[-i\boldsymbol{q}\cdot\boldsymbol{r}]\,\mathrm{d}^3r\,,$$

avec $\boldsymbol{q}=\boldsymbol{k}-\boldsymbol{K}$.

Si nous prenons la direction du vecteur $\boldsymbol{q}$ comme axe de quantification il vient:

$$\mathcal{F}_e^{m*}=-\frac{4\pi}{M}\left(\frac{\gamma}{2\pi}\right)^{\frac{1}{2}}\delta_{m,0}\frac{1}{q^2+t^2}\int_{r>R_0}\{\exp[i\boldsymbol{q}\cdot\boldsymbol{r}]\,g_e^0-(A\exp[i\boldsymbol{q}\cdot\boldsymbol{r}])g_e^0\}\,\mathrm{d}^3r$$

$$=-\frac{4\pi}{M}\left(\frac{\gamma}{2\pi}\right)^{\frac{1}{2}}\sqrt{4\pi l(l+1)}(-i)^l R_0^2\frac{\partial_{m_0}}{q^2+t^2}\left[h_e^{(1)}(itr)\frac{\partial j_l(qr)}{\partial r}-j_l(qr)\frac{\partial h_e^{(1)}(itr)}{\partial r}\right]_{r=R_0}.$$

([3]) A. B. Batiiia, Kun Huang, R. Huby and H. C. Newns: *Phil. Mag.*, **43**, 485 (1952); P. B. Daitch and J. B. French: *Phys. Rev.*, **87**, 900 (1952).

$\mathcal{F}_e^0$ est le produit de deux facteurs dont le premier

$$\left(\frac{\gamma}{2\pi}\right)^{\frac{1}{2}} \frac{8\pi}{q^2 + t^2} = \left(\frac{\gamma}{2\pi}\right)^{\frac{1}{2}} \frac{4\pi}{\gamma^2 + ((\boldsymbol{K}/2) - \boldsymbol{k})^2} = \int \varphi_d' \exp\left[i \left(\frac{\boldsymbol{K}}{2} - \boldsymbol{k}\right) \cdot \boldsymbol{r} \right] \mathrm{d}^3\boldsymbol{r} \,.$$

représente l'amplitude de probabilité pour trouver dans le deuton incident, le proton avec un vecteur d'onde $\boldsymbol{k}$. Il suffit de remplacer dans l'intégrale ci-dessus φ_d' par φ_d pour obtenir l'expression de $\mathcal{F}_e^0$ dans le cas où on s'affranchit de l'approximation de « portée nulle ». Si par exemple on choisit pour φ_d une fonction du type proposé par Hulten ($\varphi_d = c(e^{-\gamma r} - e^{-\alpha r})/r$) on remplace le facteur

$$\frac{1}{\gamma^2 + ((\boldsymbol{K}/2) - \boldsymbol{k})^2} \quad \text{par} \quad \frac{1}{\gamma^2 + ((\boldsymbol{K}/2) - \boldsymbol{k})^2} \, \frac{1}{\alpha^2 + ((\boldsymbol{K}/2) - \boldsymbol{k})^2} \,,$$

ce qui change très peu les distributions angulaires ($\alpha/\gamma \sim 7$).

Ce premier facteur présente un maximum accentué quand le proton est émis en avant (dans la direction du deuton incident). Le deuxième facteur au contraire est d'autant plus petit en valeur absolue dans la direction en avant que qR_0 est plus petit et l plus élevé.

Le comportement de ces deux facteurs explique l'aspect caractéristique des distributions angulaires qui présentent en général pour $l = 0$ un maximum pour $\vartheta = 0$ et pour $l \neq 0$, un minimum pour $\vartheta = 0$ suivi par un maximum correspondant à des angles ϑ_M d'autant plus grands que l est plus élevé [4].

3·3. *Calculs plus poussés* [5,6]. – Dans la relation (5) écrivons $S(\boldsymbol{r}_n, \boldsymbol{r}_p) = \varphi_d' F(\boldsymbol{R})$. $F(\boldsymbol{R})$ décrit le mouvement du centre de gravité du deuton (si on tient compte des forces coulombiennes on fera comme si le centre de gravité portait la charge).

La relation (5) devient:

$$\mathcal{F}_e^m = -\frac{4\pi}{M} \left(\frac{\gamma}{2\pi}\right)^{\frac{1}{2}} \int_{r > R_0} g_e^{m*}(\boldsymbol{r}) g_p^*(\boldsymbol{r}) F(\boldsymbol{r}) \, \mathrm{d}^3 r \,. \tag{6}$$

L'étude expérimentale de la diffusion élastique (d, $\mathcal{T}_1$) doit permettre de préciser la fonction F. g_p ne représente pas exactement la diffusion élastique (p, $\mathcal{T}_2$) — puisqu'on néglige l'interaction proton-neutron pour $r_n > R_0$ — mais n'en est pas très éloigné.

(4) R. Huby: *Progr. Nucl. Phys.*, **3**, 177 (1953).
(5) J. Horowitz et A. M. L. Messiah: *Journ. Phys. et Rad.*, **14**, 695 (1953).
(6) W. Tobocman: *Phys. Rev.*, **94**, 1655 (1954); R. G. Thomas: *Phys. Rev.*, **100**, 25 (1955).

Différents calculs numériques ([7-9]) ont été effectués en tenant compte des interactions coulombiennes, de la diffusion nucléaire (p, $\mathcal{M}_2$), de la diffusion nucléaire (d, $\mathcal{M}_1$) ou de certains de ces effets seulement. Le plus souvent, quand on est suffisamment au-dessus de la barrière coulombienne, les courbes de distribution angulaire présentent les mêmes pics caractéristiques que celles obtenues par la formule de Butler. Les pics sont seulement moins accentués et déplacés. Les valeurs absolues des sections efficaces sont moins fortes. Dans l'ensemble il n'y a pas de modification quant à l'utilisation des courbes de distribution angulaire pour la spectroscopie nucléaire, c'est-à-dire, pour la détermination des l. Remarquons aussi qu'un léger déplacement des pics peut toujours être obtenu en changeant la valeur de R_0 et que R_0 est dans certaines limites un paramètre ajustable.

3·4. *Valeurs absolues des sections efficaces et largeurs réduites* ([9]). – L'étude des réactions (d, p) et (d, n) devrait permettre d'obtenir sur les niveaux d'autres renseignements que la parité et le spin.

La relation (4) montre que la section efficace est proportionnelle à γ_l^2 c'est-à-dire à la probabilité d'apparition du neutron à la surface du noyau, donc à la largeur réduite. On peut donc essayer de déduire cette largeur réduite de la valeur absolue de la section efficace différentielle. Dans certain cas cette largeur réduite est connue par ailleurs (déduite par exemple de celle du noyau miroir) et on voit que la largeur réduite calculée à partir de la section efficace au moyen de la théorie de Butler est trop petite par un facteur de l'ordre de 2 à 5. Les calculs moins approchés rendent compte de cet écart mais dans l'état actuel la théorie n'est pas assez sure pour permettre une bonne détermination des largeurs réduites à partir des expériences (d, p) et (d, n).

3·5. *Résonances.* – Dans certains cas les niveaux du noyau composé (d – $\mathcal{M}_1$) sont assez distincts dans le domaine d'énergie considéré pour que l'on puisse étudier les variations des distributions angulaires (d, p) et des sections efficaces quand on passe par une résonance. Cette étude devrait permettre de voir comment les contributions dues aux processus de « stripping » et de formation de noyau composé se combinent au voisinage de la résonance. On pourrait penser que la caractéristique essentielle des distributions de stripping, l'existence d'un pic prononcé aux petits angles, devrait s'effacer quand la contributions du mécanisme « noyau composé » devient trop importants. Il n'en est pas nécessairement ainsi. Il faut tenir compte d'une part des termes

([7]) W. Tobocman et M. H. Kalos: *Phys. Rev.*, **97**, 132 (1955).

([8]) J. Yocoz: *Proc. Phys. Soc.* A **67**, 813 (1954).

([9]) R. G. Thomas: *Phys. Rev.*, **91**, 453 (A) (1953); Y. Y. Fujimoto, K. K. Kikuchi et S. S. Yoshida: *Progr. Theor. Phys.*, **11**, 264 (1954); G. Abraham: *Proc. Phys. Soc.* A **67**, 273 (1954).

d'interférences. D'autre part, dans la région externe, là où se produit le stripping, les fonctions d'onde du proton et du deuton sont fortement affectées par la résonance, leurs amplitudes au voisinage du noyau étant augmentées.

Les réacteurs qui se prêtent le mieux à cette étude sont $^{16}O(d, p)^{17}O$ [10] et $^{12}C(d, p)C^{13}$ [11]. Quand on passe par certains résonances la forme de la distribution angulaire se maintient (avec augmentation de la section efficace); dans d'autres cas, la situation est plus compliquée. Aucune analyse théorique approfondie de ces résultats expérimentaux n'a encore été effectuée.

3·6. *Polarisation.* – La théorie de Butler, comme toute approximation de Born en général, prévoit que les protons émis dans la réaction (d, p) ne sont pas polarisés. Il n'en n'en est pas de même dans le cas des approximations moins poussées.

Soit $\boldsymbol{P}$ le vecteur de polarisation du proton (valeur moyenne de l'opérateur de spin $\boldsymbol{\sigma}$). Le plan $(\boldsymbol{k}, \boldsymbol{K})$ étant un plan de symétrie pour le problème, $\boldsymbol{P}$ est perpendiculaire à ce plan. Prenons l'axe de quantification parallèle au vecteur $\boldsymbol{k} \wedge \boldsymbol{K}$, et soient P^+ et P^- les probabilités relatives pour que le spin du proton émergent soit respectivement parallèle et antiparallèle à ce vecteur. La polarisation P est donnée par

$$P \quad \begin{matrix} P^+ & P^- \\ P^- & P^+ \end{matrix} .$$

Pour calculer P dans le cadre des approximations effectuées ci-dessus il suffit de ne pas effectuer la sommation sur π dans la relation (4). On obtient ainsi le résultat:

$$P = \frac{2}{3} \frac{\sum_j \mp (2j+1)^{-1}(2l+1)^{-1} |\beta_j|^2 \{\sum_m m |^m_e | \mathcal{F}^2\}}{\sum_j (2l+1)^{-1} \beta_j^2 \{\sum_m |^m_e | \mathcal{F}^2\}} , \tag{7}$$

où les signes $\mp$ correspondent respectivement aux cas $j = l \pm \frac{1}{2}$.

Remarquons que le produit $g^*_\mu(\boldsymbol{r}_\mu) V' S(\boldsymbol{r}_n, \boldsymbol{r}_p)$ qui intervient dans (5) admet le plan $(\boldsymbol{k}, \boldsymbol{K})$ comme plan de symétrie. Il en résulte que $\mathcal{F}^m_e = 0$ si $l + m$ est impair.

[10] A. Berthelot, R. Cohen, E. Cotton, H. Faraggi, T. Grjebine, A. Leveque, V. Naggiar, M. Roclawski-Conjeaud and D. Szteinsznaider: *Journ. Phys. Rad.*, **16**, 241 (1955).

[11] K. W. Jones, M. T. Mc Ellistrem, R. A. Douglas, D. F. Herring and E. Silverstein: *Bull. Am. Phys. Soc.*, **29**, n. 7, 26 (1954) et thèse Université du Wisconsin (1954); T. W. Bonner, J. T. Eisinger, A. A. Kraus jr. and J. B. Marion: *Phys. Rev.*, **101**, 209 (1956).

D'après la relation (7), P est inférieur en valeur absolue à

$$\frac{1}{3} \quad \text{si} \quad j = l - \frac{1}{2}, \quad \text{à} \quad \frac{1}{3}\frac{l}{l+1} \quad \text{si} \quad j = l + \frac{1}{2}.$$

Des calculs numériques ont été effectués ([12]) en prenant comme point de départ la relation (6) et en ne tenant compte que de la diffusion (p, $\mathcal{T}_2$) assimilée à une diffusion par une sphère impénétrable. Ces calculs ont montré que P était positif (en accord avec une étude semi-classique de NEWNS ([13])) et que la valeur maximum était effectivement atteinte pour certains angles. D'autres calculs [8] ne tenant compte que des interactions coulombiennes ont donné une valeur négative pour P. Il convient de remarquer que nous avons supposé que les diffusion (d, $\mathcal{T}_1$) et (p, $\mathcal{T}_2$) étaient indépendantes des spins des particules. Cette hypothèse simplificatrice qui affecte peu la forme des distributions angulaires, peut être nettement moins justifiée dans le calcul des polarisations. Remarquons en particulier que les limitations de la valeur absolue de P que nous avons indiquées ci-dessus, dépendent de cette simplification.

CHESTON ([14]) dans un calcul relatif à la réaction $^{12}C(d, p)^{13}C$ (pour laquelle des expériences sont en cours), pour $Ed = 3.29$ MeV, a supposé que la diffusion (p, $\mathcal{T}_2$) faisait intervenir un terme spin-orbite. Les valeurs obtenues pour P étaient négatives mais la valeur absolue ne dépassait pas 0.26; les forces coulombiennes étaient négligées dans ce calcul. Ce problème de la polarisation devra être approfondi du point de vue théorique à la lumière des résultats expérimentaux.

([12]) J. HOROWITZ et A. M. L. MESSIAH: *Journ. Phys. et Rad.*, **14**, 731 (1953).
([13]) H. C. NEWNS: *Proc. Phys. Soc.*, A **66**, 477 (1953).
([14]) W. B. CHESTON: *Phys. Rev.*, **96**, 1590 (1954).

SUPPLEMENTO AL VOLUME IV, SERIE X
DEL NUOVO CIMENTO

N. 3, 1956
2° Semestre

On the Description of Collective Motion by the Use of Superfluous Co-ordinates.

H. J. LIPKIN

The Weizmann Institute of Science, Department of Physics - Rehovoth

This seminar summarizes some recent work at the Weizmann Institute (H. J. LIPKIN, A. DE-SHALIT and I. TALMI: *Nuovo Cimento* 2, 773 1955) in which an attempt has been made to understand certain collective aspects of the Bohr unified nuclear model on the basis of an individual particle picture. In particular, a method has been developed for treating quantum-mechanical systems having superfluous degrees of freedom and has been applied to the problem of the center of mass in the shell model and to the study of collective rotational motion.

1. - Superfluous Degrees of Freedom in the Unified Model.

A. BOHR has discussed the possibility of describing collective motions of a system of particles by defining collective co-ordinates as function of the individual particle co-ordinates and making a canonical transformation to a new system including these collective co-ordinates and the individual particle co-ordinates with respect to moving axes. The part of the transformed Hamiltonian depending upon the collective co-ordinates should then describe the rotational and vibrational energy states, while the part of the Hamiltonian depending upon the individual particle or « intrinsic » co-ordinates should describe a shell-structure in a potential which may be deformed.

The new co-ordinates defined in this way cannot be independent since there are too many of them. If the number of intrinsic co-ordinates is reduced to obtain an independent set, the resulting system is difficult to handle; furthermore, the success of the unified model indicates that one can treat the entire set of intrinsic co-ordinates *as if they were independent* and obtain some

correct results. This procedure introduces superfluous degrees of freedom into the problem. It is therefore of interest to examine the general problem of quantum-mechanical systems described with extra degrees of freedom having no physical significance.

2. – The Center of Mass in the Shell Model.

Many of the essential features of collective motion and of systems possessing superfluous degrees of freedom are illustrated very clearly in the problem of the center of mass in the shell model. The motion of the center of mass of a system of particles is that of a collective translation of the whole system; this is the simplest case of collective motion and is very closely analogous in many respect to rotational motion. Since the co-ordinates of individual particles relative to the common center of mass are not all independent, superfluous degrees of freedom are in effect introduced in the usual shell model treatment.

Consider a system of particles subject only to inter-particle forces. The Hamiltonian for the system can be written in the form:

$$H = \sum_i \frac{1}{2M} p_i^2 + V \tag{1}$$

and the following general observations can be made:

1) *Invariance.* The form of the Hamiltonian (1) is invariant with respect to translations of the co-ordinate system.

2) *Conservation law.* The total linear momentum of the system of particles $\sum_i p_i$ commutes with the Hamiltonian (1) and is a constant of the motion.

3) *Specification of Collective Motion.* One way to describe the division of particle motions into collective and intrinsic is to define a co-ordinate system which moves with the particles; in this case a co-ordinate system with its origin at the center of mass of the system. The motion of the particles with respect to the moving axes is then called the intrinsic motion; the motion of the moving co-ordinate system with respect to axes fixed in space is called the collective motion.

4) *Specification of States.* Since the operators of total linear momentum in different directions commute with one another and with the Hamiltonian (1), a complete set of eigenfunctions of (1) can be defined which are also eigenfunctions of the total momentum operator $\sum_i p_i$. These eigenfunction can be written ψ_{Pn} specified by the total linear momentum p_n and the internal quantum numbers n.

5) *Separability.* The motion of the center of mass is separable from the intrinsic motion. The wave function ψ_{Pn} can therefore be written in the form

$$\psi_{Pn} = \Phi_n(q_k) \exp[iPx_i/A\hbar], \tag{2}$$

where the intrinsic co-ordinates q_k are any independent set of the particle co-ordinates relative to the common center of mass. A is the number of particles.

6) *Translation Spectrum.* The energy value corresponding to the wave function (2) is clearly given by

$$E_{Pn} = E_n + P^2/2AM, \tag{3}$$

where E_n is the intrinsic energy dependent only upon the intrinsic part $\Phi_n(q_k)$ of the wave function. Thus for each intrinsic state there exists a continuous « translational spectrum » of energy states corresponding to different values of the total linear momentum P. This translational spectrum is similar in many respects to the rotational spectrum discussed by A. Bohr.

7) *Symmetry of eigenfunctions.* The wave functions (2) are symmetric with respect to translations of the coordinate system, changing only by a phase factor. This is in agreement with the uncertainty principle; since the momentum of the center of mass is known exactly, its position is not known at all, and all values are equally probable. The wave function (2) is not localized in space, but is spread out uniformly.

8) *Destruction of symmetry in shell model.* In the nuclear shell model, the inter-particle potential in (1) is replaced by a central potential fixed in space, and solutions are sought which are self-consistent. The shell model Hamiltonian, however, no longer has the symmetry properties of the original Hamiltonian (1): it is not invariant with respect to translations, and its solutions are localized in space and cannot be exact eigenfunctions of the original Hamiltonian. These solutions might be interpreted as describing only the intrinsic part of the motion of the nucleons; collective motion must somehow be introduced in order to obtain an exact eigenfunction having proper symmetry properties.

Another way of describing the shell model wave functions is to consider them as a wave packet of eigenfunctions of the form (2), corresponding to different values of the total linear momentum P. If these functions give good approximations to energy values, it is reasonable to assume that they contain only a single intrinsic wave function Φ_m. One can then write the shell model

wave function ψ_{sm} in the form

$$\psi_{sm} = \int \psi_{Pm} f(P)\,\mathrm{d}P, \tag{4}$$

where $f(P)$ is some function of P.

3. – A Method for Treating the Center of Mass Problem.

Let us consider for the moment a problem defined by a slightly different Hamiltonian

$$H' = \frac{1}{2M}\sum_i p_i^2 + V - \frac{1}{2AM}(\sum p_i)^2 . \tag{5}$$

Since the Hamiltonian (5) differs from (1) only by a function of $\sum p_i$ the functions (2) are eigenfunctions of (5) as well as of (1). Their energy values E'_{Pn} however are given by

$$E'_{Pn} = E_{Pn} - P^2/2AM = E_n . \tag{6}$$

The eigenvalues of the Hamiltonian (5) are thus independent of the quantum number P, and all wave functions having the same intrinsic part are degenerate. Therefore linear combinations of these functions, such as the shell model wave function (4), are also eigenfunctions of the Hamiltonian (5). The Hamiltonian (5) can therefore be used to define an alternative problem in which a calculation using wave functions localized in space gives the exact result for the original Hamiltonian H. The shell model Hamiltonian is obtained from (5) by changing the potential and by dropping the final term. Since the latter is inversely proportional to the number of particles one can assume that this is justified if A is large.

The operator (5) can be characterized by the fact that it commutes with both the position of the center of mass $\sum x_i/A$ and the momentum $\sum p_i$ and therefore depends only upon intrinsic variables. Similar operators can be constructed corresponding to other dynamic variables and can be used to calculate the expectation values of these variables with shell model wave functions. An example of such a calculation is that for the orbital contribution to the magnetic moment in a nucleus consisting of a single neutron outside closed shells. The shell model gives zero for this contribution, but it is evident that there is a small effect due to the rotation of the positively charged core about the common center of mass. This effect can be calculated by the above method.

4. – Introduction of Superfluous Co-ordinates.

The problem of the center of mass in the shell model can also be treated by introducing superfluous degrees of freedom. The results obtained are very closely analogous to those given above, but the method is formulated in a more general manner and is applicable immediately to other types of collective motion. Let us define the co-ordinate ξ_0 of the center of mass of the system of particles and let ξ_i be the co-ordinate of the i-th particle with respect to the center of mass. A transformation from the coordinates x_i to the coordinates ξ_0, ξ_i is defined as follows

$$x_i = \xi_i + \xi_0 . \tag{7}$$

The intrinsic co-ordinates ξ_i are not independent and satisfy the relation

$$\sum \xi_i = 0 . \tag{7'}$$

If the dependence expressed by equation (7′) is disregarded and the co-ordinates ξ_i are treated as if they were independent, superfluous degrees of freedom are introduced into the system. It is as if the variable $\sum \xi_i$ instead of being identically equal to zero were considered to be an additional dynamical variable. This is equivalent to adding a new variable x_0 having no physical significance to the original co-ordinate system x_i and replacing equation (7′) by

$$x_0 = \sum \xi_i A. \tag{7''}$$

The equations (7), (7″) define an ordinary transformation from the co-ordinates x_i, x_0 to co-ordinates ξ_i, ξ_0. Therefore it is merely necessary to determine the effect of adding the extra co-ordinate x_0 to the original system in order to be able to use the ξ_i, ξ_0 system.

Consider now the x_i, x_0 system, in which wave functions can be written formally in the form $\psi(x_i, x_0)$ even though the co-ordinate x_0 has no physical significance. Operators including x_0 and its canonically conjugate momentum p_0 can also be written. However, *a physical operator* is defined as an operator which contains neither x_0 nor p_0 i.e. it commutes with both x_0 and p_0. It is evident that the eigenfunctions of a physical operator can be written in the form

$$\psi(x_i, x_0) = h_m(x_0)\varphi_n(x_i) , \tag{8}$$

where the functions $h_m(x_0)$ are an arbitrary complete set of orthonormal functions and the functions $\varphi_n(x_i)$ are just the eigenfunctions of the physical operator

in the original problem before the addition of the extra co-ordinate x_0. The eigenvalues of the operator depend only upon the functions φ_n and are completely independent of the form of the functions h_m or of the superfluous quantum number m. It is therefore evident that the addition of the superfluous degrees of freedom does not change the eigenvalues of a physical operator but merely introduces a superfluous degeneracy described by the quantum number m. An infinite set of eigenfunctions of the physical operator can be found which all correspond to the same physical wave function.

It is now possible to introduce the transformation (7) (7′) to the ξ system and to calculate the eigenvalues of the physical operators in the new system. If this is done for the Hamiltonian (5), the transformed Hamiltonian is

$$H'' = \frac{\pi_0^2}{2AM} + \sum_i \pi_i^2/2M + V - (\sum_i \pi_i)^2/2AM \,, \tag{9}$$

where π_0 and π_i are the momenta canonically conjugate to ξ_0 and ξ_i respectively. The first term in (9) is just the energy of the motion of the center of mass, while the remainder has the same form as the Hamiltonian (5) in the previous treatment with Latin letters replaced by Greek. Since the motion of the center of mass is separable the eigenfunctions of (9) can be written

$$\psi = \exp[iP\xi_0/A\hbar]\varphi_n(\xi_i) \,, \tag{10}$$

where the intrinsic function φ_n has the same number of degrees of freedom as the original physical system before the separation of the center of mass motion. The extra degrees of freedom are just those introduced by the superfluous co-ordinate x_0. The functions ψ_n can be expressed in a manner analogous to the eigenfunctions of (5)

$$\psi_n(\xi_i) = \varphi_n(\chi_{\chi k}) \exp[i\beta(\sum \xi_i/A\hbar)] \,, \tag{11}$$

where the χ_k are a set of the ξ_i analogous to the q_k in (2). The energy values, are independent of the superfluous quantum number β and all eigenfunctions for the same n and different β are equivalent to the same state, as is also any linear combination, such as the shell model function. The results obtained by this method are thus equivalent to those obtained by the previously described method.

5. – Subsidiary Conditions.

The method of the introduction of superfluous co-ordinates and the use of physical operators can be used in any problem in the same manner as has been shown for the center of mass. It is often convenient, however, to remove the superfluous degeneracy by imposing a subsidiary condition which must

be satisfied by the wave functions used. One can then use a more general type of operator than the physical operator as defined above.

Let us remove the degeneracy of the set of wave functions given by equation (8) by choosing one single function $h_m(x_0)$ instead of using the complete set. This can be done by requiring that the wave function $\psi(x_i, x_0)$ satisfy a subsidiary condition of the form

$$G(x_0, p_0)\psi(x_i, x_0) = 0 , \tag{12}$$

where $G(x_0, p_0)$ is some convenient operator having a non-degenerate zero eigenvalue. If B is a physical operator, and if B' is another operator satisfying the relation $B'\psi = B\psi$ for all functions ψ satisfying the condition (12), then we say that B' is a semi-physical operator corresponding to the physical operator B and the subsidiary condition (12). The operator $B + G$, for example, is such an operator. The use of superfluous co-ordinates with subsidiary conditions has also been discussed by F. Villars (unpublished) and by S. Tomonaga (*Prog. Theor. Phys.*, **13**, 467 (1955)).

The method of subsidiary conditions can be applied to the center of mass problem to give a semi-physical Hamiltonian operator corresponding to (9) which resembles the shell-model Hamiltonian. Consider the subsidiary condition

$$G(x_0, p_0) = \frac{p_0^2}{2AM} + U(x_0) . \tag{13}$$

By adding the operator (13) to the Hamiltonian (9) one obtains the semi-physical operator

$$H''' = \frac{\pi_0^2}{2AM} + \sum_i \pi_i^2/2M + V + U(\sum_i \xi_i) . \tag{9'}$$

The undesirable term involving $(\sum_i \pi_i)^2$ has thus been eliminated. The question of whether the new potential, $U + V$ can be replaced approximately by a shell-model potential acting only on single particles depends upon the specific form of U and V.

One particular case of interest is the harmonic oscillator potential, obtained by setting $U(x) = \frac{1}{2}AM\omega^2 x_0^2/2 - \frac{3}{2}\hbar\omega/2$. (This corresponds to taking the function $h_m(x_0)$ in equation (8) as the ground state of a three-dimensional harmonic oscillator). Then by virtue of the identity

$$Ax_0^2 = (\sum_i \xi_i)^2/A = \sum_i \xi_i^2 - \sum_{i>j} (\xi_i - \xi_j)^2/A$$

the Hamiltonian (9′) becomes

$$(9'') \qquad H'''' = \frac{\pi_0^2}{2AM} + \sum_i \pi_i^2/2M + \sum_i M\omega^2\xi_i^2/2 + V - \sum_{i>j}(\xi_i - \xi_j)^2 M\omega^2/2A \,.$$

This is just the same form as the shell-model Hamiltonian. There is a central potential, in this case a harmonic oscillator well, acting independently upon each single particle, and the last two terms form a « residual interaction » between the particles. The shell-model wave functions are obtained by dropping the residual interaction terms and finding the eigenfunctions of the resulting Hamiltonian.

6. – The Rotational Problem.

The method of superfluous co-ordinates can be applied to the case of collective rotational motions. In this case one transforms from the system (x_i, x_0) to collective co-ordinates ξ_0 describing the orientation of a set of rotating axes, and intrinsic co-ordinates ξ_i which are the particle co-ordinates with respect to the rotating axes. Using Latin indices to enumerate the particles and Greek indices for vector components in space, the transformation can be written:

$$(14) \qquad x_{i\mu} = a_{\alpha\mu}(\xi_0)\xi_{i\alpha} \,,$$

$$(14') \qquad x_{0\sigma} = x_{0\sigma}(\xi_{i\alpha}) \,,$$

where the matrix $a_{\nu\mu}$ is an orthogonal matrix of determinant unity describing a rotation specified by the collective co-ordinates ξ_0. There is no natural relation for expressing x_0 in terms of the ξ_i analogous to (7″) in the center of mass case. Using the general expression (14) it is possible to obtain a Hamiltonian operator having the form given by A. Bohr:

$$(15) \qquad H = H_{\text{rot}} + H_{\text{int}} + H_{\text{coupl}} \,,$$

where H_{rot} has the form of the rotational energy of a rigid body, with functions of the ξ_i appearing instead of constant moments of inertia; H_{int} is an intrinsic energy depending only upon the intrinsic co-ordinates ξ_i and their canonically conjugate momenta; H_{coupl} depends both on the intrinsic and collective co-ordinates.

Rotational states are given by this Hamiltonian if H_{coupl} can be shown to be zero or small, and if the adiabatic approximation can be used to separate the collective and intrinsic motions. The effective moments of inertia for the rotational motion is then given by the average over the intrinsic part of the

wave function of the expressions appearing in H_{rot}. These expressions, as well as the form of H_{coupl}, depend upon the explicit form of the expression (14′). The problem is then to find the transformation which makes H_{coupl} sufficiently small, and then to calculate the moment of inertia.

A. BOHR has suggested a transformation in which the axes chosen are the principal axes of inertia of the system of particles. This corresponds to taking the three x_0's as the products of inertia of the system:

$$x_{0\sigma} = \sum \xi_{i\alpha}\xi_{i\beta} \,. \tag{14''}$$

For this case the moment of inertia obtained is that obtained by BOHR and by D. R. INGLIS (*Phys. Rev.* **96**, 1059 (1954)) for the case of irrotational flow: namely

$$\mathcal{F} = m\left[\frac{\sum(\xi_{i\alpha}^2 - \xi_{i\beta}^2)}{\sum(\xi_{i\alpha}^2 + \xi_{i\beta}^2)}\right]^2 \sum(\xi_{i\alpha}^2 + \xi_{i\beta}^2) \,. \tag{16}$$

The coupling term, however does not vanish in the general case. The only case found thus far for which H_{coupl} is identically zero is for wave functions of an anisotropic harmonic oscillator with axial symmetry having a closed shell configuration. This case has also been found by BOHR and by INGLIS, and, as has been pointed out is of little physical significance since closed shell nuclei are not deformed.

The problem then remains of finding a more general transformation which will give separation of the variables and which will give a value of the moment of inertia in agreement with observed results.

7. – Extension of the Method.

The same general method of superfluous co-ordinates can also be used for the description of more complicated types of collective motions, such as vibrations.

SUPPLEMENTO AL VOLUME IV, SERIE X
DEL NUOVO CIMENTO

N. 3, 1956
2° Semestre

Coulomb Excitation of Heavy Nuclei.

J. O. NEWTON

Atomic Energy Research Establishment - Harwell (England)

The experiments to be described were done with the aim of checking some of the theoretical predictions about the properties of the rotational states of odd A nuclei. Before considering them we shall discuss very briefly the elementary theory of the Coulomb excitation process [1].

The process of Coulomb excitation corresponds to the excitation of energy levels in a nucleus by means of the electric field of a charged particle moving past it. It is not necessary for the particle to come within the range of nuclear forces and therefore one can excite energy levels in nuclei having large Z with particles having an energy of a few MeV.

Transitions are induced by the time dependent potential

$$V(t) = \sum_{p=1}^{z_2} \frac{z_1 e^2}{|\boldsymbol{r}_1(t) - \boldsymbol{r}_p|^2},$$

where p refers to the protons in the bombarded nucleus, the suffix 1 refers to the bombarding particle and the suffix 2 to the target nucleus. $V(t)$ can be expanded in terms of its multipoles. We shall only consider the electric quadrupole transitions here because they are, with the exception of one electric dipole transition, the only ones observed up to the present time. The electric quadrupole component of $V(t)$ is

$$V_2(t) = \frac{4\pi}{5} z_1 e^2 \sum_{\mu} \sum_{p} \left\{ \frac{r_p^2}{[r_1(t)]^3} Y^*_{2\mu}(\theta_p, \varphi_p) Y_{2\mu}(\theta_1(t), \Phi_1(t)) \right\},$$

$V_2(t)$ can be regarded as a small perturbation hence we have that the pro-

[1] A. BOHR and B. MOTTELSON: *Dan. Mat. Fys. Medd.*, **27**, No. 16 (1953).

bability P for excitation is given by

$$P = \sum_{M_f} \frac{1}{i\hbar} \int_{-\infty}^{+\infty} \langle f | V_2(t) | i \rangle \exp[i\omega t] \mathrm{d}t \Big|^2$$

where i and f are the initial and final states, M_f is the magnetic quantum number of the final state and $\hbar\omega = E_f - E_i = \Delta E$. It is possible to evaluate this expression by assuming that the bombarding particle moves in a classical trajectory. A necessary requirement for this to be a reasonable approximation is that $E_i \gg \Delta E$. The result for the total cross section is

$$\sigma(E_2) = \frac{2\pi^2}{25} \frac{1}{Z_2^2 e^2} \left(\frac{mv}{\hbar}\right)^2 B_e(2) g_2(\xi) ,$$

where $B_e(2)$ is the reduced transition probability for E_2 excitation, $\xi = \Delta E \hbar^{-1} Z_1 Z_2 \sqrt{M_1}$ and $g_2(\xi)$ has been evaluated by numerical integration. A correct quantum mechanical treatment of this problem gives a result differing only slightly from the above for small ΔE [2].

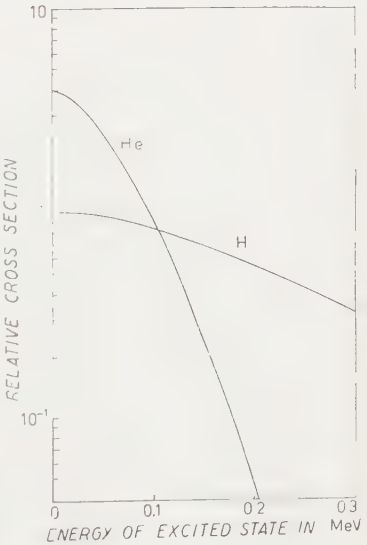

Fig. 1. – Relative cross-sections for excitation of states of various energies by 3 MeV helium and hydrogen ions in a nucleus with $Z = 92$.

ξ is roughly proportional to the time of interaction with the nucleus divided by the nuclear period for the excited state. When $\xi = 0$, $g_2(\xi)$ is approximately unity but as might be expected it falls off exponentially when ξ exceeds the order of unity. For this reason measurable yields are only obtained when ξ is less than about 2.

It is of interest to compare the values of σ ($\xi = 0$) and ξ for protons and helium ions. When $\xi = 0$ we have, for the same bombarding energy, that $\sigma(\mathrm{He}) = 4\sigma(\mathrm{H})$. We also have $\xi(\mathrm{He}) = 4\xi(\mathrm{H})$. In Fig. 1 are shown curves of cross section against ΔE for both protons and helium ions with the same E_i. From this it can be seen that helium ions are best for exciting states with low ΔE and protons for states of higher ΔE. Another factor which must be considered in deciding whether to use protons or helium ions in a particular case is the background radiation. This is in general much more intense from protons than

---

[2] L. C. Biedenharn, M. Goldstein, J. Mc Hale and R. M. Thales: *Phys. Rev.*, **101**, 662 (1956).

from helium ions both in the case of bremsstrahlung radiation and radiation from nuclear reactions.

It should also be noted that $\sigma\ (\xi \to 0)$ decreases as Z_2^{-2} and ξ increases as Z_2. It is therefore less favourable to excite heavy nuclei than light nuclei. A further difficulty in observing the γ-rays from heavy nuclei is due to the fact that the conversion coefficients are very high; in the experiments to be described they varied between 10 and 1000.

Some of the quantities which may be derived from Coulomb excitation experiments are listed below:

1) The energies of the γ-rays from states which have been excited.

2) The position of the energy levels, by comparing the observed excitation functions with the theoretical ones.

3) The quantities $B_e(2)$ from the total cross sections.

4) The spins of the excited states from the angular distributions.

1. – Details of the Experiments.

Five radioactive nuclei were bombarded with singly charged helium ions having energies up to 3 MeV. Targets of the various substances in the form of their oxides and of thickness about 0.4 mg/cm^2 were prepared on nickel backings of thickness $1.25 \cdot 10^{-2}$ cm. The γ-rays were detected in a proportional counter containing xenon at 2.2 atm pressure. Such counters have approximately four times the energy resolution of sodium iodide scintillation detectors for energies of the order of 60 keV.

In addition to the γ-rays from Coulomb excitation, γ-rays from the decay of ^{233}U, ^{237}Np, ^{239}Pu and their daughter products were also observed and had to be subtracted out.

An attempt was made to observe all three γ-rays associated with the excitation of the first two rotational states of the odd A nuclei. This was not successful in the case of ^{237}Np because the target was contaminated with iron and in the case of ^{239}Pu because the energy of one of the γ-rays was only 8 keV.

2. – Results (Analysis not yet Complete).

The γ-rays observed probably correspond to transitions between the states of angular momentum, K, $K+1$, $K+2$ of rotational bands. These are denoted by γ_{20}, γ_{21} and γ_{10} respectively. In Table I are shown the ratios $R = E(\gamma_{21})/(E(\gamma_{10})$ predicted by the first order strong coupling theory for various values of K.

TABLE I.

K	$\frac{1}{2}$	$\frac{3}{2}$	$\frac{5}{2}$	$\frac{7}{2}$
R	irregular	1.40	1.286	1.222

In the dates below I denotes the relative intensities of the various γ-rays, uncorrected for angular distribution, at a bombarding energy of 2.8 MeV; $T_{\frac{1}{2}}$ denotes the half life of the target nucleus. The excitation functions agreed in all cases with those expected theoretically for E_2 excitation of the two rotational states.

$^{238}_{92}$U this is an even-even nucleus and only one γ-ray was observed

$$E(\gamma) = (44.7 \pm 0.2)\ \text{keV}\ .$$

The L and K X-rays of Uranium were also seen.

$^{233}_{92}$U, $T_{\frac{1}{2}} = 1.6 \cdot 10^5$ years, $K = \frac{5}{2}, (\frac{7}{2})$.

TABLE II.

$E(\gamma_i)$	40.5 ± 0.2	52.3 ± 0.6	92.1 ± 1
R	1.00	1.290 ± 0.014	
I	1.00	$(1 \pm .2) \cdot 10^{-1}$	$(6.4 \pm .9) \cdot 10^{-1}$

R agrees well with the value expected for $K = \frac{5}{2}$.

$^{237}_{93}$Np, $T_{\frac{1}{2}} = 2.2 \cdot 10^6$ years, $K = \frac{5}{2}$.

TABLE III.

$E(\gamma_i)$	33.5 ± 0.2	42.9 ± 0.012	(76)
R	1.00	1.280 ± 0.012	—
I	1.00	$(4.5 \pm .5) \cdot 10^{-1}$	$(5.2\ ^{+1.6}_{-2.6}) \cdot 10^{-2}$

R again agrees well with the value expected from the measured spin of $\frac{5}{2}$. These results show that ^{237}Np has two rotational bands based on states with $K = \frac{5}{2}$ - - and $\frac{5}{2}$ —, one state having an excitation energy of 60 keV and decaying by a highly forbidden $E1$ transition to the two lower states. The data for the second band comes from measurements on the α decay of $^{241}_{95}$Am. The level scheme of this nucleus is shown in Fig. 2.

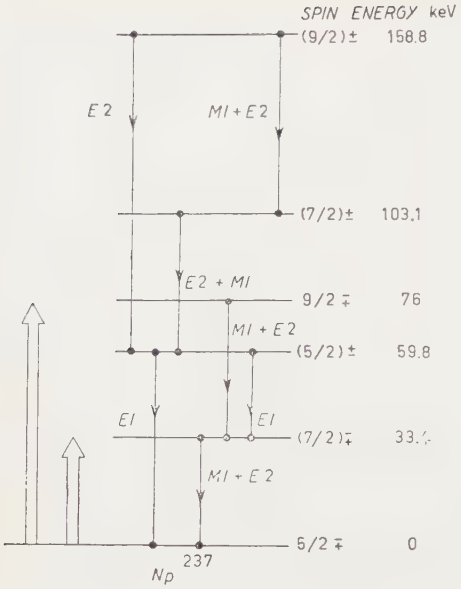

Fig. 2. – Energy levels in ^{237}Np. For references to original data see the review article by NEWTON (*Progress in Nuclear Physics*, **4**, 262 (1955)).

It will be noticed that the moments of inertia J for the two bands are very different, $3\hbar^2/J = 28.7$ keV for the ground state band and 37.2 keV for the other band. The value for the neighbouring even-even nuclei is about 44 keV. Possible reasons for the occurrence of large moments of inertia in the odd A nuclei are given in the lectures of A. Bohr.

$^{239}_{94}$Pu, $T_{\frac{1}{2}} = 2.4 \cdot 10^4$ years, $K = \frac{1}{2}$.

TABLE IV.

$E(\gamma)$	49.6 ± 0.3	57.5 ± 0.3
I	1.00	1.78 ± 0.16

It was not possible to tell from the excitation functions whether (*a*) both γ-rays originate from the same state at 57.5 keV or (*b*) one of them comes from a state at 49.6 keV. The spectrum is irregular as expected for a $K = \frac{1}{2}$ rotational band. We get values of $3\hbar^2/J$ of 37.7 keV and 72.1 keV for the possibilities (*a*) and (*b*) above. The former, which implies levels at $(7.9 \pm .4)$ keV and $(57.5 \pm .3)$ keV, seems the most likely since all odd A nuclei which have been investigated so far have values of $3\hbar^2/J$ smaller than those of the neighbouring even-even nuclei. This conclusion is supported by the fact that the favoured α groups of ^{239}Pu lead to a similar set of levels in ^{235}U (see Fig. 3 and A. BOHR, lectures).

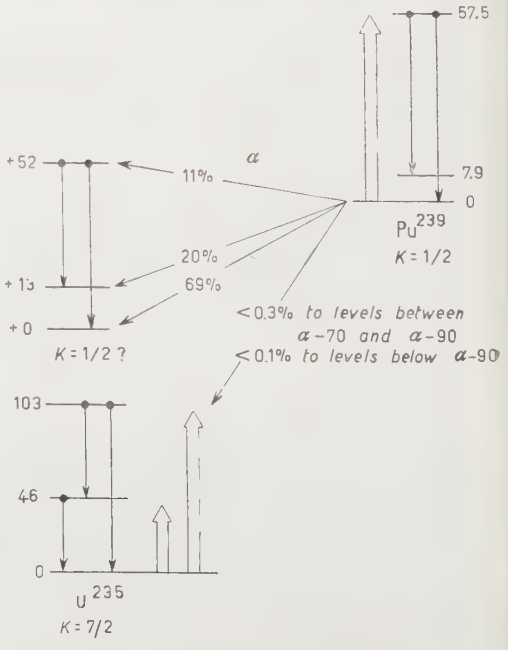

Fig. 3. – Energy levels in ^{239}Pu and ^{235}U. For references to original data see HOLLANDER, PERLNAR and SEABORG: *Rev. Mod. Phys.*, **25**, 469 (1953).

$^{235}_{92}\mathrm{U}$, $T_{\frac{1}{2}} = 7 \cdot 10^8$ years, $K = \frac{7}{2}$.

TABLE V.

$E(\gamma_i)$	46.5 ± 0.2	57.8 ± 0.6	103.8 ± 1.3
R	1.00	1.245 ± 0.015	—
I	1.00	$(6.7 \pm 0.7) \cdot 10^{-2}$	$(1.9 \pm 0.25) \cdot 10^{-2}$

The value of R does not agree too well with that expected for $K = \frac{7}{2}$. The results show that the α decay of ^{239}Pu does not lead to the ground state of ^{235}U but rather to an excited state of $K = \frac{1}{2}$. The absence of information on the decay of the $K = \frac{1}{2}$ state from ^{239}Pu decay suggests either (*a*) that its excitation is less than the L binding energy in U, in which case the decay would not have been observed, or (*b*) that the state has a very long lifetime. The former possibility seems most likely; it will also imply (*b*). In Fig. 3 are shown the level schemes of ^{239}Pu and ^{235}U as given by the α decay and Coulomb excitation data.

In Table VI are shown the values of $3^2\hbar/I$ for the various nuclei investigated.

TABLE VI.

Nucleus	$^{238}_{92}$U	$^{233}_{92}$U	$^{235}_{92}$U	$^{237}_{93}$Np	$^{239}_{95}$Pu
$(3\hbar^2/J)$ keV	44.7	34.6	31.0	28.7	37.7

SUPPLEMENTO AL VOLUME IV, SERIE X
DEL NUOVO CIMENTO

N. 3, 1956
2° Semestre

Les réactions photonucléaires avec émission de neutrons.

C. G. SCHUHL

Commissariat à l'Énergie atomique (France)
Service de Physique nucléaire - C.E.N. de Saclay

1. – Historique.

1·2. – Les premières réactions photonucléaires datent de 1934. Les auteurs, raisonnant par analogie avec l'effet photoélectrique, prévoyaient la possibilité d'éjecter un nucléon à l'extérieur d'un noyau en soumettant les noyaux à un flux de rayonnement gamma d'énergie supérieure à l'énergie de liaison des nucléons dans le noyau.

Du fait que l'on ne possédait, comme source de gamma énergiques, que les sources radioactives naturelles dont la plus énergique est celle de 2.62 MeV de ThC″, les premières réactions étudiées furent : ${}^{2}_{1}\mathrm{H}(\gamma, \mathrm{n}){}^{1}_{1}\mathrm{H}$, Q 2.22 MeV par CHADWICK et GOLDHABER [1] et : ${}^{9}_{4}\mathrm{Be}(\gamma, \mathrm{n}){}^{8}_{4}\mathrm{Be}$, (${}^{8}_{4}\mathrm{Be} \rightarrow 2\alpha$), Q 1.67 MeV par SZILARD et CHALMERS [2] où Q représente le seuil énergétique de la réaction.

1·2. – Le développement des accélérateurs a permis un développement parallèle de l'étude des réactions photonucléaires. En particulier, les gamma de 17.6 MeV et 14.8 MeV de ^{7}Li obtenus par la réaction $^{7}\mathrm{Li}(\mathrm{p}, \gamma)^{8}\mathrm{Be}$ ont permis à BOTHE et GENTNER [3] et à l'équipe de Zürich [4-6], entre 1942 et 1947, d'étudier les réactions photonucléaires sur de nombreux éléments, principalement les

(1) J. CHADWICK et M. GOLDHABER: *Nature*, **134**, 237 (1934).
(2) L. SZILARD et T. A. CHALMERS: *Nature*, **134**, 494 (1934).
(3) W. BOTHE et W. GENTNER: *Zeits. f. Phys.*, **106**, 236 (1937).
(4) O. HUBER, O. LIENHARD, P. SCHERRER et H. WAFFLER: *Helv. Phys. Acta*, **16**, 33 (1943).
(5) O. HUBER, O. LIENHARD, P. SCHERRER et H. WAFFLER: *Helv. Phys. Acta*, **17**, 195 (1944).
(6) O. HIRZEL et H. WAFFLER: *Helv. Phys. Acta*, **20**, 372 (1947).

réactions (γ, n) et (γ, p). Ils ont recherché les réactions (γ, n) et (γ, p) qu'ils pouvaient observer dans les éléments connus. Ils mesuraient le rendement des réactions photonucléaires par rapport au rendement de la réaction $^{63}Cu(\gamma, n)^{62}Cu$ qu'ils prenaient égal à 100.

Le résultat le plus important qui ressort de leur étude est que le rapport expérimental des sections efficaces des réactions (γ, p) et (γ, n): $\sigma(\gamma, p)/\sigma(\gamma, n)$ est beaucoup plus grand (100 à 1 000 fois) que le rapport théorique.

1·3. – D'autres auteurs, dont TITTERTON [7], CHASTEL [8], WILKINS et GOWARD [9] ont étudié en détails les réactions $^{12}C(\gamma, 3\alpha)$ et $^{16}O(\gamma, 4\alpha)$. Leurs résultats sont intéressants pour comprendre les noyaux formés d'un nombre entier de particules α $(Z = N = 2n)$.

1·4. – La mise au point du bêtatron, d'abord par KERST (General Electric Company) puis par WIDEROE (Brown Boveri) a permis une étude plus approfondie des réactions (γ, n) car si, d'une part, nous avons l'inconvénient d'avoir un spectre continu, nous avons, d'autre part, la possibilité de faire varier l'énergie maximum du bêtatron.

2. Les caractéristiques du spectre d'un bêtatron (bremsstrahlung).

Durant toute la période d'accélération, les électrons demeurent sur une orbite d'équilibre qu'ils parcourent environ un million de fois. Ces électrons peuvent être utilisés de deux façons différentes: directement ou bien indirectement par leur spectre de freinage (bremsstrahlung) dans un élément lourd. Dans les deux cas, l'extraction des électrons s'effectue en rompant très rapidement les conditions magnétiques de stabilité sur l'orbite d'équilibre (Fig. 1). Dans la majorité des cas, les électrons frappent une cible de tungstène (W) ou de platine (Pt) pour donner un spectre de freinage. Les caractéristiques principales des deux types de bêtatron sont résumées dans le Tableau I.

TABLEAU I.

Type du bêtatron	Energie max variable entre	Durée de l'impulsion de rayons X	Fréquence de répétition
ALLIS-CHALMERS	2 et 24 MeV	1 à 5 μs	180 Hz
BROWN BOVERI	2 et 35 MeV	1 à 10 μs	50 Hz

(7) E. W. TITTERTON: *Progress in Nuclear Physics* **4**, 1 (1955).
(8) R. CHASTEL: *Thèse* (Paris, 1952).
(9) F. K. GOWARD et J. J. WILKINS: *Proc. Phys. Soc.*, A **64**, 313 (1951).

Une première difficulté consiste à obtenir une énergie maximum bien stabilisée. KATZ, à l'Université de Saskatchewan (Canada) et GOLDEMBERG et SANTOS à São Paulo (Brésil) estiment avoir une stabilité en énergie de ± 5 keV. A Villejuif, BASILE et moi-même obtenons ± 15 keV.

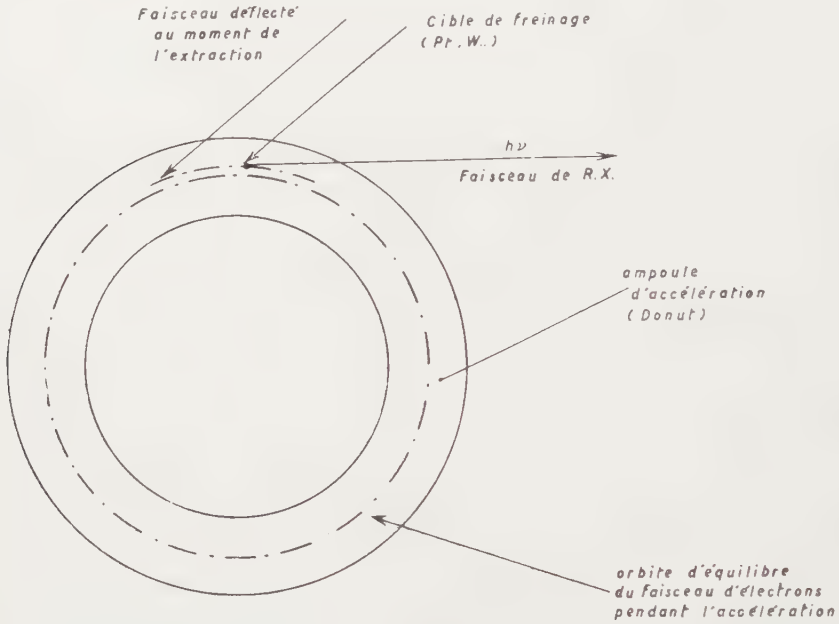
Faisceau deflecté au moment de l'extraction
Cible de freinage (Pt, W..)
hν
Faisceau de R.X.
ampoule d'accélération (Donut)
orbite d'équilibre du faisceau d'électrons pendant l'accélération

Fig. 1. – Schéma de principe du bêtatron.

Nous supposerons dans nos raisonnements que l'énergie maximum des électrons est parfaitement constante.

La forme du spectre de freinage a été calculée par HEITLER dans le cas d'une cible mince; puis par L. I. SCHIFF dans le cas d'une cible épaisse en utilisant l'approximation de Born, c'est-à-dire en supposant que la vitesse des électrons est grande après le freinage de l'électron par le champ électromagnétique du noyau. La Fig. 2 représente la forme du spectre de freinage. En ordonnées: le spectre énergétique, c'est-à-dire le nombre N de gamma d'énergie comprise entre $h\nu$ et $h\nu + \Delta h\nu$ multiplié par

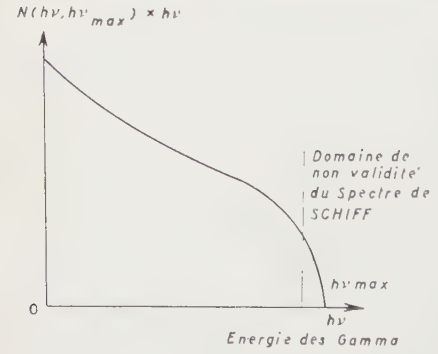

Fig. 2. – Spectre du freinage sur cibles épaisses (L. I. SCHIFF): spectre énergétique.

l'énergie de ces gamma, c'est-à-dire Nhv. En abscisses, l'énergie hv de ces gamma. Il ressort de la méthode de calcul que la portion de la courbe située vers l'énergie maximum n'est pas valable.

3. – Les méthodes utilisées dans l'étude des reactions (γ, n).

3·1. *La méthode par activation.* – Lorsque le noyau final résultant de la réaction photonucléaire est radioactif, il est possible de mesurer le rendement de la réaction à partir de sa radioactivité.

Nous appelons *activation*, la mesure de l'activité de l'isotope formé dans la réaction (γ, n) (par exemple), cette activité étant obtenue avec des cibles reproductibles irradiées à saturation et à intensité du bêtatron constante.

Cette méthode offre l'intérêt d'être simple puisqu'elle ne nécessite comme matériel expérimental que des compteurs Geiger. Dans certains cas, en particulier pour l'étude des réactions de sections efficaces faibles, elle est combinée avec les techniques de séparation chimique. Ainsi, M. DE LABOULAYE et Mlle BEYDON [10], à Saclay, ont étudié la réaction $^{109}Ag(\gamma, \alpha)^{105}Rh$ de cette manière.

C'est la méthode d'activation que BASILE et moi-même avons utilisée et nous verrons plus loin comment il est possible d'interpréter les résultats obtenus.

3·2. *Les émulsions nucléaires* sont utiles pour l'étude des réactions au cours desquelles sont émises des particules chargées. Par exemple les réactions (γ, p), (γ, α) .... C'est par ce procédé qu'ont été étudiées les réactions $^{12}C(\gamma, 3\alpha)$ et $^{16}O(\gamma, 4\alpha)$.

3·3. *La détection directe des neutrons par compteurs à* BF_3 (Fig. 3). – Le faisceau de gamma frappe la cible qui, par réaction (γ, n), émet des neutrons d'énergie pouvant atteindre 15 MeV. Ces neutrons sont ralentis dans de la paraffine et comptés par un ensemble de compteurs à fluorure de bore.

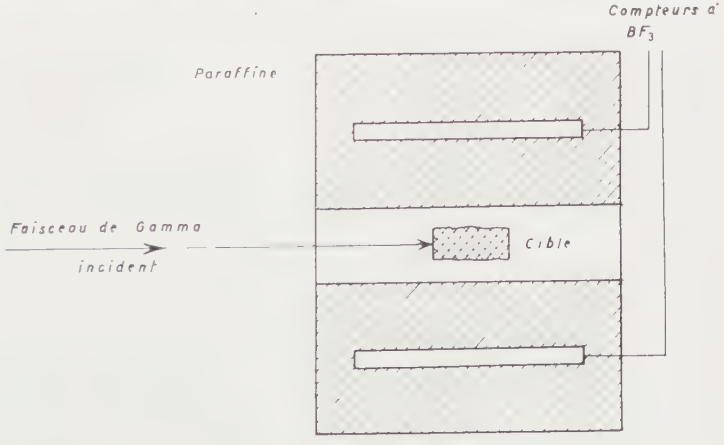

Fig. 3. – Principe de la détection directe des neutrons.

[10] H. DE LABOULAYE et J. BEYDON : *Compt. Rend. Acad. Sci.*, **239**, 411 (1954).

Cette technique permet d'améliorer les statistiques des comptages car il est possible alors d'irradier la cible plus longtemps, quelle que soit la période de l'élément final; elle permet également d'étudier des noyaux qui, par réaction (γ, n), ne donnent pas naissance à un radioélément. C'est le cas de la réaction $^9Be(\gamma, n)2^4He$. Elle offre, par contre, l'inconvénient de ne pas discriminer les différents isotopes d'un élément. Ainsi, dans le cas de l'oxygène, cette technique nous permettra-t-elle de mesurer la somme des sections efficaces des réactions (γ, n) sur les oxygènes 16, 17 et 18.

3'4. *La détection directe des neutrons par cristaux à scintillations.* – A Saclay, M. Tzara utilise, dans l'étude de la photodésintégration du deutérium, des cristaux formés de sulfure de zinc noyés dans du plexiglass (lucite).

4. – Les premiers résultats expérimentaux obtenus avec un bêtatron.

Nous ne parlerons ici que de la méthode par activation. Le résultat directement obtenu par l'expérimentateur est la courbe représentant la variation de l'activation en fonction de l'énergie maximum du bêtatron ou *courbe d'activation* (Fig. 4).

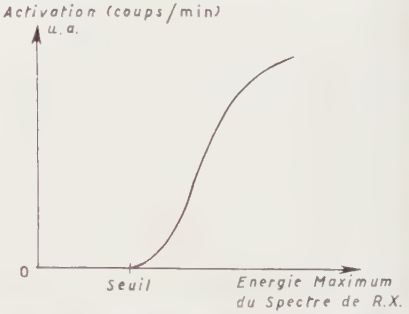

Fig. 4. Courbe d'activation type.

Or, à chaque point, nous mesurons une grandeur qui dépend de la forme de section efficace de la réaction et de la forme du spectre de freinage. L'activité est proportionnelle à

$$\mathcal{A} \propto \int_0^{h\nu_m} N(h\nu, h\nu_m)\ \sigma(h\nu)\, \mathrm{d}(h\nu)\ ,$$

c'est-à-dire à l'intégrale du produit du spectre de freinage par la section efficace (Fig. 5).

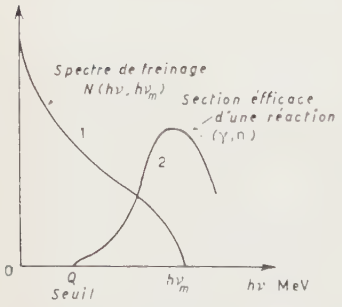

Fig. 5. La courbe d'activation est l'intégrale de la courbe produit de 1 et 2 en fonction de $h\nu_m$.

Katz et Cameron [11] à l'Université de Saskatchewan ont mis au point une méthode de calcul de la section efficace $\sigma(h\nu)$ à partir de la courbe d'activation (« Photon Difference Method »). Cette méthode suppose que la variation de σ et de ses deux premières dérivées est

[11] L. Katz et A. G. W. Cameron: *Can. Journ. Phys.*, **29**, 518 (1951).

« douce ». Par cette méthode, on obtient, pour les courbes de sections efficaces, des courbes très typiques telles que celles de la Fig. 6.

La section efficace de réaction (γ, n), calculée par la méthode de différence photonique, présente un pic assez large dont les caractéristiques sont les suivantes:

Energie du maximum de section efficace: $E_m \propto A^{-\frac{1}{3}}$ (où A est le nombre de masse des noyaux) pour $A \geqslant 40$ et à peu près constante pour $A \leqslant 40$.

Section efficace au maximum: $\sigma_m \simeq 0.1$ barn.

Largeur du pic à mi-hauteur: $\Gamma = 5$ MeV sauf pour les noyaux correspondant à des couches saturées.

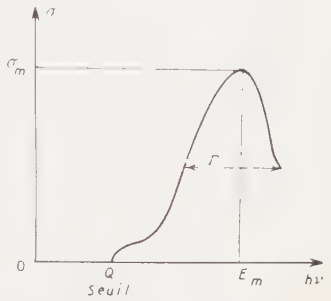

Fig. 6. – Courbe de section efficace calculée par la « photon difference method ».

Section efficace intégrée: $\sigma_{\text{int}} = \int_{n}^{24\ \text{MeV}} \sigma(h\nu)\,\mathrm{d}(h\nu) \simeq 0.02A$ MeV barn.

5. Les interprétations théoriques des premières réactions photonucléaires.

5·1. Goldhaber et Teller [12]. Ils admettent que le photon est absorbé par effet dipolaire électrique et ils examinent divers modèles classiques. En particulier, ils supposent que l'ensemble des neutrons oscille par rapport à l'ensemble des photons comme le font les atomes dans le cas des cristaux. Ils obtiennent ainsi pour E_m et σ_{int} les valeurs suivantes:

$$E_m = 40A^{-\frac{1}{6}}\ \text{MeV}\,,$$

$$\sigma_{\text{int}} = 0.015A\ \text{MeV barn}\,.$$

5·2. Steinwedel et Jensen [13] étudient un modèle fluide. Les neutrons et les protons forment deux fluides incompressibles de telle sorte que la densité en tout point soit constante ($\varrho_n + \varrho_p = \varrho_0 = \text{constante}$). Ils obtiennent:

$$E_m = 60A^{-\frac{1}{3}}\ \text{MeV}\,,$$

$$\sigma_{\text{int}} = 0.065A\ \text{MeV barn}\,.$$

---

[12] M. Goldhaber et E. Teller: *Phys. Rev.*, **74**, 1046 (1948).
[13] H. Steinwedel et J. H. D. Jensen: *Zeits. f. Naturfor.*, 5a, 413 (1950).

5·3. Levinger et Bethe [11]. Dans l'absorption dipolaire électrique des ondes électromagnétiques par un oscillateur classique simple, l'intégration sur la courbe de résonance fournit un résultat qui dépend de la charge et de la masse de l'oscillateur et non de la nature de cet oscillateur. Ce résultat pour l'absorption intégrée de l'énergie électromagnétique s'obtient en mécanique quantique (comme en physique atomique) en utilisant la règle des sommes de Thomas-Reiche-Kuhn pour l'absorption dipolaire électrique des photons par Z électrons dans un atome. Dans le cas des noyaux, nous obtenons:

$$\sigma_{\text{int}} = 0.06 \frac{NZ}{A} (1 + 0.8x) \text{ MeV barn},$$

où x est la fraction d'échange des forces nucléaires.

Ces trois théories sont relatives à l'absorption *totale* des photons, c'est-à-dire à la somme des sections efficaces de toutes les réactions énergétiquement possibles, par exemple: (γ, n), (γ, p), (γ, α), (γ, γ), (γ, γ') ..., mais elles n'expliquent pas pourquoi le rapport des sections efficaces (γ, p) et (γ, n): $\sigma(\gamma, p)/\sigma(\gamma, n)$ théorique est beaucoup plus faible que le rapport expérimental.

5·4. Courant [15] a émis l'hypothèse d'une intéraction directe des gamma sur les nucléons individuels. Un tel effet serait semblable à l'effet photoélectrique. Il favorise les réactions (γ, p) par rapport aux réactions (γ, n). Il résout en partie la difficulté présentée par les résultats des physiciens de Zürich.

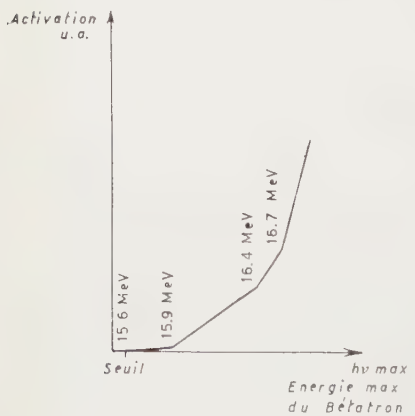

Fig. 7. – Courbe d'activation de la réaction $^{16}O(\gamma, n)^{15}O$ [Katz *et. al.*: *Phys. Rev.*, **95**, 464, 471 (1954)].

6. – La structure fine dans les réactions (γ, n).

Lors d'un examen attentif des réactions $^{12}C(\gamma, n)^{11}C$ et $^{16}O(\gamma, n)^{15}O$, les physiciens canadiens du Saskatchewan ont observé que les courbes d'activation présentaient des discontinuités de pente (ou cassures) (Fig. 7). La portion de la courbe d'activation entre deux discontinuités de pente a sa concavité vers le bas. Les auteurs supposent que les photons peuvent

[14] J. S. Levinger et H. A. Bethe: *Phys. Rev.*, **78**, 115 (1950).
[15] E. D. Courant: *Phys. Rev.*, **82**, 703 (1951).

être absorbés par résonances étroites correspondant à des niveaux d'excitation du noyau initial. La forme de la courbe d'activation s'interprète alors comme provenant de la forme de la courbe de freinage. Ces auteurs ont étudié la structure fine des réactions sur ^{7}Li, ^{12}C, ^{16}O, ^{19}F, mais ils n'ont publié aucune courbe correspondant à des noyaux de masses plus élevées. Il nous a semblé normal d'éclaircir si un phénomène se généralisait aux noyaux plus lourds. Nous avons repris l'étude de l'oxygène déjà faite par KATZ *et al.* Le Tableau II représente la comparaison de nos résultats avec ceux des autres laboratoires.

TABLEAU II. – *Discontinuités dans la courbe d'activation de la réaction* $^{16}O(\gamma, n)^{15}O$.

Auteurs	Seuil (MeV)	Energie des cassures (MeV)				
HASLAM ([15bis])	15.60	15.84	16.56	16.72	16.96	—
KATZ ([16])	15.60	15.9	16.4	16.7	16.9	17.1
BASILE-SCHUHL ([18]) . .	15.60	16.00	16.52	16.7	16.82	17.08
	± 0.03	± 0.06	± 0.06	± 0.1	± 0.08	± 0.05

Nous avons ensuite étudié le cas du phosphore ([18,19]) et celui du chlore ([20]), ce dernier élément correspondant déjà à un élément moyen.

6·1. *Cas du phosphore.* – Il se prête particulièrement bien à une telle expérience: la période de ^{30}P est courte (2.55 min) et il possède un seul isotope stable. Enfin, nous nous sommes arrêtés à l'étude de cet élément car, dans une systématique des réactions (γ, n), SHER, HALPERN et MANN obtiennent, pour son activation: $A = \text{const.}\ (h\nu_m - h\nu_0)^{\alpha}$ où A est l'activation, $h\nu_m$ l'énergie maximum du spectre de freinage, $h\nu_0$ le seuil de la réaction (γ, n) et α un nombre variant d'un noyau à l'autre entre 0.7 et 3.1 et qu'ils évaluent à 3.1 dans le cas du phosphore.

Or, dans nos études des réactions (γ, n) sur des éléments moyens et lourds, nous obtenions systématiquement $\alpha \simeq 2$. Cette forme moyenne de la courbe d'activation nous a servi pour un étalonnage en énergie du bêtatron.

([15bis]) R. N. H. HASLAM, L. KATZ, R. J. HORSLEY, A. G. W. CAMERON et R. MONTALBETTI: *Phys. Rev.*, **87**, 196 (1952).

([16]) L. KATZ, R. N. H. HASLAM, R. J. HORSLEY, A. G. W. CAMERON et R. MONTALBETTI: *Phys. Rev.*, **95**, 464 (1954).

([17]) J. GOLDEMBERG et L. KATZ: *Phys. Rev.*, **95**, 471 (1954).

([18]) R. BASILE et C. G. SCHUHL: *Compt. Rend. Acad. Sci.*, **240**, 2399 (1955).

([19]) C. G. SCHUHL et R. BASILE: *Compt. Rend. Acad. Sci.*, **240**, 2512 (1955).

([20]) R. BASILE, C. G. SCHUHL et W. SEBAOUN: *Compt. Rend. Acad. Sci.*, **241**, 387 (1955).

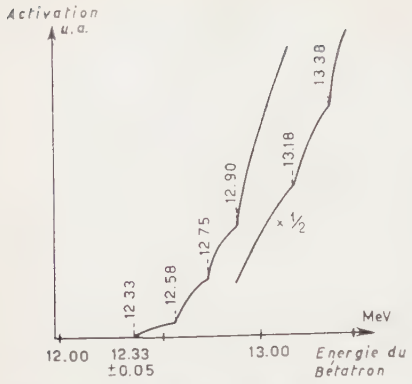

Fig. 8. - Courbe d'activation de la réaction $^{31}P(\gamma, n)^{30}P$.

La Fig. 8 représente la courbe d'activation de la réaction $^{31}P(\gamma, n)^{30}P$. Si nous traçons la courbe de la racine carrée de l'activation en fonction de l'énergie, nous avons une droite correspondant par conséquent à $\alpha = 2$. Nous retrouvons donc le résultat obtenu pour ^{63}Cu, ^{54}Fe, ^{107}Ag, ^{109}Ag. Ceci nous incite à penser que s'il est plus délicat d'observer des « cassures » lors de l'étude des noyaux lourds, car elles deviennent de plus en plus serrées, elles n'en doivent pas moins exister. D'où un effet moyen qui aboutit dans tous les cas examinés à un phénomène identique.

Le seuil obtenu (12.33 ± 0.05) MeV concorde avec les résultats expérimentaux antérieurs mais diffère notablement de la valeur calculée à partir des masses de BAINBRIDGE ([21]). Le Tableau III résume ces résultats.

TABLEAU III.

Auteurs	SHER ([22])	MC ELHINNEY ([23])	FEATHER ([24])	Masse de BAINBRIDGE ([21])	BASILE et SCHUHL ([18])
Seuils (MeV)	12.5 ± 0.2	2.35 ± 0.20	12.10 ± 0.20	12.60 ± 0.13	12.33 ± 0.05

La mesure du seuil de la réaction $^{31}P(\gamma, n)^{30}P$ permet d'améliorer notre connaissance de la mesure de la masse de ^{30}P et de calculer l'énergie maximum du spectre β^+ de ^{30}P. Nous obtenons:

Masse de ^{30}P: $(29.987\,882 \pm 0.000\,095)$ UMA .

Energie maximum du spectre β^+ de ^{30}P: (3.23 ± 0.12) MeV .

Cette valeur est en bon accord avec la valeur de (3.24 ± 0.06) MeV de GREEN et RICHARDSON ([25]) obtenue an spectromètre magnétique.

Notons, toutefois, que certaines des cassures pourraient être interprétées

([21]) K. T. BAINBRIDGE: *Experimental Nuclear Physics*, E. Segrè éd., (New York, 1953).

([22]) R. SHER, J. HALPERN et A. K. MANN: *Phys. Rev.*, **84**, 387 (1951).

([23]) J. MC ELHINNEY, A. D. HANSON et R. B. DUFFIELD: *Phys. Rev.*, A **74**, 1257 (1948).

([24]) N. FEATHER: *Advances in Physics* (1953), p. 2.

([25]) D. GREEN et R. J. RICHARDSON: *Phys. Rev.*, **96**, 858 (1954).

comme étant dues aux niveaux d'excitation du noyau résiduel. La possibilité de laisser le noyau final dans un état excité correspond à une voie nouvelle de décomposition pour le noyau composé. S'il se forme lors des réactions photonucléaires, le mode de désintégration $^{31}P(\gamma, n')^{30}P^*$ peut se produire au détriment du processus $^{31}P(\gamma, p)^{30}Si$ dont le seuil est plus bas que celui de $^{31}P(\gamma, n)^{30}P$. Ainsi la cassure de (13.18 ± 0.10) MeV située à (0.85 ± 0.05) MeV du seuil de la réaction pourrait correspondre soit à un état d'excitation de 13.2 MeV de ^{31}P, soit à l'état d'excitation de 0.8 MeV de ^{30}P. Les études expérimentales ne permettent pas de lever le doute actuellement dans ce cas.

6·2. *Cas du chlore.* – Nous avons étudié la réaction $^{35}Cl(\gamma, n)^{34}Cl^*$ où $^{34}Cl^*$ est laissé dans un état d'excitation métastable de (32.40 ± 0.04) min de période. Nous obtenons également dans ce cas des cassures situées à 13.13, 13.51, 13.72, 13.89 et 14.10 MeV.

Comme dans le cas du phosphore, la valeur du seuil obtenue (12.79 ± 0.07) MeV nous permet de calculer le bilan énergétique de la réaction $^{35}Cl(\gamma, n)^{34}Cl$ (où ^{34}Cl est dans l'état fondamental) puis la masse de ^{34}Cl et l'énergie maximum β^+ de ^{34}Cl.

Masse de ^{34}Cl: $(33.984\,781 \pm 0.000\,133)$ UMA .

Energie maximum β^+ de ^{34}Cl: (4.57 ± 0.16) MeV .

Nous sommes actuellement en train de poursuivre nos études avec des noyaux plus lourds.

7. – Conclusions.

Jusqu'à ces dernières années, bien peu d'expérimentateurs et de théoriciens s'intéressaient aux réactions photonucléaires du fait de la difficulté d'interprétation des résultats connus. Il semble que la mise en évidence des cassures soit d'un très grand intérêt car c'est à l'heure actuelle un des seuls moyens de montrer des niveaux d'excitation de 15 MeV environ. Il reste encore à vérifier le sens physique de ces cassures. C. Tzara, à Saclay, réalise une expérience sur le graphite pour vérifier que les cassures correspondent bien à des niveaux d'absorption du noyau initial [26]. Il est toutefois curieux de constater que les niveaux sont nettement séparés les uns des autres dans un domaine d'énergie qui devrait correspondre au domaine continu. Ceci peut s'expliquer du fait que les niveaux obtenus par réactions photonucléaires correspondent à l'absorption dipolaire des photons.

Enfin, une étude plus approfondie des sections efficaces relatives (γ, n), (γ, p), (γ, α), (γ, d) ... ainsi que des répartitions angulaires des particules émises fournira des renseignements intéressants sur la structure nucléaire.

---

[26] C. Tzara: *Comp. Rend. Acad. Sci.* **242**, 2340 (1956).

SUPPLEMENTO AL VOLUME IV, SERIE X
DEL NUOVO CIMENTO

N. 3. 1956
2° Semestre

A Theoretical Investigation of Nuclear Reactions with Neutrons.

M. CINI and S. FUBINI

Istituto di Fisica dell'Università - Torino
Istituto Nazionale di Fisica Nucleare - Sezione di Torino

Gli Autori riferirono in questo « Seminario » i risultati di un loro lavoro originale, che era stato già presentato al *Nuovo Cimento* per la pubblicazione, e che comparve poi nel fascicolo di Luglio 1955 (pp. 75-89) dello stesso giornale; al quale quindi rimandiamo il lettore, mentre qui ci limitiamo a riportare il sommario. [*N. d. R.*].

Summary. — A theory of the interaction of neutrons with complex nuclei is developed with the aim of obtaining a cross-section averaged over the resonances, to be compared with the results of the phenomenological model proposed by FESHBACH, PORTER and WEISSKOPF (1). It is shown what kind of assumptions have to be introduced in order that the compound nucleus formation give rise to an absorption of the incident beam, irrespective of what happens after the compound nucleus decay. The problem is reduced to the determination of the complex index of refraction of an indefinite nuclear matter, taking properly into account the effect of the Pauli principle. Subsequently this index of refraction has to be introduced into a one-body Schrödinger equation with the correct boundary conditions at the nuclear wall. By assuming nuclear forces which fit the low energy two-body data, and an average binding energy of 8 MeV per nucleon, an expression is derived for the absorption coefficient which is compared with the imaginary part of the FPW potential. At zero energy the absorption coefficient is just in the right range 0.03-0.05. For higher energies it becomes so large that already for 6-8 MeV the absorption is almost complete for medium sized nuclei. This agrees quite satisfactorily with experimental evidence.

(1) H. FESHBACH, C. E. PORTHER and V. F. WEISSKOPF: *Phy. Rev.*, **96**, 448 (1954) (to be denoted in the following as FPW).

SUPPLEMENTO AL VOLUME IV, SERIE X
DEL NUOVO CIMENTO

N. 3, 1956
2° Semestre

The Low Energy Nuclear Mechanics and the Independent Particle Model.

A. KIND

Istituto di Fisica dell'Università - Padova
Istituto Nazionale di Fisica Nucleare - Sezione di Padova

L'Autore riferì in questo « Seminario » i risultati di un suo lavoro originale, che era stato già presentato al *Nuovo Cimento* per la pubblicazione, e che comparve poi nel fascicolo di Settembre 1955 (pp. 443-449) dello stesso giornale; al quale quindi rimandiamo il lettore, mentre qui ci limitiamo a riportare il sommario. [*N. d. R.*].

Summary. — The author analizes the independent particle model of the nucleus in its definition as an approximation to *week incoherent interaction* and its applicability to general problems of low energy nuclear mechanics. In zero approximation, defined by a condition of selfconsistency, the potential wells which determine the states of the single nucleons in the nucleus have a mean depth of the order of twice the mean potential energy per nucleon. It results, for instance, that direct emission and evaporation processes of nucleons have different thresholds. It is emphasized that the optical model for nuclear reactions can be directly derived from the model considered.

PARTE SECONDA

Momenti Nucleari.

Atomic and Molecular Beam Experiments.

I. I. RABI

Columbia University - New York

Lectures edited by

E. MONTALDI

Istituto Nazionale di Fisica Nucleare - Sezione di Milano

Introduction.

Atomic and molecular beam experiments have played a vital role in the development of modern physics. For example, in the development of quantum theory, the experiments of STERN and GERLACH first directly demonstrated space quantization; in nuclear physics, they made possible the first measurements of the anomalous magnetic moment of the proton and the electric quadrupole moment of the deuteron while most recently the field of quantum electrodynamics was stimulated by the Lamb-Retherford experiments and the measurement of the anomalous g-factor of the electron. It is thought that molecular beams are capable of giving a great contribution to the fore front of physics while the use of molecular beams in the study of molecular structure should remain an interesting field for many years.

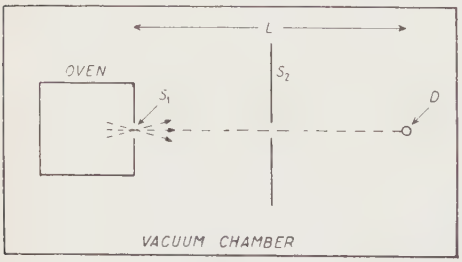

Fig. 1.

1. – The Method of Atomic and Molecular Beam.

1·1. *Atomic and Molecular Beam Technique.* – A molecular beam is produced by a source (called « oven ») placed in a vacuum chamber (Fig. 1). The beam is defined by an opening in the oven (slit S_1) and by a collimating slit (S_2), and is observed by a detector D.

In order to obtain a well defined beam, the conditions imposed on the dimensions of the apparatus are as follows:

$$S_1 < \lambda_1 , \qquad L < \lambda ,$$

where λ, λ_1 are the mean free paths in the vacuum chamber and the oven, respectively, and L is the separation of the source and detector (D). The number of particles per unit time with velocities between c and $c+\mathrm{d}c$ which strike D is given by

$$f(c)\,\mathrm{d}c \propto \frac{c}{\alpha^4} \exp\left[-\frac{c^2}{\alpha^2}\right] c^3\,\mathrm{d}c , \tag{1.1}$$

where $\alpha^2 = 2kT/M$, the symbols k, T, and M having the usual meanings. For a perfect, thin slit, the angular distribution of the particles emitted from the oven follows a $\cos\theta$ law. One can improve the intensity in the forward direction by using a « canal » instead of a slit, a technique which has been carried to a high degree of perfection by ZACHARIAS and co-workers.

Often, the limiting factor in molecular beam work is the efficiency of the detector. Several methods have been developed to detect neutral particles.

(*a*) Early methods measured the deposit of particles or chemical reactions induced in D.

(*b*) By means of a Pirani gauge, a change in pressure may be observed as the beam is collected at D.

(*c*) For the alkalis and other elements, surface ionization occurs when striking the surface of a metal having an higher work function than the ionization potential of the atoms. For the halogens, high electron affinity enables them to come off the surface as negative ions.

(*d*) Counting methods may be used for radioactive nuclei.

(*e*) The beam may be ionized by passing it through an electron stream. A mass spectrograph may be used in conjunction with this ionization method.

1·2. *Deflection of Atoms and Molecules in an Inhomogeneous Magnetic Field.* – To get an idea of the order of magnitude of the force experienced by an atomic magnetic dipole (1 Bohr magneton $\approx 10^{-20}$ erg/oersted), we may compare it with the force experienced by an elementary electric charge ($4.8\cdot10^{-10}$ esu) moving in a field of 1 V/cm (1/300 esu), which is

$$\frac{1}{300}\cdot 4.8\cdot 10^{-10} \approx 1.6\cdot 10^{-12}\ \text{dyne} .$$

The force on 1 Bohr magneton moving in a magnetic field gradient $\partial H/\partial s$ is $F = 10^{-20}\,\partial H/\partial s$. Therefore $\partial H/\partial s$ must be $1.6\cdot10^{8}$ oersted/cm in order that the elementary magnetic dipole experience a force comparable to the above

electrostatic force. In practice one can only produce gradients of approximately 10^5 oersted/cm in the laboratory and so only relatively small deflections of the beam may be obtained. For nuclear dipoles (1 nuclear magneton $= 5 \cdot 10^{-24}$ erg/oersted), the force is still another factor of 1000 smaller.

Fig. 2-*a* shows a cross-section of the type of magnetic pole pieces used in the original Stern-Gerlach experiment. A more homogeneous deflection can be produced by pole pieces such as shown in Fig. 2-*b*.

a) *b*)

Fig. 2.

The energy of a magnetic dipole, $\boldsymbol{\mu}$ in a magnetic field, $\boldsymbol{H}$ is given by

$$W_m = -\boldsymbol{\mu} \wedge \boldsymbol{H} = -g\mu_0 \boldsymbol{J} \wedge \boldsymbol{H}\,, \tag{1.2}$$

where $\boldsymbol{J}$ is the angular momentum in units of $\hbar$.

Since

$$\boldsymbol{J} \wedge \boldsymbol{H} = |J|\,|H|\cos\theta = mH$$

and since $\cos\theta = m/|J|$, we obtain finally

$$W_m = -g\mu_0 m H \tag{1.3}$$

and

$$F_m = -\frac{\partial W_m}{\partial s} = g\mu_0 m \frac{\partial H}{\partial s}\,. \tag{1.4}$$

An important aspect of this formula is that the force depends only on the space rate of change of the magnitude of H and not on its magnitude or directional properties. This is true if the change of H during a Larmor period, as seen by the moving particle, is much smaller than H (the adiabatic case).

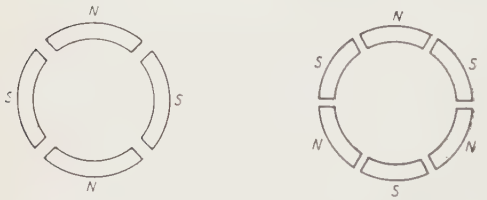

Fig. 3.

Recently, Professor PAUL of Germany has suggested an interesting magnetic arrangement for molecular beams which has already proved to be very useful in studying radioactive nuclei (HAMILTON). For a magnetic field such that $H = 0$ at a certain point in space, it may be shown that for the configuration of magnetic poles shown in Fig. 3-*a*, $H = \sqrt{H_x^2 + H_y^2} = Cr$ in the neighbourhood of the point were $H = 0$, while for the configuration shown in Fig. 3-*b*, $H = Cr^2$. The C's are constants depending on the geometry and magnetic pole strengths.

Then, for the second case, in the neighbourhood of $H = 0$

$$W_m = -g\mu_0 m C r^2 , \tag{1.5}$$

$$F_m = 2g\mu_0 m C r . \tag{1.6}$$

For negative values of $g\mu_0 m$, the expression for the force has the same form as that of a harmonic oscillator. The particles will oscillate back and forth about $r = 0$ with a period $\tau = 2\pi\sqrt{M/2g\mu_0 m C}$, where M is the mass of the particles. This system thus acts as a lens for negative values of $g\mu_0 m$, the atoms of different velocities c being focused at distances $c\tau$ from the oven.

Let us consider, now, an inhomogeneous magnetic field of length l_1, which exerts a force F on an atomic dipole. If the distance from the end of the inhomogeneous magnetic field to the detector is l_2 the total displacement, s, of an atom of mass M and velocity c originally moving parallel to the axis of the system is given by

$$S = \frac{1}{2}\frac{F}{m}t_1^2 + \frac{F}{m}t_1 t_2 ; \qquad \text{since} \quad t_1 = \frac{l_1}{c}, \; t_2 = \frac{l_2}{c},$$

we can also write

$$S = \frac{F}{2mc^2}(l_1^2 + 2l_1 l_2) ,$$

and, remembering that $mc^2/2 = kT$,

$$S = \frac{F}{4kT}(l_1^2 + 2l_1 l_2). \tag{1.7}$$

(1.7) shows that the displacement is independent of the mass of the atom.

1·3. *Deflection of Atoms and Molecules in Two Inhomogeneous Magnetic Fields.* – The simple molecular beam apparatus with one deflecting magnet suffers from a number of disadvantages. First, particles with different velocities are focused at different points, so that it is difficult to get a good intensity at the detector. Also, to obtain values for magnetic moments with this apparatus, it is necessary to measure the gradient of the magnetic field in the deflecting magnet with considerable accuracy, and this is not easy to achieve in practice. We may, however, introduce another inhomogeneous magnetic field before the collimation slit (Fig. 1). So it becomes possible, by using two inhomogeneous magnets which act in opposite directions, to refocus a certain value of m upon the detector. For certain geometrical arrangements, this focusing can be made independent of the velocities of the particles.

If a uniform magnetic field is applied in the region between the two deflecting magnets, the energy of a particle in the beam during its passage through

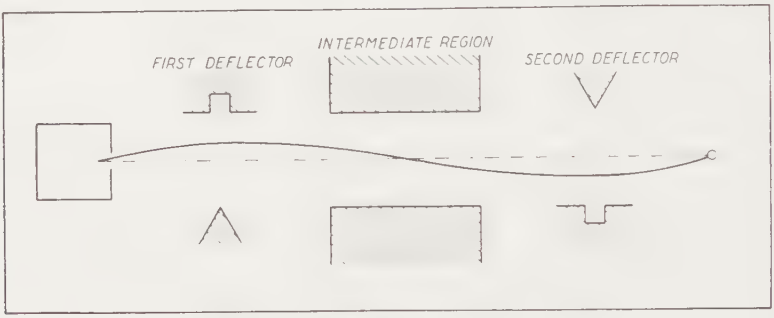

Fig. 4.

this field will depend upon its state of polarization. If the strength of the magnetic field is H_0, then the energy W_m of a particle in the magnetic substrate m is

$$W_m = -g\mu_0 m H_0 . \tag{1.8}$$

The axis of quantization is the direction of the uniform magnetic field. Thus the energy difference ΔW between two adjacent magnetic substates is

$$\Delta W = g\mu_0 H_0 , \tag{1.9}$$

corresponding to a frequency $\nu_0 = (g\mu_0/h)H_0$.

The torque $\boldsymbol{R} = \boldsymbol{\mu} \times \boldsymbol{H}_0$ will cause a precession about the field direction with the frequency ν_0 given above.

If an oscillating field $\boldsymbol{H}_1$ is applied at right angles to $\boldsymbol{H}_0$, transitions $m \rightarrow m'$, $(m' = m \pm 1)$ will be induced between adjacent magnetic substates if the frequency of the applied fields is equal to ν_0.

In the state m' the particle will fail to refocus in the next deflecting field. The resonance is therefore observed as a change in the beam intensity at the detector in the region of ν_0. Since frequency is easily measurable to great accuracy it is possible to get accurate values of g if H_0 is known. Higher accuracy can be obtained in the measurement of relative moments, as it is necessary to measure only the frequencies of the oscillating field provided the uniform field is kept constant.

1·4. *Transition Probability.* – We shall now obtain an expression for the transition probability produced between two magnetic levels by the oscillating field, in the special case of spin $I = \frac{1}{2}$. The derivation which we shall

give is a semiclassical one, and makes use of the theorem, due to EHRENFEST, which demonstrates the equality of quantum mechanical and classical averages.

Classically the rate of change of the angular momentum $\hbar \boldsymbol{I}$ of a system is given by the equation

$$\hbar \frac{\mathrm{d}\boldsymbol{I}}{\mathrm{d}t} = \boldsymbol{\mu} \wedge \boldsymbol{H} = \gamma \hbar \boldsymbol{I} \wedge \boldsymbol{H}, \tag{1.10}$$

since $\boldsymbol{\mu} = g\mu_0 \boldsymbol{I} = \gamma \hbar \boldsymbol{I}$. If we consider a rotating system of co-ordinates, then the rate of change of the angular momentum in the rotating system, $D\boldsymbol{I}/Dt$, is given in terms of $\mathrm{d}\boldsymbol{I}/\mathrm{d}t$ by

$$\frac{D\boldsymbol{I}}{Dt} = \frac{\mathrm{d}\boldsymbol{I}}{\mathrm{d}t} \quad \boldsymbol{\omega} \wedge \boldsymbol{I},$$

where $\boldsymbol{\omega}$ is the angular velocity of the rotating system. Thus the equation of motion for the angular momentum in the rotating system is

$$\frac{D\boldsymbol{I}}{Dt} = \gamma \boldsymbol{I} \wedge \left[\boldsymbol{H} + \frac{\boldsymbol{\omega}}{\gamma}\right]. \tag{1.11}$$

Equation (1.11) has the some form as (1.10) if we consider the term $\boldsymbol{H} + \boldsymbol{\omega}/\gamma = \boldsymbol{H}_{\mathrm{eff}}$ to be an effective magnetic field.

Now we specialize equation (1.11) by taking the z axis of the co-ordinate system in the direction of $\boldsymbol{H}_0$ and by assuming that the co-ordinate system rotates about the axis with angular velocity $-\omega$. Further we assume that $\boldsymbol{H}_1$ is a constant vector in the rotating system and thus is a periodic field of frequency $\omega/2\pi$ in the fixed co-ordinate system. We have

$$\boldsymbol{H} \quad H_1 \hat{i} \quad H_0 \hat{k}$$

$$\boldsymbol{\omega} \quad \omega \hat{k},$$

where $\hat{i}$ and $\hat{k}$ are unit vectors in the x and z directions, respectively, of the rotating system.

With the above specialization, equation (1.11) becomes,

$$\frac{D\boldsymbol{I}}{Dt} = \gamma \boldsymbol{I} \wedge \boldsymbol{H}_{\mathrm{eff}}$$

$$= \gamma \boldsymbol{I} \wedge \left[\left(H_0 - \frac{\omega}{\gamma}\right)\hat{k} + H_1 \hat{i}\right].$$

Thus, in the rotating system, the angular momentum vector precesses about $\boldsymbol{H}_{\mathrm{eff}}$ with angular velocity $\boldsymbol{\omega} = [(\omega_0 \quad \omega)^2 + \omega_1^2]^{\frac{1}{2}}$, where $\omega_0 = \gamma H_0$ and $\omega_1 = \gamma H_1$.

Assume that initially all the particles in the beam are polarized in the positive z direction. After a time t, the vector $\boldsymbol{I}$ of a particle turns through an angle $\bar{\omega}t$ about $\boldsymbol{H}_{\text{eff}}$. If we take new co-ordinates with the z' axis parallel to $\boldsymbol{H}_{\text{eff}}$ (Fig. 5) we can write, for the orientation of $\boldsymbol{I}$ after time t

$$\boldsymbol{I}/|\boldsymbol{I}| = -\sin\theta\cos\bar{\omega}t\hat{i}' + \sin\theta\sin\bar{\omega}t\hat{j}' + \cos\theta\hat{k}'$$

and for the direction of the original axis

$$\hat{k} = -\sin\theta\hat{i}' + \cos\theta\hat{k}' ,$$

where θ is the angle between H_0 and H_{eff}. Thus, if α is the angle between the direction of $\boldsymbol{H}_0$ and $\boldsymbol{I}$ after a time t, then $\cos\alpha$ is the scalar product of the unit vectors $\hat{k}$ and $\boldsymbol{I}/|\boldsymbol{I}|$.

$$\cos\alpha = \cos^2\theta + \sin^2\theta\cos\bar{\omega}t \tag{1.12}$$

or

$$\sin^2\frac{\alpha}{2} = \sin^2\theta\sin^2\frac{\bar{\omega}t}{2} . \tag{1.13}$$

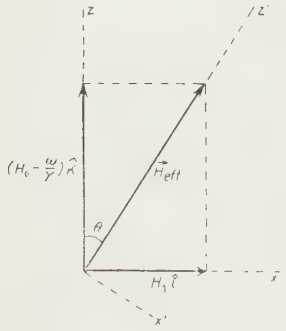

Fig. 5.

Now we make the transition from classical to quantum mechanics. For this purpose, we assume, that the expectation value of I_z is proportional to $P_{\frac{1}{2}} - P_{-\frac{1}{2}}$, where $P_{\frac{1}{2}}$ is the probability that a particle is in the magnetic substate $m = \frac{1}{2}$ and $P_{-\frac{1}{2}}$ is the probability that $m = -\frac{1}{2}$. Classically, $I_z \propto \cos\alpha$, so that, comparing the quantum and classical results, we obtain:

$$\cos\alpha \propto P_{\frac{1}{2}} - P_{-\frac{1}{2}} .$$

The special case $\alpha = 0$ corresponds to complete alignment i.e. $P_{\frac{1}{2}} = 1$, $P_{-\frac{1}{2}} = 0$, thus the constant of proportionality is unity and $\cos\alpha = P_{\frac{1}{2}} - P_{-\frac{1}{2}}$.

Because

$$P_{\frac{1}{2}} + P_{-\frac{1}{2}} = 1, \quad \text{we get} \quad P_{\frac{1}{2}} = \cos^2\frac{\alpha}{2} \quad \text{and} \quad P_{-\frac{1}{2}} = \sin^2\frac{\alpha}{2} .$$

Finally, writing $\sin\theta$ in terms of ω, ω_0 and ω_1, we get for $P_{-\frac{1}{2}}$, the probability that a transition is induced by the applied field $\boldsymbol{H}$, after a time t,

$$P_{-\frac{1}{2}} = \frac{\omega_1^2}{(\omega_0 - \omega)^2 + \omega_1^2}\sin^2\frac{t}{2}\sqrt{(\omega_0 - \omega)^2 + \omega_1^2} . \tag{1.14}$$

For systems with $I \neq \frac{1}{2}$ it is possible to derive a formula for transition probabilities by similar methods. If m and m' are two magnetic substates of I and $P_{mm'}$ is the probability of a transition from m to m' in the oscillating field, then

$$P_{mm'} = \left(\cos\frac{\alpha}{2}\right)^{4I} (I+m)!\,(I+m')!\,(I-m)!\,(I-m')!\cdot$$

$$\cdot\left|\sum_{\lambda=0}^{2I} \frac{(\operatorname{tg}\alpha/2)^{2\lambda-m+m'}}{(\lambda-m+m')!\,(I-m-\lambda)!\,(I-m'-\lambda)!}\right|^2.$$

This formula was first given by MAJORANA. The value $\cos^2\alpha/2$ is the same as for the case $I=\frac{1}{2}$ but with the same g value.

More generally, equation (1.14) for the transition probability from a spin $\frac{1}{2}$ magnetic substate holds in any two levels of a quantum mechanical system. If p and q are the two levels, the transition probability from p to q after a time t, P_{pq}, can be written

$$P_{pq} = \frac{|V_{pq}|^2}{(\Delta w - h\nu)^2 + |V_{pq}|^2}\sin^2\frac{\pi t}{h}\sqrt{(\Delta w - h\nu)^2 + |V_{pq}|^2}. \tag{1.15}$$

In this expression Δw is the energy of separation between the two levels, ν is the frequency of the perturbing field and V_{pq} is the matrix element of the perturbation hamiltonian between the states p and q. In our special case, $V_{pq} = \langle p|\boldsymbol{\mu}\cdot\boldsymbol{H}_1|q\rangle$. The time t is to be taken as the time of transit of a particle in the beam through the homogeneous magnetic field.

As ν, the frequency of the applied oscillating field, is increased through ν_0, the transition probability P_{pq} passes through a maximum. This resonance has a width arising from two sources. First, there is a minimum width arising from the fact that the molecules spend a time t in the oscillating field. Hence from the point of view of a molecule in the beam, this field is not completely periodic, but is uncertain in frequency by an amount $\Delta\nu$ given approximately by the uncertainty relation

$$t\Delta\nu = 1 \qquad \text{or} \qquad \Delta\nu = \frac{1}{t}. \tag{1.16}$$

Secondly, if the radio frequency field is very large so that $\nu_1 = \omega_1/2\pi > \Delta\nu$ it may be seen from equation (1.14) that approximately 50% of the maximum resolution takes place for $\nu - \nu_0 \simeq \nu_1$ so that the line width is increased, for large values of H_1, to $\Delta\nu \sim 2\nu_1$.

In practice it is difficult to make the uniform field H_0 completely homogeneous, and fluctuations arising from inhomogeneities give rise to a further line width. RAMSEY has proposed a new technique which overcomes the effect

of these inhomogeneities to the first order, and which produces resonances which are 40% narrower than those of the older method. In the new method the oscillating field is not applied throughout the length of the field H_0, but instead a much stronger oscillating field is applied at the beginning and the end of H_0.

The method can be understood by reference to the rotating co-ordinate system introduced above. At resonance the first oscillating field produces a precession about $\boldsymbol{H}_1$. In the region of the homogeneous field between the oscillating fields the spin of the particle will not precess relative to the rotating co-ordinate system, because at resonance the precession frequency about H_0 is equal to the rotation frequency of the co-ordinate system. Provided the two oscillating fields are in phase, the molecule will exactly double its angle of precession in the second field. This will be true independent of the velocity of the molecules and hence the time of flight of the molecules in the homogeneous field. Off resonance the molecules will arrive at the second oscillating field out of phase and thus their spin will not receive maximum deflection. In this method inhomogeneities in the homogeneous field H_0 do not add to the line width. It is possible to use a long path in H_0, hence reducing the line width.

2. – Applications to Atoms and Molecules.

2·1. *Atomic Systems in Constant Magnetic Fields.* – Only in a few simple cases, i.e. when the nuclear spin $\boldsymbol{I}=0$ or the electron total angular momentum $\boldsymbol{J}=0$, is it possible to describe the system by only one of these quantum numbers.

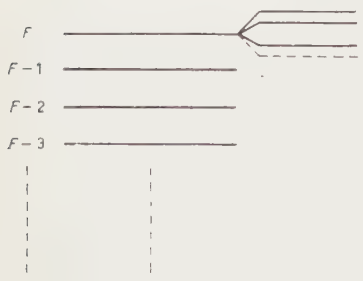

Fig. 6.

In general $\boldsymbol{I}$ and $\boldsymbol{J}$ are coupled together to give a total angular momentum $\boldsymbol{F}$, being:

$$F = I+J\,,\qquad I+J-1\,,\qquad \ldots\,,\qquad |I-J|\,.$$

The total number of these F states is $2I+1$ if $I<J$, or $2J+1$ if $J<I$.

In a weak magnetic field each energy level F splits into $2F+1$ components.

The g factor of a state of angular momentum quantum number F is given by:

$$(2.1)\qquad g_F = g_J\frac{F(F+1)+J(J+1)-I(I+1)}{2F(F+1)} + g_I\frac{F(F-1)-I(I-1)}{2F(F+1)}\,,$$

$$g_J = \frac{g_J+g_I}{2} + \frac{g_J-g_I}{2F(F+1)}\,[J(J+1)-I(I+1)]\,.$$

Transitions may be induced between the substates of F by means of a r.f. field H_1, at right angles with the constant magnetic field H_0, and g_F evaluated from the observed frequencies ($\nu = g_F\mu_0 H_0/h$). Since J and g_J are known, and the term with g_I is small compared to the term with g_J, it is possible to obtain I.

Taking into account the electric quadrupole interaction, the Hamiltonian for one atom may be written:

$$H = A\boldsymbol{J}\cdot\boldsymbol{I} + B[3(\boldsymbol{I}\cdot\boldsymbol{J})^2 - \tfrac{3}{2}\boldsymbol{I}\cdot\boldsymbol{J} - I(I+1)J(J+1)] + \\ + g_I\mu_0\boldsymbol{I}\cdot\boldsymbol{H}_0 + g_J\mu_0\boldsymbol{J}\cdot\boldsymbol{H}_0 . \tag{2.2}$$

where

$$B = \frac{eqQ}{2I\,2J\,\quad 1)I(2I\quad 1)}$$

$$eQ = \sum_i \int r_i^2\,(3\cos^2\theta_{I_i} - 1)\varrho_{m_I=I}(r_i)\,d\tau_i$$

$$eq_J = \int \frac{3\cos^2\theta_e - 1}{r_e^3}\,\varrho_e(r_e)_{m_J=J}\,d\tau_e ,$$

q is the electric field gradient in the state J. It can be shown that, for molecules

$$q_J = \frac{J\quad 1}{2J\quad 3}\,\frac{\partial^2 V_e}{\partial Z^2} .$$

where V_e is the potential from the charges external to a small sphere surrounding the nucleus, and Z is the direction of the axis of symmetry of the molecule.

In the absence of the magnetic field H_0 the Hamiltonian (2.2) becomes:

$$H = \frac{A}{2}K + e^2q_JQ\,\frac{\frac{3}{2}K(K+1) - \frac{1}{2}I(I+1)\cdot J(J+1)}{I(2I\quad 1)\cdot J(2J\quad 1)} . \tag{2.3}$$

where $K \equiv F(F+1) - I(I+1) - J(J+1)$.

The determination of any one of the quantities I, nuclear magnetic moment μ_I, quadrupole electric moment, involves the measurement of energy intervals.

In the limit of a very large magnetic field, corresponding to a Paschen-Back effect, $\boldsymbol{I}$ and $\boldsymbol{J}$ will precess independently around H_0 so that F will no longer be a good quantum number.

Instead m_I and m_J will be constants of the motion. The total Hamiltonian of the system of two nuclei becomes then:

$$W_{m_{I_1},m_{I_2},m_J} = \sum_{i=1}^{2}\left\{A_i m_{I_i} m_J + \frac{e^2 q_J Q_i}{4J(2J-1)I(2I-1)}[3m_{I_i}^2 - I_i(I_i+1)]\cdot\right.$$
$$\left.\cdot[3m_J^2 - J(J+1)] + g_{I_i}\mu_0 m_{I_i} H_0 + g_J \mu_0 m_J H_0\right\}. \tag{2.4}$$

In the case of intermediate coupling a secular equation must be solved. In the particular case of the hydrogen atom, the secular equation is quite simple.

Plotting the energy W as a function of the magnetic field strength H_0 one obtains a diagram similar to Fig. 7.

The slope of the curve, $-\partial W/\partial H_0$, gives the magnetic moment μ.

In the case of deuterium, $I = 1$ and the curves giving W as a function of H_0 look like:

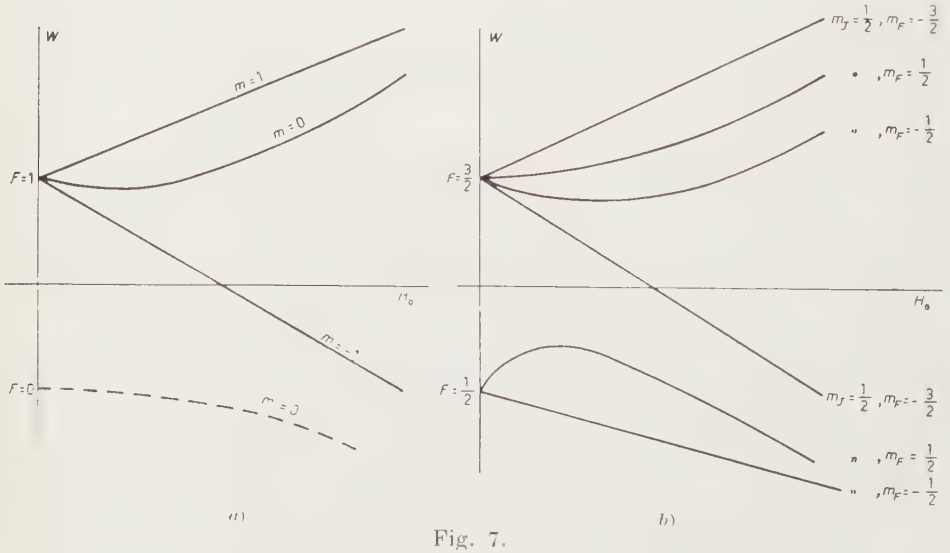

Fig. 7.

It is important to notice that, in some of the states, $\mu = -\partial W/\partial H_0$ is zero for certain values of H_0. This is used in the so-called atomic beam zero moment method. For the values of H_0 for which $\mu = 0$, the beam will not be deflected, and this independently of all velocities. The intensity as measured at the undeflected position has therefore a maximum for these values of H_0. It is possible from the number of these maxima and from their relative spacing, to obtain the nuclear spin I and the hyperfine structure (hfs) separation of the levels.

2·2. *Molecules in Constant Magnetic Fields.* – Consider a molecule with total electron angular momentum zero, that is, in a $^1\Sigma_0$ state. Then the term in the Hamiltonian $A\boldsymbol{J}\cdot\boldsymbol{I}$ is small compared to the term $g_I\mu_0 m_I H_0$, already for values of H_0 of the order of a few gauss. This is because $A\boldsymbol{J}\cdot\boldsymbol{I}$ represents the magnitude of the coupling between the nuclear magnetic moment and the magnetic field associated with the rotation of the molecule, which is in general small because of the large internuclear distance and slow angular velocity. It is not therefore necessary to have a very large field in order to produce a Paschen-Back effect.

In this case the Hamiltonian becomes:

$$H = Am_I m_J + \frac{e^2 q_J Q}{4J(2J-1)}\frac{}{I(2I-1)}[3m_I^2 - I(I+1)]\cdot \cdot[3m_J^2 - J(J+1)] + g_I\mu_0 m_I H_0 + g_J\mu_0 m_J H_0 \tag{2.5}$$

for any given nucleus. For large values of J the expression

$$\frac{3m_J^2 - J(J+1)}{J(2J \quad 1)}$$

simply becomes $\frac{1}{2}(3\cos^2\theta - 1)$.

To get an idea of how the quadrupole interaction affects the energy levels we note that when large angular momenta J are present, as it is usually the case, the quadrupole term for one nucleus may be approximated by the following formula, for which holds for $\mathcal{M}_J = 0$,

$$W_{\text{quad}} \approx \frac{e^2qQ}{I(2I-1)}\left|\frac{J(J+1)}{4J(2J-1)}\right|[3m_I^2 - I(I+1)] \approx \approx -\frac{e^2qQ}{8}\frac{3m_I^2 - I(I+1)}{I(2I-1)}. \tag{2.6}$$

In particular, for $I = \frac{3}{2}$, we have:

$$W_{\substack{\text{quad}\\ m_I=\pm\frac{3}{2}}} \approx -\frac{e^2qQ}{8}; \qquad W_{\substack{\text{quad}\\ m_I=\pm\frac{1}{2}}} \approx +\frac{e^2qQ}{8}. \tag{2.7}$$

Fig. 8-*a* shows the resultant energy levels, neglecting the terms $Am_I m_J$ and $g\mu_0 m_J H$. Fig. 8-*b* plots the resultant spectrum for $Am_I = \pm 1$.

As Fig. 8 shows, the original spectral line corresponding to a frequency $g\mu_0 H/h$ splits into three components by the quadrupole interaction. Since the $\pm\frac{1}{2}$ levels are shifted by equal amounts, to the first order, by the quadrupole interaction, the $m_I = \pm\frac{1}{2} \longleftrightarrow m_I = -\frac{1}{2}$ transition is not shifted in fre-

quency. The transitions $m_I = \pm \frac{3}{2} \longleftrightarrow m_I = \pm \frac{1}{2}$ are shifted by a frequency equal to $e^2qQ/4h$ from the original line.

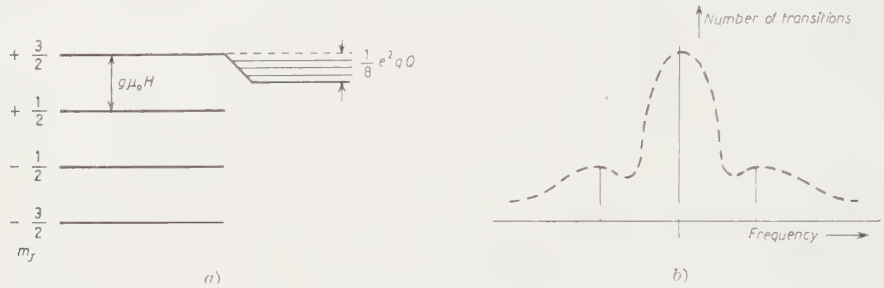

Fig. 8.

Another characteristic of the spectrum is that the central line has a larger amplitude than the satellites. The reason of this fact is the following. In practice we do not have only $m_J = 0$ as we assumed in deriving the approximate formula (2.6). We actually have $m_J = -J, -J-1, ..., +J$. This gives rise to a large number of levels closely spaced around the displacement calculated in equation (2.7). For the Paschen-Back effect, we have the selection rule $\Delta m_J = 0$ in addition to $\Delta m_I = \pm 1$. Now, the levels corresponding to neighbouring values of m_J are so close together that the frequency spectrum of our oscillator encompasses many of them. Thus, the number of transitions induced by the oscillator is proportional to the number of m_J levels within its frequency spread. This will have no effect, to the first order, on the $m_I = -\frac{1}{2} \longleftrightarrow m_I = +\frac{1}{2}$ transition since the quadrupole shift for each of these levels is identical. There will be, however, a broadening of the other transitions or, in other words, the density of m_J levels in a given frequency range will be diminished as the levels are spread out over a larger range.

Since the dependence of the quadrupole shift on m_J is proportional to $3m_J^2 - J(J+1)$, and since $m_J^2 - (m_J - 1)^2 = 2m_J - 1$, the separation of the different m_J levels will be less for smaller m_J, and hence the lines are still peaked near the displacements predicted by equation (2.4). Of course, if an incomplete Paschen-Back effect is produced, the second order (off-diagonal) terms of the quadrupole interaction, and the other neglected terms may complicate the spectrum still more.

It is therefore possible to measure e^2qQ for a large number of molecules. It is rather difficult, however, to obtain the value of Q, since the exact calculation of the electric field gradient involves an accurate knowledge of the molecular wave functions. For molecules where, from chemical data, quite pure homopolar or ionic bonding is known to predominate, it is sometimes possible to make estimates with an accuracy of 10—20%. For other molecules, one must be satisfied with even poorer accuracy. Only in the case of

the hydrogen molecule accurate wave functions are known, so that the deuterium quadrupole moment is the most accurately known.

There are other reasons motivating a detailed study of hydrogen. For example, there are many species

Atomic species: H, D, T

Molecular species: H_2, D_2, HD, HT, etc.

whose wave functions are well known, and a systematic study of these atoms and molecules provides a sensitive test of the basic ideas. By these studies, it has been possible to know, among many other things, the value of the intrinsic magnetic moment of the electron and the quadrupole moment of the deuteron.

Since the nuclei come very close together, any long range spin dependent nuclear force might show up. An upper limit has been placed on any such force.

Some of the other important measurements that have been made on hydrogen are:

(1) The nuclear magnetic moment μ_I. For many years molecular beams gave the most precise value though now nuclear induction enables greater accuracy.

(2) μ_J, the magnetic moment associated with the rotation of the molecule. These values turned out to be smaller than those predicted for a rigid molecule, which showed that this is due to the « slipping » of the electron cloud and related this irrotationability of the electrons to diamagnetic quantities.

(3) Diamagnetism of the electron cloud. It was of interest to construct a good theory of this effect since it affects the accuracy with which nuclear magnetic moments may be evaluated.

(4) The ratio of the hyperfine splittings in the atom. A simple theory predicts

$$\frac{\nu_H}{\nu_D} = \frac{1}{3}\left(\frac{m_H}{m^D}\right)\frac{\mu_P}{\mu_D},$$

where m_H, m_D are the reduced masses of the electrons in hydrogen and deuterium.

The measured ratio was too small by 0.017%. This was explained by A. Bohr in terms of the finite size of the nucleus. Inside the nucleus the interaction between the electron and nucleus becomes quite different from outside and one must divide the calculation into two parts. In the deuteron, for

example, the electron sees from the outside the sum of the proton and neutron magnetic moments, but inside the nucleus the electron sees mostly the proton magnetic moment because it is strongly attracted to the proton. Good qualitative agreement was obtained by BOHR but the more detailed calculation is extremely difficult. For deuterium, it would be sensitive to the structure of the nucleons themselves.

(5) ν_H/ν_T was also measured. As predicted by theory, the effect of penetration of the nucleus is considerably smaller since the two neutrons have opposite spins.

2·3. *Electric Field Experiments on Molecules.* – Consider a diatomic molecule such as NaCl. It's ground state is a $^1\Sigma$ state so that $\boldsymbol{J}$ is perpendicular to the line joining the centres of the nuclei. A dipole moment, μ_z, is induced in the molecule by an applied electric field, E. It may be shown that the energy of the (J, m) state of the molecule in an external electric field is given by

$$W_{J,m} = \frac{\hbar^2}{2\mathcal{I}}\left[J(J+1) + \frac{1}{2}\lambda^2\left\{\frac{J(J+1) - 3m^2}{J(J+1)(2J-1)(2J+3)}\right\}\right], \tag{2.8}$$

where $\mathcal{I}$ is the moment of inertia,

$$\lambda = \frac{\mu_z E}{\hbar^2/2\mathcal{I}}, \qquad \mu_e = -\frac{\partial W}{\partial E}. \tag{2.9}$$

The force acting on the molecule in an inhomogeneous field is

$$F = -\frac{\partial W_{J,m}}{\partial s} = -\alpha\frac{\partial (E^2)}{\partial s}. \tag{2.10}$$

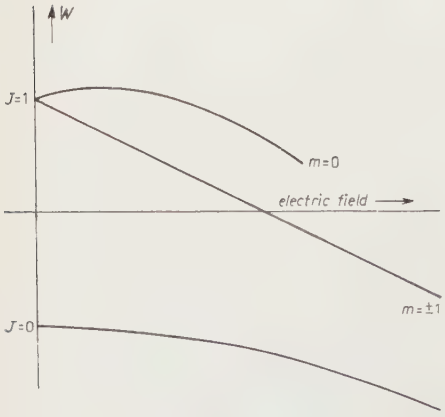

Fig. 9.

Just as in the magnetic case, a study of the complete system will involve all the internal interactions of the molecule.

From the expression of $W_{J,m}$, it may be seen that μ_e for the higher J values becomes small ($1/J^2$ dependence) so that, in practice, one can only study some of the lowest states.

Fig. 9 shows $W_{J,m}$ plotted as a function of the applied electric field for $J = 1$, $J = 0$.

Just as in the magnetic case, two inhomogeneous electric fields are used

with an intermediate region available to induce transitions between the different states of the molecules. One can take advantage of the fact that the electric moment of the $J=1$, $m=0$ state changes sign, if the second field gradient acts in the same direction as the first, and its magnitude is such that the atoms in the $m=0$, $J=1$ state are refocused upon the detector. Then transitions between this state and the others may be observed through a change in intensity of molecules reaching the detector. It should be pointed out that the $m=0 \longleftrightarrow m=\pm 1$ transitions are induced, in spite of being forbidden, because the d.c. electric field mixes s and p states.

This electrical deflection method has been very useful in the study of quadrupole coupling in molecules. The method has the advantage that it is possible to make transitions at relatively low frequencies (100 kHz to a few MHz). It should be noted, however, that the moment of inertia of a molecule varies with its vibrational state. This gives rise to a rich spectrum of resonance lines, and the results of the experiments are difficult to interpret. During the war, big advances have been made in micro-wave techniques and it was possible to obtain much higher frequencies without difficulty. Hence it became possible to make experiments in which transitions were induced between adjacent rotational levels ($J \rightarrow J \pm 1$), resulting in a spectrum which was much easier to interpret.

The set up for this type of experiment is similar to the one used in the magnetic beam experiments. The deflecting fields are inhomogeneous electric fields, which act in opposite directions, in order to obtain focusing at the detector. A homogeneous electric field and a microwave field which stimulates transitions between the leveles $J \rightarrow J \pm 1$, with $\Delta M = 0, \pm 1$, are situated between the two deflecting fields. Since the dipole moments of m levels coming from states of different J are in general different, molecules which make a transition $J \rightarrow J \pm 1$ in the microwave field will not be refocused at the detector. In the actual experiment transitions between the states $J=0$ and $J=1$ are used, because the state $J=0$ is non-degenerate and all the structure in the spectrum is due to the upper $J=1$ state. Thus the results is a relatively simple spectrum. It is necessary to have good frequency stability in this experiment, as the lines are very narrow with widths of the order of 15 kHz. The low population ($2 \cdot 10^{-6}$) of the $J=0$ state makes the intensity variation at the detector small so that the main problem in the first experiment was to find the transition resonance line.

The results of these experiments give considerable information on quantities of molecular and nuclear interest. For a diatomic molecule the separation of the J levels gives the moment of inertia of the molecule and hence the internuclear distance. A study of the variation of the moment of inertia with the vibrational state of a molecule gives information about the effective potential between the two nuclei. If these quantities are measured in molecules con-

taining different isotopes of the same element, very accurate values for the isotopic mass ratios can be obtained. For example the mass ratio of ^{35}Cl to ^{37}Cl was found to be 0.9459503 ± 0.0000015 by this method.

Again the quantity e^2qQ can be determined from the quadrupole splitting observed in molecules. It is difficult to determine q and Q independently, but the ratio of nuclear quadrupole moments for different isotopes can be determined accurately. For example, in potassium we have $Q(K_{(39)})/Q(K_{39}) = = 1.220 \pm .002$. Molecular dipole moments can also be determined.

The following Tables I and II give some values for the above quantities measured in the molecules KCl and KBr and indicates the way in which they depend on the vibrational state of the molecule. v is the vibrational quantum number, μ the molecular dipole moment, r the internuclear distance and e^2Qq/h the quadrupole coupling constant.

TABLE I.

KCl v	0	1	2	4
e^2Qq/h (K_{39})	— 5.656	— 5.622	— 5.571	— 5.511
(^{35}Cl)	0.040	0.073	0.237	0.393
r (Å)	2.6707	—	2.6872	—
μ	10.48	—	10.69	—

TABLE II.

KBr v	0	1	2
e^2Qq/h (Br)	10.244	11.224	12.204
r (Å)	2.8243	—	2.8384
μ	10.41	—	9.93

It should be noted that the values of q at the halide nuclei seem to increase with v while the q at the alkali nuclei decreases. The dipole moment μ behaves in an anomalous way. It increases with v in KCl but decreases in KBr.

These variations have not yet been explained.

We have seen that the molecular beam method gives very accurate values of the quantity e^2qQ. It is difficult, however, to determine q and Q independently since the value of q depends on the electronic structure of the molecule and our knowledge of molecular structure is not sufficient for an accurate calculation. On the other hand if Q could be determined independently, then the molecular beam data would give information useful for the theory of molecular structure.

In atoms, the coupling constant q can be estimated from the hyperfine structure splittings if the nuclear magnetic moment is known.

The constant q is proportional to $(3\cos^2\theta - 1)_{av}(1/r^3)_{av}$, while the hyperfine structure splitting is proportional to $(1/r^3)_{av}$. r is the distance of the last electron from the nucleus and the average is taken over the probability distribution of this electron. Thus if the quantity e^2qQ can be determined in an atom then the nuclear quadrupole moment can be found. A detailed description of an experiment of this type will be given in the next section.

2·4. *Determination of the Quadrupole Moment of* ^{23}Na *by an Atomic Beam Experiment.* – The nuclear quadrupole interaction in ^{23}Na must be measured in an excited state, because the ground state is a $^2S_{\frac{1}{2}}$ doublet and has no quadrupole interaction with the nucleus. The lowest excited state with a quadrupole interaction is the first $^2P_{\frac{3}{2}}$ state. ^{23}Na has spin $I = \frac{3}{2}$ hence the $^2P_{\frac{3}{2}}$ state has a hyperfine structure of 4 levels with spins $F = 0, 1, 2, 3$. A measurement of the intervals of this splitting will give the nuclear quadrupole moment.

The outline of the experimental method is as follows. The two deflecting magnets are oriented in the same direction, so that atoms passing through the apparatus without being perturbed in the intermediate region will not be refocused. Sodium resonance radiation is focused on the beam in this intermediate region, and some atoms in the beam are raised to excited states, principally the $^2P_{\frac{3}{2}}$ and $^2P_{\frac{1}{2}}$ levels. The life time of these states is of the order of 10^{-8} seconds, so that all the atoms decay again to their ground state before entering the second deflecting magnet. The deflecting fields are very strong so that the deflection depends only on the electronic magnetic quantum number m_J. If, by means of the transitions induced by the resonance radiation, an atom has reversed its m_J, it will be refocused in the second deflecting magnet and will give a signal at the detector.

Suppose now that a radio frequency field is applied in the region where the atoms are excited to the $^2P_{\frac{3}{2}}$ state. If the r.f. has the right frequency, transitions will be induced between the hyperfine levels of the $^2P_{\frac{3}{2}}$ state. These transitions will result in a change in the population of the ground state sublevels and this change can be observed at the detector. The life time of the excited $^2P_{\frac{3}{2}}$ is very short (10^{-8} s) so that a strong radiofrequency field must be used in order to get an appreciable number of transitions. Also because of this short life time there will be a considerable interference between neighbouring lines. The maximum possible change in intensity produced at the detector by the r.f. field was 1% so this put a great stability requirement on the apparatus.

In this type of experiment, atoms in the ground state are deflected in a strong magnetic field. The deflection depends on the magnetic quantum number m_J of the atoms in the initial state.

If the atoms go to an excited state, by absorbing light for example, one can tell whether they come down to the initial state or whether they go to a state with different m_J. In the former case then deflection does not change, in the latter case their deflection will be different.

As a simple numerical example of the kind of effect one might expect, let us consider an atom with $I = 0$ and $J = \frac{1}{2}$ in a magnetic field that separates the Zeeman levels as in Fig. 10.

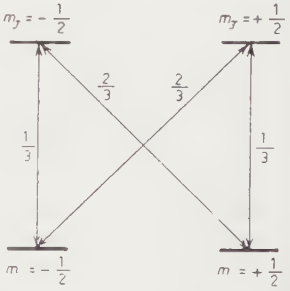

Fig. 10.

Let us suppose that the atom, originally in the ground state $m_J = +\frac{1}{2}$, by absorption of isotropic light goes to either of the excited states $m_J = \pm\frac{1}{2}$. The relative transition probability that it goes to the excited state $m_J = +\frac{1}{2}$ is $\frac{1}{3}$, and that it goes to the excited states $m_J = -\frac{1}{2}$ is $\frac{2}{3}$.

Thus the probability that the atom starts from $m_J = +\frac{1}{2}$, goes to the excited state $+\frac{1}{2}$ and decays to the ground state $m_J = -\frac{1}{2}$ is $\frac{1}{3}\cdot\frac{2}{3} = \frac{2}{9}$. It will then be recognized because its deflection in the magnetic field will change.

Identically the probability that an atom starts from the ground state $m_J = +\frac{1}{2}$, goes to the excited state $-\frac{1}{2}$ and decays to the state $m_J = -\frac{1}{2}$, is $\frac{2}{3}\cdot\frac{1}{3} = \frac{2}{9}$. Therefore the total probability that an atom will be seen is $\frac{2}{9} + \frac{2}{9} = \frac{4}{9}$, i.e. 4 atoms out of 9 will be seen in such an ideal experiment. This is called « the light effect ».

Suppose now that we apply a r.f. field with frequency equal to the energy separation between the two excited states $m_J = \pm\frac{1}{2}$, and let us suppose that the probability of an atom making a transition from either excited state to the other is $\frac{1}{2}$.

Then the probability of an atom being excited from the ground state $m_J = +\frac{1}{2}$ to the state $m_J = +\frac{1}{2}$, making the transition to the excited state $-\frac{1}{2}$ through the effect of the r.f. field, and finally decaying into the state $m_J \neq -\frac{1}{2}$ is $\frac{1}{2}\cdot\frac{1}{3}\cdot\frac{1}{3} = \frac{1}{18}$. This is called the r.f. effect.

Therefore the ratio of the r.f. effect to the light effect is in this case $\frac{1}{18}/\frac{4}{9} = \frac{1}{8}$.

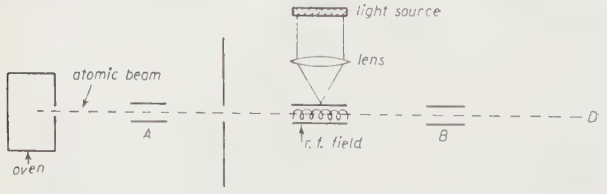

Fig. 11

The general theory of the excited state r.f. effect has been worked out by SERBER (unpublished).

The resonance atomic beam apparatus used by PERL, RABI and SENITZKY to measure the hyperfine structure of the $n = 3$ $^2P_{\frac{1}{2}}$, $^2P_{\frac{3}{2}}$ excited states of ^{23}Na, is shown schematically in Fig. 11.

A and B are strong magnetic fields arranged so that thair field gradients point in the same direction. Therefore, if an atom has to be refocused in D, the deflection in the two fields must be opposite, i.e. its m_J must change in the region between the two fields. For example, if an atom after being optically excited, decays in a state of different m_J, it will be refocused in D.

If the applied r.f. field is of the correct frequency, some of the excited atoms will change their hyperfine excited states and decay eventually in a state of different m_J, thus producing a change in the intensity of the refocused beam.

In the example given above, the excited state r.f. effect produces an increase in the number of refocused atoms.

The h.f.s. the two excited states $n=3$, $^2P_{\frac{3}{2}}$, $^2P_{\frac{1}{2}}$, $I=\frac{3}{2}$ of ^{23}Na (see Fig. 12-a) are further split in a magnetic field H as shown in Fig. 12-b for the $^2P_{\frac{1}{2}}$ state.

One may then induce transitions between the $^2P_{\frac{1}{2}}$ substates and between the $^2P_{\frac{3}{2}}$ substates by means of combined light effect and r.f. effect as explained above, and observe the change in intensity of refocused atoms in D.

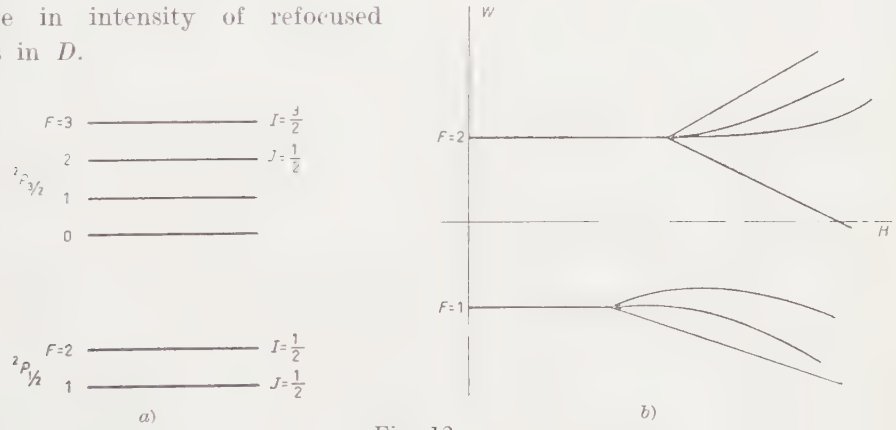

Fig. 12.

For an atom the transition probability between the states a and c is given by the formula

$$W(a,c)=\sum_{p=x,y,z}\sum_{p'=x',y',z'}\left\{\sum_b\left(|G(cbp')|^2|G(b,a,p)|^2+\right.\right.$$

$$\left.\left.\sum_{b'}\frac{G(cbp')G(b,a,p)G^*(cb'p')G^*(b'ap)}{1+4\pi^2I^2[f(bb')]^2}\right)\right\},$$

where p and p' represent the polarization for incoming and outgoing light respectively, the G's indicate matrix elements, and f is the frequency interval between the two lines.

The intensity of the observed resonances is given by

$$I \sim \frac{h_1}{(f_1 - f)^2 - g^2} + \frac{h_2}{(f_2 - f)^2 - g^2},$$

where f_1, f_2, g, h_1, h_2, are respectively the centres, the width and the heights of the individual resonances.

From the theory of magnetic dipole and electric quadrupole interaction, the difference in energy of the levels involved in the transition is given, in the case of $^2P_{\frac{3}{2}}$, by:

$$3a + b = \alpha$$

$$2a - b = \beta$$

$$a - b = \gamma,$$

where a is related to the magnetic dipole interaction and b measures the electric quadrupole interaction.

It was possible to measure only two of the energy differences α, β, γ, the third one being too weak, and it was not possible to determine to which transitions corresponded the measured energy differences. Therefore a and b could not be determined uniquely.

SUPPLEMENTO AL VOLUME IV, SERIE X
DEL NUOVO CIMENTO

N. 3, 1956
2º Semestre

Magnetic Moments of Nuclei.

A. DE SHALIT

The Weizmann Institute of Science, Department of Physics - Rehovoth

The purpose of the present talk is to summarize some of the empirical regularities found among magnetic-moments and to see to what an extent they can be explained by more or less general arguments.

As is well known the magnetic moment is given by

$$\mu = g \cdot J \,,$$

where the g-factor is the operator

$$g = \sum \frac{(g_l^{(i)} \boldsymbol{l}_i + g_s^{(i)} \boldsymbol{s}_i) \cdot \boldsymbol{J}}{J(J+1)} \,. \tag{1}$$

In this relation $g_l^{(i)}$ and $g_s^{(i)}$ are the orbital and the spin g-factors respectively of the i-th particle, $\boldsymbol{l}_i$ and $\boldsymbol{s}_i$ its orbital and spin angular momenta vector operators and $\boldsymbol{J}$ is the total angular momentum of the nucleus considered.

One result can be obtained immediately from the fact that the operator (1) is an odd one. It is seen that because of this nucleons which are paired with opposite directions of their angular momenta give no contribution to (1); the contribution of each nucleon, being proportional to an odd power of m, cancels for pairs in the states $+m$ and $-m$. This is not so for quadrupole moments, for instance, where the contribution is proportional to an even power of m and therefore adds up for particles in states with $+m$ and $-m$. One has to have a higher degree of order among nuclei to cancel quadrupole contributions, whereas the existence of « saturated » pairs of nucleons is enough to cancel magnetic moment contribution.

It is for this reason that in odd-A nuclei one may expect the main contribution to magnetic moment to come from one or a small number of nucleons. If one goes to the extreme of one-particle contribution one gets the well-known

Schmidt formula:

$$\mu = g\mathbf{j} = g_s\mathbf{j} + \tfrac{1}{2}(g_s - g_l)\cdot \begin{cases} 1 & j = l + \tfrac{1}{2} \\ -\dfrac{j}{j+1} & j = l - \tfrac{1}{2} \end{cases} \tag{2}$$

This formula thus predicts that magnetic moments of nuclei, if they are due to the contribution of a single nucleon, should fall on one of two lines (Fig. 1). This pair of lines is different of course for odd-N nuclei and for odd-Z nuclei because of the differences in the g-factors involved.

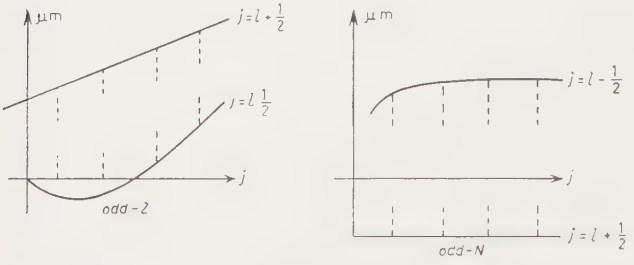

Fig. 1.

Actually the experimental points do not fall on the Schmidt lines, but they do show outstanding regularities associated with these lines.

The most striking fact is that all moments fall between the Schmidt lines (with four exceptions among the very light nuclei).

Another striking feature of the distribution of the experimental magnetic moments is their distinct grouping into two groups on each of the diagrams: there seems to be a « forbidden zone » in the middle between the Schmidt lines into which practically no magnetic moment falls.

Other regularities need a closer investigation of the data. Thus it is found that for semi-mirror nuclei (a pair of an odd Z nucleus with Z_1 and N_1 and an odd N nucleus with Z_2 and N_2 having $Z_1 = N_2$ but not necessarily $N_1 = Z_2$) the deviations of magnetic moments from the Schmidt lines are comparable and very nearly equal.

Also there is the remarkable fact that if one wants to explain deviations from the Schmidt lines as due to a small disturbance of a zeroth-order « single-particle » wave function, the same mechanism should cause deviations of opposite signs for protons and neutrons. This looks at first to be quite strange since one knows from available data on quadrupole moments that the core excitation is more or less the same for odd-N and odd-Z nuclei.

A possible explanation of the observed regularities is suggested by a theory first put forward by Blin-Stoyle [1] and further elaborated by Arima and Horie [2].

[1] R. J. Blin-Stoyle: *Proc. Phys. Soc.*, A, 1158 (1953).
[2] A. Arima and H. Horie: *Prog. Theor. Phys.*, **12**, 623 (1954).

Overlap considerations seem to indicate that, at least for undeformed nuclei, the state of lowest energy of an odd-A nucleus is obtained by coupling to zero total angular momentum as many particles as possible. We therefore take as zeroth order wave function that given by

$$\psi(j_1^2(0)j_2^2(0) \ldots j; jm) ,$$

where the notation implies that we couple a pair in j_1 to $J = 0$, a pair in j_2 to $J = 0$ and so on, and j is the state of the odd nucleon; j is also the total angular momentum and m is its Z-component; of course the wave function is properly antisymmetrized. We shall consider as a simple example a zeroth order wave function

$$\psi_0 = \psi(j_1^2(0)j; jm) . \tag{3}$$

This function can be mixed with other functions of the same total j and m such as for instance

$$\psi_1 = \psi(j_1 j_2(J_{12})j; jm) , \tag{4}$$

$$\psi_2 = \psi(j_2^2(J_2)j; jm) . \tag{5}$$

The total wave function is then

$$\psi = \psi_0 + \sum \alpha_i \psi_i . \tag{6}$$

Not all wave functions of the type (4) or (5) are equally important in determining the magnetic moment. Inasmuch as α_i are small numbers only those wave functions ψ_i will be of importance for which the matrix element $(0\ \mu\ i)$ does not vanish, since these wave functions will then contribute to μ a correction linear in α.

Since μ is a simple particle vector operator only such functions ψ_i can have $(0\ \mu\ i)$ different from zero which differ from ψ_0 by the state of just one nucleon and for which $J_{12} = 1$.

In addition j_2, the new state into which a nucleon in the state j_1 jumped in order to form ψ_i from ψ_0 should have $l_2 = l_1$ since μ commutes with l_i^2.

Thus a typical ψ_i which does contribute linearly in α to $\delta\mu$ will be

$$\psi_i(j_1 j_2(1); jm) .$$

Functions of the type (5) for instance, though perhaps appreciably mixed into the ground state wave function, do not contribute to first order in α to $\delta\mu$.

It will be shown later that of the functions (4) only those have relatively

big coefficient α for which the « jumping nucleon » has the same charge as that of the odd one. If the jumping nucleon is of opposite charge to that of the odd nucleon the amplitude of the corresponding state will in general be considerably smaller.

Thus the configurations which get mixed are mainly configurations of the same charge. Taking this result into account (it will be proved later) we can easily draw further conclusions about the behaviour of magnetic moments. For now we can assume that in (1) $g_e^{(i)} = g_e$ and $g_s^{(i)} = g_s$ for all (i), since all the nucleons which contribute anything to the magnetic moment are of the same charge. (1) can then be transformed into

$$(7) \qquad g = g_e + (g_s - g_e)\frac{(\boldsymbol{S}\cdot\boldsymbol{J})}{J(J+1)} \qquad \text{or} \qquad \mu = g_e J + (g_s - g_e)\frac{(\boldsymbol{S}\cdot\boldsymbol{J})}{J+1},$$

where $\boldsymbol{S}$ is the total intrinsic spin of the nucleons. Combining this results with the single particle Schmidt value (2) we see immediately that

$$(8) \qquad \delta\mu = (g_s - g_e)\left[\frac{\boldsymbol{S}\cdot\boldsymbol{J}}{J+1} - \begin{cases} 1/2 & j = l + \tfrac{1}{2} \\ -j/(2j+2) & j = l - \tfrac{1}{2} \end{cases}\right]$$

$$= (g_s - g_e)G$$

In (8) G is a geometrical factor which depends on the coupling of the nucleons but not on the electromagnetic properties of the nucleons. It is thus expected that the distribution of the values of G will be the same for odd neutron and odd proton nuclei. One then concludes [3] that the distribution of $\delta\mu$ — the deviations of magnetic moments from the Schmidt values — should also be the same for odd neutron nuclei and odd proton nuclei except for a factor in the scale equal to

$$(9) \qquad \frac{(g_s - g_e)_{\text{protons}}}{(g_s - g_e)_{\text{neutrons}}} \approx -1.2 .$$

This result thus accounts for the fact that deviations of odd-N nuclei are opposite to those of odd Z and also for the relative widths of the allowed proton and neutron zones. Also for semi-mirror nuclei one expects G to be nearly equal, and one immediately sees that their deviations should be comparable, and in fact the odd-proton deviation should be 20 % bigger than that of the odd neutron nucleus. This ratio is confirmed in some cases.

To come back to our original problem we want now to estimate α_1, the amplitude of a characteristic state like (4) in the mixture with the ground state (3). To do this we need the matrix element $(1/\Delta E)(0|V_{ij}|1)$. For V_{ij} we

[3] A. DE SHALIT: *Phys. Rev.*, **90**, 83 (1953).

shall take the expression

$$V_{ij} = (\tfrac{1}{4}V_s[1 - \boldsymbol{\sigma}_i\cdot\boldsymbol{\sigma}_j] + \tfrac{1}{4}V_t[3 + \sigma_i\cdot\sigma_j])\delta(\boldsymbol{r}_i - \boldsymbol{r}_j)\,. \tag{10}$$

The approximation of the δ force is taken for convenience in the actual calculation but for most purposes it might be enough to assume a range short compared with the wave length of the states concerned. V_s and V_t are the singlet and triplet interaction constants respectively. It should be remembered that these cannot be taken directly from the two-body low energy scattering results since we have taken care of a part of the interaction via the central field. However if the original r dependence of the singlet and triplet interactions is the same their ratio will remain constant also after the subtraction of the central field. It is therefore legitimate to take $|V_t| \approx 1.5|V_s|$.

It is convenient to write (10) in the form

$$V_{ij} = V^{(0)}_{ij} + V^{(1)}_{ij}(\boldsymbol{\sigma}_i\cdot\boldsymbol{\sigma}_j)\,, \tag{10'}$$

where $V^{(0)} = \frac{1}{4}V_s + \frac{3}{4}V_t$, and $V^{(1)} = \frac{1}{4}(V_t - V_s)$.

We can now show that $(0|\sum V^{(0)}_{ij}|1) = 0$. This is so because in the decomposition of $V^{(0)}_{ij}$ into Legendre polynomials $P_k(\cos\omega_{ij})$ only even k's can contribute at all [both ψ_0 and ψ_1 have the same parity, and thus P_k should have positive parity both with respect to (θ_i, φ_i) and (θ_j, φ_j)] but neither $k = 0$ nor $k = 2$ or any other k can combine states with total angular momentum zero and one thus the only contribution to $(0|\sum V_{ij}|1)$ comes from $V^{(1)}$.

As is well known for δ forces there is no triplet interaction between like nucleons (because of the Pauli principle). We thus see that if the state (4) involves excitation of unlike nucleons (of the opposite charge to that of the odd one) then its amplitude is proportional to $V_t - V_s$ whereas if it involves like nucleons its amplitude is proportional to V_s. There is another factor of 2 involved in favour of the like nucleons because of the antisymmetrization, so that on the whole the amplitude of states (4) with an excitation of like nucleons is four times bigger, on the average, than that involving the excitation of unlike nucleons. This result supplies the basis for our approximate previous treatment which led to (9).

Upon carrying out the calculation of α [2] one winds up with the following result for $\delta\mu$ caused by the mixing of $\psi(|j_1^{n_1-1}(j_1)j_2^{n_2}|(j_2)|(1)j; jm)$ with the ground state configuration $\psi(j_1^{n_1}(0)j_2^{n_2}(0)j; jm)$:

$$\delta\mu = -\tfrac{1}{2}\left|\frac{n_1 l_1(2j_2+1-n_2)}{(2j_2+1)(2l_1+1)(j+1)}\right|^{\frac{1}{2}}\frac{I}{\Delta E}\left[1+(-1)^{j-l-\frac{1}{2}}\frac{2j+1}{2}\right|\cdot$$
$$\cdot\begin{cases} -V_s(g_s - g_e) & \text{for excitation of like nucleons} \\ \tfrac{1}{2}(V_t - V_s)(g_s - g_e) & \text{for excitation of unlike nucleons,}\end{cases}$$

where $I = \int R^2_j(r)R_{j_1}(r)R_{j_2}(r)\,dr \neq 0$ and the g's are those of the *excited* nucleon.

These formulae reproduce correctly the direction of deviation and also give a zero deviation for the $p_{\frac{1}{2}}$ nucleon in agreement with the exceptionally low value observed for the deviations of these nuclei.

Although numerical values of $\delta\mu$ also improve considerably the agreement between theory and experiment, the somewhat arbitrary choice of ΔE and the absolute strength of V_s puts the weight primarily on the qualitative features of (12) rather than on its quantitative predictions. This is even more so if one notes that the same qualitative behaviour would have resulted if the zeroth order wave function would have been a combination of the type:

$$A\psi(j^4(0)j;\, jm) + B\psi(j_1^2(0)j_2^2(0)j;\, jm) + C\psi(j_2^4(0)j;\, jm)\,,$$

which is perhaps a closer approach to reality.

SUPPLEMENTO AL VOLUME IV, SERIE X
DEL NUOVO CIMENTO

N. 3, 1956
2° Semestre

On the Interpretation of H.F.S. in Molecules in Terms of Molecular Structure and Nuclear Moments.

C. H. Townes

Columbia University - New York

1. – Introduction.

A large number of hyperfine interactions in molecular spectra have been measured by the techniques of microwave and molecular beam spectroscopy. We shall discuss the interpretation of these hyperfine interactions in terms of molecular structure and the nuclear moments with which they are associated. From such interpretations, a large number of the presently known quadrupole moments of nuclei have come. Nuclear quadrupole moments are not easy to determine with precision. The following discussion will indicate some of the difficulties encountered in determining nuclear quadrupole moments and the accuracy to which they are at present known. Hyperfine structure due to magnetic dipole moments will also be mentioned, but these will be used only to examine molecular structure, since accurate independent determinations of nuclear magnetic moments are available.

Interaction between a nuclear magnetic moment and an externally applied magnetic field can be measured and the magnetic moment is then easily determined. In the case of the quadrupole moment, it is not possible to produce a strong enough external electric field to give an appreciable interaction, so one must be content with the interaction between the quadrupole moment and some of the microscopic fields produced by the electrons within an atom or within a molecule. The difficulty of determining this microscopic field is the main reason why the quadrupole moments are so hard to determine accurately.

2. – General Theory.

The nuclear quadrupole moment interacts with electronic charges, producing part of the h.f.s. observed in energy levels of atoms and molecules. This interaction, H_Q, is proportional to the inner product of the quadrupole moment tensor and the tensor $\Delta_i E_k$ of the electric field at the nucleus produced by all the charges outside the nucleus. It may be written:

$$H_Q = -\tfrac{1}{6} Q \cdot \Delta E .$$

Since the tensor Q is symmetric, has zero spur, and the components of Q along the two principal axes perpendicular to the nuclear spin are equal, the entire tensor can be expressed in terms of a single quantity $Q = (1/e) \int \varrho_n (3z_n^2 - r_n^2) \, \mathrm{d}\tau$, where ϱ_n is the nuclear charge density, e the proton charge, and z_n the coordinate along the spin axis. Similarly, ΔE is symmetric and has zero spur because of Laplace's equation. If, furthermore, there is an axis of electric symmetry, as in a linear or symmetric top molecule, ΔE may also be specified by the single quantity q, which is given by

$$q = \frac{\partial^2 V}{\partial z^2} = \int \varrho_e \frac{(3 \cos^2 \theta - 1)}{r^3} \, \mathrm{d}\tau ,$$

where ϱ_e is the charge density (of charges outside a small sphere surrounding the nucleus), r the distance from the nucleus to this charge, and θ the angle between r and the molecular axis. If the quadrupole interaction is treated as a first order perturbation, it may then be shown to have the following values in a linear molecule, or in a symmetric top molecule with no angular momentum about the symmetry axis:

$$\langle H_Q \rangle = - eqQ \, \frac{\frac{3}{4} C(C+1) - I(I+1) J(J+1)}{2I(2I-1)(2J-1)(2J+3)} ,$$

where

$$C = F(F+1) - I(I+1) - J(J+1);$$

I is the nuclear spin, J the angular momentum of molecular rotation, and $\boldsymbol{F} = \boldsymbol{I} + \boldsymbol{J}$ is the total angular momentum of the system.

There may also be contributions to the h.f.s. due to magnetic interactions. These arise (1) from the interaction between the nuclear magnetic moment and the orbital angular momentum of the electrons, and (2) from the dipole-dipole interaction due to the magnetic moment of the nucleus and the intrinsic

moment of the electrons:

$$H_{Il} = H_f(\boldsymbol{I}\cdot\boldsymbol{l})\left\langle\frac{1}{r^3}\right\rangle = H_f\Lambda(\boldsymbol{I}\cdot\hat{k})\left\langle\frac{1}{r^3}\right\rangle. \tag{1}$$

where $H_f = 2\mu_0\mu_I/I$, μ_0 is the Bohr magneton, μ_I the magnetic moment of the nucleus, Λ the component of the electron orbital angular momentum, l, along the symmetry axis of the molecule, and $\hat{k}$ is the unit vector along this axis.

$$(H_{Is})_1 = H_f\left[\frac{(\boldsymbol{I}\cdot\boldsymbol{s})}{r^3} - \frac{3(\boldsymbol{I}\cdot\boldsymbol{r})(\boldsymbol{s}\cdot\boldsymbol{r})}{r^5}\right], \tag{2}$$

where s is the electron spin and r the position vector of the electron with respect to the nucleus. There is also a term (3) which is a relativistic effect due to admixtures of s-states in the valence electron states:

$$(H_{Is})_2 = \frac{8\pi}{3}H_f\psi^2(0)(\boldsymbol{I}\cdot\boldsymbol{s}). \tag{3}$$

From these interactions, one can show that the magnetic h.f.s. for the common molecular types depends on the following constants:

$a = H_f\left\langle\frac{1}{r^3}\right\rangle$; $b = H_f\left[\frac{8\pi}{3}\psi^2(0)\right]$; $c = H_f\left\langle\frac{3\cos^2\theta - 1}{r^3}\right\rangle$; and $d = H_f\left\langle\frac{\sin^2\theta}{r^3}\right\rangle$.

In the atomic case, q for an electron in the state n, l, $m = 0$, is given by:

$$q_{nl0} = \frac{2l(2l+1)}{(2l-1)(2l+3)}\left\langle\frac{1}{r^3}\right\rangle.$$

and taking the average of $1/r^3$ with hydrogenic wave functions one gets

$$q_{nl0} = \frac{4Z^3}{n^{-3}a_0^3(2l-1)(2l+1)(2l+3)}.$$

This value is seen to decrease rapidly with increasing n and l due to the increased distance between the electron and the nucleus. In a non-hydrogen atom screening occurs and the average value of $1/r^3$ is not so easily determined. Fortunately, there are other quantities which can be experimentally measured and which depend on $1/r^3$. The spin-orbit interaction that gives rise to fine structure is given by

$$\Delta\nu = R\alpha^3 a_0^3(l - \tfrac{1}{2})\ 1/r^3\ Z,$$

where R is the Rydberg constant, α the fine structure constant, a_0 the Bohr radius and Z_i is $Z - \beta$, where β is the effective atomic screening. For a penetrating p-electron, β is about 2 or 3, indicating screening primarily due to the K-shell. By measuring the fine structure one can determine $\langle 1/r^3 \rangle$ and the value of q_{nl0} for the atomic case. In addition, magnetic h.f.s. due to electron orbital momentum also depends on $\langle 1/r^3 \rangle$, as indicated by interaction (1) above. Hence an experimental measurement of the magnetic h.f.s. and knowledge of μ_I allows determination of $\langle 1/r^3 \rangle$ and q_{nl0}.

The following Table I gives the q_{nl0} values determined from the fine structure. By comparing the values in the third column with the relative values calculated from the hydrogenic wave functions with no screening given in the fourth column, one gets an idea of the effect of screening.

TABLE I.

Electronic state	Element	Measured q_{nl0} (e. s. u.)	Relative values of q_{nl0}
$5p$	I	$45 \cdot 10^{15}$	1.00
$5d$	Cs	0.31 »	0.14
$5f$	Cs	— »	0.048
$6p$	Cs	3.4 »	0.58
$6d$	Cs	0.16 »	0.08
$6f$	Cs	— »	0.028
$7p$	Cs	1.1 »	0.36
$7d$	Cs	0.09 »	0.05

3. – Magnetic H.F.S. Interactions.

We can apply these considerations to test the usually accepted molecular models and see how well the calculated quantities agree with the actual experimental data.

Let us consider the case of a molecule formed of two atoms, each having a core of electrons whose spins and angular momenta cancel, plus one electron in a p-state. If these atoms are some distance apart, but close enough so that their valence electrons overlap slightly, one can show that the lowest state of the molecule corresponds to the singlet state, which increases slightly the electron charge between the two atoms, forming the normal covalent bond. In an actual molecule, the internuclear distance is so small that appreciable distortion of the atomic states may take place. However, the singlet combination of the two atomic states may still be a reasonable approximation. How good an approximation it is seems to be shown especially clearly by examination of molecular hyperfine structure.

Consider first the oxygen molecule, which has one normal covalent bond, but has other valence electrons which are in a rather unusual state, so that the ground state of O_2 is $^3\Sigma$ rather than the much more common $^1\Sigma$. Its structure may be represented schematically in this way:

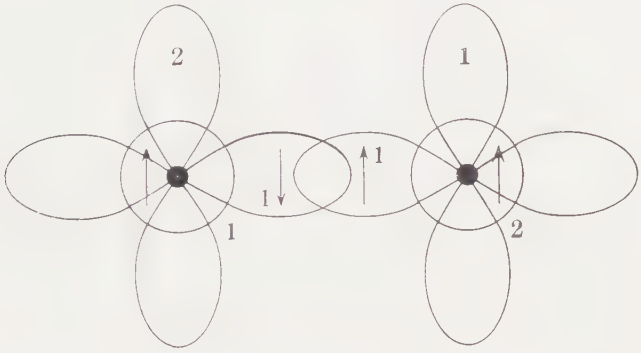

Two p-electrons with opposite spins form one covalent bond, while the other six p-electrons form two 3-electron bonds, each of which contributes a net spin of $\frac{1}{2}$ to give the molecular $^3\Sigma$ state. Total angular momenta along the axis of the molecule is zero.

One can measure the value of the constant c by putting into an O_2 molecule a ^{17}O atom which gives rise to h.f.s., and the value obtained for c can be compared with the value calculated from the measurement of c on isolated atoms. One gets $c_{exp} = 1.1c_{th}$. The electrons are therefore somewhat more compressed in their molecular orbits than in the atom. From the measurement of b one also finds that the p bond involves a 2.5% admixture of $2s$-state. These deviations from h.f.s. expected indicate the extent to which the simple structure of above is valid.

Another molecule with magnetic h.f.s. which has been studied is NO. This molecule has an odd number of electrons. Two different structures are usually considered:

$$\overset{\circ}{N}=O \qquad \bar{N}=\overset{+\circ}{O}$$

In one case the nitrogen has one unpaired electron, and in the other case the N atom becomes negative, and the O atom remains with one odd electron. In both cases $\Lambda = 1$, and we have a $^2\Pi$ state. The actual state is expected to be a mixture of these two states. The percentage to which these states are present was believed to be, from various indirect chemical arguments, 40-50%.

If we evaluate $\langle 1/r^3 \rangle$ with respect to the nitrogen nucleus, in the first

state we find:

$$\left\langle \frac{1}{r^3} \right\rangle = 23 \cdot 10^{24} \text{ cm}^{-3},$$

while it is much smaller in the other case:

$$\left\langle \frac{1}{r^3} \right\rangle = 0.5 \cdot 10^{24} \text{ cm}^{-3}.$$

If these states were present with equal probability, we would expect a total $\langle 1/r^3 \rangle$ for NO of $11.7 \cdot 10^{24}$ cm^{-3}. The actual measured value is $15 \cdot 10^{24}$ cm^{-3}. Measurements of d and use of the above value of $1/r^3$ allow determination of $\sin^2\theta$. One finds $\sin^2\theta = 0.90$, while in the atom it is 0.80. Measurement of b shows that there is a 2% admixture of s-state. These results for NO give a particularly detailed test of the validity of using simple atomic orbitals for h.f.s., and show that at least in such a case, approximately 10% accuracy can be expected from predictions made on the basis of atomic wave functions.

4. – Examples of Quadrupole Interactions.

Quadrupole h.f.s. is different from magnetic h.f.s. in that it depends on all charges in the molecule. Magnetic h.f.s. depends only on those electrons (usually one) which have unpaired angular momentum. However, since closed shells of electrons about a nucleus contribute nothing to the quadrupole h.f.s. because they are spherical, we shall see that quadrupole effects depend also primarily on the valence electrons.

The electronic structure of neutral chlorine has seven valence electrons. The first two are in s-orbits; these contribute nothing to q since they are spherically symmetric states. The remaining five p-electrons are distributed in three p-orbits. This leaves the chlorine atom in a p-state, and one expects a contribution to q due to the non-spherical symmetry of the p-state.

One can represent the chlorine ground state schematically so:

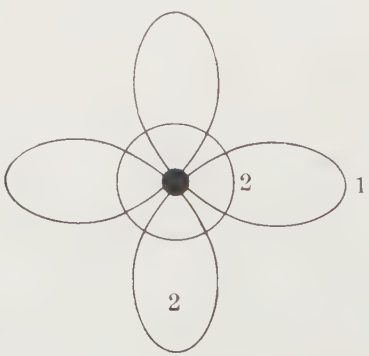

Clearly another electron in the p-shell would close the shell, producing a spherically symmetric state, and one would expect $q = 0$. Thus the ion Cl^- should have $q = 0$. For neutral chlorine, the measured value of eqQ is -110 MHz. If one assumes that in Cl^+ the missing electron is taken from the odd p-orbit, one would expect a value of about -220 MHz for eqQ in Cl^+. With these facts in mind, one can look at chlorine in various molecules and by measuring eqQ get an idea as to the type of chemical binding. For example:

for	CH_3I	$eqQ = -75$	MHz,	slightly ionic,
»	I^+Cl^-	» $= -82$	»	slightly ionic,
»	F^-Cl^+	» $= -145$	»	—
»	K^+Cl^-	» $= -0.3$	»	strongly ionic,
»	$ClCN$	» $= -83$	»	—
»	$CsCl$	» < 2	»	strongly ionic.

Similar effects have been see for bromine, except that the bromine nucleus has the opposite sign for Q.

In a molecule the contributions to q come from:

i) Valence electrons; these contribute about $20 \cdot 10^{24}$ cm^{-3} to $\langle 1/r^3 \rangle$.

ii) Closed shells distorted by valence electrons and by neighboring atoms; these contribute about $1 \cdot 10^{24}$ cm^{-3} to $\langle 1/r^3 \rangle$.

iii) Neighboring atoms and ions; these contribute about $0.2 \cdot 10^{24}$.

Let us look at the valence contribution. We can write the wave function as a superposition of states of given n, l and m:

$$\psi = \sum_{nlm} a_{nlm} \psi_{nlm} .$$

Then, of course, for ϱ_e, in the integral for q, we use $\psi^* \psi$.

Suppose we have a case where

$$\psi = a_s \psi_s + a_p \psi_p + a_d \psi_d .$$

We wish to evaluate $q = e \int \psi^* \psi ((3 \cos^2 \theta - 1)/r^3) \, d\tau$.

The term in $\psi_s^* \psi_s$ contributes nothing by spherical symmetry. We expect the effect of $\psi_p^* \psi_p$ to be very much greater than $\psi_d^* \psi_d$ because of the strong $1/r^3$ dependence. Of the cross terms, the ones containing s and p or p and d give nothing because of parity. The term in s and d is not entirely negligible if the coefficients a_s and a_d are both large. However, if $a_p{}^2$ is as large as about 0.5, then the contribution from the $\psi_p^* \psi_p$ term is much more important. We can write therefore that $q \simeq q_p |a_p|^2$. In a mostly pure p-state the amount of admixture of other states will affect the chemical properties of the molecule much more markedly than it affects q.

5. – Conclusion.

In cases where the effect of strongly penetrating p-valence electrons is important, such as in the halogens, it is possible to make a fairly good evaluation of q. In the light elements, however, where the valence effects do not predominate, and in the elements with other than strongly penetrating p-valence electrons, such as the alkalis, effects such as close shell distortions become important and evaluation of q is much more difficult.

We have seen that h.f.s. interaction in molecules can be used as a sensitive probe of molecular structure, but for getting Q the problem is more difficult. In experiments with microwave spectroscopy, molecular beams, r.f. spectroscopy, etc., one obtains values for eqQ to very high accuracy, but values of q are not known to better than 10 or 30% for molecules. In atomic spectroscopy one can evaluate q to a higher accuracy, but here the experimental hyperfine splitting is seldom known to better than 30%. Thus, except in the case of deuterium, where the coupling constant eqQ has been measured with great precision and q can be calculated fairly accurately because the molecular wave function of hydrogen is rather well known, measurements of nuclear quadrupole moments cannot be expected to be much more accurate than about 25%. The quadrupole moment of the deuteron is probably known within an error of 2%. There are in addition a few cases where atomic h.f.s. has been measured by r.f. spectroscopy. In these cases the accuracy of determination of quadrupole moments is limited to about 5% by our lack of knowledge of the polarization of closed shells by the valence electrons.

BIBLIOGRAPHY

A complete bibliography and details can be found in C. H. Townes and A. L. Schawlow: *Microwave Spectroscopy* (New York, 1955).

Also for magnetic h.f.s.

R. A. Frosch and H. M. Foley: *Phys. Rev.*, **88**, 1337 (1952).
S. L. Miller, C. H. Townes and M. Kotani: *Phys. Rev.*, **90**, 542 (1953).
G. C. Dousmanis: *Phys. Rev.*: to be published.

For quadrupole h.f.s.

C. H. Townes and B. P. Dailey: *Journ. Chem. Phys.*, **17**, 782 (1949).
B. P. Dailey and C. H. Townes: *Journ. Chem. Phys.*, **23**, 118 (1955).

PARTE TERZA

Nuove specie d'atomi: il positronio e gli atomi mesici.

New Atoms.
(Positronium and Mesonic Atoms).

S. DeBenedetti

Carnegie Institute of Technology - Pittsburgh, Pa.

Atomic Physics is the main source of our knowledge on the properties of the best known among the elementary particles: the electron. Since nature has not provided us with atoms containing the other elementary particles, it is natural that attempts have been made to produce such systems artificially. These attempts have met with some success in recent years.

Though the time of survival of the new atoms is short, the study of their properties is possible, in some cases with amazing accuracy. Thus, the study of positronium, composed of an electron and a positron, has proved fruitful for the investigation of detailed quantum electro-dynamical effects. The muonic atoms, normal atoms in which one of the electrons has been replaced by a negative μ-meson, have been used for the determination of nuclear sizes; and the pionic atoms yield information on the interaction of low energy π-mesons with nuclei.

These notes will be concerned with the description of the studies on these atoms, and of the techniques used for their experimental investigation.

CHAPTER I

Positronium [1]

1. – The Annihilation Process.

Thus far it has not been possible to prepare the atom of positronium in sufficient quantities for the application of conventional chemical or spectro-

[1] Reference is made to the following review articles on this subject: M. DEUTSCH: *Progress in Nuclear Physics*, **3**, 131 (1953); S. DeBENEDETTI and H. C. CORBEN: *Annual Review of Nuclear Science*, **4**, 191 (1954).

scopic methods to its study: this atom has been discovered and its properties have been investigated only through the observation of its annihilation radiation. It is therefore necessary that, before entering in the discussion of the atom of positronium, we present some of the theory and of the experiments on the annihilation of electron pairs.

1'1. *Two Quantum Annihilation.* – The phenomenon of annihilation of a positive and negative electron was predicted by Dirac as a necessary consequence of his electron theory. In this theory the annihilation process is described as a transition of an electron from a state of positive energy to one of negative energy. The energy difference, equal to $2mc^2$ if the two particles are at rest, is radiated in the form of electromagnetic radiation. If the particles are at rest and do not interact with any other body, conservation of momentum requires that at least two quanta are emitted. In most cases, two photons, each of energy mc^2, are radiated in opposite directions. In the theory, the phenomenon is treated as a second order effect (Fig. 1, *a* or *a'*).

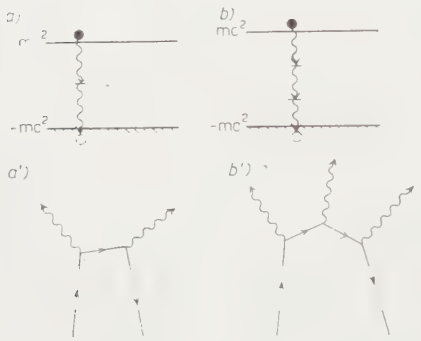

Fig. 1. – The annihilation phenomenon with the emission of two (*a* and *a'*) or three (*b* and *b'*) γ-rays. *a* and *b* are schematic representations of the transition from a positive to a negative energy state; *a'* and *b'* are Feynman's diagrams.

The annihilation cross-section $\sigma_{2\gamma}$ can be obtained, at least as an order of magnitude, considering that it must have the dimensions of a surface formed with the constants c, h, m, e; the constant e, in particular, must enter at the fourth power, since we are dealing with a second order process. Thus $\sigma_{\gamma 2}$ must inconta as factor $\alpha^2\lambda_c^2$, where $\alpha = 1/137 = e^2/hc$ is the fine structure constant, and $\lambda_c = h/mc$ is the Compton wave length. The velocity dependence of σ must be $1/v$, as it follows from statistical considerations, since the reaction occurs between particles of small speed and the products are high velocity quanta; expressing this velocity dependence through the dimensionless factor c/v, one obtains

$$\sigma_{2\gamma} \approx \alpha^2\lambda_c^2 \frac{c}{v} = r_0^2 \frac{c}{v} , \tag{1}$$

where $r_0 = e^2/mc^2$ is the classical electron radius.

A complete computation shows that

$$\sigma_{2\gamma} = \pi\alpha^2\lambda_c^2 \frac{c}{v} = \pi r_0^2 \frac{c}{v} , \tag{2}$$

is the spin averaged two-quantum annihilation cross section for electron-positron pairs. This formula holds if the relative kinetic energy T is between the limits $\alpha^2 mc^2 \ll T \ll mc^2$.

Since the probability of the annihilation process depends on the overlap of the wave functions of positron and electron, the annihilation occurs almost exclusively from S states. Moreover, since photons carry one unit of angular momentum parallel or antiparallel to their direction of propagation, the two quanta of annihilation can arise only from a state of angular momentum 0 or 2. As a consequence, the ${}^3S$ states of a pair are to be excluded as sources of two quantum annihilation radiation.

From this selection rule one can obtain separately the cross-section for annihilation in singlet or triplet collisions: with obvious notation:

$$(3) \qquad {}^3\sigma_{2\gamma} = 0 \,, \qquad {}^1\sigma_{2\gamma} = 4\sigma_{2\gamma} = 4\pi r_0^2 \frac{c}{v} \,.$$

If T is not negligible compared to mc^2, the energy available for the annihilation radiation is sensibly different from $2mc^2$ and one must take into account the energy dependence of the matrix elements. In this way Dirac obtained [2]

$$(4) \qquad \sigma_{2\gamma} = \frac{\pi r_0^2}{\gamma + 1} \left[\frac{\gamma^2 + 4\gamma + 1}{\gamma^2 - 1} \ln (\gamma + \sqrt{\gamma^2 - 1}) - \frac{\gamma + 3}{\sqrt{\gamma^2 - 1}} \right] ,$$

where $\gamma = (E/mc^2) = 1 + (T/mc^2)$. This expression reduces to (2) in the limit $\gamma \to 1$ $(v \ll c)$.

However, in view of our atomic problems, we are more interested in the low energy range. For $T \lesssim \alpha^2 mc^2$ the Coulomb attraction between electron and positron distorts appreciably the trajectories of these particles, and the plane wave approximation, used in the derivation of (2), is no longer valid. Since the rate of transition is proportional to the probability of finding the positron at the position of the electron, the plane wave cross-section must be multiplied by a factor $|\psi(0)|^2$, where ψ is a properly normalized Coulomb wave function. For positive energy unbound states one has [3]

$$(5) \qquad |\psi(0)|^2 = \frac{2\pi\xi}{1 - \exp[-2\pi\xi]} \qquad \xi = \frac{\alpha}{\beta} = \frac{c}{137v} \,.$$

The correction introduced is negligible for $\xi \ll 1$ $(T \gg \alpha^2 mc^2/2)$. For $\xi \gg 1$ $(T \ll \alpha^2 mc^2/2,\ p \ll \alpha mc)$ (5) reduces simply to

$$(6) \qquad |\psi(0)|^2 = 2\pi\xi = \frac{2\pi c}{137 v} \,.$$

[2] P. A. M. Dirac: *Proc. Camb. Phil. Soc.*, **26**, 361 (1930).

[3] See for instance, W. Heitler: *The Quantum Theory of Radiation* (Oxford, 1944), p. 84.

In the case of positronium, we are faced with a positron and an electron bound in a negative energy state, described by a hydrogen-like wave function for atomic number $Z = 1$ and reduced mass $\mu = m/2$. For an S state of total quantum number n

$$|\psi(0)|^2 = \frac{1}{\pi}\left(\frac{1}{2na_0}\right)^3 . \tag{7}$$

(where $a_0 = \lambda\!\!\!^{-}_c/\alpha$ is the Bohr radius) expresses the density of positron at the position of the electron. Thus the mean life ${}^1\tau_{2\gamma}$ of the ${}^1S$ states (*parapositronium*) is

$$\frac{1}{{}^1\tau_{2\gamma}} = {}^1\sigma_{2\gamma} v \frac{1}{\pi}\left(\frac{1}{2na_0}\right)^3 = \frac{1}{2}\frac{\alpha^5}{n^3}\frac{mc^2}{\hbar} = \frac{1}{1.25\cdot 10^{-10} n^3} \text{ sec}^{-1} . \tag{8}$$

The ${}^3S$ states (*ortho-positronium*) are stable against two quantum annihilation and would live indefinitely if higher order processes did not occur.

1·2. *Three Quantum Annihilation.* – Pairs in the ${}^3S$ state, for which the second order mode of decay is forbidden, annihilate in a third order process (Fig. 1, *b* or *b'*) with the emission of 3 γ-rays. The annihilation probability is, in this case, of the order of 137 times smaller than in the singlet.

The detailed calculation of the three quantum effect has been carried out by several authors ([4-6]). The first to give the correct result were Ore and Powell who obtained:

$$\frac{{}^1\tau_{2\gamma}}{{}^3\tau_{3\gamma}} = \frac{4}{9\pi}(\pi^2 - 9)\alpha = \frac{1}{1115} \cong \frac{\alpha}{8} . \tag{9}$$

Thus the mean lives of the ${}^3S$ atomic states of a pair are 1115 times longer than those of the corresponding ${}^1S$ states. Numerically, for positronium triplet

$${}^3\tau_{3\gamma} = 1.4\cdot 10^{-7} n^3 \text{ sec} . \tag{10}$$

The ratio of three quantum to two quantum events from positrons annihilating in free collisions with electrons with random oriented spins, is

$$\frac{\sigma_{3\gamma}}{\sigma_{2\gamma}} = \frac{\frac{3}{4}{}^3\sigma_{3\gamma}}{\frac{1}{4}{}^1\sigma_{2\gamma}} = \frac{3}{1115} = \frac{1}{372} . \tag{11}$$

([4]) E. M. Lifshitz: *Dokl. Akad. Nauk SSSR*, **60**, 211 (1948).
([5]) D. Ivanenko and A. Sokolov: *Dokl. Akad. Nauk SSSR*, **61**, 51 (1948).
([6]) A. Ore and J. L. Powell: *Phys. Rev.*, **75**, 1696 (1949).

In this expression the cross-sections for 2 and 3 quantum annihilation have been averaged over the spin directions.

ORE and POWELL have also computed some of the physical characteristics of the three quantum annihilation radiation and, namely, its energy distribution. The computed spectrum is reproduced in Fig. 2.

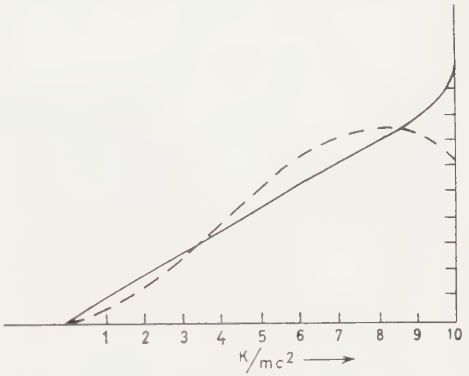

Fig. 2. – Theoretical spectrum of triplet annihilation radiation. The full curve is the result of the complete theory; the dotted curve is the distribution anticipated from statistical factors [From A. ORE and J. L. POWELL: *Phys. Rev.*, **75**, 1696 (1949)].

1·3. *Experimental Work on Positrons and their Annihilation.* – Positrons were discovered in the cosmic radiation in 1933 (7), and soon recognized as the anti-electrons predicted by Dirac theory. It was found that they were produced in cosmic ray showers (8) and could be created by γ-rays from radioactive sources (9) with a cross-section proportional to the square of the atomic number (10). The production in pairs was experimentally demonstrated by pictures of cloud chamber tracks (11).

The annihilation radiation was first observed by THIBAUD (12) from targets in which positrons were focused. The discovery of artificial radioactivity supplied convenient sources of positive electrons, in all respect similar to those created by the materialization of γ-ray energy (13).

An experimental measurement of e/m for the positron showed that this quantity is the same as the electron's e/m within 0.01 per cent (14). Similarly, a crystal spectrometer measurement of the wave length of the annihilation line (15), and a β spectrometer measurement of the energy of the annihilation radiation (16), have proven that the mass of the positron must be the same as that of the electron within one part in 10^4.

(7) C. D. ANDERSON: *Phys. Rev.*, **43**, 491 (1933).
(8) P. M. S. BLACKETT and G. P. S. OCCHIALINI: *Proc. Roy. Soc.*, A **139**, 699 (1933).
(9) P. M. S. BLACKETT, J. CHADWICK, G. P. S. OCCHIALINI: *Proc. Roy. Soc.*, A **144**, 235 (1934).
(10) S. DEBENEDETTI: *Compt. Rend.*, **200**, 1389 (1935).
(11) L. SIMONS and K. ZUBER: *Proc. Roy. Soc.*, A **159**, 383 (1937).
(12) J. THIBAUD: *Compt. Rend.*, **197**, 1629 (1933); *Phys. Rev.*, **45**, 781 (1934).
(13) F. JOLIOT: *Compt. Rend.*, **197**, 1622 (1933); *Compt. Rend.*, **198**, 81 (1934).
(14) L. A. PAGE, P. STEHLE and S. B. GUNST: *Phys. Rev.*, **89**, 1273 (1953).
(15) D. E. MULLER, H. C. HOYT, D. J. KLEIN and J. W. M. DUMOND: *Phys. Rev.*, **88**, 775 (1952).
(16) G. LINDSTRÖM: *Festskrift Manne Siegbahn* (1951).

The simultaneous emission of two opposite quanta was demonstrated for the first time by KLEMPERER [17]; BERINGER and MONTGOMERY [18] verified that the two quanta made an angle of 180° with the error of the order of 1°.

Numerous authors [19-22] have studied the relative polarization of the two quanta, finding them perpendicularly polarized in agreement with the theory.

One can conclude that the experiments have confirmed in considerable detail the consequence of Dirac theory proving beyond any reasonable doubt its applicability to positrons and electrons. Experiments on three quantum annihilation, to be described later in connection with positronium, have also verified the theoretical expectations for this effect.

2. – The Free Atom of Positronium.

2·1. *Formation of Positronium in Gases.* – The possible existence of an atomic system composed of a positive and a negative electron was considered by MOHOROVICIC [23] as early as 1934. Before this atom had been discovered, it had already received the appropriate name positronium [24]. But the credit for the discovery and for the study of positronium goes to DEUTSCH who, with elegant experiments, pointed out its formation when positrons stopped in certain gases.

If the positrons from a radioactive source are allowed to travel in a gaseous medium, they lose their energy through the usual ionization and excitation processes. The great majority of the positrons reach the end of their ionized path without annihilating, since the cross-section for energy loss is much greater than that for annihilation. After the end of their ionized path, and before their annihilation occurs, the following possibilities should be considered: 1) the positrons may be further slowed down in elastic molecular impacts until they annihilate in a collision with the electrons of the gas molecules; 2) after some elastic impacts the positrons are captured by an atom or a molecule, and annihilate while bound to it; 3) some positrons may capture an electron from the surrounding molecules and form an atom of positronium which eventually annihilates as a free atom in the gas.

DEUTSCH thought that this last possibility could be experimentally pointed out through an enhancement of triplet annihilation events. This is because

[17] O. KLEMPERER: *Proc. Camb. Phil. Soc.*, **26**, 361 (1930).
[18] R. BERINGER and C. G. MONTGOMERY: *Phys. Rev.*, **61**, 222 (1942).
[19] E. BLEULER and H. L. BRADT: *Phys. Rev.*, **73**, 1398 (1948).
[20] R. C. HANNA: *Nature*, **162**, 332 (1948).
[21] C. S. WU and I. SHAKNOV: *Phys. Rev.*, **77**, 136 (1950).
[22] F. L. HEREFORD: *Phys. Rev.*, **81**, 482 (1951).
[23] S. MOHOROVICIC: *Astron. Nacht.*, **253**, 94 (1934).
[24] A. E. RUARK: *Phys. Rev.*, **68**, 278 (1945).

in the collisions of a free positron the ratio of 3 quantum to 2 quantum emission corresponds to that to be expected from random orientation of the spin, and is 1/372 (11); while when positronium is formed, presumably in the triplet state 3 times more frequently than in the singlet, the random distribution of the spin is removed: each triplet positronium atom annihilates in three quanta (unless it is decomposed or transformed into singlet in molecular collisions).

In the absence of positronium formation the positron mean life is inversely proportional to the gas pressure, while, if positronium is formed, the characteristic mean life of this atom, $1.4 \cdot 10^{-7}$ s, should be observed independently of pressure. Positronium formation should also produce an increase in the number of three quantum annihilation and a change in the spectrum of the annihilation radiation.

The first observations indicating that the annihilation probability is not always proportional to the gas pressure, are due to SHAERER and DEUTSCH ([25]). The subsequent work of DEUTSCH ([26]) revealed the $1.4 \cdot 10^{-7}$ s pressure independent mean life, establishing the formation of positronium.

The experiment (Fig. 3) was conducted as follows. A source of ^{22}Na (a substance which emits positrons of 0.56 MeV maximum energy immediately followed by a 1.3 MeV γ-ray) was deposited in front of a fast scintillation counter. The counter was protected by an absorber of appropriate thickness to prevent the direct counting of the positrons. The pulses in this first counter were mostly due to the nuclear γ-ray of 1.3 MeV and were practically simultaneous with the emission of a positron. On the side opposite to the counter the source was uncovered, and the positrons emerged into a chamber whose gaseous atmosphere could be controlled. A second scintillation counter, protected from the direct radiation of the source by a lead plug, was introduced in the opposite side of the chamber in order to

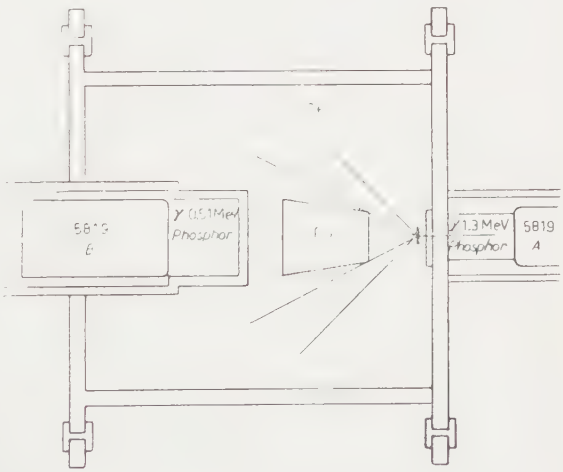

Fig. 3. Equipment used by DEUTSCH for the measurement of positron mean life in gases [From M. DEUTSCH: *Progr. in Nucl. Phys.*, **3**, 131 (1953)].

([25]) J. W. SHEARER and M. DEUTSCH: *Phys. Rev.*, **76**, 462 (1949).
([26]) M. DEUTSCH: *Phys. Rev.*, **82**, 455 (1951); **83**, 866 (1951).

detect the annihilation radiation of the positrons stopped in the gas. Thus the time elapsed between a pulse in the first counter and one in the second, was a measure of the survival time of a positron. This time was measured by means of a multichannel delayed coincidence arrangement from which the positron decay curves could be directly obtained.

Different gases behaved in different ways in regard to the positron lives. In O_2, for instance, the annihilation probability was proportional to the pressure; no effect of positronium formation could be found in the air. The mean life observed in Freon (CCl_2F_2) was, instead, practically independent of pressure from a fraction of atmosphere up to 2 atm. Extrapolated to 0 pressure the measured life was equal, within experimental error, to the theoretical value (10) for the triplet positronium atom (Fig. 4).

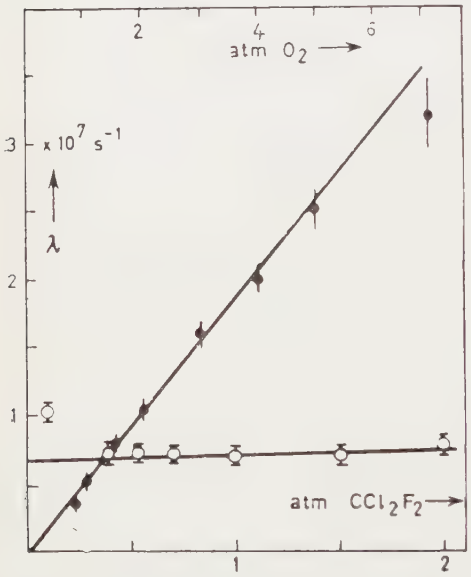

Fig. 4. – Pressure dependence of annihilation probability for O_2 (points) and Cl_2F_2 (open circles) showing the formation of positronium in this second gas. [From M. DEUTSCH: *Phys. Rev.*, **83**, 866 (1951)].

In this manner the atom of positronium was discovered.

In order to be more accurate about the sequence of events one should say that Deutsch's measurements, besides proving the existence of positronium, were also an independent determination of the mean life of its triplet state. At the time of the experiments, there were three different calculated values for this quantity: the experimental data pointed out to the right one ([5]), which was later confirmed by repeated computations ([27]).

2·2. *Annihilation Radiation from Positronium.* – Triplet positronium, besides decaying with characteristic mean life, also emits a characteristic annihilation radiation. The presence of this atom can be revealed in a simple manner by a measurement of the energy of the annihilation radiation: the spectrum of triplet annihilation is continuous (Fig. 2) while that of singlet annihilation presents a sharp line at mc^2. A NaI scintillation spectrometer was often used by DEUTSCH to distinguish between the two spectra.

The increase in intensity of three quantum annihilation is obviously accompanied by a decrease in the two quantum process. This effect was detected

([27]) J. M. RADCLIFFE: *Phil. Mag.*, **42**, 1334 (1951).

by POND ([28]), who studied the formation of positronium by observing the decrease in the coincidence counting rate of two counters responding to the singlet annihilation radiation.

But the most direct way of observing triplet positronium, is to detect the emission in coincidence of the three quanta of annihilation radiation. This was done in experiments performed at the Carnegie Institute of Technology ([29]). The source (Fig. 5) was a thin ^{22}Na sample at the center of a small Al container holding SF_6 vapors at different pressures: increasing the pressure the number of positrons stopping in the vapor increases, and so does the formation of positronium. This is accompanied by an increase in the triple coincidence rate of three NaI counters symmetrically located in a plane containing the source. The energy of the coincident rays was measured with differential pulse height selectors and was found to vary, as a function of the angles, as predicted by the laws of conservation of energy and momentum (Fig. 6).

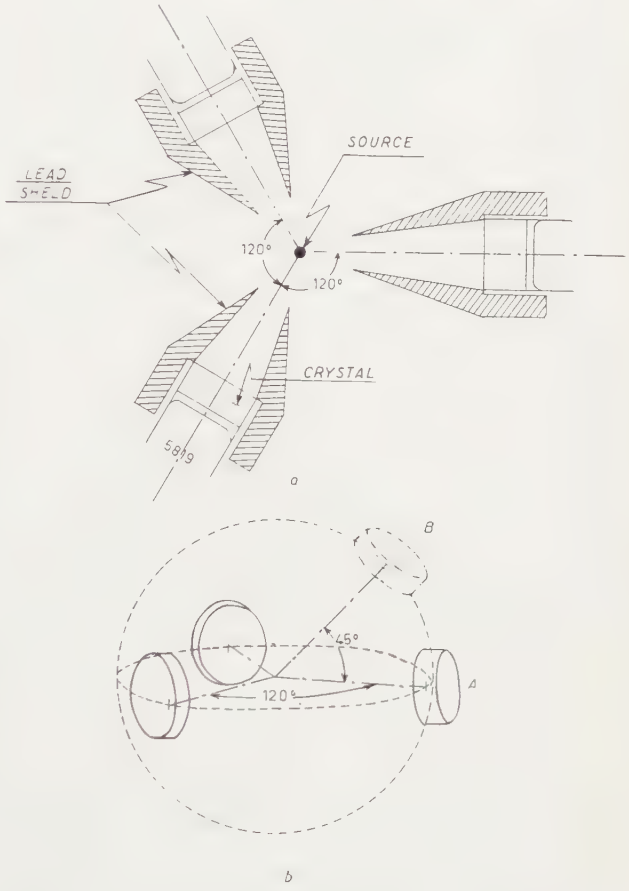

Fig. 5. – Instrument for the observation of three-quantum annihilation of triplet positronium. *a*) top view. *b*) perspective of the scintillating crystals. One of the counters was brought to position *B* for background counting. [From S. DEBENEDETTI and R. T. SIEGEL: *Phys. Rev.*, **94**, 955 (1954)].

Since for each angular configuration of the γ-rays their energy is determined, the three quantum annihilation spectrum can be obtained from a measurement of angular distribution. The spectrum experimentally determined in this manner is in satisfactory agreement with the theoreti-

([28]) T. A. POND: *Phys. Rev.*, **85**, 489 (1952).
([29]) S. DEBENEDETTI and R. T. SIEGEL: *Phys. Rev.*, **85**, 371 (1952); **94**, 955 (1954).

cal curve of Fig. 2. The experiment was sufficiently accurate to show the effect of the energy dependence of the matrix elements, since the data did not agree with the distribution obtained from the statistical factors alone (dotted curve Fig. 2).

The polarization of the triplet annihilation radiation was also studied. The polarization properties were computed by DRISKO [30], and the experiment [31] confirmed a particularly simple theoretical prediction concerning the polarization of any one of the quanta relative to the plane of emission of all three.

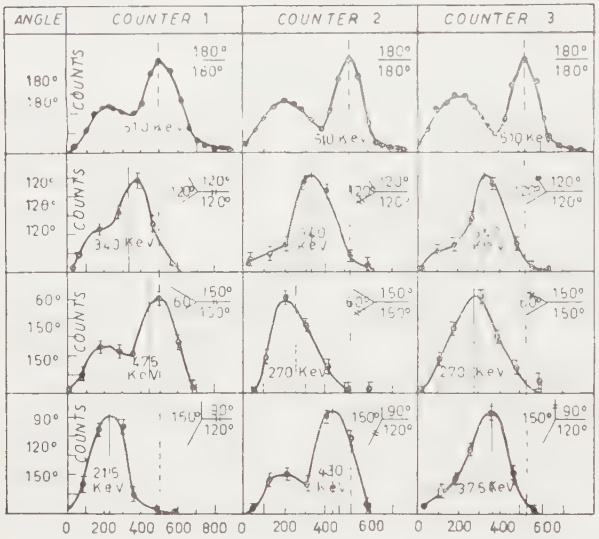

Fig. 6. – Pulse height spectra of three quantum annihilation radiation for different angular arrangements of the counters. Top three curves are calibration curves obtained with two quantum annihilation. [From S. DEBENEDETTI and R. T. SIEGEL: *Phys. Rev.*, **94**, 955 (1954)].

2·3. *Chemical Properties of Positronium.* – The word chemical may appropriately be used in connection with the formation and decomposition of positronium [32], which depends on the interaction of this atom with the molecules of the surrounding gas.

Positronium triplet is formed in most gases (such as H_2, He, N_2, A, SF_6, CCl_2F_2), but a contamination of NO, O_2 or halogen molecules prevents its observation. The percentage of positrons forming positronium in the favorable cases is of the order of 20%.

Since the binding energy of positronium (6.8 eV) is smaller than the ionization potential I of most molecules, some energy has to be supplied when the positron captures an electron. Thus only positrons of kinetic energy larger than I – 6.8 eV can capture electrons. Positrons which are slowed down below this limit are lost for positronium formation and annihilate in free collisions with the molecules.

---

[30] R. DRISKO: *Phys. Rev.*, **102**, 1542 (1956).

[31] L. LEIPUNER, R. SIEGEL and S. DEBENEDETTI: *Phys. Rev.*, **91**, 198 (1953).

[32] Most of the information on this subject is unpublished. It can be found in reports by DEUTSCH in the M.I.T. Lab. of Nuclear Science and Engr. Progress Reports (1952 and 1953).

In agreement with these considerations, Deutsch found that the application of an electric field (dc or ac) increases the amount of positronium formed, since it reaccelerates the slow electrons.

The quenching of orthopositronium by NO is related to the odd number of electrons in this molecule. In a collision, the odd electron is readily exchanged with the electron of an atom of positronium. The cross-section of the NO molecule for ortho → parapositronium conversion is $8 \cdot 10^{-17}$ cm². NO_2, which also has an odd number of electrons, effectively produces triplet to singlet conversion, while N_2O (with 22 electrons) does not.

The O_2 molecule also induces ortho → para conversion because of its magnetic field. The cross-section is in this case much smaller: $4 \cdot 10^{-19}$ cm².

The large cross-section of the halogens ($\approx 10^{-16}$ cm²) for the suppression of orthopositronium is possibly due to an actual chemical combination between these molecules and positronium.

These observations of Deutsch indicate the possibility of more extensive studies of the chemical properties of the element positronium.

2·4. *The Fine Structure of Positronium.* – To the physicist the work on the energy levels of the positronium atom is more interesting than its chemical properties. The present status of positronium spectroscopy is characterized by the fact that the spectral lines have not been observed, but their fine structure is known with great accuracy.

The main contribution to the fine structure is due to the interaction between the magnetic moments of the two electrons. In as S state the interaction energy is given by the formula [33]

$$W_m = \frac{8\pi}{3} \mu^2 \boldsymbol{\sigma}_1 \cdot \boldsymbol{\sigma}_2 |\psi(0)|^2 , \tag{12}$$

where $\mu = e\hbar/2mc$ is the Bohr magneton and $\boldsymbol{\sigma}$ the spin matrix vector. Considering (7) and remembering that $\boldsymbol{\sigma}_1 \cdot \boldsymbol{\sigma}_2 = 1$ for triplets, and $\boldsymbol{\sigma}_1 \cdot \boldsymbol{\sigma}_2 = -3$ for singlets one obtains:

$$\begin{cases} {}^3W_m = \dfrac{\alpha^4}{12} \dfrac{mc^2}{n^3} & \text{(triplet)}, \\ {}^1W_m = -\dfrac{\alpha^4}{4} \dfrac{mc^2}{n^3} & \text{(singlet)}. \end{cases} \tag{13}$$

The ortho and para positronium S terms are thus separated by $(\alpha^4/3)(mc^2/n^3)$ due to first order coupling of the magnetic moments.

[33] E. Fermi: *Zeits. f. Phys.*, **60**, 320 (1930).

There are, however, other contributions to the fine structure splitting which may be computed with modern quantum-electrodynamical methods. The largest of these, also of the order of $\alpha^4 mc^2$, is due to what may be called the « annihilation force ». This can be visualized considering that the coulomb attraction between the positive and negative electron does not act all the time in the triplet state, since, in this state, positronium may virtually annihilate and reproduce itself with a one-quantum annihilation and pair production process (Fig. 7).

When all the quantum electrodynamic corrections to the fine structure of positronium are computed to the order α^5, one obtains [34] for the difference in energy between ortho and para positronium ground states:

$$\Delta W = \frac{\alpha^4 mc^2}{4}\left[\frac{7}{3} - \frac{\alpha}{\pi}\left(\frac{32}{9} + 2\ln 2\right)\right] + \frac{i\alpha^5 mc^2}{4} . \tag{14}$$

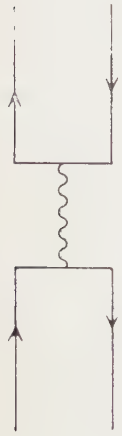

The imaginary term arises from the real mean life of the singlet state decaying through two quantum annihilation. Numerically, the real part is

$$\Delta W = 2.0337 \cdot 10^5 \text{ Mc /s} . \tag{15}$$

This theoretical value was obtained after the splitting had been measured by DEUTSCH with the methods described in the following section. We shall see that (15) is in excellent agreement with the experimental result (22).

Fig. 7. – Feynman's diagram corresponding to the virtual annihilation and re-creation of triplet positronium. This effect results in a decrease of positron-electron attraction (annihilation force).

2·5. *Zeeman Effect.* – In order to find the Zeeman splitting one has to diagonalize the matrix of the perturbing energy $\boldsymbol{\mu}\cdot\boldsymbol{H}$, where $\boldsymbol{\mu} = (e\hbar/2mc)\cdot(\boldsymbol{\sigma}_1 + \boldsymbol{\sigma}_2)$ is the magnetic moment of positronium, and $\boldsymbol{H}$ the external magnetic field. The matrix elements of interest are easily found from

$$\begin{cases} (\boldsymbol{\sigma}_1 - \boldsymbol{\sigma}_2)_z \, {}^3\psi_{\pm 1} = 0 , \\ (\boldsymbol{\sigma}_1 - \boldsymbol{\sigma}_2)_z \, {}^3\psi_0 = 2 \, {}^1\psi_0 , \\ (\boldsymbol{\sigma}_1 - \boldsymbol{\sigma}_2)_z \, {}^1\psi_0 = 2 \, {}^3\psi_0 . \end{cases} \tag{16}$$

Thus the $m = \pm 1$ states of the triplet do not split. For the other states,

[34] R. KARPLUS and A. KLEIN: *Phys. Rev.*, **87**, 848 (1952); T. FULTON and R. KARPLUS: *Phys. Rev.*, **93**, 1109 (1954).

one has to solve the secular equation

$$\begin{vmatrix} \lambda - {}^3W & \frac{eh}{mc} H \\ \frac{eh}{mc} H & \lambda - {}^1W \end{vmatrix} = 0 , \tag{17}$$

where ${}^1W$ and ${}^3W$ are the unperturbed singlet and triplet energies. The perturbed energy levels are given by the roots of this equation:

$$\begin{cases} {}^3E = \lambda_1 = \dfrac{{}^1W + {}^3W}{2} + \dfrac{\Delta W}{2}\sqrt{1 + x^2} , \\ {}^1E = \lambda_2 = \dfrac{{}^1W + {}^3W}{2} - \dfrac{\Delta W}{2}\sqrt{1 + x^2} , \end{cases} \tag{18}$$

where $\Delta W = {}^3W - {}^1W$ and where one has introduced

$$x = \frac{2eh}{mc} \frac{H}{\Delta W} .$$

The splitting of the levels as a function of H is shown in Fig. 8. It is important to observe that the magnetic field introduces an admixture of singlet state in the triplet term with $m = 0$. For a given field the admixture ratio $|{}^1\psi_0|^2/|{}^3\psi_0|^2$ equals $x^2/4$.

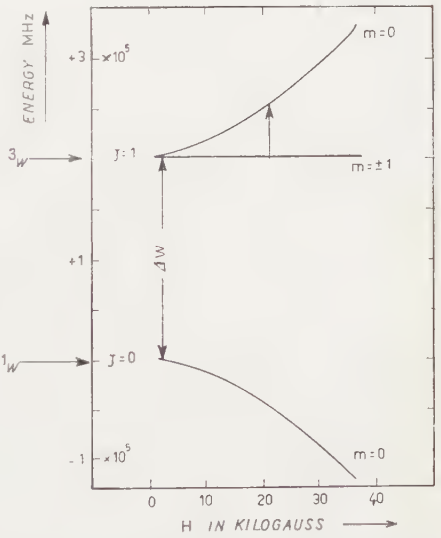

Fig. 8. – Splitting of positronium levels in a magnetic field. W_0 is here the singlet energy without field.

2·6. *Magnetic Quenching and First Determination of the Fine Structure Splitting of Positronium.* – As a result of the admixture of ${}^1S_0$ in the ${}^3S_0$, the number of triplet annihilations due to positronium decreases when a magnetic field is applied. This is because $\frac{1}{3}$ of what was pure triplet state in absence of the field, has now a finite probability of decaying as singlet. The dependence on the field of the number of triplet annihilation $n_{3\gamma}$, is given by

$$n_{3\gamma} = \frac{2}{3} + \frac{1}{3} \frac{|{}^3\psi_0|^2}{|{}^3\psi_0|^2 + |{}^1\psi_0|^2} \frac{{}^1\tau}{{}^3\tau} = \frac{2}{3} + \frac{1}{3} \frac{1}{1 + (x^2/4)} \frac{{}^1\tau}{{}^3\tau} . \tag{19}$$

For very strong fields the three-quantum effect is reduced to $\frac{2}{3}$ of its initial value for no field (Fig. 9); for intermediate fields the triplet annihilation rate

depends on x. Since this variable includes ΔW a measurement of $n_{3\gamma}$ as a function of H, is a determination of the fine structure splitting of positronium.

The measurement was performed by DEUTSCH and DULIT ([35]) who measured the triplet annihilations in a varying magnetic field through the analysis of the annihilation radiation with a scintillation spectrometer. The result (Fig. 9) was

$$\Delta W = 9.4 \cdot 10^{-4} \text{ eV} = 2.26 \cdot 10^{5} \text{ Mc/s}, \tag{20}$$

with an error of 15%.

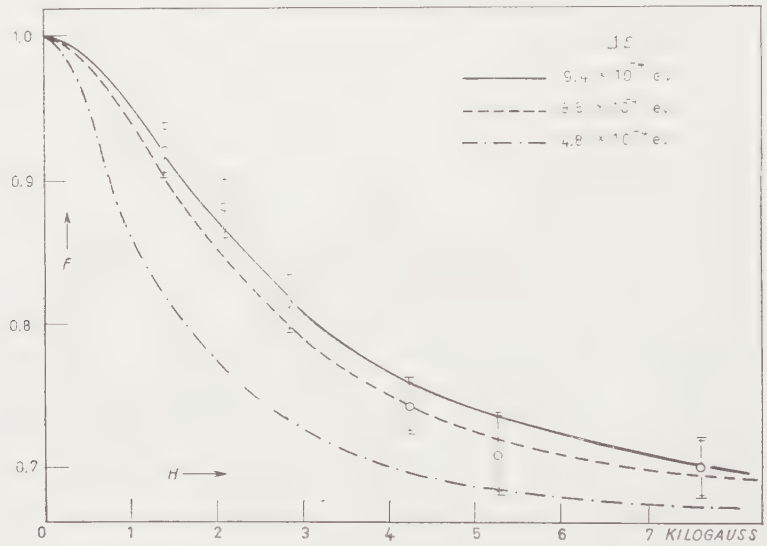

Fig. 9. – Magnetic quenching of triplet positronium. [From M. DEUTSCH and E. DULIT: *Phys. Rev.*, **84**, 489 (1952)].

This is to be compared to the theoretical values $\alpha^4 mc^2/3 = 4.8 \cdot 10^{-4}$ eV for uncorrected dipole interaction and $7\alpha^4 mc^2/12 = 8.5 \cdot 10^{-4}$ eV including the α^4 correction term due to the annihilation force. It is seen that the experimental result clearly points out the effect of the annihilation force. The correction terms of the order α^5 are too small to be revealed by this experiment.

2·7. *Resonance Quenching.* – A much more accurate determination of the fine structure splitting was made possible by the introduction of a resonance method ([36]). With a magnetic field present, a radiofrequency signal is fed

([35]) M. DEUTSCH and E. DULIT: *Phys. Rev.*, **84**, 489 (1952).
([36]) M. DEUTSCH and S. C. BROWN: *Phys. Rev.*, **85**, 1047 (1952).

to a cavity containing positronium. If the frequency ω is such that

$$\hbar\omega = {}^3E - {}^3W = \frac{{}^1W - {}^3W}{2} + \frac{\Delta W}{2}\sqrt{1 + x^2}\,; \tag{21}$$

transitions from the $m = \pm 1$ level to the $m = 0$ level ($x^2/4$ mixture of singlet and triplet) are induced (arrow in Fig. 8). Such transitions induce singlet decay of the $m = \pm 1$ levels of the triplet which were not affected by the magnetic field alone.

If ω and H are measured, equation (21) can be solved for ΔW. The resonance (Fig. 10) is sharp: its width is mainly due to the natural width of the

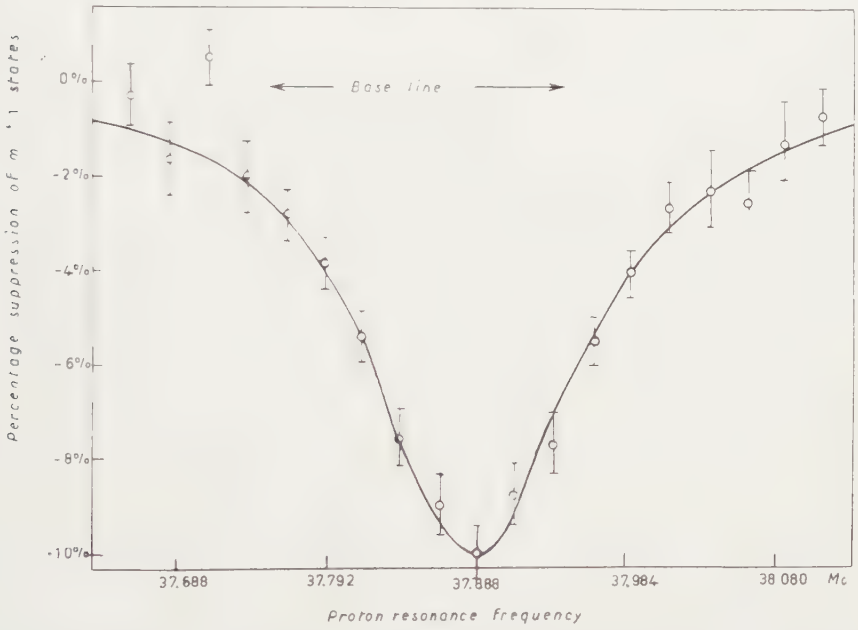

Fig. 10. – Resonance quenching of positronium in a magnetic field. The proton frequency is a measure of the field; the frequency in the positronium cavity was 3012.9 MHz. (Courtesy of Mr. WEINSTEIN).

$m = 0$ level, which is $6.2 \cdot 10^{-3}$ times the value of the energy ΔW to be measured. The value of H was measured, in the latest experiments ([37]), with the proton resonance method. The value experimentally found is

$$\Delta W = (203\,380 \pm 40)\ \text{Mc/s}\,. \tag{22}$$

([37]) R. WEINSTEIN, M. DEUTSCH and S. BROWN: *Phys. Rev.*, **94**, 758 (1954); **98**, 223 (1955).

The theoretical computation developed after this result had been obtained leads to the value (15). There is complete agreement within the limits of the stated experimental errors.

The elegance of these experiments, the fundamental nature of the problems investigated, and the accuracy of the results make the study of the free atom of positronium one of the outstanding achievements in physics in recent years.

Looking back on this work, one has the comforting feeling that it may still be possible for an experimentalist to give some basic contribution to our knowledge of the physical world relying on his ingenuity and originality, rather than doing the experiment of most obvious interest, which usually involves the greatest weight of dollars and machinery.

3. – Behaviour of Positrons in Condensed Materials.

In this section we want to discuss the behaviour of positrons in solids, in relation to the possibility of formation of positronium within these materials. It must, however, be made clear from the beginning that even if a bound state of an electron and a positron existed in solid matter, the wave function of this state could be considerably different from that of free positronium. The expression positronium in solids has to be understood in a very broad sense.

Apart from the question of formation of positronium, however, the results obtained in experiments on the behaviour of positrons in solids are worth reporting since the study of positron annihilation may present a new tool for the investigation of the solid state.

3·1. *The Width of the Annihilation Line.* – The first evidence showing that the details of the annihilation process were related to the motion of the electrons within a solid absorber was found experimentally by DuMond and coworkers ([38]) in the course of their precise measurement of the annihilation line by means of the curved crystal γ-ray spectrometer. These authors found that the annihilation line had a measurable width which was naturally interpreted as a Doppler effect resulting from the electron's motion.

The experiments were performed with a source of ^{64}Cu, with the positrons stopping in Cu. The natural line width was 0.096 X U. This corresponds to a velocity of the center of mass of the annihilating pair of 0.004c, equal to the speed of an electron of 4.1 eV. The observations could be accounted for assuming that the annihilating positrons were at rest, and the electrons had a kinetic energy of 16 eV. The observed width shows that the annihilating

([38]) J. W. M. DuMond, D. A. Lind and B. B. Watson: *Phys. Rev.*, **75**, 1226 (1949).

positrons are practically at rest, and that only the conduction electrons contribute to the annihilation, since the inner electrons have much greater velocities.

Similar work done with a β-spectrometer ([39]) led to a line width of the same order of magnitude.

3·2. *The Angular Distribution of the 2-Quantum Annihilation Radiation.* – More accurate information on the state of motion of the electrons involved in the process of annihilation is obtained from the measurements of the angular distribution of the annihilation radiation.

In 1942 BERINGER and MONTGOMERY ([18]) had shown, using Geiger counters in coincidence, that the two γ-rays of annihilation are emitted in opposite directions within an angle of the order of one degree. With the increased efficiency in γ-ray detection due to the advent of scintillation counters, it became possible to measure the angle between the γ-ray with far greater precision, and departures from antiparallelism of the order of 10^{-2} radians were found.

In the first experiments to reveal this effect ([40]) the positron source (shavings of Cu containing some ^{64}Cu) was surrounded by an Au absorber in which most of the positrons annihilated. The annihilation source was about 1 mm thick in the direction perpendicular to the direction of observation of the annihilation radiation. The counters in coincidence were on opposite sides of the source at 120 cm of distance from it. Coincidence counts were observed when the counters were slightly out of alignement relative to the source, a clear indication of the imperfect antiparallelism of the annihilation rays.

Such deviations from antiparallelism are obviously related to the momentum of the annihilating pair. If the momentum has a value p, in the direction perpendicular to that of observation, the angle between the γ-rays is p/mc. The observed angular distribution corresponded to an average angle of the order of 1/137 of a radian or to a momentum of the order of $mc/137$. This result is most easily interpreted assuming that the positron is effectively at rest, and that most of the momentum is contributed by the conduction electrons.

The theory of this phenomenon was developed by Primakoff neglecting the attraction between positrons and electrons. He showed that, in this approximation, the positrons are thermalized before annihilation by losing their energy to the metal lattice; their wave function is a wave of long wave length modulated by the repulsion of the ionic cores and can be considered constant outside the ionic core, zero within it. Thus, in order to compute the properties of annihilation, it is necessary to know the wave function of the

([39]) D. LIND and A. HEDGRON: *Ark. f. Fysik*, **5**, No. 2, 29 (1952).

([40]) S. DEBENEDETTI, C. E. COWAN, W. R. KONNEKER and H. PRIMAKOFF: *Phys. Rev.*, **77**, 205 (1950).

electrons only outside of the ionic core: here, this can be represented by plane waves of wave length appropriate to the distribution of momenta in a degenerate gas having a density equal to that of the conduction electrons. According to this view, the angular distribution curve observable with good resolution should consist of two parts: a central peak due to the Fermi distribution of electron momenta, and a somewhat wider, but considerably less intense, tail due to the momentum of the positron resulting from the modulation of its wave function.

Applied to Au, this theory gave an average momentum in sufficient agreement with the experimental result. The experiments, however, were not precise enough to verify the more detailed consequence of the theory and to test the assumptions made.

The original work in Au was extended to other substances by several authors ([41-43]), sometimes with some improvements in technique. Recently, with the use of more efficient scintillation counters, several groups ([44-46]) have succeeded in increasing the angular definition to 10^{-3} radians and have obtained much more detailed information. In some of the new experiments, the annihilation source does not consist anymore of an absorber surrounding the radioactive material, but of an interchangeable thin (≈ 1 mm) strip bombarded by the positrons from radioactive samples (usually ^{22}Na). The counters are protected from the direct radiation of these samples by means of heavy absorbers, and their angle of acceptance of the radiation from the annihilation source is defined by slits in Pb blocks. The experiments measure the distribution of one component of the momenta, say p_x, with a resolution which is considerably smaller than the half-width.

The work on metals (Fig. 11) has brought to a verification of Primakoff's assumption. The dependence on the angle λ around 180° is in most cases (Fig. 11*a*) parabolic. It can be described by the function $1 - (\lambda mc/p_{max})^2$ as expected from an undistorted Fermi distribution.

The curves of Fig. 11*a* exhibit a sharp break for $\lambda = p_{max}/mc$ where p_{max} is the maximum momentum computed for a 0 Fermi distribution. In all cases, agreement with the experiment is reached assuming that the number of free electrons per atom is given by the position of the element in the periodic chart: 1 for the alkali, 2 for Be and Mg, 3 for Al, 4 for Sn and Pb, 5 for Bi. For angles larger than p_{max}/mc the parabolae are followed by a tail

---

([41]) J. B. Warren and G. M. Griffiths: *Can. Journ. Phys.*, **29**, 325 (1951).
([42]) H. Mayer-Leibnitz: *Zeits. f. Naturfor.*, **6**a, 663 (1951).
([43]) R. E. Green and A. T. Stewart: *Phys. Rev.*, **98**, 486 (1955).
([44]) L. A. Page, M. Heinberg, J. Wallace and T. Trout: *Phys. Rev.*, **98**, 206 (1955).
([45]) A. T. Stewart: *Phys. Rev.*, **99**, 594 (1955).
([46]) G. Lang, S. DeBenedetti and R. Smoluchowski: *Phys. Rev.*, **99**, 596 (1955).

as expected. These tails, however, are too large to be accounted for exclusively by the modulation of the positron wave function and are probably due to the annihilation of the positron against the swifter electrons of the atomic cores.

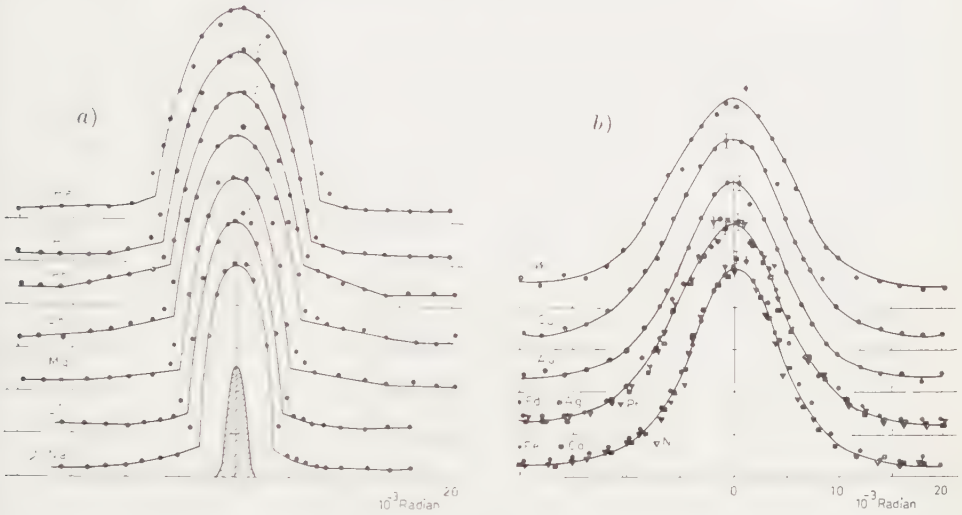

Fig. 11. – Angular distribution of annihilation radiation from various metals. Shaded area shows instrumental resolution. [From G. Lang, S. DeBenedetti and R. Smoluchowski: *Phys. Rev.*, **99**, 596 (1955)].

This view seems corroborated by the fact that the metals for which the ratio (ionic volume)/(cell volume) is larger, exhibit relatively greater tails: in the case of the transition metals and noble metals (see Fig. 11*b*), where the cores nearly touch each other, the size of the tails is so great that these blend with the parabolae and cannot be resolved.

No evidence of positronium formation in metals is obtained from the angular distribution curves. Indeed these curves show no effect of positron-electron attraction since they can be interpreted assuming a velocity independent annihilation probability equivalent to a $1/v$ cross-section.

A semiconductor, Ge, was studied at Carnegie Institute of Technology ([47]). The angular distribution was parabolic for both n and p type impurities. The maximum angle corresponds to a maximum Fermi momentum for an electron gas of 4 electrons per atom. It appears that the electrons of a partly filled band cannot be distinguished from those of a completely filled band since, in both cases, the distribution in momentum is mainly determined by the Fermi statistics.

([47]) G. Lang: personal communication.

The case of ionic crystals was also studied. For several alkali halides tested the angular dependence is more nearly linear, instead of being quadratic. The curves are triangular in appearance. Their width increases with decreasing atomic number of the halogen, as if the positron chose to annihilate against the negatively charged ion.

In the work on insulators ([44]) particular attention was given to those substances where positron mean lives of the order of 10^{-9} s had been detected by BELL and GRAHAM ([48]) (see description of this work in Section 3·1).

Fused quartz and crystal quartz were compared, since the long positron life had been found in fused samples and not in crystalline samples of this material. The data showed a sharp peak at zero radians in the angular distributions obtained with fuse quartz, a peak which was not present in crystal quartz. Other experiments ([43]) showed a similar peak in Teflon which is another of the substances exhibiting a long positron life: the size of the Teflon peak increases with temperature (Figure 12), as does the value of the long positron life.

These experiments show the existence of pairs annihilating with nearly zero total momentum in the insulators which are

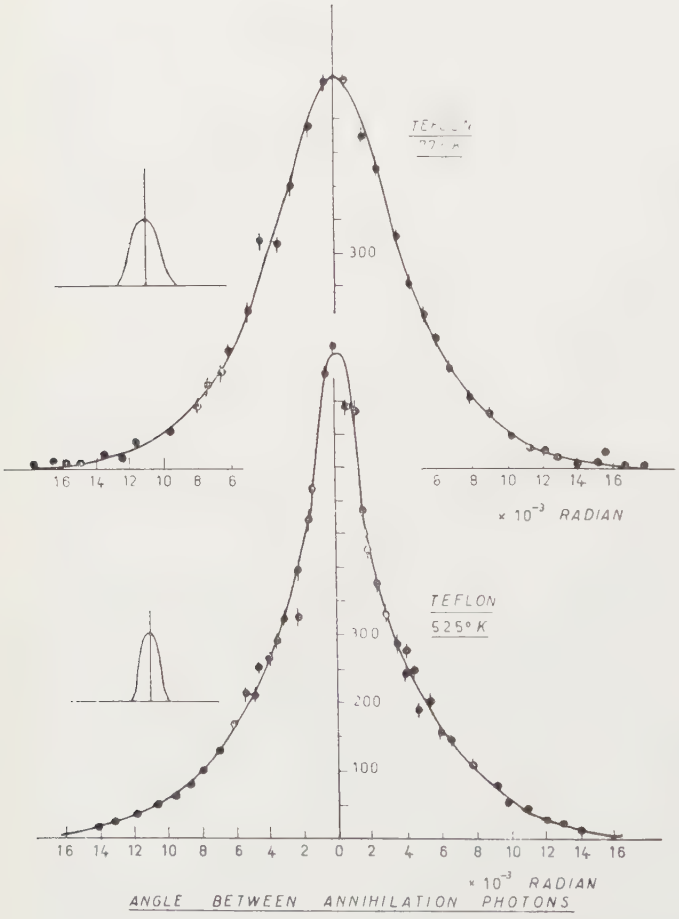

Fig. 12. – Angular distribution of annihilation radiation in Teflon. Angular resolution shown for each curve. [From A. T. STEWART: *Phys. Rev.*, **99**, 594 (1955)].

([48]) R. E. BELL and R. L. GRAHAM: *Phys. Rev.*, **90**, 644 (1953).

characterized by long positron mean lives. Most probably these pairs are atoms of positronium at rest. If formed in the triplet state, these atoms may live longer than free positrons: when annihilating as singlet, the two quanta show zero momentum since the momentum of the electron cancels that of the positron.

It appears that the simplest explanation of the angular correlation experiments is that positronium is formed in certain insulators (usually those substances exhibiting a positron mean life of the order of 10^{-9} s), while in metals the positron at rest annihilates in free collisions, mostly with the conduction electrons. As we will see, however, this view concerning the behavior of slow positrons in metals is not easy to reconcile with the experimental information on positron mean lives.

3·3. *Thermalization and Diffusion of Positrons.* – The mechanism of thermalization of the positrons has made the object of several theoretical investigations. First PRIMAKOFF ([48]), considering the energy lost in the collisions between the positron and the crystal lattice, reached the conclusion that the thermalization time in Au would be of the order of $3 \cdot 10^{-10}$ s. This was thought to be shorter than the annihilation time, estimated of $25 \cdot 10^{-10}$ s, neglecting positron-electron attraction. It is instead somewhat longer than the actual annihilation mean life, which is now known to be $\approx 1.5 \cdot 10^{-10}$ s.

According to GARVIN ([49]) however, there is a much more effective mechanism of thermalization in metals, due to the collisions between the positron and the conduction electrons. This author estimates that, as a consequence of these collisions, the positrons should become thermalized in $\approx 10^{-15}$ s.

A more refined viewpoint is taken by LEE-WHITING ([50]) who considers that the positron's charge is, in a conductor, screened by the increased electron density in its vicinity. The effect of electron screening on the electron-positron collisions is evaluated and a thermalization time of the order of 10^{-12} s is found.

All these authors agree in the conclusion that most positrons have time to reach thermal energy before annihilating, at least in metals.

An attempt to point out the existence of thermal positrons was performed by MADANSKI and RASETTI ([51]). A positron source was mounted at one end of an evacuated tube containing an electrode which could be charged negatively in order to collect the thermal positrons diffusing out of the source material. No evidence of thermal positron diffusion was found, despite the fact that an effect about 100 times background was expected. Several surfaces were tried including Cu, Pt at 1 450 °C (to eliminate surface layer of absorbed

---

([49]) R. L. GARVIN: *Phys. Rev.*, **91**, 1571 (1953).
([50]) G. E. LEE-WHITING: *Phys. Rev.*, **97**, 1557 (1955).
([51]) E. MADANSKI and F. RASETTI: *Phys. Rev.*, **79**, 397 (1950).

gases), K evaporated in vacuum, liquid Ga, insulators such as glass, mica, etc., all with negative results.

The authors present the possible following reasons for the failure of this experiment: *a*) positrons do not diffuse, but are trapped in potential minima; *b*) positrons diffuse within the condensed materials but are trapped at the surface; *c*) positronium is formed. Positronium atoms could diffuse from the absorber, but being neutral, would not be collected on the negative electrode.

The negative result of this experiment probably requires different interpretations for different cases. In insulators, for instance, it is possible that some positrons form positronium, (where it may be located in imperfections of the crystal) while others may get trapped at fixed location. In metals instead, the positron may move freely, and be prevented from escaping out of the material by electrical image forces or other surface effects.

3·4. *The Mean Life of Positrons in Condensed Materials.* – In order to predict the value of positron mean lives, let us consider first the model of annihilation in free collisions, and examine a specially simple case, such as that of an alkali metal. According to the model of Primakoff which accounts so well for the angular distribution, we have to imagine a positron practically at rest in a Fermi gas of electrons. The annihilation probability per unit time can be written as $1/\tau = Nv\sigma$; N is the number of free electrons per unit volume, which, as we have seen, is the number of atoms times their valence, v is the electron velocity and σ the annihilation cross section. If one uses for σ the plane wave value, one has $1/\tau = N\pi r_0^2 c$; this formula predicts a mean life of $2.9 \cdot 10^{-9}$ s for Li, $10.2 \cdot 10^{-9}$ s for K, $16 \cdot 10^{-9}$ s for Ca. These predictions however, are much longer than the experimentally measured mean lives. It is natural to look for the reason for this discrepancy in the fact that we have thus far neglected the attraction between positron and electron, while implicitly considering the repulsion between the positron and the atomic cores.

As a first attempt to take into account the electrostatic attraction one can simply apply the Coulomb correction factor ([6]) to the annihilation cross section. After averaging over the Fermi momentum distribution one obtains $1/\tau = -3\pi(mc/137p_{max})\pi r_0^2 cN$. Numerically for the alkali this formula gives $1.7 \cdot 10^{-10}$ s for Li, $4.2 \cdot 10^{-10}$ s for K, $5.6 \cdot 10^{-10}$ s for Cs.

Though these estimates are obviously very rough, one is led to expect that the differences of the positron mean lives in the alkali metals should be at least 10^{-10} s and it becomes worth while to try to detect such differences with sufficiently fast instrumentation.

The first work of comparison of positron mean lives in different substances was performed by DeBenedetti and Richings ([52]). The time between the

([52]) S. DeBenedetti and H. J. Richings: *Phys. Rev.*, **85**, 377 (1952).

nuclear γ-ray of ^{22}Na and the annihilation radiation from solid absorbers was measured with an error of $5 \cdot 10^{-11}$ s. The positron mean lives were found to be the same within this error in all the metals tested (including Li, K, Al, Pb) (Fig. 13). Only in certain insulators, such as quartz, paraffine, Teflon, the mean lives were measurably longer, apparently of a few 10^{-10} s.

This work was continued and extended by BELL and GRAHAM ([48]) who, using a much more elaborate technique, made an absolute measurement of the mean lives. These were found to be $(1.5 \pm 0.5) \cdot 10^{-10}$ s in all metals.

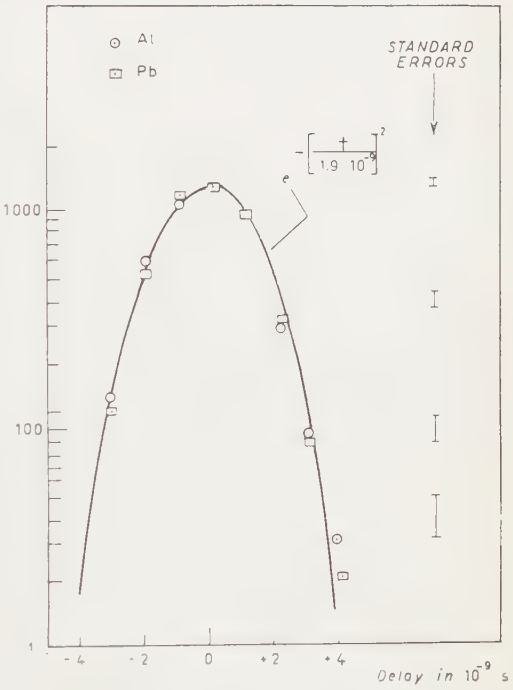

Fig. 13. - Delay curves showing the equality of positron mean lives in Al and Pb. [From S. DEBENEDETTI and H. J. RICHINGS: *Phys. Rev.*, **85**, 377 (1952)].

According to BELL and GRAHAM the fact that the measured mean life of positrons in metals is the same as that of singlet positronium has to be interpreted as evidence for the existence of positronium in these substances. It is, however, difficult to conceive the presence of a singlet positronium atom within the lattice and within the degenerate gas of conduction electrons, so completely undisturbed by its surroundings that it would decay with the same mean life as the free atom. Even if the positronium wave function in metal was the same as in the gas, the frequent spin exchanges would make the mean life four times longer. The small value of the mean life in metals could be due to a concentration of electrons near the positron, produced by the electrostatic attraction, but not necessarily identified with positronium.

Whether or not positronium is formed in metals, the positron-electron attraction must play an important role in the interpretation of the mean lives, while not affecting the angular distribution. It is possible that more extensive theoretical analysis will explain this apparently contradictory situation. Some recent work by FERRELL ([53]) already shows that an approximate consideration

([53]) R. A. FERRELL: personal communication.

of the Coulomb attraction leads to shorter mean lives without affecting appreciably the angular distribution curve.

Before closing the subject of the mean life of positrons in metals, one should mention that an increase of mean life in superconductors has been reported ([54,55]), but this very interesting effect has not been confirmed by more recent investigations ([56]). Similarly, the angular distribution of the annihilation radiation is not affected by the superconducting state ([57]).

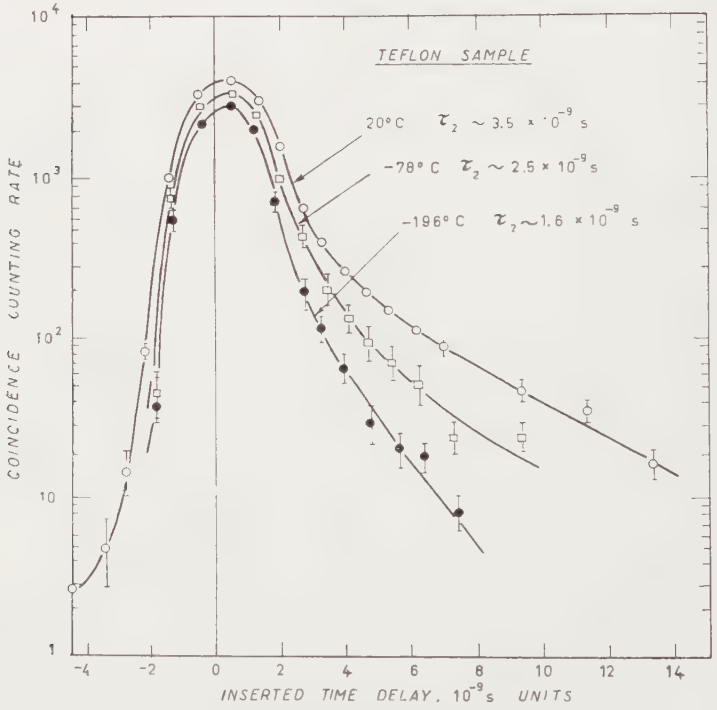
TEFLON SAMPLE
20° C $\tau_2 \sim 3.5 \times 10^{-9}$ s
-78° C $\tau_2 \sim 2.5 \times 10^{-9}$ s
-196° C $\tau_2 \sim 1.6 \times 10^{-9}$ s
COINCIDENCE COUNTING RATE
INSERTED TIME DELAY, 10^{-9} s UNITS

Fig. 14. – Delay curves showing the two positron mean lives in Teflon, and their temperature dependence. [From R. E. Bell and R. L. Graham: *Phys. Rev.*, **90**, 644 (1953)].

The positron decay curves in several insulators, also measured by Bell and Graham, show a complex structure, corresponding to two different mean lives (Fig. 14): one, τ_1, of the order of 10^{-10} s, and the other, τ_2, of the order of 10^{-9} s. When present, this second mean life accounts for $\approx 30\%$ of the

([54]) W. E. Millet: *Phys. Rev.*, **94**, 809 (1954).
([55]) H. Talley and R. Stump: *Phys. Rev.*, **94**, 809 (1954); **96**, 904 (1954).
([56]) E. Madanski: personal communication.
([57]) R. Stump: *Phys. Rev.*, **100**, 1256 (1955).

annihilations. As a typical example, τ_2 is not found in crystal quartz, but is present with 30% abundance in fused quartz. The value of τ_2 depends on the substance, and, for a given substance, increases with temperature (from $(1.6 \pm 0.4)\cdot 10^{-9}$ s in Teflon at $-196°$ to $(3.5 \pm 0.4)\cdot 10^{-9}$ s for Teflon at 200°).

The authors remark that a connection seems to exist between regularity of structure and shortness of τ_2. They suggest that the two mean lives can be attributed to the presence of positronium (which may be possibly located in some irregularity of the lattice): τ_1, is, within errors, the parapositronium mean life, and τ_2 is interpreted as the mean life of the ortho state in the solid. The value of τ_2 measures the rapidity of triplet to singlet conversion in collision with the lattice structure.

Though some details remain to be explained (such as the temperature dependence of τ_2) the existence of positronium in the substances exhibiting the second mean life seems well established since it is confirmed by the angular correlation measurements, and by the abundance of three-quantum annihilations (see next section).

3·5. *Three Quantum Annihilation Rates.* – The number of triplet annihilations in solids has been studied experimentally by the direct measurement of triple coincidences. The triple coincidence rate is found the same for all conductors. The experimental determination of the ratio of triplet to singlet annihilations is difficult since it involves the knowledge of source intensity and counter efficiency. The various attempts made ([58,29,59]) agree with the theoretical value 1/372 (see (11)) within experimental errors.

In the insulators which exhibit the second mean life, the three-quantum annihilation rate is greater ([60]). In Teflon, it decreases when the temperature is lowered showing a correlation with the peakedness of the angular distribution and with the value of the second mean life. A similar behavior is found in water, glycerine, and methyl alcohol ([61]), while no temperature effect was found in a metal (zinc) ([62]).

The results obtained with the three experimental methods used thus far (angular correlation, mean lives, and triple coincidences) help in building a picture of the behavior of slow positrons in solids. Though this picture cannot always be interpreted in a simple manner, these studies have proven that the positron is a simple probe, which can easily be introduced in solid matter, and which sends signals, in the form of annihilation radiation, conveying

([58]) J. A. Rich: *Phys. Rev.*, **81**, 140 (1951).
([59]) J. K. Basson: *Phys. Rev.*, **96**, 691 (1954).
([60]) R. L. Graham and A. T. Stewart: *Can. Journ. Phys.*, **32**, 678 (1954).
([61]) R. T. Wagner and F. L. Hereford: *Phys. Rev.*, **99**, 593 (1955).
([62]) R. T. Wagner and F. L. Hereford: *Phys. Rev.*, **99**, 665 (1955).

information on the nature of the medium where it is located. Some of the results agree easily with the previous knowledge of this medium, others seem more difficult to interpret and open new problems. It seems established, however, that positron techniques are useful in the study of solid state.

CHAPTER II

Mesonic Atoms

1. – μ-Mesonic Atoms.

1·1. *The formation of mesonic atoms.* – Atomic systems containing mesons were first considered in the discussion of the classical experiment of CONVERSI, PANCINI and PICCIONI [63] on the capture of the μ-mesons by nuclei. Before this experiment, it was known that about 50% of the μ-mesons stopping in heavy materials decayed with a mean life of $\approx 2\ \mu$s giving rise to energetic electrons. It was inferred that the mesons decaying in this manner were those of positive sign, and that the negative mesons were captured by nuclei in a time much shorter than 10^{-6} s. The experiment of CONVERSI, PANCINI and PICCIONI was performed in order to verify this assumption. The result was that in heavy elements, such as Fe, the positive mesons did not undergo radioactive decay, as if they were indeed captured by nuclei; but, in light elements, such as C, the meson decay occurred apparently unaffected by the presence of nuclei.

This fact could be interpreted in one of the two following ways:

a) the mesons did not reach the proximity of the nucleus in a time comparable to their own mean life;

b) the mesons did not interact with nuclei as strongly as one had assumed.

The question thus opened was of the greatest importance being equivalent to ask whether the meson which had been discovered in the cosmic radiation could be identified with the one predicted by Yukawa as a quantum of the nuclear force field.

To answer this question the mechanism of approach of a meson to a nucleus was treated theoretically by FERMI and TELLER [64] in a paper which can be considered as an investigation on the formation of mesonic atoms.

---

[63] M. CONVERSI, E. PANCINI and O. PICCIONI: *Phys. Rev.*, **71**, 209 (1947).
[64] E. FERMI and E. TELLER: *Phys. Rev.*, **72**, 399 (1947).

FERMI and TELLER discuss the energy loss of a negative meson near and after the end of its ionized range. They observe that when the meson velocity has been reduced to a value of the same order as that of the valence electron (meson energy $\approx 2\,000$ V), the usual formalism of ionization-excitation losses is no more valid. For the discussion, the further energy degradation is divided in steps. In the first step the energy is reduced from 2 000 V to 0, in a time of $2.6 \cdot 10^{-14}$ s for graphite, $2.2 \cdot 10^{-14}$ s for iron. After this the meson energy becomes negative. The meson is bound to an atom, and approaches the nucleus, traversing freely the electronic orbits since the exclusion principle does not apply to this extraneous particle. Down to a radius $r_1 = (m/\mu)^{\frac{1}{3}} r_k = 0.17\ r_k$ (r_k is the radius of the electronic K shell and $0.17 r_k$ corresponds to a mesonic orbit of total quantum number ≈ 6) the energy loss can be computed considering the energy transferred by the meson to an atomic cloud of degenerate electron gas. From $r_1 = 0.17 r_k$ to $r_2 = 4.5 \cdot 10^{-11}\ Z^{-5/21}$ cm (corresponding to a mesonic orbit of total quantum number $\approx 1.4 Z^{0.38}$) the mechanism of energy transfer to the atomic electrons is more properly described as an Auger effect. And finally, for $r < r_2$, in the last quantic jumps, the predominant mechanism of energy loss in the emission of electromagnetic radiation which emerges as such from the atom (mesonic X-rays).

The total time for reaching the K mesonic shell starting from 2 000 eV is evaluated as $9.2 \cdot 10^{-14}$ s for C, and as $6.1 \cdot 10^{-14}$ s for Fe. This result shows that the observed radioactive decay of the meson in C cannot be explained assuming that the mesons do not approach the nucleus with sufficient speed. Thus, the mesons originally discovered in cosmic rays do not interact strongly with nuclei and cannot be identified with Yukawa particles.

These mesons later received the name of μ-mesons. Soon afterwards, however, a meson of somewhat greater mass was discovered: it was called the π-meson, and it was found to interact strongly with nuclei, as YUKAWA has predicted for the nuclear force quanta.

Both μ- and π-mesons, of negative sign, form mesonic atoms according to the mechanism described by FERMI and TELLER. Some of the properties of these atoms will be described in what follows.

1·2. *Elementary Properties of Mesonic Atoms.* – The simplest evaluation of the energy and of the structure of mesonic atoms can be obtained by using the theory of Bohr and a hydrogen-like model. In this approximation, the energy of a mesonic state of total quantum number n, is given by

$$E_n = -\frac{\alpha^2}{2} \frac{Z^2}{n^2} \mu c^2 , \tag{23}$$

where μ is the meson mass. The radius of the corresponding trajectory is

$$a_n = \frac{n^2}{\alpha Z} \frac{\hbar}{\mu c} . \tag{24}$$

The energies involved are about 200 times greater than those of the corresponding atomic states, and the radii about 200 times smaller. The center of mass correction is much more important for mesons than for electrons, and for a quantitative evaluation, chiefly in light elements, μ has to be substituted by the reduced mass of the meson-nucleus system.

This evaluation of the energy is valid provided that the meson finds itself in a potential represented by Ze^2/r. In « electronic » atoms, the most important correction to the Coulomb potential is due to electron screening. This effect, however, is negligible for the first orbits of the mesonic atoms since the probability of finding K electrons within the K mesonic orbit is only $(m/\mu)^3 \approx 10^{-7}$.

An important correction to the simple Bohr estimate comes, instead, from the finite size of nuclei. Since nuclear radii are of the order of $(\hbar/\mu c)A^{\frac{1}{3}} \approx \approx (\hbar/\mu c)(2Z)^{\frac{1}{3}}$ the K mesonic Bohr orbit is within the nucleus if

$$\frac{1}{\alpha Z}\frac{\hbar}{\mu c} < \frac{\hbar}{\mu c}(2Z)^{\frac{1}{3}}, \tag{25}$$

which is satisfied for $Z \gtrsim 30$. Thus, already for elements of medium atomic weight, the energy of the states must be computed considering that the electrostatic field in which the meson moves is due to a charge distribution of finite size.

Only the case of the μ-meson will be discussed in this section since this particle interacts very weakly with nucleons and its state of motion depends exclusively on the distribution of electric charge. The case of π-mesons, where the effect of specific nuclear forces is important, will be discussed later.

A theoretical investigation of the properties of μ mesonic atoms was undertaken by WHEELER ([65]). If nuclei are assumed to be spheres of constant charge density, the potential within the nucleus varies with the second power of the radius as for an oscillator. For small Z, the effect of the finite nuclear size can be treated as a small perturbation to the hydrogen-like levels; in the opposite case of Z very large, the position of the levels can be computed in first approximation from the oscillator potential, and the Ze^2/r dependence outside the nucleus is treated as a perturbation. At the limit $Z \to \infty$ the force constant of the oscillator potential is $Ze^2/R^3 \approx (8Ze^2/A)(mc^2/e^2)^3$ and gives rise to equally spaced levels separated by ≈ 8.7 MeV (for Z/A the same as for heavy nuclei).

Even for the heaviest nuclei the pure oscillator potential is a poor approximation and WHEELER computed the energy by numerical integration of the Klein-Gordon equation (the spin of the μ-meson was not yet known). For Pb the binding energy of the K shell, which would be 21 MeV for a point nucleus, is reduced to 9.56 MeV for a nuclear radius of $8.3 \cdot 10^{-13}$ cm; a change

([65]) J. A. WHEELER: *Rev. Mod. Phys.*, **21**, 133 (1949).

of 53 keV in the binding energy of this state is expected for a 1% change in the nuclear radius.

These theoretical estimates pointed out the interest of measuring the spectra of μ mesonic X-rays for the experimental determination of nuclear radii.

The intensity of the X-rays lines depends upon the competition between radioactive transitions and Auger effects. The probability for emission of dipolar electromagnetic radiations w_r is proportional to the third power of the energy and to the square of the size of the dipole. Thus its dependence on μ and Z is $(\mu Z^2)^3(\mu Z)^{-2} = \mu Z^4$. The transition probability w_H computed for the corresponding lines of the usual hydrogen atom ([66]) can be used directly after multiplication by these factors. Thus we can write

$$w_r = \frac{\mu Z^4}{m} w_H . \tag{26}$$

The Auger probabilities, instead, are, for a given change in quantum numbers, nearly independent of Z. For their evaluation, one can make use, in a good approximation, of the formulae and of the computations of conversion electron coefficients, since the mesonic orbits — like the nucleus — are very small compared to the orbits of the electrons. Accurate calculations specifically developed for the mesonic atoms, are however, available ([67]).

As anticipated by FERMI and TELLER, the fluorescent yield of a given line increases with Z; X-ray lines of the K series should be radiated for all elements while those of the L, M, and higher series will be missing for the lower atomic numbers.

Once the μ-meson has reached the ground state of the atom, it remains in this state until captured by one of the nuclear protons according to the reaction:

$$p + \mu^- \rightarrow n + \nu . \tag{27}$$

The probability of this process is proportional to the number of nuclear protons, and may be assumed to depend directly on the density of the $1S$ mesonic wave function at the nucleus. Thus, for small Z, where the nuclear size correction is negligible, the capture probability w_c is proportional to Z^4. In general we can express it as

$$w_c = \text{const} \cdot \sum_{\text{all protons}} |\psi \text{ (at each proton)}|^2 . \tag{28}$$

This expression has been evaluated by Wheeler taking into account the effect

---

([66]) For a tabulation of w_H see for instance H. BETHE: *Handb. der Phys.*, **24**, **1**, p. 444.

([67]) G. R. BURBRIDGE and A. H. DEBORDE: *Phys. Rev.*, **89**, 189 (1953).

of the finite nuclear radius on φ. The results are expressed by introducing a quantity Z_{eff} such that

$$w_c = \frac{1}{\tau_0}\left(\frac{Z_{\text{eff}}}{Z_0}\right)^4 . \tag{29}$$

where τ_0 is the μ-meson mean life. Z^4_{eff} is a function of Z proportional to the computed Z dependence of the capture probability, and Z_0, to be determined from the experiment, is a constant which measures the strength of the interaction (27). For Z_{eff} WHEELER finds the numerical formula

$$Z_{\text{eff}} = Z[1 + (Z/37.2)^{1.54}]^{-1/1.54} . \tag{30}$$

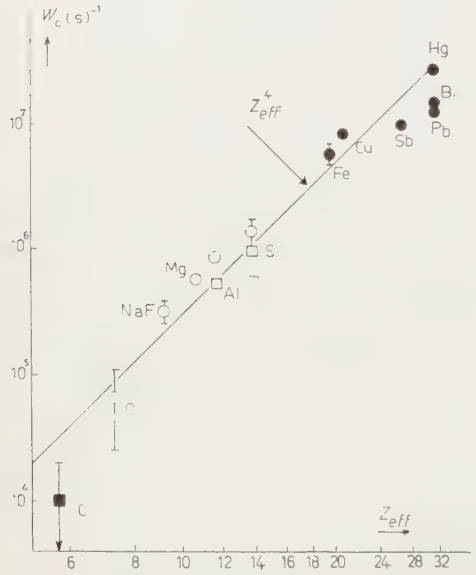

Fig. 15. – Values of w_c obtained from the experimental values of μ-mesonic mean lives by means of formula (31). Open circles from reference ([68]); squares from reference ([69]); full points from reference ([70]).

The mean life of a μ-meson in the ground state of an atom satisfies the relation:

$$\frac{1}{\tau_{1s}} = \frac{1}{\tau_0} + w_c = \frac{1}{\tau_0}[1 + (Z_{\text{eff}}/Z_0)^4]. \tag{31}$$

For $Z_{\text{eff}} = Z_0$, $\tau_{1s} = \tau_0/2$.

1·3. *Experiments on the Mean Life of μ-Mesonic Atoms.* – After the experiment of CONVERSI, PANCINI and PICCIONI, it became of interest to study the mean life of negative mesons in different substances in order to obtain the strength of the interaction (27) between μ-meson and nucleons and to verify the formation of mesonic atoms (revealed by the Z^4_{eff} dependence of the capture probability).

TICHO ([68]) measured the mean lives of μ-mesons in H_2O, NaF, Mg, Al, S with the results of Fig. 15. The Z dependence of the capture probabilities obtained from this experiment corresponds to the power 3.7 ± 0.85. The value of the constant Z_0 is near to 11.

([68]) H. K. TICHO: *Phys. Rev.*, **74**, 1337 (1948).

([69]) A. ALBERIGI-QUARANTA and E. PANCINI: *Nuovo Cimento*, **11**, 607 (1954).

([70]) J. W. KEUFFEL, F. B. HARRISON, T. N. K. GODFREY and G. T. REYNOLDS: *Phys. Rev.*, **87**, 942 (1952).

These results were recently verified by ALBERIGI-QUARANTA and PANCINI [69] who measured the mean lives in Al, C, S, and found a (3.8 ± 0.5) power of Z, and a Z_{eff} of 11.1. Both these experiments were performed with Geiger counters.

For heavier atomic numbers the measurement of μ-meson mean life becomes difficult for two reasons, *a*) the mean life becomes so short that the random delays in the firing of Geiger counters interfere with its observation; *b*) the number of delayed decay electrons decreases since most of the mesons are captured by the nuclei.

These difficulties have been circumvented in the work of KEUFFEL, HARRISON, GODFREY and REYNOLDS [70]. These authors have made use of large scintillation counters in the place of Geiger counters. They measure the meson life by observing the time between its arrival and its capture, revealed by the emission of nuclear γ-rays. The experimental arrangement is shown in Fig. 16. Here the arrival of the meson is revealed by a $A + S_1$ coincidence, its stopping in the target by a $A + S_1 - X$ anticoincidence; a $A + S_1 - X + S_2$ pulse can be due, among other things, to electromagnetic radiation emitted when the meson is captured by a target nucleus; and finally a $(A + S_1 - X) + S_2$ delayed coincidence measures (presumably) the meson survival time. The delayed coincidences were measured with a chronotron described in ChapterIII. The interpretation of the data is complicated by the presence of delayed coincidences due to other effects such as: bremsstrahlung from μ^- decay electrons (mean life 2.2 μs); neutrons produced by protons stopping in the target and detected in S_2 with a delay due to their time of flight (delays always smaller than 0.032 μs); random delays (uniformly distributed in time). When the measured delay curves are corrected for these effects, one obtains the results of Fig. 15. These show a Z_{eff}^4 dependence up to Cu ($Z = 29$; $Z_{\text{eff}} = 20.6$) but indicate mean lives considerably shorter than predicted by the Z_{eff}^4 law for the heavy elements.

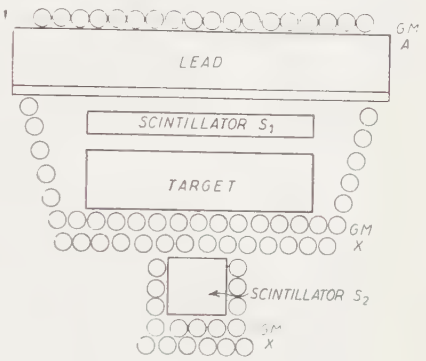

Fig. 16. – Apparatus for the measurement of mean lives of heavy μ-mesonic atoms. [From J. W. KEUFFEL, F. B. HARRISON, T. N. K. GODFREY and G. T. REYNOLDS: *Phys. Rev.*, **87**, 942 (1952)].

These results were discussed theoretically by KENNEDY [71], who pointed out the possible influence of detailed nuclear effects, such as shell structure, on the value of the mean life. It appears from these considerations that a

[71] J. M. KENNEDY: *Phys. Rev.*, **87**, 953 (1952).

more complete experimental study, involving a larger number of elements, and possibly an artificial source of mesons, is desirable.

1·4. *Measurement of Nuclear Radii from μ-Mesonic X-Rays.* – The first evidence of electrons produced by X-rays from the μ mesonic atom of Pb was obtained in cloud chamber pictures by CHANG in 1949 ([72]). In an experiment performed with scintillation counters BUTEMONT ([73]) was able to detect the *K* line of μ mesonic carbon using cosmic rays as a source of mesons. The Auger electrons from μ-mesonic atoms have been observed in photographic emulsions ([74,75]) and were studied semi-quantitatively.

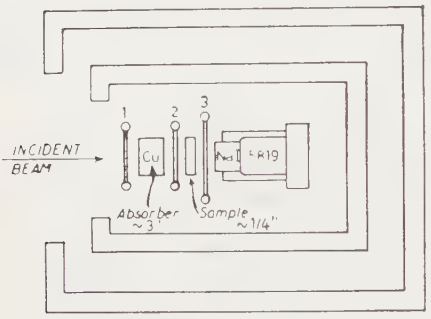

Fig. 17. – Apparatus for the measurement of X-rays from μ-mesonic atoms. [From V. L. FITCH and J. RAINWATER: *Phys. Rev.*, **92**, 789 (1953)].

But the first accurate measurements of μ-meson X-ray energies are due to FITCH and RAINWATER ([76]), who used electronic techniques and a meson beam from the Columbia University synchro-cyclotron at Nevis.

The negative mesons, emerging from a target bombarded by 385 MeV protons are focussed with magnets and collimated through a channel in the cyclotron shielding wall. In this manner, a parallel beam is obtained, containing 90% π-mesons, 10% μ-mesons, and a few per cent electron contamination. The momentum of all these particles is the same, and their energy corresponds to 115 MeV, 130 MeV and 214 MeV respectively. The range of the μ-meson is somewhat greater than that of the π-mesons: the pions are stopped in a Cu absorber (Fig. 17), while the muons penetrate the Cu, and are brought to rest in a sample of the element whose X-rays one wants to study. It was verified that in a C sample the μ-mesons decay with their characteristic mean life.

Four scintillation counters were used for the study of the X-rays. Of these, 1, 2 and 3 were fast organic counters and 4 a NaI crystal. 1 and 2 responded in coincidence to the particle traversing the Cu absorber; the anticoincidences $1 + 2 - 3$ revealed a particle stopped in the sample; a $1 + 2 - 3 + 4$ pulse

([72]) W. Y. CHANG: *Rev. Mod. Phys.*, **21**, 166 (1949).
([73]) F. D. S. BUTEMONT: *Phil. Mag.*, **44**, 208 (1953).
([74]) COSYNS, C. DILWORTH, G. P. S. OCCHIALINI, SHOENBERG and PAGE: *Proc. Phys. Soc.*, A **62**, 801 (1951).
([75]) W. F. FRY: *Phys. Rev.*, **83**, 594 (1951).
([76]) V. L. FITCH and J. RAINWATER: *Phys. Rev.*, **92**, 789 (1953).

announced a non-ionizing radiation, detected in NaI, and coincident with a μ-meson stopped in the sample. For each $1+2-3+4$ event the height of the pulse in 4 was analyzed with a multichannel pulse height selector, in order to obtain the X-ray spectrum.

As a guide in the interpretation of the results the energy of the terms was recomputed taking into account the more recent data for the μ-meson mass

TABLE I. *Energies of μ mesonic orbits in* MeV *computed for* $\mu = 210\ m_e$.

Z	Dirac Energies $R=0$			Dirac Energies $R = 1.3\cdot10^{-13}\ A^{\frac{1}{3}}$ cm		
	$E(1s)$	$2p_{\frac{3}{2}} \to 1s$	$2p_{\frac{1}{2}} \to 1s$	$E(1s)$	$2p_{\frac{3}{2}} \to 1s$	$2p_{\frac{1}{2}} \to 1s$
13	0.4849	0.3631	3.628	—	—	—
22	1.3917	1.0455	1.0432	1.282	0.935	0.933
29	2.4300	1.8277	1.8208	2.12	1.52	1.51
51	7.7071	5.8332	5.7627	5.22	3.41	3.37
82	21.328	16.414	15.857	10.11	5.48	5.30

($\mu = 210\ m_e$ was used) and the spin $\frac{1}{2}$ of this particle. The energies obtained using Dirac equation are reported in Table I for $R = 0$, and $R = 1.3A^{\frac{1}{3}}\ 10^{-13}$ cm. It is seen from this Table that the effect of the finite nuclear radius is expected to reduce the energy of the K transition in Pb from ≈ 16 to ≈ 5 MeV; in the same element the splitting between the $2p_{\frac{1}{2}} \to 1s$ and the $2p_{\frac{3}{2}} \to 1s$ transitions computed for a purely Dirac magnetic moment of the μ-meson is about 200 keV.

The experimental investigation covered the K lines of a number of elements, (Fig. 18), ranging in Z from 13 (Al) to 83 (Bi). For the light elements the pulse height distribution shows simple photopeaks, and the effect of finite nuclear radius is relatively small. In the heavy elements where the K line has an energy of several MeV, the NaI counter responds mostly through pair production, and each X-ray line gives rise to a multiple peak, whose structure depends on the escape of the positron annihilation radiation. The shape of these peaks has to be interpreted in order to obtain the effects of the nuclear radius and of the fine structure splitting.

In order to analyze the pulse height distributions, FITCH and RAINWATER compared them with similar curves obtained from γ-rays of known energy. The γ-rays from ^{24}Na (1.38 and 2.76 MeV), and from $^{12}C^*$ (4.43 MeV from the reaction $^4He - {}^9Be \to {}^{12}C^* - n$) were used for the comparison. Experiments with the $^{12}C^*$ γ-rays showed that the highest peak in the distribution corresponds to the γ-energy minus $2mc^2$ (the two annihilation quanta having escaped from the NaI). The curves of the meson X-rays of Pb are accordingly interpreted assuming that the highest peak corresponds to the energy of the $2p_{\frac{1}{2}} \to 1s$

transitions, minus $2mc^2$. It was found in this manner that the $2p_{\frac{3}{2}} - 1s$ energy in Pb is 6 MeV. Comparison with Table I shows that the Pb nucleus is smaller than predicted for $r_0 = 1.3 \cdot 10^{-13}$ cm. The values of r_0 obtained from the μ mesonic X-rays in Pb and other elements are shown in Table II. It is seen that $r_0 = 1.2 \cdot 10^{-13}$ cm accounts for the results in all cases.

These results verify the constant density of nuclear matter, and agree with the data obtained by electron scattering. A more detailed discussion of nuclear radii can be found in the lecture by Dr. COOPER.

The pulse height distribution curves of Pb and other heavy elements, were also used in an attempt to measure the magnetic moment of the μ-meson. Some indications of a fine structure splitting in agreement with Dirac theory

TABLE II. – *Measured energies (in* MeV*) and corresponding values of* r_0*, for* $\mu = 210\ m_e$.

Z	$E(2p_{\frac{3}{2}} \to 1s)$	r_0
22	0.955	1.17
29	1.55	1.21
51	3.50	1.22
82	6.02	1.17

were found, but the interpretation of the curves is not unambiguous. Though all conclusions are presented as «tentative» by the authors, one can state that no disagreement is found with the assumption that the magnetic moment of the meson has the Dirac value $e\hbar/2\mu c$.

1·5. *Other Effects on* μ*-Mesonic* X*-Rays.* – The success of the experiments on the X-rays from μ-mesonic atoms has attracted to the problem the renewed interest of the theorists. COOPER and HENLEY ([77]), after discussing the effect of nuclear size, meson mass, spin and magnetic moment on the energy of the terms, pass to the evaluation of other corrections to the energy levels. Among these they consider the discretness of the charge distribution (contributing less than 0.1% even in heavy nuclei), the radial variation in nuclear charge density, the nuclear quadrupole splitting (of the same order as the fine structure splitting for heavy nuclei with large quadrupole moments) and the effect of nuclear polarization (estimated to 1% of the $2p \to 1s$ transition in Pb). Essentially the same effects are discussed in an article by WHEELER ([78]) who points out that μ-mesons can be used as a nuclear probe particle and that accurate mea-

([77]) L. N. COOPER and E. M. HENLEY: *Phys. Rev.*, **92**, 801 (1953).
([78]) J. A. WHEELER: *Phys. Rev.*, **92**, 812 (1953).

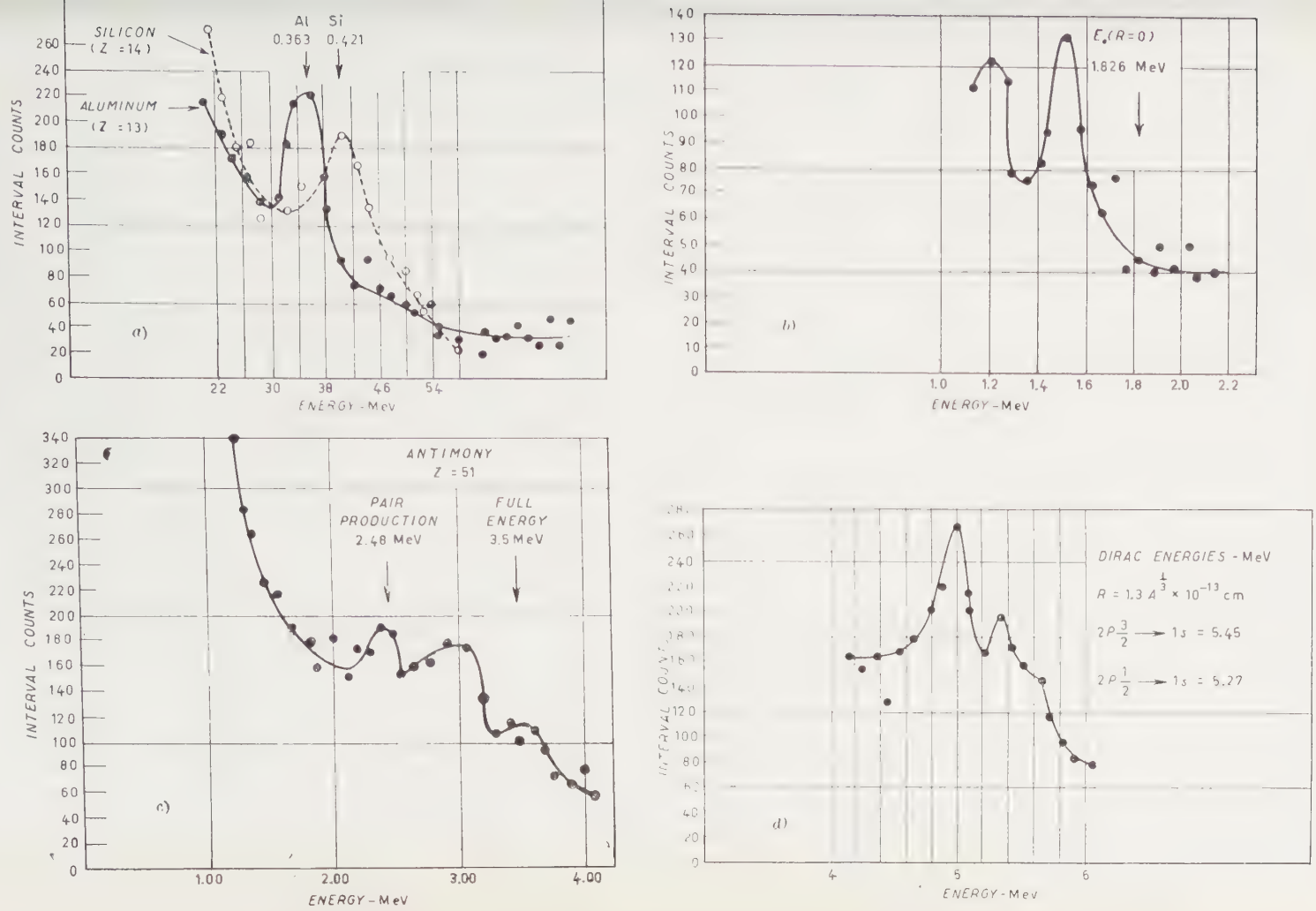

Fig. 18 *a*), *b*) *c*), *d*). – Typical scintillation spectra of μ-mesonic X-rays of the K series. [From V. L. Fitch and J. Rainwater: *Phys. Rev.*, **92**, 789 (1953)].

surements on μ-meson X-rays can give information on quadrupole moments, nuclear charge distribution, nuclear polarizability and compressibility. The effect of nuclear distortion was considered also by LAKIN and KOHN ([79]) who estimate a shift of (16 ± 9) keV for $Z = 80$. The detailed effect of nuclear size and charge distribution has been treated by HILL and FORD ([80]) who have computed electronically accurate values of the energy of the $1s$, $2s$, $2p$ and $3d$ states in Pb for various parameters describing the nuclear charge.

The nuclear fine structure effects form the subject of a paper by JACOBSOHN ([81]) who considers the admixture of nuclear levels produced by the quadrupole field of a μ-meson. In particularly favorable cases this effect should split a line into components separated of ≈ 100 keV, the amount of splitting depending on the quadrupole moment of the first excited nuclear state. The mixing of nuclear levels should also result in γ-rays following the $2p \rightarrow 1s$ transition.

The excitation of nuclear rotational states has been discussed by WILETS ([82]) who concludes that, for nuclei with large deformations, the $2p$ levels of the mesonic atoms should exhibit a splitting of size comparable to that of the mesonic fine structure.

Apart from the nuclear effects, one has also to consider the quantum electrodynamical corrections. Though none of the small nuclear effects has been as yet detected experimentally, some data exist on the quantum electrodynamical corrections to the mesonic levels. According to the theory ([83,84]) the self energy corrections, which depend on $1/\mu^2$, are negligible, but the vacuum polarization should increase the binding energy of some $0.1\,\%$ in light elements ($Z \approx 10$).

The energy of soft μ X-ray lines has been measured by the Columbia group ([85]) by comparison with the absorption edges of ordinary atoms. One finds in this manner that, for instance, the $2p \rightarrow 1s$ transition in C lies between the (electronic) K edges of elements 74 and 77; thus, the transition energy is less than 76.123 keV. From this experimental energy limit one can obtain a limit of the value of the meson mass: without taking into account vacuum polarization one has $\mu < 209.99\ m_e$, and, including vacuum polarization corrections, $\mu < 208.95\ m_e$. Both these values are in agreement with the Berkeley measurements which yield $\mu = (206.9 \pm 0.2)\ m_e$ ([86]).

([79]) W. LAKIN and W. KOHN: *Phys. Rev.*, **94**, 787 (1954).
([80]) D. L. HILL and K. W. FORD: *Phys. Rev.*, **94**, 1617 (1954).
([81]) B. A. JACOBSOHN: *Phys. Rev.*, **96**, 1637 (1954).
([82]) L. WILETS: *Dan. Mat. Fys. Medd.*, **29**, No. 3 (1954).
([83]) L. L. FOLDY and E. ERICKSEN: *Phys. Rev.*, **95**, 1048 (1954).
([84]) A. B. MICKELWAIT and H. C. CORBEN: *Phys. Rev.*, **96**, 1145 (1954).
([85]) S. KOSLOV, V. FITCH and J. RAINWATER: *Phys. Rev.*, **95**, 291 (1954).
([86]) W. H. BARKAS: personal communication.

However, when the same work is performed on the $3d \to 2p$ line of phosphorus the mass limits obtained are $\mu \sim 207.67\ m_e$ (no vacuum polarization) and $\mu \sim 206.89\ m_e$ (with vacuum polarization). The fact that the first limit disagrees with the Berkeley value, while the second is consistent with it, can be considered as evidence for the vacuum polarization effect.

In conclusion, one can state that more accurate measurements of μ mesonic X-ray energy are highly desirable and could be used to investigate several interesting points. However, the experimental techniques need to be considerably improved before one can hope to verify some of the theoretical predictions.

2. π-Mesonic Atoms.

2·1. *Problems Presented by π-Mesonic Atoms.* – The problems of the π-mesonic atoms are essentially different from those of the μ-mesonic atoms.

The negative pions interact so strongly with nuclei that, despite the shorter value of their mean life ($2.55 \cdot 10^{-10}$ s), they are captured by the nucleus (even in hydrogen) before having had time to decay in any appreciable amount. The problem of competition between decay and capture from the atomic ground state does not exist, the capture being always overwhelmingly more probable. The mean life of the $1s$ state is too short for a direct delayed coincidence measurement, and it could possibly be studied only through a measurement of width.

Another kind of competition, however, arises in these atoms: the competition between electromagnetic transitions and direct nuclear capture from excited states. We have seen that the radiative probability varies as Z^4 (26); if one assumes that the capture probability w_c varies as the number Z of nuclear protons, times the square of the wave function near the origin (the wave function is 0 at the origin for $l \neq 0$), one obtains, as a generalization of (28)

$$w_c \approx \text{const}\ Z^{2l+4}, \qquad (Z \text{ small}), \tag{31}$$

where l is the orbital angular momentum. Thus, the nuclear capture from excited states of a given n and $l > 0$ can overcome the emission of radiation for Z sufficiently large. Experimentally, this can be observed through the decrease with Z of the intensity of a given X-ray line. A first experimental problem, therefore, is the measurement of the X-ray intensities from various transitions (such as $2p \to 1s$, $3d \to 2p$, $4f \to 3d$) in different elements, in order to find the nuclear capture probability of the pion from the corresponding initial states (such as $2p$, $3d$, $4f$, etc.).

Intensity studies have shown that, as a consequence of nuclear capture

from the $2p$ state, the $2p \to 1s$ transition is completely suppressed for $Z > \approx 10$; because of nuclear capture from the $3d$ state the $3d \to 2p$ transition has negligible intensity for $Z > \approx 20$. Thus, for π-mesons, the energetic X-ray lines are missing and the nuclear radius effect is always a minor correction.

There is, however, another effect which may influence the energy of the lines. It is known that, in addition to the electrostatic interaction, there are short range forces acting between the nucleus and the π-meson. These « specifically nuclear » forces are responsible for the scattering of π-mesons by nucleons and can be expected to perturb the position of the energy terms of π-mesonic atoms. Investigations on the « specifically nuclear » shifts of the X-ray lines are interesting in connection with the fundamental problem of pion-nucleon interaction; they have provided information on the pion-nucleon interaction at 0 energy, where the scattering method cannot be used.

The theoretical and experimental work on these questions will be presented in the following sections.

2·2. *π-Mesonic Hydrogen and Deuterium.* – The capture of negative pions in hydrogen and deuterium, has been studied by Panofsky and co-workers ([87]) and their classical results have to be considered in any attempt of interpretation of heavier π-mesonic atoms.

The capture of pions at rest by hydrogen and deuterium, occurs only if the pions stop in the pure substances. Panofsky failed to find any hydrogen effect even in a light substance, such as LiH, where, according to the estimates of Fermi and Teller, $\frac{1}{4}$ of the pions should be captured in H. Presumably the reason for this behavior is that the pionic hydrogen atom is a small neutral body which is not bound to a fixed position by molecular forces. Even if formed in a substance like LiH, it would move to the vicinity of the heavier nucleus: here the meson would leave the proton and pass to the larger charge of the other nucleus.

When the negative pions are stopped in pure hydrogen the following reactions are observed with about equal frequency:

$$\begin{cases} \pi^- + \mathrm{p} \to \mathrm{n} + \gamma\,, & (\sim 50\%), \\ \pi^- + \mathrm{p} \to \mathrm{n} + \pi^0 \\ \qquad\qquad \hookrightarrow 2\gamma & (\sim 50\%). \end{cases} \tag{32}$$

It is obvious that non-radiative capture such as $\pi^- + \mathrm{p} \to \mathrm{n} + \text{Kin. En.}$ is not possible because of conservation of momentum. In the case of deuterium.

([87]) W. K. H. Panofsky, R. L. Aamodt and J. Hadley: *Phys. Rev.*, **81**, 565 (1951).

instead, two nucleons are left in the final state and non-radiative capture becomes possible: it is, indeed, the most frequent of the three possible processes, which are given below together with their intensities:

$$(33)\qquad \begin{cases} \pi^- + \mathrm{d} \to \mathrm{n} + \mathrm{n}\,, & (\approx 70\%), \\ \pi^- + \mathrm{d} \to \mathrm{n} + \mathrm{n} + \gamma\,, & (\approx 30\%), \\ \pi^- + \mathrm{d} \to \mathrm{n} + \mathrm{n} + \pi^0\,. & (\approx 0\%). \end{cases}$$

The first two of these reactions are probably the prototype of the nuclear capture process in heavier atoms where the capture of a π-meson is accompanied by the formation of a star.

From detailed balance comparison ([88]) with the cross section of the inverse, charge symmetrical reaction $\mathrm{p} + \mathrm{p} \to \mathrm{d} + \pi^+$ one concludes that the meson is the $2p$ state of pionic deuterium, and is captured by the nucleus at a rate of $0.94 \cdot 10^{10}\ \mathrm{s}^{-1}$. Since the radiation probability to the ground state is considerably larger ($17.2 \cdot 10^{10}\ \mathrm{s}^{-1}$) the meson reaches the $1s$ state before being captured. From these data one can estimate the capture probability from $2p$ states in heavier elements using (31) and (26). Thus one has

$$(34)\qquad \frac{w_c}{w_r} = 17 Z^{-2}\,.$$

This estimate would make $w_c = w_r$ for $Z \approx 4$.

Some improvements on these considerations ([89]) do not modify the main conclusion that nuclear capture should overcome radiative transition from the $2p$ state at some very low Z.

2·3. *Experimental Studies of π-Mesonic X-Ray Intensities.* – The first experiments on the X-rays from π-mesonic atoms were performed at the University of Rochester ([90]) with equipment similar to that described in the section about μ-mesonic X-rays. Using an absorber thickness to stop in the target the π-mesons, the pionic X-rays of the K series were found at roughly the expected energy for Be, C, O. The intensities reported are 0.13 ± 0.03 X-ray per meson stopped in C and 0.21 ± 0.07 X-ray per meson stopped in $\mathrm{H_2O}$.

This work was followed by experiments at the Carnegie Institute of Tech-

([88]) K. Brueckner, R. Serber and K. Watson: *Phys. Rev.*, **81**, 575 (1951).

([89]) A. M. L. Messiah and R. E. Marshak: *Phys. Rev.*, **88**, 678 (1952).

([90]) M. Camac, A. D. McGuire, J. B. Platt and H. J. Schulte: *Phys. Rev.*, **88**, 134 (1952).

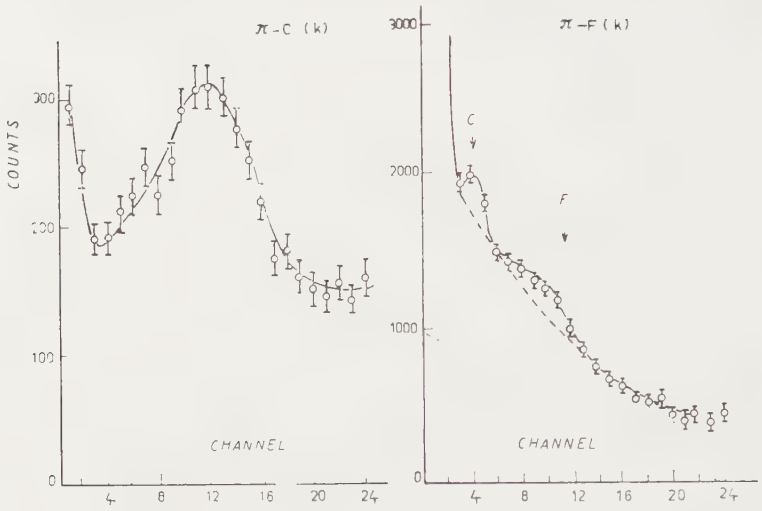

Fig. 19. – The curve at the left is the pulse height distribution for the K-line of pionic Carbon. The curve at the right is obtained with a sample of LiF. In this second curve a weak hump at the position expected for the fluorine K-line is noticeable; the small C peak is at the position of the Carbon K-line and is due to mesons stopping in the organic counters.

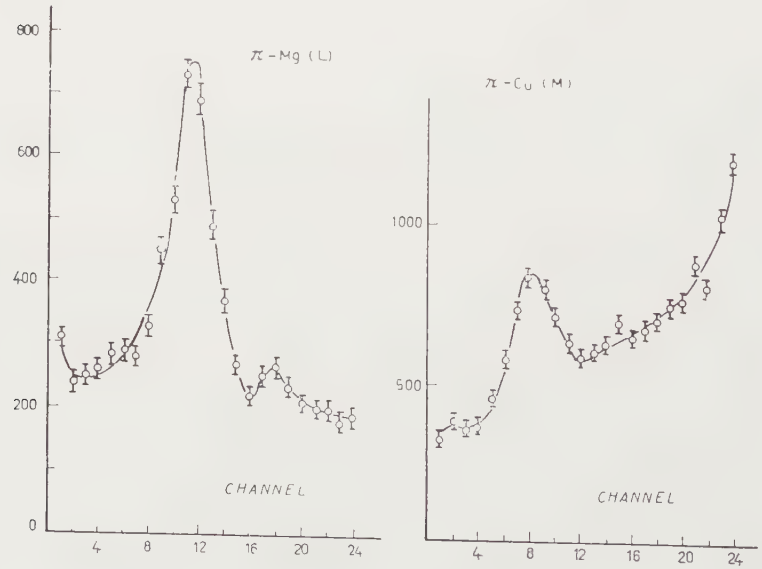

Fig. 20. – The L-line of pionic Magnesium (left) showing the main peak ($3 \rightarrow 2$) around channel 12 and a smaller peak (possibly $4 \rightarrow 2$) around channel 18. The M line of pionic Calcium (eight) around channel 8; the curve rises towards the L-line which lays beyond channel 24.

nology ([91]) which did not confirm the unexpected increase in intensity from C to O. In this work the relative intensities of the K lines were measured in Be, B, C, N, O and F (Fig. 19); furthermore, lines of the L series were observed and their intensity was measured in 14 different elements (Fig. 20) from $Z = 6$ to $Z = 23$. The results obtained are shown in Fig. 21. More recent data of the Rochester Group ([92,93]), shown in the same figure, agree with the general trend of the Carnegie Tech results. The Rochester work, which is a study of absolute yields, has been used to provide the scale of the ordinates in Fig. 21.

The measurements are performed by analyzing the pulse height selector curves obtained for a certain number of anticoincidence counts. The uncorrected relative yields are the ratio of the area under the photopeaks and the number of anticoincidences, which is assumed to correspond to the mesons stopped in the target. The main error in the determination of the photopeak area is probably due to the subtraction of background. A number of corrections are needed to obtain the relative yields. These include a correction for the absorption of the X-rays, and one for the energy dependence of the detection efficiency. An absolute value of the detection efficiency is needed for the absolute yields.

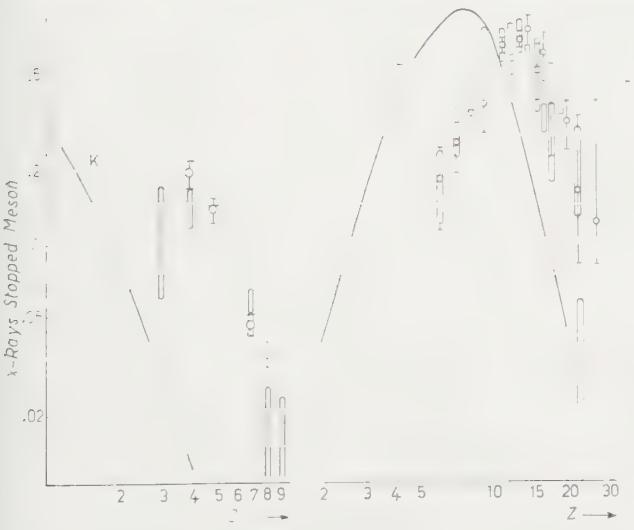

Fig. 21. – Intensity of mesonic X-rays of the K and L series. Elongated points from reference ([91]); round points with errors from reference ([92]) and ([93]). Curves from formulae (35) and (36) with $\tau_N = \tau_\pi$.

Though some uncertainty may be left in the details, the main facts can be expressed as follows: the K series is weak (yield $\lesssim 10\%$) in all the elements studied, probably because the absorption from the $2p$ state is large compared to the radiative transition probability even in Li, the lightest of the elements tried; the L se-

([91]) M. B. Stearns, S. DeBenedetti, M. Stearns and L. Leipuner: *Phys. Rev.*, **93**, 1123 (1954).

([92]) M. Camac, A. D. McGuire, J. B. Platt and H. J. Schulte: *Phys. Rev.*, **99**, 897 (1955).

([93]) M. Camac, M. L. Halbert and J. B. Platt: *Phys. Rev.*, **99**, 905 (1955).

ries increases in intensity with Z in the light elements, reaches a maximum (with yield around 100%) for $Z \approx 10$, and then decreases for $Z \approx 16$ due to nuclear capture from the $3d$ state.

2·4. *Interpretation of π-Meson X-Ray Intensities.* – The X-ray yields can be expressed by the following relation

$$Y = P_i \frac{w_r}{w_r + w_A + w_c}, \tag{35}$$

where P_i expresses the probability that the meson reaches the initial state i; w_r is the probability for emission of radiation of the lines considered, while w_A and w_c are respectively the Auger and the nuclear capture probabilities from the initial state i. The value of w_r can be obtained from formula ([26]) and w_A has been computed by BURBRIDGE and DEBORDE ([67]).

The factor P_i depends on the previous history of the meson cascading from one level to another; one generally assumes for the last quantic jumps that $P_i = 1$ for $l = n - 1$, and $P_i = 0$ for all other states. The reason for this assumption is that the statistical weight of the states goes as $2l + 1$, and thus, no matter what model is made of the capture of the meson in the atom, only the orbits of highest angular momentum (circular orbits) are occupied after a sufficiently large number of transitions. The cascading can be studied in greater detail, assuming different initial conditions, and using the computed w_r and w_A to follow the branching in the successive steps. One verifies in this manner that the above estimate of the factor P_i cannot be too far from the truth.

If the meson approaches the nucleus going through the states with $l = n - 1$, the total quantum number n must change by one unit at the time. Thus only one line should be observed for each series. Experimentally, the K_α $(2p \to 1s)$ line accounts for $(80 \pm 5)\%$ of the K series intensity and the L_α $(3d \to 2p)$ for about the same fraction of the L intensity. These observations are not too strongly in disagreement with the simplified picture of cascading which we will accept for the continuation of this order of magnitude discussion.

It is now possible, in principle, to solve equation (35) in order to obtain a value of capture probability w_c for each line observed. The data, however, are affected by too much uncertainty to justify a detailed tabulation of capture probabilities, and we will try only to interpret the general trends. For this we will express the yields by means of a single parameter τ_N which we may call the «mean life of the meson in nuclear matter». τ_N is defined by

$$w_c = \frac{1}{\tau_N} \int_0^R \Psi\Psi^* 4\pi r^2 \, \mathrm{d}r \,. \tag{36}$$

The integral extends over the nuclear volume, and expresses the probability of finding the meson within the nucleus. If the meson were always within the nucleus, its mean life would be just τ_N.

In Fig. 21 one shows, together with the experimental yields, the curves computed from (35) and (36), for $\tau_N = \tau_\pi = \hbar/\mu c^2 = 4.7 \cdot 10^{-24}$ s (μ is here the mass of the π-meson). The comparison shows a similarity in the trends together with some definite discrepancies. The yields of the K series can be accounted for by assuming $\tau_N \approx 10\tau_\pi$ for $2p$ states. The disagreement between theory and experiment for low Z values in the L series is most disturbing since in this part of the curve the yields should depend exclusively upon electromagnetic effects (radiation and Auger). The decrease of the L yields for $Z > 15$ is interpreted as due to nuclear capture and requires a τ_N a few times larger than τ_π, for mesons in the $3d$ states.

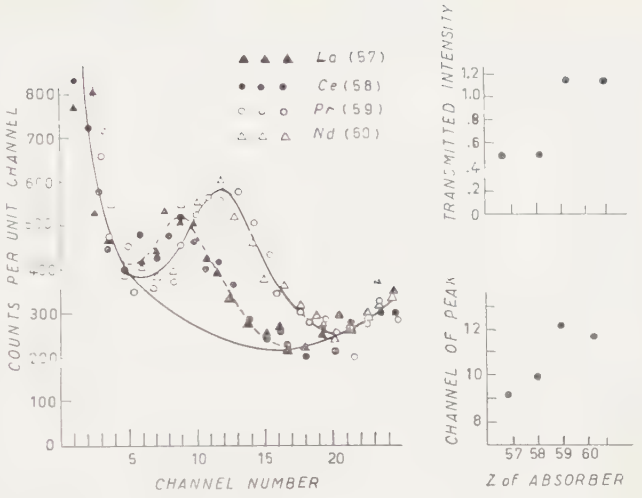

Fig. 22. – *a*) Critical absorption measurements on the M-line of π-mesonic phosphorus in La, Ce, Pr and Nd, providing a limiting value for the π^- mass.

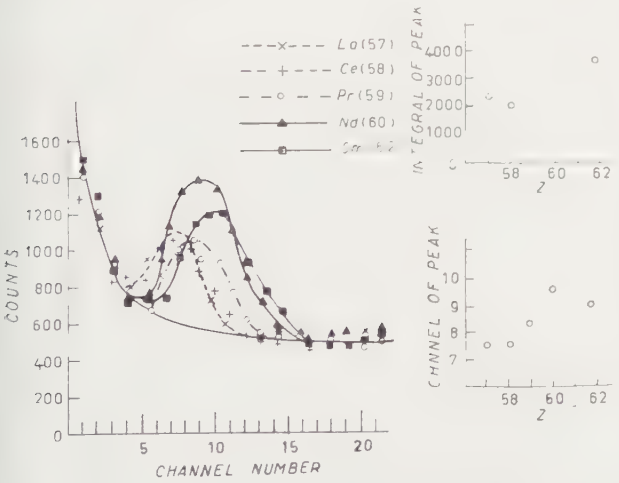

Fig. 22. – *b*) Critical absorption measurements of the K-line of Be in Nd, Sm, Pr, Ce, La, showing the « nuclear shift » of the line. (Reference (94) and (95)).

2·5. *The Measurement of the π-Meson Mass.* – Before proceeding to the ex-

(94) M. Stearns, M. B. Stearns, S. DeBenedetti and L. Leipuner: *Phys. Rev.*, **95**, 1353 (1954).

(95) M. B. Stearns, M. Stearns, S. DeBenedetti and L. Leipuner: *Phys. Rev.*, **69**, 804 (1954); **97**, 240 (1955).

perimental study of the « specifically nuclear » energy shifts, the mass of the π-meson was measured with the mesonic X-rays ([94]). A precise value of the pion mass, on which the π-Rydberg depends, was needed for the interpretation of all energy determinations; it was also advisable to check by means of a mass measurement the techniques to be used in the experiments on nuclear effects.

In order to study the mass of the meson it was necessary to use lines for which nuclear effects could be neglected. The lines of the M series ($4f \to 3d$ transitions) satisfy this requirement since they involve only states whose overlap with the nucleus is extremely small.

The technique of critical absorption was used for the measurement of the energy. In order to obtain a maximum accuracy in the mass determination the experiment was performed on lines whose energy was expected to be very close to an edge. Curves showing the transmission of the X-rays in successive elements are shown in Fig. 22*a*, and the comparison between theory and experiment is given in Table III. The result of the mass measurement is

$$272.2\ m_e \leqslant m_\pi \leqslant 273.6\ m_e\ . \tag{37}$$

TABLE III. – *Comparison of computed and experimental energies, and π-meson mass limits.*

	Line Studied	P $4f \to 3d$	Al $4f \to 3d$	K $4f \to 3d$
theoretical	Klein-Gordon energy (keV) (for $m_\pi = 272.5\ m_e$)	40.39	30.31	64.90
	Vacuum polarization correction (keV)	0.100	0.065	0.190
	Computed energy (keV)	40.49	30.37	65.09
experimental	Absorbers bracketing transmission discontinuity	Ce(58) Pr(59)	Sn(50) Sb(51)	Hf(72)
	K edges (keV)	40.45 42.00	29.19 30.49	65.35
	Meson mass limits	$\geqslant 272.2\ m_e$	$\leqslant 273.6\ m_e$	$\leqslant 273.6\ m_e$

2·6. *The Measurement of Nuclear Shifts of the K Lines.* – The energies of the K lines of the elements from Li to F have been studied at the Carnegie Institute of Technology ([95]). The energy was measured by comparison with that of lines presumably unaffected by specifically nuclear interaction effects (μ-me-

sonic lines, or π lines of the L and M series); for Li, Be and B the critical absorption method was also used (Fig. 22*b*).

In all cases investigated the energy of the π-K lines was found lower than expected from a computation by means of the Klein-Gordon equation and including vacuum polarization and finite nuclear size correction. The results are shown in Fig. 23.

Similar measurements were made at the University of Rochester ([92]) where negative shifts were also found. The energy was determined by comparison with X-rays from an artificial radioactive source; no critical absorption measurements were made. The results of the Rochester group agree within the stated errors with those of Carnegie Institute of Technology, with the exception of nitrogen; the reason for this discrepancy is not clear and is probably instrumental.

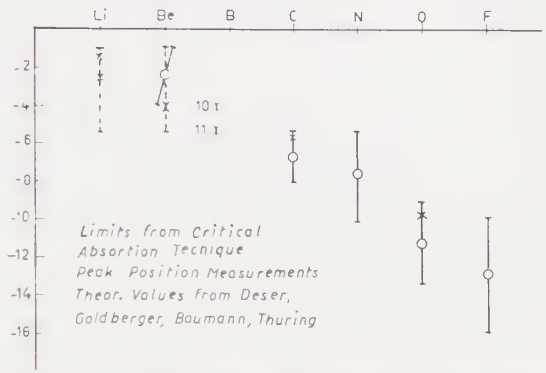

Fig. 23. Percentage difference between the observed energy of $2p \to 1s$ lines and the values computed in absence of « specifically nuclear » effect. [From M. B. Stearns, M. Stearns, S. DeBenedetti and L. Leipuner: *Phys. Rev.*, **97**, 240 (1955)].

The crosses in Fig. 23 represent the result of a theoretical calculation ([96]) based on a comparison with the scattering of pions by nucleons, in the assumption that the effects of the individual nucleons in a heavy nucleus are simply additive. According to this view, the scattering length a of a heavy nucleus is related to the scattering length of the neutron and of the proton by the simple formula

$$a = Na_n + Za_p .$$

In turn, according to charge independent symmetric meson theory, the scattering lengths of negative mesons by nucleons are given by

$$a_n = a_3 , \qquad a_p = \tfrac{2}{3}a_1 + \tfrac{1}{3}a_3 ,$$

where a_1 and a_3 are the nucleon-meson scattering lengths for isotopic spin $\frac{1}{2}$ and $\frac{3}{2}$ respectively. In the Born approximation the nuclear scattering length

---

([96]) S. Deser, M. L. Golberger, K. Baumann and W. Thirring: *Phys. Rev.*, **96**, 774 (1954).

corresponds to a δ-function potential

$$V = -\frac{2\pi\hbar^2}{\mu} a\,\delta(r) = -\frac{2\pi\hbar^2}{\mu}\left[Na_3 + Z\left(\frac{2a_1}{3} + \frac{a_3}{3}\right)\right]\delta(r)\,. \tag{38}$$

The energy shifts of the $1s$ state can now be computed as a perturbation du to this potential:

$$\Delta E = \int V\psi\psi^* 4\pi r^2 \mathrm{d}r = -|\psi(0)|^2 \frac{2\pi\hbar^2}{\mu} a\,. \tag{39}$$

Finally, remembering that $|\psi(0)|^2 = (1/\pi)(Z^3/r_0^3)$ where $r_0 = \hbar^2/\mu e^2$ is the meson's Bohr radius) and introducing the ionization potential of the pionic atoms $E = -Z^2e^2/2r_0$, one obtains for the fractional shift of the S level

$$\frac{\Delta E}{E} = \frac{4Z}{r_0} a = \frac{4Z}{r_0}\left(\frac{2}{3} Za_1 + \frac{3N + Z}{3} a_3\right)\,. \tag{40}$$

For $N = Z$ this expression reduces to:

$$\frac{\Delta E}{E} = \frac{8}{3}\frac{Z^2}{r_0}(a_1 + 2a_3)\,. \tag{41}$$

From these formulae the theoretical points of Fig. 23 are obtained using the values of a_1 and a_3 given by OREAR ([97]), namely $a_1 = 0.16$ and $a_3 = -0.11$, in units of the μ-meson Compton wave length $\hbar/\mu c$.

Vice-versa, one could obtain the value of $a_1 + 2a_3$ from the general trend of the observed energy shift. If the experimental determinations were much more accurate, they could be used to obtain a_1 and a_3 separately through ([40]).

The sign of the observed energy shifts agrees with the assignment of the sign of the scattering lengths, which was chosen arbitrarily before these experiments. The agreement between theoretical and experimental points is generally considered as a confirmation of the values of meson nucleon scattering phases at zero energy, which were previously obtained by extrapolation of higher energy scattering data.

Though the agreement between theory and experiment is encouraging, one cannot consider that the interpretation of the energy shifts in terms of elementary particles scattering phases is definitely proven to be correct. One should mention in this connection that an entirely different interpretation has been suggested ([98]), according to which the energy shifts are a higher order effect resulting from the capture of the π-mesons by nuclei.

([97]) J. OREAR: *Phys. Rev.*, **96**, 176 (1954).
([98]) K. A. BRUECKNER: *Phys. Rev.*, **98**, 769 (1955).

It is possible that both mechanisms contribute to the observed effect, but one has the impression that the contribution predicted from the scattering phases is more important since it agrees, within the rather large errors, with the experimental data. More accurate experimental results may allow to distinguish between the two interpretations. In this connection it would be interesting to measure the effect on two isotopes of the same element, in order to see whether the difference could be accounted for by adding the effect of the extra neutron. H and D would be the most interesting case, but their study presents great experimental difficulties because of the energy range of the K mesonic line, and of the smallness of the expected shifts. ^{10}B and ^{11}B seems a more hopeful possibility, though it may still lay beyond the limits of accuracy of the experimental techniques used thus far ([98a]).

Chapter III

Instrumentation.

The experimental work on the new atoms would not have been possible without the progress in instrumentation achieved in the last decade, after the introduction of scintillation counters. Kallmann's discovery of transparent scintillants was followed by a major change in the experimental techniques used in nuclear physics. In a modern laboratory the new scintillation counters have almost entirely replaced the Geiger counters because of their higher speed, greater efficiency for γ-rays, and energy-proportional response.

An exhaustive survey of the instrumentation in a modern nuclear physics laboratory is beyond the scope of these lectures. In the following pages we intend to review some of the experimental techniques used in the work on the new atoms. In the lectures, the information on the techniques was presented as part of the description of experimental work, but it has seemed more appropriate to collect the treatment of instrumentation as a separate part of these notes.

([98a]) After these notes had been prepared the energy of π-mesonic X-rays has been measured more accurately by D. West and E. F. Bradley [*Phyl. Mag.*, **8**, 1, 97 (1956)] who used a proportional counter as detector, and by M. Stearns and M. B. Stearns [*Phys. Rev.*, **103**, 1534 (1956)] who have improved the scintillation counter method. These last authors have measured the difference between ^{10}B and ^{11}B, and found it in agreement with the neutron (isotopic spin triplet) scattering length.

The reader who is interested in a more complete treatment is referred to the many review articles and books on the subject ([99-103]).

1. – Scintillation Detectors for Fast Coincidences.

The techniques of scintillation counting is at least as old as nuclear physics since the very existence of the nucleus was proven by Rutherford's experiments on the scattering of α-particles, experiments which were performed by visual observation of scintillations on a ZnS screen. The use of the technique was limited by the fact that scintillating substances such as ZnS are not transparent to their own light and can therefore be used only in connection with radiations which lose a great amount of energy in a thin surface layer. After the introduction of the gas discharge counters, the method of scintillation counting was considered almost exclusively of historical interest, until the situation was reversed with the discovery of transparent scintillants.

The transparency of certain substances to their own fluorescent radiation is explained as follows. A molecule at thermal equilibrium is in its lowest electronic state, while excited rotational and vibrational states may be populated. The absorption of energy, either from a photon or from a fast charged particle, usually produces a transition to an excited electronic state; this transition is accompanied by a change in the effective potential between the nuclei which maintain their original position (Franck-Condon principle). After the transition the nuclei find themselves in the new potential, usually at a position far removed from the position of equilibrium. Before the molecule has had time to re-radiate the absorbed energy, the nuclei have adjusted themselves in the new potential, finding a vibrational-rotational level compatible with the prevailing temperature. In so doing they dissipate part of the absorbed energy, and the energy available for the fluorescent radiation is smaller than that required for the excitation of the molecule. The emission band of the substance is of longer wave length than the absorption band.

The behavior of substances such as naphthalene, anthracene and stilbene is explained in this manner. In order to account for the scintillating properties of mixtures of organic materials, one has to consider some mechanism of energy

([99]) R. K. Swank: *Ann. Rev. Nucl. Sci.*, **4**, 111 (1954).

([100]) J. B. Birks: *Scintillation Counters* (New York, 1953).

([101]) R. E. Bell: *Ann. Rev. Nucl. Sci.*, **4**, 93 (1954).

([102]) I. A. D. Lewis and F. H. Wells: *Millimicrosecond Pulse Techniques* (New York, 1954).

([103]) P. R. Bell: *The Scintillation Method*, pp. 133-164 in «*Beta and Gamma Ray Spectroscopy*», edited by K. Siegbahn (Amsterdam, 1955).

transfer within the substance. If, for instance, small amounts (one percent or even less) of anthracene are mixed to a naphthalene crystal ([101]) the spectrum emitted by the mixture is the anthracene spectrum. This shows that the energy travels through the crystal until it finds one of the molecules of lower excitation energy: this molecule becomes excited and eventually emits its own fluorescent spectrum. It seems that the energy propagates by means of migration of « excitons », rather than by emission and absorption of photons.

The phenomenon of energy transfer is used in liquid and plastic scintillants. In liquid scintillants a small amount of scintillating substance is dissolved in an appropriate solvent (for instance 5 g of p-terphenyl in one liter of toluene); some of the energy lost by the ionizing particles in the solvent is collected by the scintillant in solution and is transformed into photons. Similarly, the scintillating substance may be dissolved in a transparent plastic (for instance 36 g of p-terphenyl per liter of polystyrene) to obtain plastic scintillators.

If the scintillant in solution emits radiation of too short wave length, the excitation energy can be transferred to a « second solute » which radiates its own spectrum, of more convenient light. For instance, 3 g of terphenyl per liter of phenylcyclohexane, is a liquid scintillant having a maximum spectral emission at 3 350 Å; the addition of 0.01 g per liter of 1.6-diphenyl-1,3,5-hexatriene shifts the maximum of spectral emission to 4 500 Å, with improvement of multiplier response.

Transparent inorganic scintillants can also be made, by adding controlled amounts of impurities to an ionic crystal. The ionizing radiation may excite an electron to the conduction band, or form excitation waves. Thus the energy may be transferred to one of the impurity centers which becomes excited and emits an optical photon.

A fairly recent tabulation of the properties of various scintillators can be found in the paper by SWANK ([99]). Some of the data are reported in Table IV.

The most important factors in the selection of a scintillator for a coincidence experiment are the height and the duration of the pulse. The quantities tabulated are the pulse height relative to anthracene and the scintillation mean lives. The pulse height given is proportional to the integrated intensity $N = N_0 \int \exp[-t/\tau]\,dt$, while for very fast work the initial intensity $N_0 = N/\tau$ is more important. Though the integrated intensity of anthracene is the largest among the organic scintillators, the initial intensity is not: for terphenyl in toluene, whose pulse height is 35% of that of anthracene, the initial intensity is five times greater, since the mean life is 15 times shorter.

The average energy spent to produce a photon is of the order of 50 eV, for β-rays in anthracene, though the data of different authors vary from

---

([104]) E. J. BOWEN, E. MIKIEWICZ and F. W. SMITH: *Proc. Phys. Soc.*, A **62**, 26 (1949).

TABLE IV.

	Substance	Pulse Height (*)	Mean life of light emission	Wave length of Maximum emission
organic	Anthracene $C_{14}H_{10}$	100	$32 \cdot 10^{-9}$ s	4 400 Å
	Trans-stilbene $C_{14}H_{12}$	60	$6.4 \cdot 10^{-9}$ s	4 100 Å
liquids	5 g p-terphenyl per liter Toluene	35	$2.2 \cdot 10^{-9}$ s	3 550 Å
	3 g p-terphenyl per liter Phenylcyclohexane	27	$< 2.9 \cdot 10^{-9}$ s	3 350 Å
	Same, plus 0.01 g/l 1,6 diphenyl-1,3,5-hexatriene	35	$8.0 \cdot 10^{-9}$ s	4 500 Å
plastics	36 g p-terphenyl per liter Polystyrene.	28	$\leqslant 3.0 \cdot 10^{-9}$ s	3 550 Å
	Same, plus 0.2 g/l 1,1,4,4-tetraphenyl-1,3-butadiene .	39	$4 \cdot 10^{-9}$ s	4 450 Å
inorganic	NaI(Tl)	210	$250 \cdot 10^{-9}$ s	4 100 Å

(*) Integrated height output for β rays, relative to anthracene.

26 eV to 70 eV, probably due to the difficulty of obtaining samples of anthracene of the same purity. The corresponding initial pulse height in anthracene is 600 photons per μms per MeV, and in terphenyl in toluene 3 000 photons per μms per MeV.

The light pulses are viewed with a sensitive phototube which transforms them into electrical pulses. The electrical pulses are amplified through a process of electron multiplication within the phototube itself, which is then called a photomultiplier.

With proper optical design one can direct to the photocathode a large fraction of the scintillation light, provided one uses a multiplier whose cathode is deposited on the inside of the tube envelope (5819 type). For this the scintillant is cemented to the outside glass envelope with transparent cement, while the other faces are covered with reflecting or diffusing white materials. The efficiency in light collection is obviously much smaller in tubes like the 1P21, where the light has to traverse the evacuated region of the tube before reaching the photocathode.

For many applications it is convenient to locate the multiplier at some distance from the scintillant. This is necessary, for instance, when the scin-

tillant is in a magnetic field which would prevent the mechanism of electron multiplication. In this case one makes use of transparent plastic rods (« light pipes », optically joined to the scintillant and to the photomultiplier glass envelope), through which the light travels, being totally reflected at the surface. It has been proven ([105]) that no light is lost provided the light pipe and the photocathode have a cross sectional area at least as large as that of the scintillant.

However, the use of large samples, of multiple reflections, and of long light pipes is objectionable from the point of view of speed, because of the variations in the time of flight of photons travelling along different paths.

In a good phototube, about 10% of the photons reaching the photocathode produce photoelectrons. In general, the number of photoelectrons per photon depends on the spectrum of the scintillant and on the spectral response of the photocathode.

The efficiency of light collection and photoproduction does not affect only the pulse height, but also the time resolution. This is because the ultimate limitation to the resolving time is given by the fluctuation in the time of appearance of the first photoelectron at the photocathode. These fluctuations are obviously smaller when the total number of photoelectrons is large. Quantitatively ([106]) one can show that the fluctuation $\bar{t}$ (first moment about the mean) of the time of appearance of the first Q of N photoelectrons, is given by

$$\bar{t} = \frac{Q\tau}{N}\left\{1 + \frac{Q+1}{2N} + \ldots\right\}, \tag{42}$$

where τ has been previously defined.

The photoelectrons are directed towards a first positive dynode, out of which a larger number of secondary electrons emerge, until the pulse, conveniently amplified, is collected at the photomultiplier plate. Gains of the order of 10^6 are easily obtained in conventional multipliers provided with 9 or 10 dynodes.

The gain, however, is not obtained without further losses in time resolution. The process of multiplication takes a certain time, and this time is not the same for all electrons involved. The fluctuations in the multiplication time are estimated to $\approx 10^{-9}$s in tubes such as the 1P21, and to $\approx 5 \cdot 10^{-9}$ s in tubes such as the 5819, where the electrons have to travel a longer distance between the photocathode and the first dynode.

([105]) R. L. Garvin: *Rev. Sci. Inst.*, **23**, 755 (1952).
([106]) R. F. Post and L. I. Schiff: *Phys. Rev.*, **80**, 1113 (1950).

2. – Fast Coincidence Circuits.

Several circuits capable of determining the simultaneity between two ionizing events with an error of less than 10^{-9} s have been developed. These circuits are characterized by their extreme simplicity, since any added element decreases the speed of response.

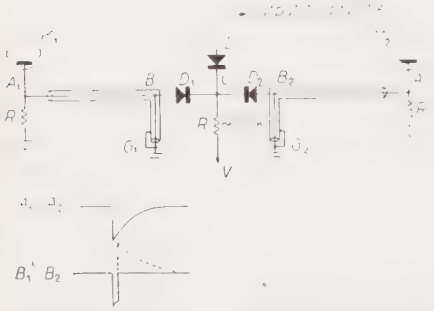

Fig. 24. Fast coincidence circuit of DeBenedetti and Richings [*Rev. Sci. Instr.*, **23**, 37 (1952)].

The positron mean lives in solids were first investigated with the circuit of Fig. 24, developed at the Carnegie Institute of Technology ([107]). Let us discuss the pulse shapes obtained in the specific case of an electron losing 500 kV in a fast scintillant, say terphenyl in toluene, viewed with a multiplier having a gain of $\approx 10^6$. Neglecting multiplier time straggling, the initial current at the anodes of the multipliers, is of the order of 10 mA, and decays with a time constant of $2.2 \cdot 10^{-9}$ s. This current goes to ground through a cable, and, in parallel, through its characteristic resistance R_0. If a 200 Ω cable is used the anode time constant is of the order of 10^{-9} s and the pulses raise to a maximum of the order of one volt. The pulses arrive at positions B_1 and B_2 after the time required for propagation in the cables A_1B_1 and A_2B_2. At a later time the reflection from the grounded ends of the cables G_1 and G_2 reach B_1 and B_2; these reflections are of sign opposite to that of the original pulse, and are delayed by twice the time of propagation in B_1G_1 and B_2G_2. In the ideal case of no time straggling the length of B_1G_1 and B_2G_2 limits the duration of the pulse at B_1.

After the pulses at B_1 and B_2 are shaped in this manner, the coincidences are selected by means of the three crystal diodes D_1, D_2 and D_3. D_1 and D_2 work as Rossi tubes. They conduct to ground (G_1 and G_2) the current produced by the negative voltage V in the resistance R.

If, to simplify the discussion, the diodes have a forward resistance $r \ll R$, and an infinite back resistance, the static voltage at C is $Vr/2R$. The parameters are chosen to make this voltage ≈ 0.1 V. When a negative pulse (0.1 V or larger) interrupts the current in one of the diodes the voltage raises with a time constant rC (C is the stray capacitance at point C) towards a maximum value Vr/R. If both diodes are cut off by simultaneous pulses the

([107]) S. DeBenedetti and H. Richings: *Rev. Sci. Inst.*, **23**, 37 (1952).

voltage at C starts rising with time constant RC towards the value V: the rise stops when one of the pulses ends, or when C has reached the voltage of the smaller pulse. Though the initial increase of the voltage at C is only a factor two greater for coincidences than for single counts, if the pulses last longer than RC ($\approx 10^{-10}$ s) and are higher than $Vr/2R$ ($\approx .1$ V), coincident pulses give much larger signals than single ones.

The third diode, D_3, has a rectifying action which prevents the addition of two pulses following each other within the rise time of the subsequent amplifier. Its non-linear behavior also helps in the selection of the coincidences.

This circuit works with pulses of the order of 1/10 of a volt: unlike circuits using vacuum tubes it can be used without preamplification and without using the multipliers at voltages higher than rated. Its efficiency depends on pulse height and resolving time, but it is probably 100% for pulses produced by 500 kV electrons. Tests with the annihilation radiation (to which organic counters respond with a continuous Compton spectrum) showed an efficiency of $\approx 50\%$ for a resolving time $\tau = 2 \cdot 10^{-9}$ s: a resolving time of 10^{-9} s was obtained for an efficiency of $\approx 30\%$.

The circuit used by BELL and GRAHAM [1] in their positron mean life work is described in a paper by BELL, GRAHAM and PETCH [108]. The resolving time of this circuit reaches the minimum possible value determined by the statistical fluctuations in the emission of the first photo-electron. This remarkable result is achieved by applying up to 2 400 V to a 1P21 tube; in such operating condition (which not all tubes are able to stand), the multiplication factor is at least 10^8 and a single photoelectron produces a pulse large enough (≈ 3 V) to cut off an ordinary vacuum tube.

The theoretical limit in resolving time depends on circuit efficiency; it can be defined as the time required for a 90% coincidence efficiency. This is the time required for a 95% probability of the appearance of the first photoelectron in both the photocathodes. Since $0.05 \approx \exp[-3]$, this time is $3\bar{t}$, where $\bar{t}$ is computed from formula (42) for $Q = 1$, and for the appropriate N. Thus the minimum resolving time depends on pulse height, and on the energy of the particles detected; if one assumes with BELL *et al.* $N = \frac{1}{3}$ photoelectrons per kilovolt in anthracene, one obtains the curve a and b of Fig. 25. In the same figure the line for terphenyl in toluene would probably be somewhat lower. The value of N could be made considerably greater if a multiplier having a photocathode on the glass envelope could be used without increasing the multiplier time straggling. In Fig. 25, curve c corresponds to the idealized case of terphenyl in toluene ($\tau = 2.2 \cdot 10^{-9}$ s), 100% light collection ($0.35 \cdot 20 = 7$ photons per kV) and 25% photoelectric efficiency (1.7 photoelectrons per kV).

---

[108] R. E. BELL, R. L. GRAHAM and H. E. PETCH: *Can. Journ. Phys.*, **30**, 35 (1952).

The operation of Bell's circuit is best understood from the simplified diagram and the wave forms of Fig. 26. The tubes V_1 and V_2 conduct 10 mA in static conditions; during the time of propagation of the pulse in L_2 they have an effective plate resistance of 25 Ω. A pulse at the anode of multiplier V_1 cuts off V_2 immediately (i.e., when the effects of the first photoelectron are felt at the anode). The current in V_2 is interrupted for $\approx 10^{-7}$ s, during which time the plate voltage would be decreased of 0.25 V. However, the pulse reflected from L_2, reestablishes the static plate voltage after twice the time of propagation in L_2. If tubes V_2 and V_3 are cut off simultaneously (within twice the propagation in L_2) the variation of voltage at the plate is greater. The diode V_5 is used as a nonlinear element which stresses the difference in pulse sizes.

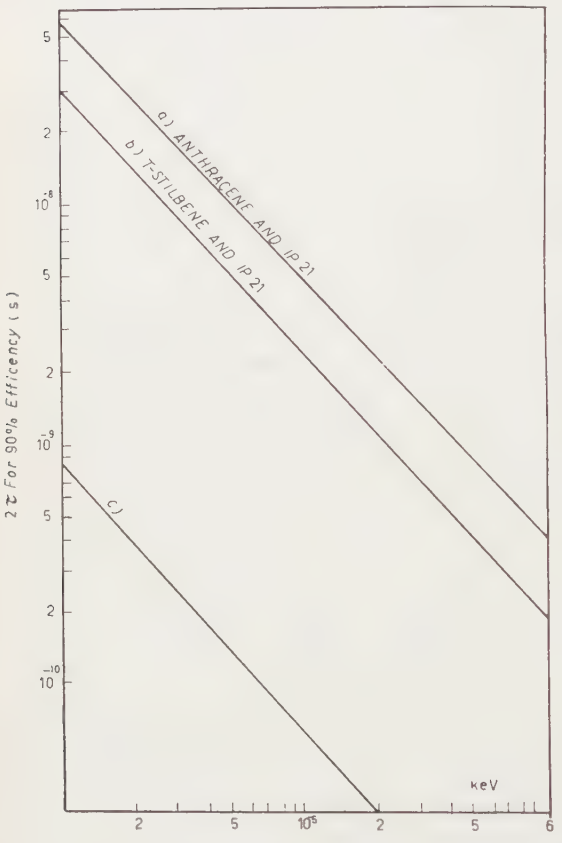

Fig. 25. – Minimum resolving times for 90% efficiency of coincidence apparatus curve *a*) and *b*) after Bell *et al.*, (reference ([108])); curve *c* refers to optimum conditions described in the text.

Fig. 27 shows the circuit with some of its auxiliary equipment. The 100 Ω cables on the plate circuit are used to control the delay between the two channels. With this circuit one reaches the theoretical limit of resolving time as shown in the curves *a* and *b* of Fig. 25.

The resolving time of a fast coincidence circuit is the error in the measurement of the time between two events, when this measurement is performed only once. For instance, if, in a rare cosmic ray event, the time of flight of a particle is measured, the error is given by the instrument resolving time. If, however, the measurement is repeated automatically many times, as in most cases where a radioactive source is used, the error in the time determination can be considerably smaller. In practice one measures the coincidence rate for different artificially introduced delays (coincidence curve) for the

events whose time difference one wants to study (delayed coincidence curve), and for events known to be simultaneous (prompt coincidence curve). If the simultaneous events have the same pulse height distribution as the ones to be measured, accuracy in time measurement is limited only by the statistical errors affecting the points in these curves. For instance, BELL *et al.* ([108]) find that the mean life of the 411 kV γ-rays of ^{198}Hg is $1 \cdot 10^{-11}$ s, with an error evaluated at $1.7 \cdot 10^{-11}$ s. The equal pulse height distributions for the comparison curves are easily achieved in the case of comparison of positron mean lives in different substances, since the energy of the radiations is always the same. For the measurement of mean lives of γ-rays of different energies, elaborate precautions are required. The absolute measurement of the mean life of positrons in solids was also performed by comparison; for details the paper by BELL and GRAHAM ([48]) should be consulted.

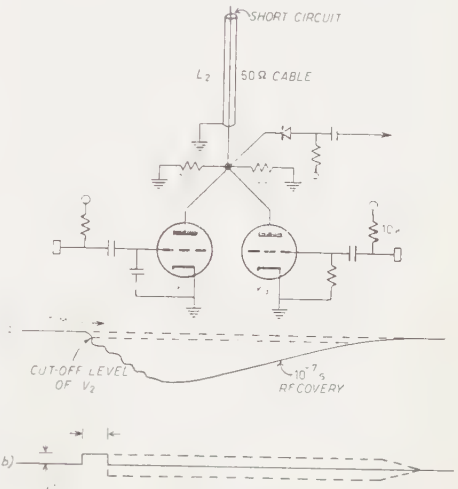

Fig. 26. – Simplified diagram of the circuit of BELL *et al.*, (reference ([108])) with wave forms showing a pulse at the grid (*a*) and at the plate (*b*) of V_2.

Once the curves to be compared are obtained in the proper conditions and with sufficiently small errors, the unknown mean life T is found using the fact that the centroid of the « delayed » curve is displaced of T relative to the centroid of the « prompt » curve ([109]). Other analytical properties of these curves have been discussed by NEWTON ([110]) and by RICHINGS ([111]).

The coincidence circuits described above are those which have been used in the measurement of positron mean lives in solids. Many other circuits have been described in the literature. Of these, one should mention the one described by GARWIN ([112]) which has been frequently used in experiments with large accelerators because of its adaptability to multiple coincidence-anticoincidence work, and the circuit of FISHER and MARSHALL ([113]) which makes use of a gated beam tube.

([109]) Z. BAY: *Phys. Rev.*, **77**, 419 (1950).
([110]) T. D. NEWTON: *Phys. Rev.*, **78**, 490 (1950).
([111]) H. RICHINGS: Carnegie Institute of Technology, Thesis, unpublished.
([112]) R. L. GARWIN: *Rev. Sci. Inst.*, **21**, 569 (1950); **24**, 618 (1953).
([113]) J. FISHER and J. MARSHALL: *Rev. Sci. Inst.*, **23**, 417 (1952).

A word should be said about the multiple delayed coincidence circuits which permit the simultaneous recording of the numbers of coincidences for

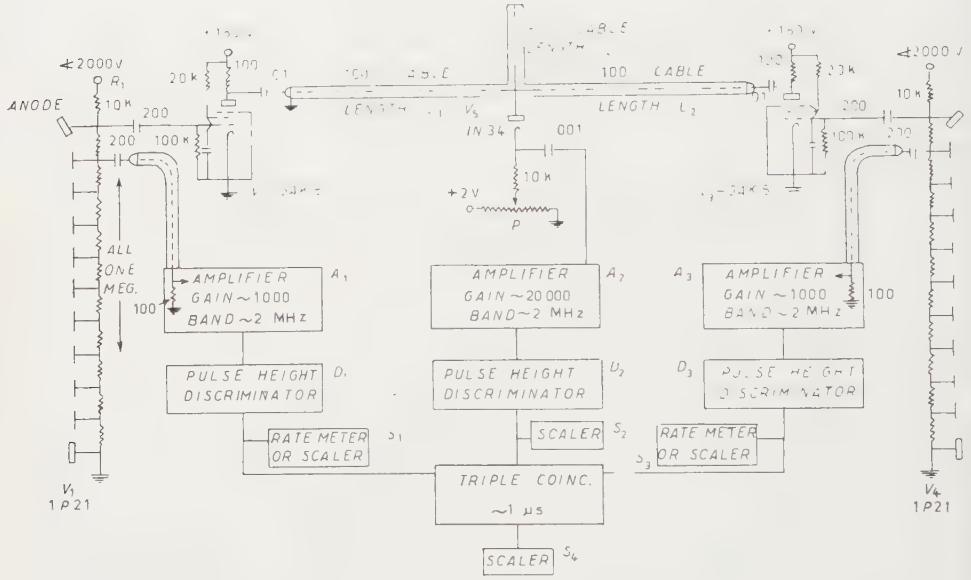

Fig. 27. – Schematic block diagram of the coincidence circuit of Bell *et al.* (Reference [108]).

various delays. These circuits are not among those of shortest resolving time, but have the advantage of reducing the time necessary for the collection of data. They are therefore essential in cosmic ray work [114], and have been used for the mean life of μ-mesonic atoms. One of these circuits, which has received the name of chronotron [115,116] measures delays up to 256 mμs, with a precision of 2 mμs. It was used by Keuffel *et al.* [70] in the work described in Chapter II.

The pulses from the two scintillation counters are first limited in size and duration, and are shaped to a height of 10 V and a width of 25 mμs. Then, these equalized pulses from the two counters are applied at the opposite ends of a 100 Ω coaxial cable. The interval between them is determined by finding the position along the cable where they meet. If, for example, the pulses

---

[114] B. Rossi and N. Nereson: *Rev. Sci. Inst.*, **17**, 65 (1945).

[115] S. H. Neddermayer, E. J. Althaus, W. Allison and E. R. Schatz: *Rev. Sci. Inst.*, **18**, 488 (1947).

[116] J. W. Keuffel: *Rev. Sci. Inst.*, **20**, 197 (1949).

are simultaneous, they meet in the middle. The meeting point is ascertained by means of 10 crystal diodes spaced along the cable at 16 mμs intervals. The diode closest to the meeting point transmits the largest pulse. The outputs of these diodes (0.5 μs in duration) are simultaneously displayed on an oscilloscope and photographed. Inspection of the photograph tells between which two detectors the pulses met, and to which of these two detectors the meeting was closest.

Another method of simultaneous counting in many delay channels consists in transforming the time separation between two pulses into pulse height ([114,117]). The delay can then be read on a multichannel pulse height selector, of the kind described in a later section.

3. – Scintillation Spectrometry.

The measurement of energy with scintillation counters is made possible by the proportionality between the energy spent by the charged particle within the scintillating material and the number of photons emitted. The linear relationship between energy lost and light output holds for fast particles, for which the energy loss per unit length is small. A measurement in anthracene for electrons of energy between 30 to 3 200 keV ([118]), showed that the linearity is valid for energy larger than 125 keV, with a decrease of pulse height per kilovolt below 125 keV. Densely ionized radiation, such as α-particles, produce smaller pulses than electrons of the same energy (the ratio being about 1/10 at 4 MeV).

Continued irradiation of anthracene by an intense α source causes a noticeable decrease in the scintillation efficiency, proving that the radiation damages the crystal and affects its scintillation ability ([100]). Assuming that the smaller light output per keV of heavily

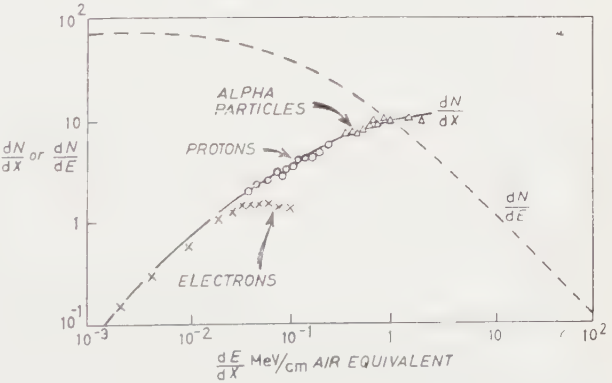

Fig. 28. – Specific photon emission versus specific energy loss in anthracene. [From R. K. Swank: *Ann. Rev. Nucl. Sci.*, **4**, 111 (1954)].

([117]) F. Lepri, L. Mezzetti and G. Stoppini: *Rev. Sci. Inst.*, **26**, 936 (1955).
([118]) J. I. Hopkins: *Rev. Sci. Inst.*, **22**, 29 (1951).

ionizing particles is due to the presence of damaged molecules along the track. Birks has succeeded in interpreting quantitatively the observations. Fig. 28 shows the experimental information on this effect, together with the theoretical curve. Experimental data for different substances and different kinds of radiations can be found in the literature ([119]).

The resolution of a scintillation spectrometer is limited by the statistical fluctuations in the number of photoelectrons. For good resolution, therefore, the substance having the larger integrated light output should be used, and care should be taken to collect all the possible light. This means not only suitable optics, but also electronics of time constant longer than the scintillation time. Independent circuits must be used when both energy resolution and time resolution are wanted, as it will be described in the following section. If m is the average number of photoelectrons for a certain energy lost in the crystal, a simple statistical consideration shows that the total width of the line at half maximum must be at least $100\sqrt{(2 \ln 2)/m} = 100 \cdot 2.36 m^{-\frac{1}{2}}$, in percent of the pulse height. Thus, the line width can be estimated from the data on the number of photoelectrons. Under ideal conditions (100% light collection and $\frac{1}{4}$ photoelectron per photon at photocathode) there should be about 1 photoelectron per 200 eV lost in anthracene. In practice, however, Hopkins ([118]) with anthracene and 5819, observes only one photoelectron for an energy loss of 1.4 to 2.4 keV; Borkowski and Clark ([120]) estimate from experimental data that 200 eV electron energy lost in NaI crystal release one photoelectron in a 5819 photocathode, under mounting conditions which they describe. Using their best tube and their best NaI sample, these authors obtain a full width at half maximum of 7.6% for the 661 keV ^{137}Cs photopeak.

Lack of homogeneity in the scintillant and in the multiplier photocathode increase the line width. This last effect can be partially compensated by using a short light pipe, in order to distribute the light more uniformly over the photocathode. Variation in resolution of factors of 2 can be expected changing scintillators and tubes.

For the study of β energies organic crystals are used, specially anthracene which has the highest integrated pulse height. Crystals containing heavy elements are not advisable since the scattering of electrons increases with Z. In NaI, for instance, 80% to 90% of the entering electrons would scatter out before stopping. Even with organic crystals, special care has to be taken in order to reduce the scattering effects: hollow crystals and split crystals ([121]) may be used to this end.

([119]) C. J. Taylor, W. K. Jentschke, M. E. Remley, F. S. Ely and P. G. Kruger: *Phys. Rev.*, **84**, 1034 (1951).

([120]) C. J. Borkowski and R. L. Clark: *Rev. Sci. Inst.*, **24**, 1046 (1953).

([121]) B. H. Ketelle: *Phys. Rev.*, **80**, 758 (1950).

It has been possible to apply the technique of scintillation spectrometry not only to the determination of the energy of monochromatic conversion lines or to the study of maximum energies, but also to the analysis of β spectral shapes. BELL ([103]) obtains Kurie plots which are linear to 50 kV using a hollow crystal spectrometer in a hydrogen atmosphere. Allowed and forbidden β-shapes can be distinguished with the technique of scintillation spectrometry which is obviously of great interest for the study of β spectra from weak sources.

X-ray and γ spectra are studied, instead, with scintillants containing heavy elements. Among them, NaI is by far the most convenient, and the only one used in practice. Here the presence of a heavy atom is desirable because of its large photoelectric cross-section. Organic scintillants respond to γ-rays of not too low energy almost exclusively by Compton effect, showing a continuous distribution of pulse height for each line; NaI, instead, presents photopeaks which can be resolved with much greater ease. For energy greater than 1 MeV some complications arise because of pair production. A γ-ray of energy $h\nu$ produces a peak at energy $h\nu$ (photoeffect, and pair production followed by absorption within the crystal of the two γ-rays of positron annihilation), another at energy $h\nu - mc^2$ (pair production with the escape of one annihilation quantum) a third at $h\nu - 2mc^2$ (escape of both annihilation γ's) and a continuous Compton distribution.

Several attempts have been made in order to remove the multiple peaks, which are troublesome in the case of complex spectra. The most direct method involves the use of a scintillator large enough to absorb all the energy of the γ-rays. Total absorption γ-ray spectrometers using liquid scintillants or NaI have been described ([122]). Coincidence methods have also been used. The first of these was a « Compton coincidence » spectrometer ([123]) where the pulse height due to a Compton electron is measured for a given angle of γ-ray scattering. For energies above 1 MeV one can analyse the height of the pulses in the main crystal of the spectrometer only when in coincidence with two annihilation photoelectrons revealed by two auxiliary counters at opposite sides of the main one ([124]): in this manner only the line at $h\nu - 2mc^2$ is observed. Inversely, one can use an anticoincidence circuit to suppress the signal arising from photons not completely absorbed in the primary NaI counter ([125]).

These methods, however, are cumbersome and have not been used extensively in research work. The main value of scintillation spectrometry remains its simplicity, its wide angle of acceptance, and its large efficiency; these advantages in many cases overcome the disadvantages of the large line width and of the ambiguity of interpretation for complex spectra.

([122]) R. S. FOOTE and H. W. KOCH: *Rev. Sci. Inst.*, **25**, 746 (1954).
([123]) R. HOFSTADTER and J. A. MCINTYRE: *Phys. Rev.*, **78**, 619 (1950).
([124]) H. I. WEST and L. G. MANN: *Rev. Sci. Inst.*, **25**, 129 (1954)
([125]) R. D. ALBERT: *Rev. Sci. Inst.*, **24**, 1096 (1953).

4. – Pulse Height Selecting Circuits.

Linear and reliable pulse height selecting circuits are essential in scintillation spectroscopy. A series of review articles on the techniques used for this purpose has been written by VAN RENNES ([126]).

The most direct method of pulse height selector consists of a visual analysis of a record of all pulse heights, such as may be obtained by photographing the deflections of an oscilloscope, followed by the enumeration of the pulses in each pulse height interval. A pulse height selecting circuit performs this work automatically.

The simplest such circuit consists of a pulse height discriminator which passes only the pulses higher than a preset voltage V_1. Measuring the counting rate as a function of V_1, one obtains what is called an integral bias curve. The number of pulses in an interval between V_1 and V_2 can be obtained by subtracting the corresponding counting rates, and the number in a small interval around V_1 is proportional to the derivative of the curve obtained.

The operation of subtraction can be performed automatically using two discriminators followed by an anticoincidence circuit. The first discriminator D_1 admits all pulses higher than V_1; the second, D_2, admits all pulses higher than V_2. The anticoincidence circuit cancels the output of D_1 when it occurs simultaneously to a pulse from D_2. In this way only pulses in the interval $V_1 < V < V_2$ are counted ([127]).

The speed of such a differential discriminator cannot be faster than the total rise time of the pulses in an amplifier of considerable gain. In practice, this circuit cannot be made faster than $\approx 1\,\mu s$. It is therefore impossible to ascertain the simultaneity of pulses from two detectors, after their height has been measured, with resolving times better than $\approx 1\,\mu s$. When speed is desired one makes first the time measurement by means of a fast coincidence circuit, and then one discards the pulses of unwanted height by means of differential pulse height selectors acting on a slow coincidence circuit (Fig. 27).

A multichannel pulse height selector records simultaneously the number of pulses in each pulse height interval. It can be built through the repetition of many single channels of the kind described above. An instrument of this design has the advantage of a relatively short dead time compared to the circuits to be described below.

When high counting rates are not required, one may employ entirely different techniques, which allow the use of a great number of channels without

([126]) A. B. VAN RENNES: *Nucleonics* (July, p. 20; August 1952, p. 22; September 1952, p. 32; October 1952, p. 50).

([127]) J. E. FRANCIS, P. R. BELL and S. C. GUNDLACH: *Rev. Sci. Inst.*, **22**, 133 (1951).

a linear increase in the number of components. These techniques, which often involve the use of « memory » units from computing machines, are developed around a pulse height to counts (analogue to digital) converter first introduced by WILKINSON ([128]).

Wilkinson's original instrument is a 100 channel pulse height analyser, using a message register (not preceded by scalar, dead time $\approx 10^{-1}$ s) for each channel. In his scheme each pulse to be measured produces a square pulse whose duration in time is proportional to the height of the imput signal (height to time conversion or lay-down-circuit). This square pulse is then used to gate an oscillator, allowing the passage of a number of wave crests proportional to the pulse height to be measured. In this manner the information to be handled is transformed in a number (coding, or analogue to digital conversion).

The next operation is the decoding of the information: this is done by « reading » the number of crests for each imput pulse, and registering how many times any given number is read. The number of crests is read by two « rings of ten » ([129]) in series, able to store electronically numbers up to 100. If, for instance, a pulse of height 27 arrives, the first ring (ring of units) will stop at position 7, and the second ring (of tens) at position 2. The various elements of the ring operate relays (20 in all) in such a way that in the example considered the 2nd relay of the decade ring and the 7th of the unit ring close. The inner contact of each of the ten relays of the « units » ring is connected to the inner contacts of each of the ten relays of the « tens » ring via a telephone message register. The outer contacts of all relays of the units ring are connected to ground, and the outer contacts of all relays of the tens ring go to a vacuum tube. This tube passes a large current pulse at a convenient time after the two rings have stopped at the position recording the proper pulse height. In this manner the pulse of pulse height « 27 » is recorded in one and only one message register, corresponding to its own height. After the height of a pulse is thus recorded, the rings are automatically reset to 0, and the instrument is made ready to accept and analyze the amplitude of the next imput pulse.

The speed of this circuit is limited by inertia of the mechanical message registers. It is, however, possible to achieve a considerable gain in speed by using scalers to record the information in each channel, and by substituting the relays with vacuum tubes. However, the apparatus to read and register the information becomes so cumbersome that one of the main advantages of Wilkinson's circuit is lost.

Wilkinson's method, however, can be used in connection with relatively fast schemes of registration if one makes use of the memory elements developed

---

([128]) D. H. WILKINSON: *Proc. Camb. Phot. Soc.*, **46**, 508 (1950).

([129]) T. K. SHARPLESS: *Electronics*, **21**, 3, 122 (1948).

for computing machines. In the first method used for this purpose ([130]) the information is stored in the form of ultrasonic pulses traveling in a column of mercury (mercury delay line). The pulses, introduced at one end of the line by means of a quartz crystal, employ 1.2 m s to reach the opposite end, where they are collected by a second quartz crystal. Since pulses separated of 1 μs can be resolved, there are, at any given time, 1200 locations on the line where one can, or cannot, store a pulse. These 1200 « yes or no » keep traveling in the line since, after being collected by the second crystal, they are fed back to the first (the pulses are each time reshaped to correct for the delay line distortions). The 1200 locations are divided in N (say 100) groups, corresponding to the N pulse height channels. Within each group the $1200/N$ available locations (say 12) are used to record on a binary scale the number of counts in the corresponding channel. Thus $2^{1200/N}$ (say 2^{12}, or 40000) counts can be recorded in each channel.

Appropriate circuits to « write » new information on the line and to « read » the numbers stored are described. It is possible to display the information on the face of an oscilloscope, where the 1200 locations are disposed in a rectangular array: each channel corresponds to a column and each power of 2 to a row, in such a way that a luminous dot in the 5^{th} row of the 23^{rd} column means 2^5 counts in channel 23.

In recent years the progress of the art of pulse height sorting has followed the progress in memory techniques for computing machines. Recently, a pulse height selector of 256 channels, and capable to store 2^{16} pulses in each channel has been built at the Argonne National Laboratory ([131]). This instrument has a magnetic core memory; its average dead time is about 80 μs. The number of counts in each channel is shown directly in an oscilloscope where the spectral distribution curve (composed of 256 points) is exhibited on a linear scale.

([130]) G. W. Hutchinson and G. G. Scarrot: *Phil. Mag.*, **42**, 792 (1951).
([131]) T. Brill: personal communication.

SUPPLEMENTO AL VOLUME IV, SERIE X
DEL NUOVO CIMENTO

N. 3, 1956
2° Semestre

μ-Mesonic Atoms.

L. N. COOPER (*)

The Institute for Advanced Study - Princeton, N. J.

Yesterday professor DEBENEDETTI brought the μ-meson from a relativistic velocity in the cyclotron to a bound state in the target. Today perhaps we can begin in the target and consider some of the details of the analysis of μ mesonic atoms and some of the things that can be learned from these atoms.

In brief, from a study of mesonic atoms we can learn about the nucleus — its charge distribution, perhaps its spin, quadrupole moment and its susceptibility to polarization. Also we may learn some of the properties of the meson such as its spin, its magnetic moment, its mass and its non-electromagnetic nuclear interaction. Naturally we cannot learn everything at once. We can learn some of the above things if we know the others. It also turns out, and this is perhaps somewhat surprising, that one can study the effect of vacuum polarization with μ mesonic atoms.

To give some idea of what the situation is like in a mesic atom let us consider the lowest levels of the nucleus-meson system. The level structure is as given in Fig. 1.

Table I gives some of the calculated transition energies (calculated on the basis of a uniform sphere of nuclear charge to $R = 1.3 \cdot A^{\frac{1}{3}} \cdot 10^{-13}$ cm) and some of the observed transition energies.

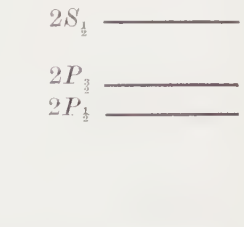

Fig. 1. – Lowest levels of a mesic atom.

(*) Present address: University of Illinois, Urbana, Illinois.

As can be seen from Table I for $r_0 = 1.3$ the calculated transition energies are smaller than the observed transition energies. The guiding direction of the analysis of E. M. HENLEY and myself of the mesic atom was to find what effect was large enough to explain the large transition energies, or what effects would shift the $1S$ level downwards ([1]).

TABLE I.

	Z	Observed $2P_{\frac{1}{2}} - 1S_{\frac{1}{2}}$ transition energies	Calculated $2P_{\frac{1}{2}} - 1S_{\frac{1}{2}}$ transition energies ($r_0 = 1.3$)	r_0 required to fit observed data
Titanium	22	0.955	0.935	1.17
Lead	82	6.02	5.48	1.17

The meson nucleus-system to a good approximation can be treated as being described by the following Hamiltonian:

$$H = H^N + H^\mu + H^e , \tag{1}$$

where H^N is the total nuclear Hamiltonian, H^μ is the free meson Hamiltonian

$$H^\mu = \boldsymbol{\alpha}\cdot\boldsymbol{p} + \beta\mu , \tag{2}$$

and H^e is the static electric interaction of the meson with the Z protons:

$$H^e = \sum_{i=1}^{Z} \frac{e^2}{\boldsymbol{r} \quad \boldsymbol{R}_i} , \tag{3}$$

where $\boldsymbol{R}_i$ is the position vector of the i-th proton and $\boldsymbol{r}$ is the position vector of the μ-meson.

In using this Hamiltonian we have neglected the interaction of the meson with atomic electrons, the nuclear spin, and non-electromagnetic μ-nuclear interactions. However all of these are very small. We shall consider as small those effects which shift the energy levels by less than 1% as the experiment of FITCH and RAINWATER ([2]) was accurate to about 1%.

If we average H^e over the nuclear ground state we get:

$$V = \langle \psi_0 | H^e | \psi_0 \rangle , \tag{4}$$

([1]) L. N. COOPER and E. M. HENLEY: *Phys. Rev.* **92**, 801 (1953).
([2]) V. L. FITCH and J. RAINWATER: *Phys. Rev.*, **92**, 789 (1953).

where the nuclear coordinates $R_1 \ldots R_z$ do not appear in V. Then the Schrödinger equation for the entire system:

$$(H^N + H^\mu + H^e)\Psi = W\Psi, \tag{5}$$

separates into:

$$H^N\psi = E\Phi, \tag{6}$$

and

$$(H^\mu + V)\Phi = \varepsilon, \tag{7}$$

where $W = E + \varepsilon$ and $\Psi(R_1 \ldots R_z, r) = \psi(R_1 \ldots R_z)\Phi(r)$.

For a uniform nuclear charge distribution to R, V becomes

$$V = -\frac{Ze^2}{R}\left(\frac{3}{2} - \frac{1}{2}\frac{r^2}{R^2}\right) \qquad r \leqslant R \tag{8}$$

$$V = -\frac{Ze^2}{R} \qquad r > R$$

Equation (7) can be expanded into large and small components to get

$$\left[H_s - \frac{(\varepsilon - V)^2}{2\mu} + \frac{1}{8\mu^2}\nabla^2 V + \frac{1}{2\mu^2}\frac{1}{r}\frac{dV}{dr}S\cdot S + \ldots\right]\Phi_2 = \varepsilon\Phi_2, \tag{9}$$

$$\text{where} \quad H_s = \frac{\nabla^2}{2\mu} + V.$$

This is effectively an expansion in $(E - V)/2\mu$ and since for a potential like (8) $(E - V)$ is bounded the error incurred by neglecting the dotted terms can be estimated and for lead was less than 1%. The solutions of this equation can be obtained by solving

$$H_s\Phi = \varepsilon\Phi, \tag{10}$$

which is just the non relativistic Schrödinger equation, and treating the extra terms in Equation (9) as perturbations. This yields the results shown in Table I.

We must now consider what corrections must be made to the energy levels derived above.

1. – Meson Properties.

1·1. *Meson Spin and Magnetic Moment.* – The meson spin was assumed above to be $\frac{1}{2}$. This would seem to be so if $\pi \to \mu + \nu$ or if $\mu \to e + 2\nu$. Unless the meson has an enormous anomalous moment the energy levels above would not be shifted very much. However the data do not seem to indicate a large anomalous magnetic moment.

1·2. *Meson Mass.* – In deriving the results given in Table I, one used for the meson mass $\mu = 210\ m_e$ [3]. For small change of the meson mass one can estimate by perturbation procedures what the shift in the energy levels will be. This turns out to be

$$\Delta\varepsilon_{\mu k} = -(\varepsilon_k - \overline{V}_k)\Delta\mu/\mu\,, \tag{11}$$

where ε_k is the energy for a meson of mass $210\ m_e$ in the state specified by quantum number k, $\overline{V}_k = \langle \varphi_k | V | \varphi_k \rangle$, and $\Delta\mu$ is the change in meson mass. For the case of lead since the potential is harmonic inside the nucleus and Coulomb outside, $\Delta\varepsilon$ is very small for relatively large values of $\Delta\mu$.

2. – Nuclear Properties.

Effects due to the discreteness of the nuclear charge distribution and to nuclear quadrupole moments are also very small. In fact the experiment was done with elements like lead for which the quadrupole moment was zero in order not to complicate the spectra.

2·1. *Nuclear Polarization.* – We should now consider how the nuclear polarization will affect the energy level structure. To give an idea of what this effect is consider the following. The μ-meson enters the nucleus. Since it is negatively charged the nucleus shrinks (due to the decrease in Coulomb energy). The shrunk nucleus being more compact has a larger electric potential. Thus the $1S$ level of the mesic atom will be shifted downwards. Instead of calculating the polarization using some nuclear model for which we would

[3] The current best value of the μ-meson mass in $207\ m_e$ [F. M. Smith, W. Birnbaum and W. H. Barkas: *Phys. Rev.*, **91**, 765 (1953)]. For the heavy elements this maker very little difference in the calculated $2S$-$1S$ transition energy. For the light elements the $1\frac{1}{2}$ % decrease in mass decreases the calculated $2P$-$1S$ transition energy by about $1\frac{1}{2}$ % but the vacuum polarization correction at the same time increases this calculated transition energy by about $\frac{1}{2}$ %.

have to estimate nuclear compressibility, etc., let us go back to our original Hamiltonian and use $H' \quad V \quad H'$ as a perturbation. Then employing some general quantum mechanical arguments and our knowledge of nuclear energy levels we can obtain an overestimate of the levels shift due to the nuclear polarization, which overestimate itself is not large enough to explain the transition energies observed by FITCH and RAINWATER.

We treat H'

$$H' = H^e - \langle \psi_0 | H^e | \psi_0 \rangle \,, \tag{12}$$

as a perturbation on $H^N + H_s$.

The first order correction $W^{(1)}$ to the total energy is zero. It is in the second order that polarization effects appear. For the S-state meson:

$$W^{(2)} = \sum_{N,m} \frac{\langle 00 | H' | Nm \rangle \langle Nm | H' | 00 \rangle}{\Delta E} \,, \tag{13}$$

where $a\,b$ is $\psi_a \psi_b$ the state vector for the unperturbed nucleon in state a and the unperturbed meson in state b, and

$$\Delta E = E_0 + \varepsilon_0 - E_N - \varepsilon_m \,.$$

H' can be expanded in spherical harmonics to give:

$$H' = -e^2 \sum_{l=0}^{\infty} H'_l = -e^2 \sum_{l=0}^{\infty} \sum_{i=1}^{E} f_l(r, R_i) P_l(\cos \vartheta_i) \,, \tag{14}$$

where ϑ_i is the angle between the meson and the i-th nucleon position vector, and $f_l(r, R_i)$ is some radial function.

We can rewrite Equation (13) as

$$W^{(2)} = e^4 \sum_{l=0}^{\infty} W_l^{(2)} \,, \tag{15}$$

where

$$W_l^{(2)} = \sum_{N,m} \frac{\langle 00 | H'_l | Nm \rangle \langle N\,m | H'_l | 00 \rangle}{\Delta E}$$

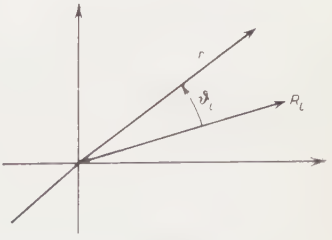

Fig. 2.

and this is so because the angular functions are such that the nucleons must make the same multipole transitions as the meson.

Then we can use the closure theorem to get for $W_l^{(2)}$

$$W_l^{(2)} = \frac{1}{\Delta E} \langle 00 | H_l'^2 | 00 \rangle \,, \tag{16}$$

where now ΔE is unknown. However we certainly overestimate if we choose for ΔE the smallest energy consistent with the multipole transition considered. When this is done one has a value for $W_l^{(2)}$ which is certainly larger than the actual value. The actual matrix element $00|H_l'^2|00$ can be computed with some simple assumption about the ground state of the nucleus.

The result of calculations like this give a value for lead of

$$W_{\max}^{(2)} = -0.185 \text{ MeV} . \tag{17}$$

Although this is reasonably large, it is considerably smaller than would be necessary to explain the large observed $2P - 1S$ transition energy. It must also be remembered that $W_{\max}^{(2)}$ of eq. (17) is a gross overestimate of $W^{(2)}$. One can introduce various refinements into the calculation and the value for $W^{(2}$ is then greatly reduced.

2·2. *The Vacuum Polarization.* – The vacuum polarization increases the nuclear potential due to the virtual creation and annihilation of an electron positron pair.

The increase in potential produces only a small effect, comparatively, in the heavy elements (of the order of a $1\,\%$ shift in the energy levels) but for the light elements where one can observe higher transitions $3D - 2P$ and calculate the expected transition energies very exactly, one can actually see the presence of the vacuum polarization (4).

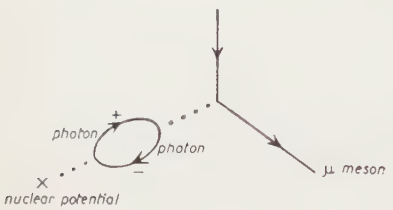

Fig. 3.

None of the effects discussed above seriously disturb the energy level scheme given in Table I, and this is particularly true for the heavy elements. Thus in order to explain the large observed $2P - 1S$ transition energy one has two alternatives:

1) to assume an anomalous μ-meson-nuclear interaction;

2) to make the nucleus charge denser.

There has been some evidence for an anomalous μ-nuclear interaction from the high energy μ-meson scattering (5). However the experiments are very difficult to interpret and the conclusions one can draw from them are still not certain.

(4) S. Koslov, V. Fitch and J. Rainwater: *Phys. Rev.*, **95**, 291 (1954).
(5) I. B. McDiarmid: *Phil. Mag.*, **45**, 933 (1954).

On the other hand the electron scattering experiments also indicate a denser nuclear charge distribution (6) so that, for the heavier elements at least, this seems to be the only consistent explanation. A nuclear charge distribution characterized by a uniform density to a radius of $R = 1.2 \cdot A^{\frac{1}{3}} \cdot 10^{-13}$ would be consistent with the observed $2P - 1S$ μ-mesonic transition energies from lead to titanium.

If now we need an anomalous μ-nuclear interaction to explain the high energy scattering of μ-mesons this interaction would have to be very strongly energy dependent in order not to be seen in the mesonic atom.

(6) B. Hahn, D. G. Ravenhall and R. Hofstadter: *Phys. Rev.*, **101**, 1131 (1956).

PARTE QUARTA

Fisica dei reattori

Nuclear Reactor Physics.

A. M. WEINBERG

Oak Ridge National Laboratory, Oak Ridge, Ten.

Lectures collected by

G. CAGLIOTI, K. SAHAI and B. L. YOUTZ

International School of Physics, 1955 - Varenna

and edited by

U. L. BUSINARO

Laboratori CISE - Milano

Introduction.

In this brief summary it is our intention to give an outline of only the most important topics in nuclear reactor theory.

Nuclear reactor theory deals with the problem of the neutron distribution in nuclear reactors. This distribution determines the heat production which is of course needed for the design of practical reactors. This theory by no means exhausts the whole of the analysis needed to design a high-powered reactor. On the contrary reactor engineering analyses—such as heat transfer, fluid flow, mechanical design etc—are also necessary for the design of chain reactors.

A central goal of reactor technology is to produce useful work from nuclear reactors.

Thus as the nuclear technology matures, it takes on, more and more, the characteristics of any thermodynamic technology.

Our concern here, shall be however only with the nuclear aspects of reactor.

CHAPTER I.

Application of Nuclear Theory to Chain Reactor.

1. – Important Nuclear Processes.

We begin by listing the nuclear processes which figure most directly in « nuclei combustion » and then we shall apply standard nuclear theory to these processes, in so far as they are involved in nuclear chain reactors.

In order of importance, the nuclear processes involved in a chain reactor are:

a) Neutron induced fission.

b) Neutron capture, especially the n-γ type, but also n-α and n-p.

c) Neutron scattering, both elastic and inelastic.

d) n-2n, γ-n and β-decay processes.

Reaction *a*) is the most important one because this is the reaction without which nuclear fire would not ignite.

Reactions *b*) come second in order of importance, because they tend to quench the nuclear fire. The establishment of a chain reaction always involves the balance between the n-fission reaction as opposed to the n-capture reactions.

Reactions *c*) are third among the most important processes in reactor considerations. Elastic scattering, on the whole, determines the size of the reactor because it affects the distance a neutron travels from the time it is born until it is caught by another fissionable atom to produce more neutrons. Thus, reactions of this sort, in which the neutron does not change its identity, are primarily determinative of the size scale of the chain reaction, rather than whether or not the chain reaction will run at all.

Of course, scattering can imply a change in neutron energy, especially if there is inelastic scattering and, since the neutron energy determines the ratio of fission to capture probabilities, such scattering processes may have bearing on the question of whether or not one can ignite nuclear fire in a chain reactor of any size.

The reactions *d*) are of much less importance then the other three in the operation of a reactor. n-2n reaction might be expected to give a useful multiplication of neutrons to aid the chain reaction. However, their importance is small even if Be or D (which have comparatively large n-2n cross-sections) are the principal materials of the reactor, since the neutron energy for the n-2n reactions is higher than the energy of the bulk of the neutrons in the reactor.

One might also expect that the γ-rays reaction would contribute useful neutrons since there are many γ-rays, produced in the fission process, which have energies higher than the energy necessary to liberate a neutron from, say ^{9}Be (1.6 MeV) or ^{2}H (2.2 MeV). However, the γ-n cross-sections are about three orders of magnitude less than the Compton cross-section per electron, hence, the γ-ray energies are very rapidly degraded below the γ-n thresholds by Compton scattering, and the contribution of γ-n reactions is also small.

Thus the possibility of a chain reaction based on a combination of γ-n and n-γ reactions, e.g. a sphere of mixed H_2 and D_2 in which γ-rays produce neutrons, and these, in turn, produce γ-rays, can be immediately dismissed.

β-processes are of great practical importance in reactor technology, because of the problem of the disposal of radioactive products formed in the fission process, but, as it has little to do with reactor physics, this matter will not be discussed further.

2. – Cross Section Theory.

We shall now apply the standard theory of cross-sections to the most important nuclear processes in reactors.

The whole problem in reactor design is to balance the yield of neutrons from the various production processes against the loss of neutrons by capture processes and leakage from volume.

One has to write down the balance equation for these processes in which the nuclear cross-sections appear as parameters—which are usually obtained experimentally. Unfortunately not all of the important cross-sections are available: for example the capture cross-sections for many of the fission fragments have not been measured. Hence it is necessary to make « educated guesses » for certain cross-sections, by relying on cross-section theory.

The basis of these guesses is the well-known Breit-Wigner single resonance formula. For radiative capture of a neutron of energy E, taking into consideration only neutrons of zero orbital momentum l, one has [1]:

$$\sigma_{n,\gamma}(E) = \pi \left(\frac{\hbar}{p}\right)^2 \frac{g_c}{g_1} \frac{\Gamma_n \Gamma_\gamma}{\Gamma^2/4 + (E - E_1)^2}, \tag{I.1}$$

where p is the momentum of the neutron in the center of the mass system, Γ_n and Γ_γ are, respectively, the neutron and γ-ray partial width of the reso-

---

[1] See, for instance, I. M. Blatt and V. F. Weisskopf: *Theoretical Nuclear Physics* (New York, 1952), p. 425.

nance state that occurs at energy E_1, $\Gamma \cong \Gamma_n + \Gamma_\gamma$ is the total width, and g and g_1 are the statistical weights of the compound nucleus and of the initial state respectively. These are given by:

$$\text{(I.2)} \qquad \begin{cases} g_1 = (2I+1)(2\cdot\tfrac{1}{2}+1) = 2(2I+1) \\ g = 2J+1 \,. \end{cases}$$

where I is the spin of the target nucleus and J the spin of the compound nucleus.

For $I > 0$ one may approximate:

$$\text{(I.3)} \qquad \frac{g}{g_1} \cong \frac{1}{2}$$

In general the widths Γ_n and Γ_γ are not independent of energy. This is a very well-known fact as far as the neutron widths are concerned; for the radiation widths recent Brookhaven experiments indicate a very slight dependence of Γ_γ on neutron energy (2).

One may factor the neutron width, as follows:

$$\text{(I.4)} \qquad \Gamma_n = \frac{2\gamma^2}{(I)^2} \,,$$

where γ is called the reduced neutron width and is almost energy independent, and I is the amplitude of the wave function at the nuclear surface. The dependence of I for the neutron upon the angular momentum $l\hbar$, is given in the following Table I.

TABLE I.

l	$I_l(a)$	$I_l(a)$ for $pa/\hbar \ll 1$
0	$(\hbar/p)^{\frac{1}{2}} \exp[-ipa/\hbar]$	$(\hbar/p)^{\frac{1}{2}}$
1	$(\hbar/p)^{\frac{3}{2}}([1/a + ip/\hbar]) \exp[-ipa/\hbar]$	$(\hbar/p)^{\frac{1}{2}}(\hbar/pa)$
...		
l	$(\hbar/p)^{l+\frac{1}{2}} a^{l+1}(-\partial/a\partial a)^l(1/a \exp[-ipa/\hbar])$	$(\hbar/p)^{\frac{1}{2}}(\hbar/pa)^l C_l$
	$(C_l = 1\cdot 3\cdot 5\cdot \ldots \cdot (2l-1)$ and a = nuclear radius.	

Table I shows that for $l = 0$ one has $\Gamma_n \cong (2\gamma_n^2/\hbar)p$, which is the well-known relation $\Gamma_n \sim \sqrt{E}$.

(2) J. S. LEVIN and D. J. HUGHES: *Phys. Rev.*, **101**, 1328 (1956).

For $l > 0$ we have an additional factor $(pa/\hbar)^{2l}$. Therefore, for low energy neutrons, the contribution of the higher angular momentum states to the cross-section, is very small.

In the capture and fission processes occurring in thermal or intermediate chain reactions, we are concerned primarily with neutron energies below a few kilovolts, so we must usually consider only the $l = 0$ states. This is not the case, however, of elastic and inelastic scattering, since the fission neutron spectrum includes neutrons of several MeV energies.

We now apply the Breit-Wigner formula to obtain a broad description of the energy dependence of the n-γ type reactions. In the case of many well separated resonances, we can obtain an average cross-section at relative energy E by integrating equation (I.1) over the whole energy in order to obtain the area under a single resonance curve, and then divide by the average distance D between resonances of the same angular momentum and parity.

In the integration all quantities except the:

$$[(\Gamma^2/4) + (E - E_1)^2]^{-1} ,$$

are considered to be constant. By making the substitution for Γ_n in the case of $l = 0$ and for small $pa/\hbar$, one obtains, for the average capture cross-section over a resonance:

$$\sigma_{n,\gamma}(E) = \frac{4\pi^2}{D} \frac{\hbar}{p} \frac{g_c}{g_1} \frac{\gamma_n^2 \Gamma_\gamma}{\Gamma_\gamma + 2\gamma_n^2(p/\hbar)} . \qquad (l = 0). \tag{I.5}$$

It has been shown ([3,5]), that

$$\gamma_n^2 = fD , \tag{I.6}$$

where f is a proportionality factor of the order of 10^{-13} cm.

Taking into account (I.6) and the fact that the sum of g_c/g_1 over all possible angular momenta compatible with the spin of the bombarded nucleus and of the captured neutron, is equal to unity, one obtains:

$$\sigma_{n,\gamma}(E) = \frac{1.8 \cdot 10^{16} f}{E^{\frac{1}{2}}} \frac{\Gamma_\gamma}{\Gamma_\gamma + 4.4 \cdot 10^9 f D E^{\frac{1}{2}}} \text{ F } (*) , \qquad (l = 0), \tag{I.7}$$

([3]) H. A. Bethe: *Rev. Mod. Phys.*, **9**, 69 (1937).

([4]) H. Feshbach, D. C. Peaslee and V. F. Weisskopf: *Phys. Rev.*, **71**, 145 (1947).

([5]) Of the numerous works of Wigner and coworkers in nuclear reaction theory, see, for instance, the review article by Wigner in *Am. Journ. Phys.*, **17**, 99 (1949).

(*) The F is used to indicate the cross-section unit « Fermi » 10^{-24} cm^2, term also known as barn.

Γ_γ, D are expressed in eV, while f in cm, this formula was first given in this form by WIGNER [5].

In order to consider the contributions of higher angular momentum states, one has to add a correction factor to (I.7). A rough expression for this factor may be obtained assuming that the neutrons of angular momentum $l \leq ap/\hbar$, (i.e. neutrons that, classically, strike the nuclear sphere of radius a) contribute to the cross-section according to their statistical weight $2l+1$ while the neutrons with an angular momentum $l > ap/\hbar$ do not contribute at all [5].

One finally obtains this way:

$$\overline{\sigma_{n,\gamma}(E)} = \frac{1.8\cdot 10^{16} f}{E^{\frac{1}{2}}} \frac{\Gamma_\gamma (1 + A^{\frac{2}{3}} E/10^7)}{\Gamma_\gamma + 4.4\cdot 10^9 f D E^{\frac{1}{2}}}. \tag{I.8}$$

although the correction for higher l's tends to be an underestimate.

This is a useful formula by which one can estimate nearly all the intermediate energy average capture cross-sections needed in nuclear reactor work.

We shall now examine the general behaviour of the nuclear cross-sections as predicted by equations (I.1) and (I.8).

At thermal energies, capture is determined almost entirely by the presence of nearby resonance. Thus we can determine the thermal energy dependence by considering the behaviour of equation (I.1) at low energy, *i.e.*:

$$\sigma_{n,\gamma} \to \pi \left(\frac{\hbar}{p}\right)^2 \frac{g}{g_1} \frac{\Gamma_n \Gamma_\gamma}{E_1^2}. \tag{I.9}$$

Since, as we have seen previously $\Gamma_n \sim p$ for low energies, we have

$$\sigma_{n,\gamma} \sim \frac{1}{p^2} \sim \frac{1}{v^2}.$$

which is the well-known $1/v$ law.

In the low resonance region, where the neutron width $4.4\cdot 10^9 \cdot f D E^{\frac{1}{2}}$ is much less than Γ_γ, we see from (I.8) that the average capture cross-section goes roughly as $1/v$ also, due to the factor $(1.8\cdot 10^{16} f)/E^{\frac{1}{2}}$. These two $1/v$ dependences must not be confused, of course; the thermal $1/v$ law refers to the actual capture cross-section, the resonance $1/v$ law only to the average cross-section.

At still higher energies where Γ_γ becomes much less than the neutron width, we find that the average cross-section behaves like $1/E$. At extremely high energies the limiting value of $0.4 A^{\frac{2}{3}} \Gamma_\gamma / D$ is approached.

Fig. 1 qualitatively summarizes the general behaviour here discussed of the capture cross-section.

In spite of their great importance in reactor calculations, only few n-γ cross-sections are measured in the keV energy region, and most of these not for monoenergetic neutrons, but for a somewhat degraded fission spectrum, the average energy of which is usually assumed to be about 1 MeV ([6]).

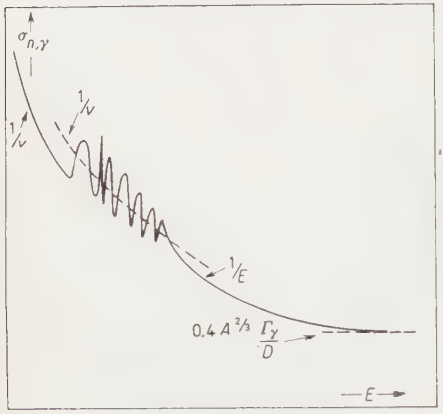

Fig. 1. Qualitative behaviour of $\sigma_{n,\gamma}$ cross section, as function of energy.

Formula (I.8) may be used to evaluate n-γ cross-section in the keV region, using experimental data for Γ_γ, f and D obtained in the first 100 electronvolt, with a velocity selector ([7]).

3. – Neutron Induced Fission.

We shall here describe the most important of the nuclear processes enumerated at the beginning of this section, i.e. neutron induced fission, limiting ourselves, however, to those aspects which are essential to the working of a chain reaction.

From the well-known odd-even effect in neutron binding energy, one may expect, and this indeed is what happens, that heavy elements containing an odd number of neutrons are more susceptible to fission than those containing an even number of neutrons, since in the former the addition of a slow neutron produces about 1 MeV additional excitation energy.

A neutron captured in a fissionable material leads to fission or only to γ-rays emission with different probabilities. If we define the quantity α as the ratio of the radiative capture to fission cross-section:

$$\alpha = \frac{\sigma_{n,\gamma}}{\sigma_f},$$

the probability that a captured neutron produces fission is $1/(1+\alpha)$, while the probability of radioactive capture is $\alpha/(1+\alpha)$.

One may thus write the chemical equation for the reaction of neutrons with fissionable material as:

([6]) D. J. Hughes, W. D. Spatz and N. Goldstein: *Phys. Rev.*, **75**, 1781 (1949).

([7]) E. Vogt: *Report NDE*-14 (1955); R. S. Carter, J. A. Harvey, D. J. Hughes and V. E. Pilcher: *Phys. Rev.*, **96**, 113 (1954); J. A. Harvey, D. J. Hughes, R. S. Carter and V. E. Pilcher: *Phys. Rev.*, **99**, 10 (1955) and also reference ([2]).

(I.10) 1 neutron + fissionable material →

$\alpha/(1+\alpha)$ absorption products (such as ^{236}U, ^{234}U or ^{240}Pu) +

+ $2/(1+\alpha)$ fission products (such as ^{87}Kr, ^{139}I, etc) +

+ approx. 7 β-rays and neutrinos + approx. 10 γ-rays +

+ approx. 180 MeV total energy + η neutrons.

η, defined as the number of neutrons produced per neutron absorbed, must not be confused with ν, the number of neutrons produced per fission, to which it is related by:

(I.11) $$\eta = \frac{\nu}{1+\alpha}.$$

Equation (I.10) can be used to discuss the possibility of the chain reaction and the economy of the neutrons.

If there were no losses of neutrons (such as leakage from reactor volume, or parasitic capture from structural materials), the condition $\eta > 1$ would be sufficient to ensure the establishment of a chain reaction. Since there are always processes which cause neutrons to be lost, η must exceed 1 in order that a chain reaction may be possible.

The non-productive capture processes in a reactor are characterized by a quantity P_0 defined as the probability that a neutron has to be absorbed by fuel. Hence $1 - P_0$ is the probability that the neutron is lost by parasistic capture or leakage. The product ηP_0, called the criticality constant, C, determines whether the neutron population in a reactor will be critical ($C = 1$), divergent ($C > 1$), or convergent ($C < 1$).

P_0 and C are « extensive » quantities, i.e. they depend upon the geometry of the system.

For a chain reaction to occur, we have seen that it is essential that $\eta > 1$. It is often useful, however, to have also $P_0\eta > 1$. In such a case one may use the $P_0\eta - 1$ neutrons remaining after 1 neutron has been used to sustain the chain reaction, to produce new fissile material. This may be obtained by inserting in the reactor some « fertile » material such as ^{238}U or ^{232}Th. In the case of ^{238}U the reaction leading to the fissile material ^{239}Pu is:

(I.12) $$\eta + {}^{238}U \rightarrow {}^{239}U \xrightarrow[\beta^-]{24 \text{ min.}} {}^{239}Np \xrightarrow[\beta^-]{2.3 \text{ days}} {}^{239}Pu\,.$$

If $P_0\eta - 1 > 1$, the process of convertion is self-sustaining (breeding process).

A useful quantity in classifying the reactor with regard to the possibility of converting fertile in fissile material, is the conversion ratio, C.R., defined

as the ratio of the atoms of fuel produced to the atoms of fuel consumed. One always has:

$$\text{C.R.} \leqslant \eta - 1 \,. \tag{I.13}$$

If a C.R. $\geqslant 1$ can be realized, one has the possibility of converting all the world's ^{238}U or ^{232}Th into fissionable material.

To summarize:

$\eta > 1$ for a chain reaction,

$\eta \geqslant 2$ to burn all the ^{238}U or ^{232}Th .

The values of ν, η, α for ^{233}U, ^{235}U, ^{239}Pu and natural uranium for thermal neutrons are given in Table II. From the values of α we see that capture competes quite strongly with fission especially in the case of ^{239}Pu.

TABLE II. – *Experimental values of* ν, η, α *for thermal neutrons* (*).

	^{233}U	^{235}U	^{239}Pu	Natural U
ν	2.54 ± 0.04	2.46 ± 0.03	2.88 ± 0.04	
η (thermal)	2.31 ± 0.03	2.08 ± 0.03	2.03 ± 0.03	1.34 ± 0.02
α (thermal)	0.098 ± 0.002	0.184 ± 0.008	0.42 ± 0103	

From the values for η we see that to achieve a conversion ratio > 1 would be very difficult for any fuel other than ^{233}U, using thermal neutrons.

In addition one should keep in mind that α is strongly energy dependent. We give in Table III rough experimental values for α at various neutron energies.

TABLE III. – *Rough experimental values of* α *as a function of neutron energy* (+).

Neutron energy	^{233}U	^{235}U	^{239}Pu
10^2 eV	Probably	0.5	0.7
10^3	< 0.1	0.5	0.6
10^4	at all	0.35	0.4
10^5	energies	0.13	0.18
10^6		0.1	0.1

(*) These values are taken from recent American data: see D. J. HUGHES and J. A. HARVEY: *Report Brookhaven National Laboratory, No.* 325 on neutron cross-section.

(+) See the preceding reference and also the proceedings of U.N. Atom for Peace Conference.

Since α is so small at high energies, it is for breeding purposes advantageous to use fast neutrons, as the value then approaches the theoretical upper limit $\eta = \nu$. This principle was utilized in the first breeder reactor of Argonne.

In the resonance region of cross-sections, the value of α fluctuates widly. For instance in the first resonance at ^{239}Pu, that appears at about 0.3 eV, $\alpha = 0.8$. η decreases as the temperature rises, thus giving a certain temperature stability to the thermal chain reaction based on ^{239}Pu. The relatively great values listed in Table II, are obtained in spite of very great fission cross-section. This may be seen looking at Table IV, where we have reported the thermal cross-sections for fissionable material.

TABLE IV. – *Thermal cross-sections in* F (*).

	^{233}U	^{235}U	^{239}Pu	Natural U
$\sigma_{scatt.}$		10 ± 2	9.6 ± 0.5	8.3 ± 0.2
$\sigma_{abs.}$	585 ± 10	687 ± 7 (*)	1065 ± 15 (*)	7.68 ± 0.07 (*)
$\sigma_{fiss.}$	533 ± 10	580 ± 8	750 ± 15	4.18 ± 0.06

(*) The absorption does not obey the $1/v$ law exactly, so to obtain the average cross-section over a Maxwellian distribution, one divides by $2/\sqrt{\pi}$ (as is usually done for $1/v$ absorption) and then multiplies by the following factors: 0.981 for ^{235}U; 1.075 for ^{239}Pu; and 0.99 for natural U.

Another important aspect of the neutron induced fission is the energy spectrum of emitted neutrons. This spectrum is roughly Maxwellian and is given by the distribution function:

$$N(E) = 0.488 \exp[-E] \sinh \sqrt{2E}\,, \tag{I.14}$$

E is the energy of the emitted neutrons in MeV; $N(E)$ is normalized to 1 neutron.

With regard to the temporal sequence with which the neutrons per fission are emitted, not all neutrons may be considered as emitted immediately (prompt neutrons). Some are delayed and come off following the β-decay of the fission products. With ^{235}U, 0.755% of the neutrons emitted in thermal fission are delayed, and 0.422% are delayed neutrons in the case of ^{239}Pu. For fast fission the figure is 2.42% with ^{232}Th and 1.74% with ^{238}U.

The importance of these delayed neutrons is very great with regard to the possibility of controlling nuclear reactors. In fact if the reactor is operated in a regime where the delayed neutrons are necessary for the maintainance of the chain, the time scale of the reaction increases; this greatly simplifies the control of the reactor.

Chapter II.

The Mathematical Theory of Chain Reaction.

1. – Definitions.

The mathematical theory of chain reactions is somewhat analogous to the boundary value problems in non-relativistic quantum mechanics. It is, however, a little more complicated on account of the fact that the operators are not generally Hermitian, and it is often necessary to introduce the adjoint function.

In a chain reactor one essentially has fuel and chain-carriers (i.e. neutrons) which react with more fuel to produce more neutrons and so on. Since the primary aim of a reactor is to produce energy, a problem of fundamental technological importance is the possibility of predicting the power distribution within a reactor, for the purposes of designing, cooling, etc. The power is proportional to the flux; hence we consider the function $\varphi(\boldsymbol{x}, E, t, \boldsymbol{\Omega})$ which represents the distribution of neutron flux in space ($\boldsymbol{x}$) ,energy (E), time (t) and direction of motion ($\boldsymbol{\Omega}$).

However, for almost all practical purposes, it is sufficient to assume that the distribution is either spherically symmetric or capable of being represented by the first two spherical harmonics. It is, therefore, sufficient to consider only the total flux:

$$\Phi(\boldsymbol{x}, E, t) = \int \varphi(\boldsymbol{x}, E, t, \boldsymbol{\Omega})\, \mathrm{d}\boldsymbol{\Omega} \,. \tag{II.1}$$

By definition of flux,

$$\Phi(\boldsymbol{x}, E, t) = n(\boldsymbol{x}, E, t) \cdot v \,, \tag{II.1'}$$

where $n(\boldsymbol{x}, E, t)$ is the density of neutrons per unit energy per unit time and v is the velocity of the neutrons. The neutron flux is the sum of the velocities of all the neutrons in a given cubic centimeter and of a given energy.

If one has the flux distribution, one can easily obtain the power distribution in the reactor, since power distribution is given by:

$$P(\boldsymbol{x}, t) = \text{const} \times \int \Sigma_f (E, \boldsymbol{x}) \Phi(\boldsymbol{x}, E, t)\, \mathrm{d}E \,. \tag{II.2}$$

where Σ_f is the « macroscopic » fission cross-section (*).

(*) Macroscopic cross-section is defined as the product of the number, N, of nuclei per unit of volume, times the « microscopic » cross-section σ. Thus the dimension of macroscopic cross-section is inverse length.

We recall here the definition of the criticality constant C, given in the preceding section. C may be written as the ratio of the number of neutrons in one generation to the number in the preceding generation, and is equal to ηP_0.

Now P_0, that is the probability that a neutron has to be absorbed by fuel, is the product of two factors:

f = probability that a neutron, absorbed in the reactor, may be absorbed in the fuel;

P = the non-leakage probability, or the probability of the neutron being absorbed somewhere in the reactor. Thus we have:

$$C = \eta f P \,. \tag{II.3}$$

In a system in which the neutrons are monoenergetic, ηf is constant for all neutrons, and so depends only on the material of the reactor. It is an « intensive » quantity, independent of size. P, on the other hand, depends upon the geometry of the reactor and is an « extensive » quantity.

In chain reactors, it is useful to characterize the geometry—i.e. the size and shape of the reactor—by specifying a certain geometric invariant, (independent of coordinate system) of the reactor. The relevant invariant turns out to be the wave number and corresponding mode of oscillation of the reactor as a geometric object. To determine the fundamental modes of vibration of a system, we write down, as in acoustics, the wave equation:

$$\nabla^2 \Psi + B^2 \Psi = 0 \tag{II.4}$$

using the condition that $\Psi = 0$ on the boundary; the meaning of Ψ will soon become clear.

For a slab of thickness H, one has:

$$\left\{ \begin{array}{l} \Psi \quad \cos \dfrac{\pi x}{H} \,, \\ B^2 = \dfrac{\pi^2}{H^2} \,, \end{array} \right. \tag{II.5}$$

B^2 is called in reactor theory « the geometric buckling ». It can be shown that the buckling is a monotonic function of the surface to the volume ratio of the object, provided that object is of sufficiently simple shape. The usefulness of the buckling B^2, as a characterization of the reactor geometry, stems from the fact that the non-leakage probability P, of a bare reactor, is always a

function of the geometric buckling:

$$P = P(B^2) . \tag{II.6}$$

In an infinite system $B^2 \to 0$ and $P \to 1$ which means that there is no leakage. We define the « infinite multiplication constant », as the criticality constant in an infinitely large system:

$$k = C_\infty = \eta f . \tag{II.7}$$

Evidently k is the number of neutrons produced per neutron absorbed in an infinite system.

In general one has

$$C = kP(B^2) . \tag{II.8}$$

Thus to determine the criticality condition for a general reactor we have two problems: the determination of the multiplication constant for similar infinite system and the determination of $P(B^2)$.

One has, by definition

$$k = \frac{\int \nu \, \Sigma_f \, \Phi \, \mathrm{d}E}{\int [\Sigma_f \Phi + \Sigma_c \Phi] \, \mathrm{d}E} . \tag{II.9}$$

Σ_f and Σ_c are the macroscopic fission and radiative capture cross-section, respectively. Thus, to carry out the calculation of k one must know the distribution of neutrons.

Similarly, to determine the nonleakage probability, one must know the distribution of neutrons.

This can be illustrated by referring to the slab reactor considered before. The neutron distribution is roughly shown in Fig. 2. Since the neutrons closest to the edge are more likely to leak out than those near the center, it is apparent that P must depend upon the relative number of neutrons at each point of the reactor, i.e. on the neutron distribution. Besides, also the energy distribution of neutrons must be known in order to compute P, since the scattering properties are often sensitive to energy.

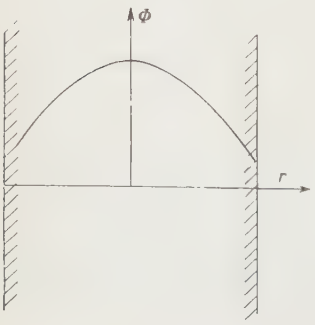

Fig. 2. – Thermal neutron distribution in a slab bare reactor.

2. – The First Fundamental Theorem.

With regard to the problem of neutron distribution, we shall now state what is often called the « First Fundamental Theorem ». The theorem reads.

The stationary neutron distribution $\Phi(\boldsymbol{x}, E)$ in a critical, bare, uniform reactor is separable in space and energy,

$$\Phi(\boldsymbol{x}, E) = \varphi(E)\psi(\boldsymbol{x}) \,. \tag{II.10}$$

The spatial distribution is the fundamental solution of the wave equation (II.4), i.e., it is the solution which is positive throughout the reactor and vanishes on the extrapolated boundary. The geometric buckling, B^2, must satisfy the critical equation

$$C = kP(B^2) = 1 \,, \tag{II.11}$$

where $P(B^2)$ is the non-escape probability already defined.

A simple illustration of the theorem is afforded by a one velocity reactor in which the neutrons are produced, diffused and absorbed without change of energy. In this case the neutron distribution Φ_s, in a trivial sense, is separable in space and energy.

Restricting ourselves, therefore, to such one-velocity systems, we write down the well-known diffusion equation for a stationary (i.e. just critical) reactor.

$$D\nabla^2\Phi_s + (\nu\Sigma_f - \Sigma_a)\Phi_s = 0 \,, \tag{II.12}$$

where D is the diffusion coefficient. E.g. (II.12) represents the balance, in unit volume, between leakage of neutrons (first term) and net-production (second term = production — absorption).

On considering the diffusion equation (II.12) one sees that automatically Φ satisfies the wave equation, if we write (II.12) as:

$$\nabla^2\Phi_s + \frac{k-1}{L^2}\Phi = 0 \,, \tag{II.13}$$

taking

$$k = \frac{\nu\Sigma_f}{\Sigma_a} \,, \qquad L^2 = \frac{D}{\Sigma_a} \quad \text{and} \quad \Sigma_a = \Sigma_f + \Sigma_c \,, \tag{II.14}$$

L is called diffusion length.

If (II.13) is viewed as wave equation, then the buckling B^2 is:

$$B^2 = \frac{k-1}{L^2} . \tag{II.15}$$

For the slab geometry, we have found, using the condition on the boundary, that $B^2 = \pi^2/H^2$. (see (II.5)). Comparing this expression with (II.15), we have the condition that the extensive quantity π^2/H^2 must be equal to the intensive quantity $k-1/L^2$; the latter is called material buckling.

By equating the geometrical to the material buckling

$$B^2 = \frac{k-1}{L^2} , \tag{II.16}$$

one obtains:

$$\frac{k}{1 + L^2B^2} = 1 = C , \tag{II.17}$$

since in a just critical reactor $C = 1$.

Since, by definition, $C = kP(B^2)$, one has in this very simple case

$$P(B^2) = \frac{1}{1 + L^2B^2} . \tag{II.18}$$

The geometric buckling, evidently satisfies the equation required by the first fundamental theorem.

As far as one-velocity systems are concerned, the theorem is almost trivially true, since the wave equation and reactor equation are the same. In more general cases, the reactor equation, instead of (II.12), is an integro-differential equation and is not a wave equation. In such cases, the fundamental theorem is a very useful, and not entirely obvious, general result. We will postpone to a subsequent paragraph, the demonstration of the first fundamental theorem in general cases.

3. – Bare, One-Velocity Critical Reactors.

The criticality condition (II.17) obtained for the bare, one-velocity reactors and the expression for the geometrical buckling—for instance (II.5) for a slab reactor—allows us to compute the size of the reactor required for criticality.

In the case of a sphere, for example, the fundamental mode gives the geometrical buckling

$$B^2 = \frac{\pi^2}{R^2} , \tag{II.19}$$

where R is the radius of the sphere. Thus:

$$R = \frac{\pi L}{\sqrt{k-1}} . \tag{II.20}$$

The size scale of a just critical one velocity reactor is thus determined by the diffusion length, L. This diffusion length is a fundamental length related to the root mean square distance, $\sqrt{r^2}$, a neutron travels from birth to death. Precisely:

$$L^2 = \frac{1}{6} \overline{r^2} . \tag{II.21}$$

From equation (II.20), we see that the multiplication constant, k, determines the number of these fundamental lengths, L, that must be taken to balance neutron leakage by neutron production.

If the reactor had been taken in the shape of a cylinder instead of a sphere, the radius would be given by the same equation (II.20), but with π replaced by the first root of the Bessel function of zero order, i.e. 2.405.

4. – Non-Steady Reactors.

Before going on we shall discuss here, briefly, why the criticality constant, C, plays such a central role in reactor theory.

By denoting the total neutron population in the n-th generation by N_n, we see, according to our previous definition, that:

$$C = \frac{N_{n+1}}{N_n} . \tag{II.22}$$

In the limit of small population change per generation, we may write:

$$N_{n+1} = N_n \left(1 + \frac{l}{N_n} \frac{\Delta N}{\Delta t}\right), \tag{II.23}$$

where $\Delta N/\Delta t$ is the rate of change of population and « l » is the average time between generations.

By comparing (II.23) with (II.22) one obtains in the limit in Δt:

$$\frac{1}{N} \frac{\mathrm{d}N}{\mathrm{d}t} = \frac{C-1}{l} , \tag{II.24}$$

so that:

$$N = N_0 \exp\left[\left(\frac{C-1}{l} t\right)\right] . \tag{II.25}$$

There is, then, an exponential build-up in population with a time constant $l/(C-1)$. That is, the criticality constant determines at what rate a non-steady reactor will grow or wane.

The criticality constant also determines how far a reactor is from the « just-critical » state.

This has a great practical importance in reactor design: if one is building a chain reactor, which is to run for some time, it is necessary to design it so that one may have an available criticality constant greater than unit. Then, as the fuel is consumed and the fission-product poisons grow, one can still obtain criticality.

The difference, $C-1$, is often called the excess reactivity of the reactor and, in practical cases, is sometimes as great as 0.25.

On account of the great importance of the criticality constant, it is necessary to be able to calculate its value for a given configuration, even though this does not represent a « just-critical » situation. For this reason we need to develop a mathematical stratagem, whereby the « first fundamental Theorem », which is usually applied to the « just-critical » situation only, can be applied.

To show how this mathematical stratagem develops, we begin by reminding that in all cases

$$C = \eta f P(B^2) = \frac{\nu}{1+\alpha} f P(B^2) \,. \tag{II.26}$$

If we have a reactor configuration in which the actual value of ν is just, say, ν, but this configuration is not critical, we may consider a reactor identical in every respect, except that we change ν to ν' so that the comparison reactor is « just-critical ». Then:

$$\frac{\nu'}{1+\alpha} f P(B^2) = 1 \,, \tag{II.27}$$

and

$$C_{\text{non-critical}} = \nu/\nu' \,. \tag{II.28}$$

For example, for ^{235}U we said $\nu = 2.54$. If for our actual reactor the ν necessary to obtain criticality, is $\nu' = 2.35$, then the value of the criticality constant for this reactor is just:

$$C = 2.54/2.35 = 1.08 \,.$$

5. – Generalization of the First Fundamental Theorem.

We shall now derive the First Fundamental Theorem for a reactor in which not all neutrons have the same energy.

Since the Fundamental Theorem requires that the neutron distribution be a solution of the wave equation which vanishes on the boundary, we can seek an oscillating solution over the whole space which gives the correct value to the distribution on the geometric boundary of the reactor (*).

This means replacing the actual finite reactor with a similar reactor of infinite extent and considering the oscillating solutions of the reactor equation.

The equivalence of this oscillating solution to the boundary value solution is obvious for systems of a very high degree of symmetry. It is less obvious but, none the less, true that in the most general reactor case (to the order of approximation with which we are concerned) this method of replacing the finite reactor with an infinite one, and computing the first fundamental mode over the whole of space, does provide a solution to the actual reactor problem, in as much as it gives a neutron distribution, which satisfies the reactor equation and is zero on the boundaries for all relevant energies.

We now consider a uniform, homogeneous reactor in which neutrons are produced at energies other than those at which they are absorbed, but in which the fissions are caused only by thermal neutrons. This is almost the case in most moderated reactors.

The equation describing the thermal distribution for such a reactor is:

$$D\nabla^2\Phi_s(\boldsymbol{x}) - \Sigma_a\Phi_s(\boldsymbol{x}) + q(\boldsymbol{x}) = 0, \tag{II.29}$$

(diffusion) (absorption) (production)

where $q(\boldsymbol{x})$, the rate of production of thermal neutrons, will be given by:

$$q(\boldsymbol{x}) = \int_{\substack{\text{volume}\\ \text{of reactor}}} \Sigma_f\Phi(\boldsymbol{x})\cdot\nu\cdot K(\boldsymbol{x};\boldsymbol{x}')\,\mathrm{d}\boldsymbol{x}', \tag{II.30}$$

if we assume a uniform reactor. K is the probability that a fast neutron produced at $\boldsymbol{x}'$ will appear as a slow neutron at $\boldsymbol{x}$.

Since we replace the actual reactor by an equivalent infinite reactor, and since we are assuming a homogeneous, isotropic medium, it is true that K depends only on the distances between $\boldsymbol{x}$ and $\boldsymbol{x}'$; hence we replace $K(\boldsymbol{x};\boldsymbol{x}')$ with $K(|\boldsymbol{x}-\boldsymbol{x}'|)$.

The quantity K, called the « slowing down kernel », is best determined experimentally, but this is often difficult, especially for terminal energies other than thermal. It is therefore, necessary to develop a theory for determining K at any energy. In this simple case of ours, assuming that no nuclear process

(*) Actually by transport theory, the zero solution must occur slightly outside the geometric boundary.

other than scattering occurs during the slowing down, we shall view K as an experimentally given quantity.

Equation (II.29) and (II.30) constitute an integro-differential reactor equation. That the *general* solution of this type of equation will be the solution of the wave equation follows from the fact that these equations are invariant under the translation-rotation group. To see this in the *special* case described by (II.29) and (II.30), we prove that if Φ_s satisfies the wave equation and B^2 satisfies the criticality equation, then Φ_s satisfies the reactor equation.

In general, we may represent the solution Φ_s of (II.29) by a Fourier integral in three dimensions:

$$\Phi(\boldsymbol{x}) = \int_{\text{all space}} g(\boldsymbol{k}) \exp[i\boldsymbol{k}\cdot\boldsymbol{x}]\,\mathrm{d}\boldsymbol{k}\,. \tag{II.31}$$

If we differentiate this twice, in order to get the Laplacian operator and impose the condition that Φ_s satisfies the wave equation (II.4), we get:

$$-k^2\Phi_s + B^2\Phi_s = 0 \quad \text{or} \quad k^2 = B^2\,. \tag{II.32}$$

Thus the vector $\boldsymbol{k}$ is limited to a sphere of radius B and can be represented in terms of a unit vector, $\boldsymbol{\Omega}$, as $\boldsymbol{k} = B\boldsymbol{\Omega}$. Thus:

$$\Phi_s(\boldsymbol{x}) = \int_{\text{unit sphere}} q_1(\boldsymbol{\Omega}) \exp[iB\boldsymbol{\Omega}\times\boldsymbol{x}]\,\mathrm{d}\boldsymbol{\Omega}\,. \tag{II.33}$$

Substituting this value of Φ_s in equation (II.30), we get:

$$q(\boldsymbol{x}) = \nu\Sigma_f \int_{\text{volume}} K(|\boldsymbol{x}'-\boldsymbol{x}|)\left(\int_{\text{unit sphere}} q_1(\boldsymbol{\Omega}) \exp[iB\boldsymbol{\Omega}\times\boldsymbol{x}']\,\mathrm{d}\boldsymbol{\Omega}\right)\mathrm{d}\boldsymbol{x}'\,. \tag{II.34}$$

Multiplying by $\exp[iB\boldsymbol{\Omega}\cdot\boldsymbol{x}]\cdot\exp[-iB\boldsymbol{\Omega}\cdot\boldsymbol{x}]$ and rearranging the order of integration, we obtain:

$$q(\boldsymbol{x}) = \nu\Sigma_f \int_{\text{angle}} q_1(\boldsymbol{\Omega}) \exp[iB\boldsymbol{\Omega}\times\boldsymbol{x}]\cdot \cdot\left(\int_{\text{volume}} K(|\boldsymbol{x}'-\boldsymbol{x}|) \exp[iB\boldsymbol{\Omega}\times(\boldsymbol{x}'-\boldsymbol{x})]\,\mathrm{d}\boldsymbol{x}'\right)\mathrm{d}\boldsymbol{\Omega}\,. \tag{II.35}$$

In performing the integration over $\boldsymbol{x}'$, it is clear that there can be no dependence on $\boldsymbol{\Omega}$, since we are integrating a spherically symmetric function, K, times a factor which is, essentially, a plane wave in all directions. This integral is, in fact, just the Fourier transform of $K(|\boldsymbol{x}'-x|)$, say $K(B^2)$.

Then, since $\overline{K}(B^2)$ can have no angular dependence, it may be taken out of the integral over angles and the remaining integral is just the Fourier representation of $\Phi_s(\boldsymbol{x})$. Thus we have

$$q(\boldsymbol{x}) = \nu\Sigma_f\Phi_s(\boldsymbol{x})\overline{K}(B^2)\,, \tag{II.36}$$

where, explicitely

$$\overline{K}(B^2) = 4\pi\int_0^\infty r^2K(r)\frac{\sin Br}{Br}\,\mathrm{d}r\,. \tag{II.37}$$

In (II.36) we have derived a rather remarkable result: the rate of production of *slow* neutrons at any point in the reactor is just proportional to the rate of production of *fast* neutrons at that same point.

By putting the expression (II.36) for $q(\boldsymbol{x})$ in equation (II.29), we have:

$$D\nabla^2\Phi_s - \Sigma_a\Phi_s + \nu\Sigma_f\Phi_s\overline{K}(B^2) = 0\,, \tag{II.38}$$

which means that we have reduced the integro-differential equations (II.29), (II.30) to a wave equation, provided that B^2 is chosen in such a way that

$$-DB^2\Phi_s - \Sigma_a\Phi_s + \nu\Sigma_f\Phi_s\overline{K}(B^2) = 0\,, \tag{II.39}$$

which proves the First Fundamental Theorem.

From the latter condition and by using (II.14), we find that:

$$\frac{k\overline{K}(B^2)}{1 + L^2B^2} = 1 \qquad (\mathrm{C})\,, \tag{II.40}$$

for a just-critical reactor.

As concluding remarks, let us firstly discuss in more detail the idea of using a wave-like solution to infinity as a representation of the neutron flux distribution in the actual finite reactor.

One assumption made in this is that the extrapolated boundary of the reactor for fast neutrons is the same as that for slow neutrons. This is not true in general and will lead to some complication, except for the case of a very large reactor. But, outside this complication, the oscillating solutions, (which are essentially a representation in terms of positive and negative image sources) will always add together in such a way that the source function at the boundary is zero, as required independently of the shape of the reactor.

Another interesting detail appears, upon close examination of the critical equation (II.40). In the general case, this will be a trascendental equation with many solutions for B^2. It turns out in all cases of practical interest,

that, if $k > 1$, there will be one, and only one, of these solutions which is positive, and this is the solution called the « material buckling », (this is given by (II.16), for one-velocity reactors), the intensive quantity set equal to the « geometrical buckling » for criticality.

There will be, however, many negative solutions for B^2 (sometimes called the « complex material buckling »). These are important in considering non-uniform reactors, in which the neutron flux distribution is not separable in space and energy. In such cases the neutron distribution can be built up by the solutions of the wave equation, in which the wave numbers are equal to the complex material bucklings, as we shall discuss later, in detail.

6. – The Second Fundamental Theorem.

At the beginning of this section we have shown, examining the one-velocity reactor, that the non-leakage probability of thermal neutrons is $1/1 - L^2B^2$. Since $C = kP(B^2)$ for all cases, we can then view $K(B^2)$ as the non-leakage probability for fast neutrons during the slowing-down time. This is a statement of what is often called the Second Fundamental Theorem, namely that:

The fast neutron non-leakage probability is just the Fourier Transform of the slowing-down kernel,

$$P_f = K(B^2) \,. \tag{II.41}$$

One may interpret the non-leakage probability for slow-neutrons as the Fourier Transform of a diffusion kernel. In fact, $P_s = 1/(1+L^2B^2)$ is the Fourier transform of an exponential function which, represents, indeed, the diffusion theory distribution for slow neutrons from a point source of slow neutrons.

7. Application of the First and Second Fundamental Theorems.

7·1. *All-Thermal Model.* – One may apply the First and Second Fundamental Theorems to derive again the critical condition for the simple model of chain reaction, in which all neutrons are considered to be produced as thermal neutrons, i.e. one-velocity chain reactor.

In such a case the slowing down kernel is a delta function

$$K(r) = \delta(r)/4\pi r^2 \,. \tag{II.42}$$

In order to write the critical condition (II.40) we need the Fourier Trans-

form $K(B^2)$ of the slowing-down kernel (II.42):

$$\overline{K}(B^2) = \int_0^\infty \delta(r) \frac{\sin Br}{Br} \, dr = 1 \,. \tag{II.43}$$

If we put this last expression in (II.40), we obtain the critical equation for the one velocity—e.g. all thermal—reactor already given in (II.17).

7·2. *Very Large Reactors.* – For very large reactors, i.e. reactors for which $k \sim 1$, it is possible to obtain a simple expression for the critical condition (II.40).

Since in a very large reactor B^2 is small, we may substitute, in the expression (II.37) for $K(B^2)$, the $\sin Br$ by the first two terms of its development in MacLaurin series:

$$\overline{K}(B^2) \simeq 4\pi \int_0^\infty r^2 K(\pi) \left(1 - \frac{r^2 B^2}{6}\right) dr = 1 - B^2 \frac{\overline{r^2}}{6} \,, \tag{II.44}$$

where $\overline{r^2}$ is the mean square slowing down distance. Thus from (II.44) and the criticality condition (II.40), we get the extremely useful result, for any large reactor, that:

$$B^2 = \frac{k-1}{L^2} \frac{}{\overline{r^2}/6} = \frac{k-1}{M^2} \,. \tag{II.45}$$

where M^2 which is called the migration area and is equal to $L + \overline{r^2}/6$, that is $\frac{1}{6}$-th the mean square distance a neutron travels from birth, as a fast neutron, to capture, as a slow neutron.

It should be noted that (II.44) is independent of the slowing-down model used; the result is numerically valid if $k \approx 1$. Thus the critical size R of a bare reactor, is always given by:

$$R = \text{const} \cdot \frac{M}{\sqrt{k-1}} \,, \tag{II.45a}$$

the constant depending on the shape of the reactor.

The one group equation for R, (II.20), is a special case of (II.45) in which $L = M$. Of course in the one group case it is not necessary to require $k \approx 1$ for the simple result (II.45*a*) to be valid.

Since η for natural uranium is 1.34, so that k is always near unity for unenriched reactors, one may remark that the results of this paragraph are of great importance in reactors which use unenriched fuel .

7·3. *Group Model for Slowing-Down.* – In the « Group Model » of the slowing-down process, it is assumed that the neutrons makes all but the last of the

collisions required to bring it down to thermal energy without any energy change, and then suddenly loses all its energy at the last collision.

In this case, the neutron distribution from a point source is given by:

$$K(r) = \frac{\exp[-r/L_1]}{4\pi L_1^2 r} \,. \tag{II.46}$$

which is obtained by the solution of

$$\nabla^2 K - K/L_1^2 = \delta(r) \,. \tag{II.47}$$

The quantity L_1^2 is $\frac{1}{6}$-th the mean square slowing-down distance in (II.44). The Fourier Transform of K is simply

$$\overline{K}(B^2) = \frac{1}{1 + L_1^2 B^2} \,. \tag{II.48}$$

The expression (2.48) for the non-leakage probability of fast neutrons, during slowing-down, is similar to the non-leakage probability $1/(1 + L^2 B^2)$ for thermal neutrons. One can therefore consider a reactor to which the « group model » for slowing-down is applicable, as a reactor whose neutrons are divided into two groups: a fast group which diffuse with diffusion length L_1 and a thermal group with diffusion length L. This model is called the « Two Group Reactor Model ».

In this case the criticality condition is

$$C = \frac{k}{1 + L^2 B^2} \cdot \frac{1}{1 + L_1^2 B^2} = 1 \,. \tag{II.49}$$

This equation, a quadratic in B^2, involves all the essential complications of the actual slowing-down model, since it has one root positive and another root negative, the latter leading to the complex material buckling, mentioned earlier.

7·4. *Many Group Model.* – Equation (II.49) appears as a particular case of a more general equation, obtained in the « many group model », in which the process of slowing-down is broken up into energy intervals, in each of which cross-sections and diffusion coefficient are constant. In this case the slowing-down kernel is given by the relation:

$$K(|\boldsymbol{x} - \boldsymbol{x}'|) = \tag{II.50}$$

$$= \iint \ldots \int K_1(|\boldsymbol{x} - \boldsymbol{x}_1|) K_2(|\boldsymbol{x}_1 - \boldsymbol{x}_2|) \ldots K_n(|\boldsymbol{x}_{n-1} - \boldsymbol{x}'|) \, \mathrm{d}\boldsymbol{x}_1 \, \mathrm{d}\boldsymbol{x}_2 \ldots \mathrm{d}\boldsymbol{x}_{n-1} \,,$$

where each $K_i(r)$ is a formula like (II.46). Thus by the convolution theorem for Fourier Transform, we obtain:

$$\overline{K}(B^2) = \overline{K}_1(B^2)\overline{K}_2(B^2) \ldots K_n(B^2) . \tag{II.51}$$

The two group result for G given in (II.49) involves two such « group » kernels.

7·5. « *Fermi* » *Age or Continuous Slowing-down Model.* – As a limiting case of the « many group model », we can introduce the infinite group or continuously slowing-down picture, in which the number n of intervals tends to infinity.

Then one has:

$$\overline{K}(B^2) = \lim_{n\to\infty} \prod_n \frac{1}{1 + L_n^2 B^2} . \tag{II.52}$$

Putting

$$\tau = \lim_{n\to\infty} \sum L_n^2 \tag{II.53}$$

it can be seen that (II.52) becomes:

$$\overline{K}(B^2) = \exp[-B^2\tau] , \tag{II.52'}$$

τ is called the neutron « age » or the « Fermi age » and is equal to $\frac{1}{6}$-th of the mean square difference travelled by a fast neutron to thermalization. Since neutrons lose energy as they diffuse outward, τ is a measure of the neutron energy.

Equation (II.52'), (which shows that the Fourier Transform of the slowing-down kernel is gaussian in B^2), permits us to write the criticality equation for an infinite group slowing-down model, in the form:

$$C = \frac{k \exp[-B^2]}{1 + L^2B^2} = 1 . \tag{II.54}$$

Equation (II.54), which is called the Fermi or continuous critical equation, is particularly useful for heavy moderators (e.g. graphite), in which, on the average, a neutron has to make many collisions in slowing-down from an average fission energy of approximatively 2 MeV to thermal energies.

It is interesting to note that by an inverse Fourier Transform of equation (II.52'), one gets again a Gaussian for $K(r)$, the actual slowing-down kernel:

$$K(r) = \overline{\overline{K}(B^2)} = \frac{\exp[-r^2/4\tau]}{(4\pi\tau)^{\frac{3}{2}}} . \tag{II.55}$$

Using indium foils as detectors near a point source of energetic neutrons in a moderator, one finds that the neutron distribution is, in fact, Gaussian, even for moderators as light as heavy water. This is, however, not strictly true at large distance from the source, where the neutrons that have gone through without making a collision, begin to have a predominant influence. In these region the tail of the distribution is found to be not Gaussian but exponential.

One may write down the differential equation describing slowing-down with Gaussian distribution. This equation is adequate for most moderators of interest in chain reacting systems. Evidently the well-known equation of heat conduction, namely:

$$\nabla^2 K = \frac{\partial K}{\partial \tau} \qquad S \,, \tag{II.56}$$

where S denote the source distribution, will have a Gaussian solution if S is a delta function: hence (II.56) may be taken as the differential equation for slowing down of neutrons. Herein $K(r, \tau)$ is proportional to the rate of production per cm^3 of neutrons at r at an energy corresponding to the « age ».

8. – The Approach to Criticality.

In the preceding paragraphs we have mainly dealt with neutron distribution in « just critical » assemblies. It is also very important to see what happens to the neutron in a subcritical reactor, as criticality is approached.

Criticality can be approached either by gradually increasing the size of the reactor, thus decreasing the geometrical buckling, or else adding additional fuel (say ^{235}U), thus increasing the multiplication constant. Both of these methods increase C. While carrying out « critical » experiments, it is essential to know how close one is to criticality, so that the reactor should not be made supercritical inadvertently.

To see how the neutron distribution changes as C is increased, we write the neutron balance equation (or reactor equation), using two types of neutron sources: the fission source and an extraneous neutron source, The latter source is necessary to sustain the chain reaction in a subcritical assembly, so as to have a stationary neutron distribution. Thus the balance neutron equation is:

$$D\nabla^2 \Phi_s - \Sigma_a \Phi_s + \nu\Sigma_f \int K(|\boldsymbol{x} - \boldsymbol{x}'|)\Phi_s(\boldsymbol{x}')\,\mathrm{d}\boldsymbol{x}' + \tag{II.57}$$

$$+ \int H(|\boldsymbol{x} - \boldsymbol{x}'|)S(\boldsymbol{x}')\,\mathrm{d}\boldsymbol{x}' = 0 \,.$$

Here $H(|\boldsymbol{x}-\boldsymbol{x}'|)$ is the slowing-down kernel of the extraneous neutron source and may be different from K. S represents the number of neutrons emitted by the extraneous source per second per unit volume.

We seek solutions of (II.57) which are a superposition of solutions of the wave equation. Considering not just the fundamental mode but all modes, we write for the n-th mode wave equation:

$$\nabla^2\psi_n + B_n^2\psi_n = 0 \,. \tag{II.58}$$

The ψ_n's all satisfy the boundary conditions and form a complete orthogonal set of functions. We can thus, develop the flux Φ_s and the extraneous source distribution S, in series of the ψ_n's:

$$\Phi_s = \sum a_n\psi_n \,; \qquad S = \sum s_n\psi_n \,. \tag{II.59}$$

By substituting (II.59) in (II.57) and making use of the second fundamental theorem applied to the ψ_n, namely:

$$\int \psi_n(\boldsymbol{x}')K(|\boldsymbol{x}-\boldsymbol{x}'|)\,\mathrm{d}\boldsymbol{x}' = \overline{K}(B_n^2)\psi_n(\boldsymbol{x}) \,, \tag{II.60}$$

and finally of the orthogonal properties of the ψ_n's, we easily get

$$[-DB_n^2 - \Sigma_a + \nu\Sigma_f\overline{K}(B_n^2)]a_n + S_n\overline{H}(B_n^2) = 0 \,. \tag{II.61}$$

Solving for a_n one then obtains, for the neutron distribution in a subcritical reactor with an extraneous source:

$$\Phi_s(\boldsymbol{x}_1) = \sum_n \frac{S_n\overline{H}(B_n^2)}{(DB_n^2+\Sigma_a)(1-C(B_n^2))}\psi_n(\boldsymbol{x}) \,, \tag{II.62}$$

where $C(B_n^2)$ is the value of the criticality constant corresponding to the n-th-mode buckling B_n^2.

It is no longer true, from (2.62), that in a subcritical reactor the distribution is determined by the fundamental solution of the wave equation. For example, suppose, $k = 0$: then $C = 0$ and we get a neutron distribution as in a dead block of material with a source in it.

Let us see what happens in the approach to criticality. As k is increased, each $C(B_n^2)$ increases. However, the $C(B_0^2)$ corresponding to the fundamental mode, with buckling B_0^2, approaches unity faster, since the B_0^2 of the fundamental mode is lower than for higher modes. In other words, the leakage of « fundamental mode neutrons » is always less than that of higher mode neutrons,

and this is the reason why $C(B_0^2)$ approaches 1 faster than any higher $C(B_n^2)$.

Thus, as one approaches criticality, the neutron distribution changes from a distribution characterized by the source, to one characteristic of the multiplying medium (see Fig. 3), this latter being the wave function for the zeroth order mode, i.e.

$$\Phi_s \to \frac{S_0 \overline{H}(B_0^2)}{(DB_0^2 + \Sigma_a)(1 - C(B_0^2))} \psi_0(\boldsymbol{x}) \,. \tag{II.63}$$

In an actual experiment BF_3 counters are placed at various points, to measure the neutron flux. One starts with the extraneous source neutrons and gradually builds up the concentration of fissionable material (or increases

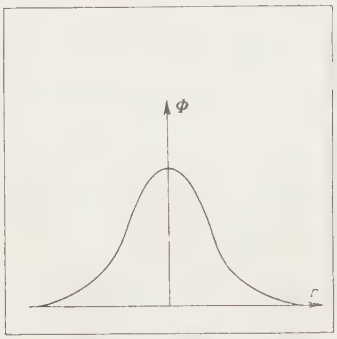

Fig. 3*a*. – Source neutron distribution: $k = 0$.

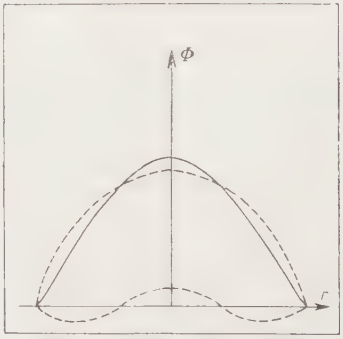

Fig. 3*b*. – Neutron distribution in approaching criticality: $k \to 1$.

the reactor size). The multiplication rate R is defined as the ratio of the total number of neutrons produced, to the total number of neutrons produced by the source. Since only the zeroth mode contributes to the integral over the reactor, the multiplication rate is found immediately from (II.63), viz.

$$R \cong \frac{\int (\Sigma_a + DB_0^2)\Phi_s \, \mathrm{d}\boldsymbol{x}}{\int S_0 \overline{H}(B_0)\psi_0 \, \mathrm{d}\boldsymbol{x}} \frac{1}{1 - C(B^2)} \,. \tag{II.64}$$

Thus as $C \to 1$, $R \to \infty$. From the measurement of R, one may deduce the value of the criticality constant C. In making such a measurement, however, one should remember that the BF_3 counting rate, early in the experiment, will be sensitive not only to changes in C, but also to changes in the flux distribution of neutrons from the source function to the fundamental mode

function. The placing of BF_3 counters is, therefore, a matter of considerable importance.

As one approaches $C = 1$, however, the fundamental mode tends to swamp out all others, and then changes in the BF_3 counting rate are truly a measure of the change in C.

9. – Non-Thermal Reactors.

Until now we have considered only reactors in which all of the fissions occur at thermal energies, none at higher energies. This is a good approximation to the original moderated, natural uranium reactors.

However, now, with the availability of pur fissionable material, one must also consider reactors in which appreciable fission occurs at other than thermal energies.

There are, at least, two practical considerations that make the high energy reactors seem desirable: we saw previously that the ratio of the capture to fission cross sections, decreased considerably with energy so that η became considerably greater than 2 (especially for the ^{238}U–^{239}Pu system) thus making « breeding » more possible at higher energy. Secondly, a fast reactor can be made of much smaller size than a thermal reactor, an important consideration especially in designing portable reactors. For a limited size reactor and, hence limited amount of moderator, the moderator to fuel ratio decreases with the size and the average neutron energy, at which fissions must occur, increases. Thus it is necessary to develop the mechanics for calculating critical conditions of a system in which fissions occur at any energy.

9·1. *The Slowing-down Density.* – First we consider, in some detail, the energy distribution of the neutrons in a reactor.

Since the slowing-down kernel $K(r)$ represents the probability that a fast neutron, produced at one point, appears as thermal at another point, a distance « r » away, this will evidently be proportional to the so called « slowing-down density », i.e. the number of neutrons crossing the energy E per cm^3 per second at « r ». It is therefore, useful to derive an expression for the slowing down density. For this purpose it is necessary to consider the kinematics of scattering.

Assuming isotropic scattering, in the center of gravity system, it turns out that the average energy after collision is a fixed fraction of the average energy before collision, independent of the magnitude of this initial energy. Thus the ratio of E_0, the energy before collision, to E, the energy after collision, is a constant. We will define the natural logarithm of this ratio, as

the « lethargy » u:

$$u = \log \frac{E_0}{E} . \tag{II.65}$$

Per collision, on the average, the lethargy jumps by equal intervals. Thus, to get the number of collisions that a neutron makes in going from, say, 10 MeV to 1 MeV, one simply calculates the difference in lethargy between these energy states and divides this by the average gain in lethargy per collision.

Now, this latter quantity, i.e. the distance in lethargy space that neutrons travel, on the average, per collision, can be calculated from simple kinematics, assuming isotropic scattering. The result, in terms of the atomic weight, A, of the moderator nuclei, is

$$\xi = 1 + \frac{\alpha^2}{1 - \alpha^2} \ln \alpha^2 , \tag{II.66}$$

where

$$\alpha = \frac{A - 1}{A + 1} .$$

For all but very light nuclei, one has, with good approximation:

$$\xi \cong \frac{2}{A + \frac{2}{3}} . \tag{II.67}$$

Values of ξ for the most important moderators are given in the following table:

TABLE V. – *Values of* ξ.

Hydrogen	Deuterium	Berillium	Graphite
1	0.725	0.22	0.158

Now, we can compute the slowing-down density, $q(\boldsymbol{x}, u)$ from the number of collisions occurring at lethargy u per unit lethargy per cm³ per second. For doing so, one has simply to multiply this latter quantity by the average gain in lethargy per collision, that is:

$$q(\boldsymbol{x}, u) = \Sigma_s \Phi(\boldsymbol{x}, u) \cdot \xi , \tag{II.68}$$

where $\Phi(\boldsymbol{x}, u)$ is the neutron flux per unit lethargy and Σ_s is the macroscopic scattering cross section.

In section *II.7* we found that a slowing-down kernel, $K(r)$, good for all

moderators but hydrogen, is the Gaussian kernel (II.55). From the proportionality between the slowing-down kernel and the slowing-down density, that we have noted above, one sees that q is related in the same way as K, i.e. as a Gaussian, to the « Fermi age » τ. Thus, if we can express τ in terms of lethargy, we can obtain a differential equation like (II.56), which describes the slowing-down process in space and lethargy.

9·2. *The « Fermi Age ».* – One can simply generalize the definition of τ given above, when we were mainly interested in thermal reactors: τ gives one sixth of the mean square distance a neutron travels in going from energy E_1 to energy E. Using this definition of τ and the fact that the neutron motion is statistically random during the slowing-down, one can add up the mean square distances for each step of the slowing process to obtain the total τ.

To calculate the mean square distance a neutron travels in going through an increment $\mathrm{d}u$ of lethargy space, we first realise that the number of collisions that occurs is: $\mathcal{N} = \mathrm{d}u/\xi$. Secondly one must recall that, for a random walk, the mean square distance is given by:

$$r^2 = 2 \cdot \mathcal{N} \cdot \lambda \cdot \lambda_t \,, \tag{II.69}$$

where λ is the mean free path $= 1/\Sigma_s$ and λ_t is the transport mean free path given by

$$\lambda_t = 3D \cong \frac{\lambda}{1 - 2/3A} \,, \tag{II.70}$$

where A is the atomic weight of the target nuclei.

Adding terms of type (II.69), together, to cover the total lethargy interval, from $u' = 0$ to $u' = u$, we have for the Fermi age:

$$\tau(u) = \int_0^u \frac{D}{\Sigma_s} \frac{\mathrm{d}u}{\xi} \,. \tag{II.71}$$

9·3. *Slowing-Down Differential Equation.* – The expression (II.71) for τ permits the construction of a differential equation for the slowing-down in space and lethargy. This equation is obtained by the already given differential equation (II.56), for the Gaussian slowing-down kernel, simply by changing from the age τ to the lethargy u, as independent variable, i.e.

$$\frac{D(u)}{\Sigma_s \xi} \nabla^2 q(\boldsymbol{x}, u) = \frac{\partial}{\partial u} \big(q(\boldsymbol{x}, u)\big) \,, \tag{II.72}$$

where we assume that ξ and Σ_s are independent of space.

Using (II.68), (II.72) can be written as an equation for $\Phi(\boldsymbol{x}, u)$

$$D(u)\nabla^2\Phi(\boldsymbol{x}, u) = \frac{\partial}{\partial u}\left(\Sigma_s \xi \Phi(\boldsymbol{x}, u)\right). \tag{II.73}$$

Equation (II.73) is the so-called « slowing-down differential equation », which will be taken as fundamental in describing the slowing-down process.

Now, to determine the criticality condition and the neutron distribution, it is only necessary to write down the material balance equation at each energy : the solution of the equation will be found by applying the First Fundamental Theorem.

9·4. *Neutron Energy Distribution in Infinite Uniform Systems.* – First of all, let us investigate, the form of the neutron energy distribution, in an infinite medium, where the neutrons are produced everywhere equally at high energy and are slowed down without any high energy absorption.

Since there will be no spatial dependence for Φ in equation (II.73), one has merely

$$\xi\Sigma_s\Phi(u) = Q\,, \tag{II.74}$$

where Q, the number of neutrons produced at high energy per cm³ is a constant. Thus we have the result that, if there is no leakage or absorption, the slowing-down density, q, is equal to Q, the number of high energy neutrons produced per cm³ per second.

Replacing u by E, as the variable, and noting that:

$$\Phi(u)\,\mathrm{d}u = \Phi(E)E\,\mathrm{d}E \tag{II.75}$$

we have

$$\Phi(E) = \frac{Q}{\xi\Sigma_s E}. \tag{II.76}$$

This is the well-known $1/E$ rule, which is really a very good approximation to the distribution of moderatly high energy neutrons in a thermal reactor, in which there is no absorption at high energy. It is because of the energy distribution that the velocity selectors using reactor neutrons are ineffective above about 1000 eV.

To consider the effect of absorption we must include a term $\Sigma_a(u)\Phi(\boldsymbol{x}, u)$ on the left side of equation (II.73). Again neglecting the spatial term, solving for Φ and converting to energy, as independent variable, one obtains

$$\Phi(E) = \frac{Q}{\xi\Sigma_s E}\exp\left[-\int_E^{E_0}\frac{\Sigma_a}{\xi\Sigma_s}\frac{\mathrm{d}E'}{E'}\right], \tag{II.77}$$

where the exponential is really a measure of the effectiveness of absorption (Σ_a) when compared with the slowing-down by scattering ($\xi\Sigma_s$). In a large reactor, this is an extremely good representation of the energy distribution of the higher energy neutrons.

One can now calculate the loss of neutrons due to absorption, in passing from energy E_2 to a lower energy E_1.

We compute the neutron flux at energy E_2 and compare it to the flux appearing at E_1. Then the probability of escaping absorption, called the « resonance escape probability » is:

$$p(E_2 \to E_1) = \frac{q(E_2)}{q(E_1)} = \frac{\xi\Sigma_s E_2 \Phi(E_2)}{\xi\Sigma_s E_1 \Phi(E_1)} = \exp\left[-\int_{E_1}^{E_2} \frac{\Sigma_a}{\xi\Sigma_s} \frac{\mathrm{d}E'}{E'}\right]. \tag{II.78}$$

Actually this is true only to first order, where the absorption is not so strong as to change the basic $1/E$ character of the energy distribution. At very sharp resonances, (II.78) tends to overestimate the loss; the equation is corrected by replacing Σ_s by $\Sigma_{\text{total}} = \Sigma_s + \Sigma_a$ in the denominator of the integrand.

9·5. *Finite Non-Thermal Critical Reactor.* – Now we shall take into account the finite size of the reactor, but still consider only a uniform, stationary system, so that we can still use the First Fundamental Theorem (i.e. replace $\nabla^2\Phi$ by $-B^2\Phi$ in all equations where it occurs). Thus the slowing-down equation with capture

$$D(u)\nabla^2\Phi(\boldsymbol{x}, u) - \Sigma_a(u)\Phi(\boldsymbol{x}, u) = \frac{\mathrm{d}}{\mathrm{d}u}\left(\xi\Sigma_s\Phi(\boldsymbol{x}, u)\right), \tag{II.78}$$

immediately becomes:

$$-B^2 D(u)\Phi(\boldsymbol{x}, u) - \Sigma_a(u)\Phi(\boldsymbol{x}, u) = \frac{\mathrm{d}}{\mathrm{d}u}\left(\xi\Sigma_s\Phi(\boldsymbol{x}, u)\right). \tag{II.80}$$

The leakage caused by the finite size is mathematically the same as a true absorption and the solution can be written immediately by analogy to (II.77):

$$\Phi(\boldsymbol{x}, E) = \frac{Q}{\xi\Sigma_s E} \exp\left[-\int_{E}^{E_0} \frac{B^2 D(E') + \Sigma_a}{\xi\Sigma_s} \frac{\mathrm{d}E'}{E'}\right] = \tag{II.81}$$

$$= \frac{Q}{\xi\Sigma_s E} \exp\left[-B^2\tau(E_0 \to E)\right] \exp\left[\int_{E}^{E_0} \frac{\Sigma_a}{\xi\Sigma_s} \frac{\mathrm{d}E'}{E'}\right].$$

This is a very good approximation to the energy distribution, in a reactor of finite size for the neutrons of energy below the fission spectrum.

To complete the problem and to arrive at the criticality constant we must now write down the material balance equations, both of fast and thermal neutrons:

$$\text{(II.82)} \qquad \begin{cases} D(E)\nabla^2\Phi(\boldsymbol{x}, E) - \Sigma_a\Phi(\boldsymbol{x}, E) + S(\boldsymbol{x}, E) = \dfrac{\partial}{\partial E}\left(\xi\Sigma_s E\Phi(\boldsymbol{x}, E)\right), \\ D(E_t)\nabla^2\Phi_t(\boldsymbol{x}) - \Sigma_a\Phi_t(\boldsymbol{x}) + S(\boldsymbol{x}, E_t) = \xi\Sigma_s E_t\Phi(\boldsymbol{x}, E_t), \end{cases}$$

where:

$$S(\boldsymbol{x}, E) = \nu f(E)\left\{\int\Sigma_f(E')\Phi(\boldsymbol{x}, E')\,dE' + \Sigma_f(E_t)\Phi_t(\boldsymbol{x})\right\},$$

represents the source for production of neutrons, both by fast and thermal fissions and $f(E)$ is the energy distribution function of the neutrons produced in fission.

The term $S(\boldsymbol{x}, E_t)$ is usually neglected, since very few of the neutrons produced in fission are at thermal energies at birth.

In (II.82), $\Phi_t(\boldsymbol{x})$ is the actual neutron flux at thermal energy; this is not to be confused with $\Phi(\boldsymbol{x}, E_t)$ which is the flux of nascent neutrons per unit energy interval, just above thermal energy, as computed by the first of equations (II.82).

The problem, now, is to seek solutions of the integro-differential equation (II.82). Again, if we assume a uniform, stationary reactor, we can apply the First Fundamental Theorem and thus get the ordinary differential equations whose solutions are of the type

$$\text{(II.83)} \qquad \Phi = \frac{S}{\xi\Sigma_s E}\exp\left[-B^2\tau(E_0 \to E)\right]\exp\left[-\int\frac{\Sigma_a}{\xi\Sigma_s}\frac{dE'}{E'}\right],$$

as we found previously in equation (II.81).

Here, however, S involves Φ so we need a self consistency condition to obtain a valid solution. This condition turns out to be just the criticality equation:

$$\text{(II.84)} \qquad C = \nu\int_0^\infty\frac{dE}{E}\,\frac{\Sigma_f(E)}{\xi\Sigma_s(E)}\int_E^\infty dE' f(E')\exp\left[\int_E^{E'}\frac{\Sigma_a(E'')}{\xi\Sigma_s(E'')}\frac{dE''}{E''} - B^2\tau(E' - E)\right]$$

$$= \frac{\nu\Sigma_f(E)}{\Sigma_a(E_t)}\cdot\frac{1}{1 + L^2B^2}\int_{E_t}^\infty dE' f(E')\exp\left[-\int_{E_t}^{E'}\frac{\Sigma_a(E'')}{\xi\Sigma_s(E'')}\frac{dE''}{E''} - B^2\tau(E' - E_t)\right] = 1.$$

The criticality condition (II.84) may be written in a more compact way as:

$$\text{(II.85)} \qquad C \equiv k_{\text{fast}}\exp\left[-B^2\tau_{\text{fast}}\right] + \frac{k_{\text{slow}}}{1 + L^2B^2}\exp\left[-B^2\tau_{\text{slow}}\right] = 1,$$

where the new parameters introduced are defined by comparison with (II.84); k_{fast} may be defined as the multiplication constant for other than thermal fission, i.e. k_{fast} represents the number of neutrons produced by non-thermal fission; while τ_{fast} and τ_{slow} are the average Fermi age for neutrons causing non-thermal and thermal fission respectively.

The version (II.85) of the criticality condition may appear rather artificial and in fact, it is so, in the case of intermediate bare reactors (which use enriched fuel) in which non-thermal fission occurs over a broad lethargy range.

With natural uranium thermal reactors, however, the situation is different. Here non-thermal fission is confined essentially to fast fission in ^{238}U, i.e. in a narrow lethargy interval above the ^{238}U fission threshold. Thus one can assume that all non-thermal fissions are caused by neutrons which have not been moderated at all, i.e. neutrons for which $\tau_{\text{fast}} = 0$.

For such natural uranium reactors, it is customary to introduce a « fast effect factor » ε, defined as the number of neutrons produced by all fissions per neutrons produced by thermal fission. ε is related to k_{fast} by

$$\varepsilon = \frac{1}{1 - k_{\text{fast}}} . \tag{2.86}$$

The criticality condition then becomes for a natural uranium reactor:

$$\frac{\varepsilon k_{\text{slow}} \exp\left[-B^2 \tau_{\text{slow}}\right]}{1 + L^2 B^2} = 1 . \tag{2.87}$$

10. – Non Uniform Reactor Systems.

Till now have considered uniform chain-reacting systems, i.e. systems in which the « intensive » properties are not functions of the position in the reactor.

The most common non uniformity met with, in a reactor, is a reflector. The purpose of a reflector is two-fold; the most obvious is to reduce the neutron leakage. This has the effect of increasing the criticality constant, C. Such increased reactivity, caused by the reflector, can be exploited by making the reactor smaller than it would be without a reflector; this involves a reduction in the amount of expensive fissionable material used in the reactor. Excess reactivity may be used also to allow the reactor to be run for a longer period, without a change of fuel. At the beginning of the operation, the excess criticality can, of course, be taken up by control rods of Cadmium or Boron steel, which are strongly neutron absorbing and, as the criticality falls in the running of the reactor, these rods are gradually moved out. Still another reason for

putting a reflector around a reactor is that it makes the neutron density more uniform through the reactor.

As the Fig. 4 shows, the reflector raises the neutron distribution at the edge of the reactor, so that the central region flux tends to be much less peaked than it would be without a reflector. This is a most important point, technologically, for the following reason: the ultimate aim, in designing a reactor, is to extract the heat from the system, and it is clear that the heat-extracting mechanism must be such as to cool the most active point adequately. (In a bare reactor this is at the center.) If the cooling system is working to capacity at the center, then as the power is less at the edges, the coolant is idling there. An aim of reactor design is, therefore, to achieve a uniform neutron density and, consequently the maximum utilization to the fuel and coolant throughout the reactor.

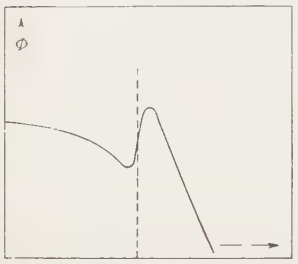

Fig. 4. - Thermal neutron distribution in a Material Testing Reactor type reactor.

Finally, if the experiment requires a high slow-neutron density, this can be attained in a reflector, which, because of its small capture—i.e. long neutron lifetime—may, in some cases, have a neutron density larger than that in the reactor. This finds a useful application in irradiation experiments, production of isotopes and so on.

A typical reactor with neutron thermal flux greater in the reflector than in the reacting core is the Material Testing Reactor (M.T.R.) whose thermal flux distribution is of the type of that given in the above Fig. 4.

10·1. *Neutron Distribution Equations for Non-Uniform Reactor.* – In large reflected reactors, i.e. in reactors whose dimensions are large in comparison with the migration length, the neutron distribution in the reactor core, far from the edges, is well approximated by the distribution that would be there if the reactor were uniform and bare—i.e. given by the First and Second Fundamental Theorems. Such a distribution is called the asymptotic neutron distribution; it is the zero mode solution of the wave equation.

On the other extreme, for reactors, such as M.T.R. or, for instance, the small swimming-pool reactor exibited at the Atoms for Peace exhibition of Geneva, both of which use enriched fuel, the reactor dimensions are not very large compared to the migration length and the neutron distribution scarcely has space to acquire the shape characteristic of the asymptotic solution (see the above Fig. 4).

The basis for making an estimate of the neutron distribution in such a system is usually the neutron balance equation, based on the continuous slowing-down model.

Since generally, the diffusion coefficient, D, and cross-sections may be arbitrary functions of space, the reactor equations for a non-uniform reactor are

$$\text{(II.88)}\qquad \begin{cases} \operatorname{div} D(\boldsymbol{x}, u)\operatorname{grad}\Phi(\boldsymbol{x}, u) - \Sigma_a(\boldsymbol{x}, u)\Phi(\boldsymbol{x}, u) + \\ \qquad + \nu f(u)\left\{\int_0^u \Sigma_f'(\boldsymbol{x}, u)'\Phi(\boldsymbol{x}, u')\,\mathrm{d}u' + \Sigma_f(\boldsymbol{x}, u_t)\Phi_t(\boldsymbol{x})\right\} = \dfrac{\partial}{\partial u}\{\xi\Sigma_s\Phi\}\,, \\ \operatorname{div} D(\boldsymbol{x}, u_t)\operatorname{grad}\Phi_t(\boldsymbol{x}) - \Sigma_a(\boldsymbol{x}, u_t)\Phi_t(\boldsymbol{x}) = \xi\Sigma_f\Phi(\boldsymbol{x}, u_t)\,, \end{cases}$$

where, in the thermal equation, we have not written the fission-source term, for $f(u_t) \simeq 0$. The notations in (II.88) are the same as in the reactor equations (II.82) for uniform systems. The solution of (II.88) is both tedious and difficult, especially as D may vary arbitrarily, depending on the disposition of material in the reactor. Therefore, one approaches the problem by calculating the criticality constant iteratively from its definition (II.22) namely $C = N_{n+1}/N_n$, where N_n is the number of neutrons in the n-th generation.

In order to see how the iteration proceeds, we suppose that the high energy neutrons are initially distributed uniformely in the reactor. These will proceed to diffuse and multiply and be absorbed as given by equation (II.88).

Their initial uniform distribution may be viewed as a superposition of fundamental spatial modes. (In the case of a uniform reactor, these modes are also solutions of the wave equation; in a reflected reactor case, the various modes will be much more complicated functions).

In proceeding from fast to slow neutrons—i.e., as the neutron undergoes moderation—higher harmonics decay faster then the fundamental. This may be seen by recalling that in a uniform reactor, the neutron distribution has a term in it proportional to $\exp[-B^2\tau(u)]$, and B^2 for a higher mode is larger than for a lower.

The decay of the higher spatial neutron distribution, can also be understood by noting that the higher harmonics correspond to a smaller reactor, so that the neutron distribution in these modes, would tend to leak out most easily.

From this rough consideration, one can see that, after a few successive iterations, the spatial dependence of the neutron distribution settles down to the shape characteristic of the fundamental mode. The heigth of the distribution, however, changes: it increases if the reactor is super-critical and decreases if it is sub-critical.

Thus the computation of C requires one to carry out successive iterations until the spatial dependence of the distribution has settled down, and then to take the ratio of the heights in successive iterations.

The mathematical techniques used to solve equations of type (II.88) vary. For example it has become standard practice, in the United States, to divide the lethargy into intervals $u_i - u_{i-1}$, thus breaking the partial differential

equation into a sequence of ordinarily differential equations. Each of these is then integrated over the lethargy interval and the results averaged. Thus the term on the right hand side of (II.88) becomes $\xi\Sigma_s(\Phi(u_i) - \Phi(u_{i-1}))$ and (II.88) becomes a set of coupled differential equations.

Each has a term corresponding to neutrons entering the lethargy interval, and another term corresponding to neutrons which leave it. If the number of lethargy groups is larger than 3, high speed computing equipment is almost a necessity. The three group theory, which can be handled without a machine, often gives good results, but with electronic equipment, calculations have been made using up to a hundred groups.

The above described calculation gives merely C, and to obtain the critical reactor size, it is found to be practical, especially if one is using a high speed computer, to calculate the criticality constant for two given configurations and then interpolate the value of the reactor size for $C = 1$.

This method is specially useful since the alternative approach, namely that of setting up and attempting to solve a boundary value problem, tends to get out of hand.

11. – Microscopic Reactor Theory; General Remarks

We have so far been dealing with the behavior of the reactor as a whole, i.e. we have been concerned with « macroscopic reactor theory ».

In macroscopic theory we have taken the intensive parameters as « given », and then calculated the extensive quantities C and Φ. The task of determining the intensive quantities of a reactor—primarily the multiplication constant k—was, historically, the more important problem since it was involved in heterogeneous natural U reactors such as the original graphite reactors. The calculation of the intensive parameters is called « microscopic reactor theory ».

For a homogeneous thermal reactor, using ^{235}U, the determination of k is simple if we ignore the energy distribution of the neutrons. The multiplication constant k is given by:

$$k = \eta f = \frac{\nu}{1 + \alpha} \frac{\Sigma_{a,\text{fuel}}}{\Sigma_{a,\text{fuel}} + \Sigma_{a,\text{elsewhere}}}, \tag{II.89}$$

where the parameters were defined in Sect. *II.1*.

The original problem of microscopic theory was the determination of how best to dispose the fuel in the body of the reactor in order to achieve a multiplication constant k that is greater than unity. This is not easy since the value of η in natural U exceeds unity by only about 30%.

It is found that introducing the uranium in the form of lumps or rods,

rather than homogeneously, greatly reduces resonance absorption in ^{238}U and therefore improves the multiplication constant. This comes about because resonance capture in ^{238}U is concentrated in lines. If neutrons of all energies enter a lump of uranium the neutrons at the ^{238}U resonance energies will be filtered out by the surface layer, and there will be relatively few resonance neutrons available to be absorbed in the lump interior.

The effect of lumping the uranium, is measured by the so called « resonance absorption integral »,

$$I_{\text{eff}} = \int \sigma_a(E) \frac{dE}{E} . \tag{2.90}$$

The experimental value for I_{eff} goes from 260 F, for a thin foil of natural U, to about 20 F for a large lump of natural U. It is this « effective » resonance integral which is to be used in equations (II.78) in estimating the resonance escape probability in heterogeneous reactor.

Another effect of lumping uranium is that the probability of fast fission in ^{238}U is increased because the bulk of the ^{238}U is exposed to undegraded fission neutrons with energy higher than the fission threshold.

The fast effect defined as the ratio of neutrons produced by all fission to neutrons produced by thermal fission is denoted by ε.

For heterogeneous systems the calculations of the thermal utilization f is much more complicated than in homogeneous systems, because the neutron densities in the moderator and fuel are different.

In order to deal with the computation of k in such reactors it is useful to put in evidence the different contribution to the neutron multiplication, expressing k as the product of four factors:

$$k = \eta \varepsilon p f . \tag{II.91}$$

These factors have already been defined as follows: η gives the number of neutrons produced per neutron absorbed by fuel; ε is the fast fission factor (see (II.86)); p the resonance escape probability (see (II.78)), and f the thermal utilization given by the ratio of thermal neutrons absorbed by fuel to the total number of thermal neutrons absorbed. For a heterogeneous system p may be put in the form:

$$p \sim \exp\left[- \frac{N_U}{N_m \sigma_s \xi} \cdot I \right] , \tag{II.92}$$

where N_U is the number of atoms of fuel per cm^3, and N_m that of moderator; I is the resonance integral.

We can roughly see, looking at the definitions of f and p, what is the

expected behavior of the product fp, (i.e. essentially k) as the volume ratio of fuel to moderator changes.

If there were no moderator, the thermal utilization would be equal to unity. As the proportion of moderator is increased, the absorption in the latter competes increasingly with the absorption in the fuel and f falls off.

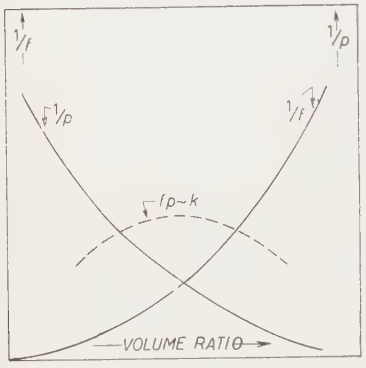

Fig. 5. – Qualitative behaviour of $1/f$, $1/p$ and $fp \simeq k$ as function of the volume ratio — i.e. the ratio of the moderator to fuel volume.

On the other hand p shows a reverse trend: it is unity in the case of moderator only and gradually decreases as fuel is added. The product fp, as is shown in the Fig. 5 would therefore, have an optimum value, and hence so also will k.

The exact determination of the optimum lattice parameters, i.e. volume ratio and rod radius, depends on what one seeks to optimize, Thus if minimum uranium holdup is required, it proves in practice necessary to optimize so that k is nearly a maximum. On the other hand if minimum reactor size rather than minimum fuel holdup were the primary consideration, thus implying maximum material buckling, one should have to minimize the dimensions, so that the criticality constant

$$C = k \frac{\exp[-B^2\tau]}{1 + L^2B^2},$$

rather than simply k would have to be an optimum. In general the maximum of C and of R do not occur at the same dimensions.

11·1. *The Thermal Utilization.* – We shall now deal a little more with the thermal utilization since the calculation of this quantity is somewhat involved. In a homogeneous system one can write the thermal utilization as follows:

$$f = \frac{\Sigma_{a0} V_0}{\Sigma_{a0} V_0 + \Sigma_{a1} V_1}, \tag{II.93}$$

where the subscript zero and one refer to « fuel » and moderator (plus coolant etc.) respectively, and V is the volume of the material in question.

In a heterogeneous reactor, this simple expression is modified, because the neutron density in moderator and fuel are different. The moderator and fuel cross-sections must be weighted with the average neutron densities in

both the regions. Thus if d (called the « disadvantage factor ») is the ratio of relative neutron density in moderator and fuel, then for a heterogeneous system one has

$$f = \frac{\Sigma_{a0} V_0}{\Sigma_{a0} V_0 + \Sigma_{a1} V_1 d} . \tag{II.94}$$

The theoretical problem of heterogeneous reactor theory is primarily concerned with computing d.

In order to see how such calculations are made, we suppose that the fuel is in a square lattice of cylindrical rods. We first assume cylindrical cell boundaries, for simplicity. If we focus our attention then on a particular cell, and require the boundary condition that the normal derivative of the flux be zero, so that the boundary is a surface of symmetry, we can attempt to find solutions of the simple diffusion equation, giving the slow neutron flux distribution Φ_0 in the fuel element and Φ_1 in the moderator.

The ratio of the average values of these is:

$$d = \Phi_1^{\mathrm{Av}} / \Phi_0^{\mathrm{Av}} . \tag{II.95}$$

We can obtain a qualitative picture of the thermal flux distribution, by remembering that in the fuel slow neutrons are absorbed and fast neutrons are produced. These fast neutrons diffuse out of the fuel and are changed to slow neutrons in the moderator with very little absorption. Thus the slow neutron flux is higher in the moderator than in the fuel in some case by as much as a factor 2. A discontinuity in shape occurs at the boundary due to the difference in diffusion coefficients in the two materials (see the Fig. 6).

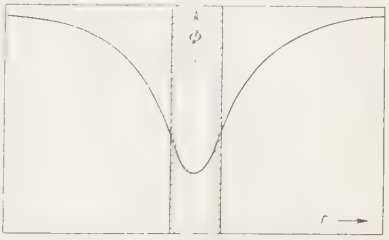

Fig. 6. – Neutron flux distribution in a cilindrical cell.

The actual calculation of d is usually done on the basis of ordinary diffusion theory even though the assumption that the angular distribution can be represented by the first two spherical harmonics is not really valid in many practical cases. Still the error is rather small and the more elaborate methods require extensive computation, so that the zero-order diffusion theory is usually used.

12. – Reactor Kinetics; General Remarks.

In order to conclude our rapid survey of reactor design problems, we shall now turn to a brief discussion of the kinetics of reactors, when they are not

in their steady state. In our previous discussion, everything has referred to the steady state ($C = 1$), except in Sect. *II.4* where, to illustrate the importance of the criticality constant, we have sketched the time dependence of the neutron distribution in non-critical reactors, and in Sect. *II.10* in which we show how to calculate C from its definition in terms of neutron population from generation to generation, by means of the iterative process. This latter calculation is very closely related to that aspect of reactor kinetics, which deals with the way in which a reactor finds its fundamental spatial mode after having been perturbed out of that mode by some extraneous initial condition.

A more important practical aspect is the problem of how the neutron population rises and falls, within the fundamental spatial mode after the higher modes have decayed away. This has essentially to do with the way in which a chain reaction builds up when the control rods are pulled out of the reactor. (Pulling out the control rods a certain distance determines the rate of change of the power level of the reactor. When the desired level is reached, the control rods are reinserted to the point where the criticality constant is just one, and this desired level will be maintained until the rods are inserted further thus making C less than one).

It should be mentioned, at this point, that reactors in first approximation are described by linear equations: only the shape of the distribution, not the absolute intensity is determined by the equations.

Actually a reactor is a slightly non-linear device: the entering nuclear parameters are not quite power independent. For example, increasing the power level increases the temperature of the reactor so that the reactor may expand, and this would cause the criticality constant to decrease; which tends to bring the power level back down.

Mathematically this means that C is a function of N; hence the neutron population, in a reactor left to itself levels off at a value given by equation

$$C(N) = 1 \,. \tag{II.96}$$

12·1. *The Green's Function for a Reactor.* – We now consider in more detail, how the fundamental mode is re-established when a reactor has been perturbed out of that fundamental mode. To do this, we will solve the problem of a critical reactor ($C = 1$) operating in its fundamental mode, $\psi_0(\boldsymbol{x})$ to which one extra neutron is added at the point $\boldsymbol{x}'$ at time $t = 0$. We are then essentially calculating the Green's Function for the reactor.

The time-dependent equation for uniform bare thermal-reactors is:

$$D\nabla^2\Phi - \Sigma_a\Phi + \nu\Sigma_f\int K(|\boldsymbol{x} - \boldsymbol{x}'|)\Phi(\boldsymbol{x}')\,\mathrm{d}\boldsymbol{x}' = \frac{1}{v}\frac{\partial\Phi}{\partial t}\,, \tag{II.97}$$

where we neglect the effect of the delayed neutrons.

The general solution to (II.97) is of the form:

$$\Phi(\boldsymbol{x}, t) = \sum a_n \psi_n(\boldsymbol{x}) \exp[\lambda_n t] , \tag{II.98}$$

where the ψ_n's are all of the solutions of the wave equation (II.58).

Now the initial condition, we are assuming, is that at $t = 0$

$$\Phi(\boldsymbol{x}, 0) = \psi_0(\boldsymbol{x}) + v\delta(|\boldsymbol{x} - \boldsymbol{x}'|) , \tag{II.99}$$

where $\psi_0(\boldsymbol{x})$ is the fundamental mode and $v\delta(|\boldsymbol{x} - \boldsymbol{x}'|)$ represents the normalized flux due to a single neutron of velocity v at the point $\boldsymbol{x} = \boldsymbol{x}'$. Using (II.99) one can determine the coefficient a_n of the expansion (II.98), one obtains

$$\Phi(\boldsymbol{x}, t) = (1 + \psi_0(\boldsymbol{x}'))\psi_0(\boldsymbol{x}) + \sum_{m>0} \psi_n(\boldsymbol{x}')\psi_n(\boldsymbol{x}) \exp[\lambda_n t] , \tag{II.100}$$

which is recognized as the Green's function for a heat conduction-type probelm.

Introducing (II.100) into (II.97) one obtains for the reciprocal time constants λ_n,

$$\lambda_n = \Sigma_a v(1 + L^2 B_n^2 - k\overline{K}(B_n^2)) . \tag{II.101}$$

As we said before, each higher mode corresponds to a smaller reactor, and, since the expression in parenthesis is essentially $(1 + L^2 B_n^2)(1 - C(B_n^2))$, for these higher modes λ_n will be a larger negative number than for the lower modes. Thus the higher modes die away more quickly than the lower modes. For a just-critical reactor $C(B_0^2) = 1$, and λ_0 goes to zero, meaning that the zero mode will persist. For an order of magnitude estimate of the λ's for the higher modes, in case $k \cong 1$ it should be observed that the bracket in (II.101) approaches unity and the lifetime of the modes approach the generation time of the neutrons. This time amounts to something between 0.001 and 0.1 seconds, so these times are too small to be very important in starting up a reactor.

12·2. *The Importance Function.* – Another interesting piece of information that we may deduce from our solution of (II.97), concerns the long term effect of adding an extra neutron at a point.

Using just the stationary part of equation (II.100) we can calculate the ultimate fractional increase in neutron population flux due to this added neutron. It is just:

$$\text{Fractional increase} = \frac{(1 + \psi_0(\boldsymbol{x}'))\psi_0(\boldsymbol{x}) - \psi_0(\boldsymbol{x})}{\psi_0(\boldsymbol{x})} = \psi_0(\boldsymbol{x}') . \tag{II.102}$$

Thus the total fractional amount, by which the flux is increased is just equal to the flux at the point at which the addition occurred. This amount is just a measure of the «importance» of one neutron at that point in the reactor: if the point is one of high flux, the added neutron will very likely produce progeny; if it is a point of low flux, the added neutron will more probably leak out. We can describe this by means of an importance function, $I(\boldsymbol{x})$, and for the case of a bare uniform thermal reactor, we see that:

$$I(\boldsymbol{x}) = \psi_0(\boldsymbol{x}) \,. \tag{II.103}$$

The usefulness of the importance function is seen when we consider the effect produced by adding an absorber to a reactor.

If the absorber is uniformly distributed, the change in criticality constant is given by

$$\delta C \simeq \frac{\Sigma_a}{\Sigma_R} \,, \tag{II.104}$$

where Σ_a is the absorption coefficient of the absorber and Σ_R that of the reactor as a whole. If, however, the absorber is located at a given point, then we must multiply the absorption cross section in the numerator of (II.104), by the flux of neutrons at that point and also by the importance function at that point and similarly in the denominator but integrated over the volume of the reactor. Since the functions are orthonormal, this integral gives unity, so we have the result:

$$\delta C = \frac{\Sigma_a \psi_0(\boldsymbol{x}) I(\boldsymbol{x})}{\Sigma_R} \,. \tag{2.105}$$

For the reactor under consideration, where the importance function is given by (II.103), we have the result that the change in criticality is just the change that would occur for a uniform distribution of absorber, but weighted by the square of the flux at the point at which the absorber is placed. In a cubical reactor, for instance, where the flux distribution is represented by a cosine in each of the three directions, an absorber is eight times as effective if placed in the center, as, if it is uniformly distributed throughout the volume.

All of this, of course, applies only to a bare reactor, where the distribution is represented by the asymptotic solution of the wave equation.

In the actual reactor, especially one with reflectors, the non-asymptotic solutions are excited. In this case, the reactor equations are not self-adjoint, so one cannot expand $\psi(\boldsymbol{x}, t)$ in terms of the ψ_n's. Rather, the importance function is the adjoint of the actual solution. The adjoint is computed as the solution of the equation adjoint to the actual reactor equation. If, as in the

group picture, the reactor equations are a system of linear equations of the form

$$H \Phi = 0 , \tag{II.106}$$

where H_{ij} is a matrix operator and Φ_j is the flux of the j energy group, the adjoint equations of (II.106), for the importance function I_j, are:

$$\tilde{H}_{ij} I_j = 0 , \tag{II.107}$$

where H_{ij} is the transpose of H_{ij}.

12·3. *Delayed Neutrons.* – We are now interested in discussing briefly just how the neutron population rises and falls as a whole in the fundamental mode as the criticality constant is changed.

For the sake of safety and control, a reactor *must* be arranged in such a way that the criticality constant *never* exceeds unity by more than the fraction of delayed neutrons. If this precaution is not observed then the time scale for control of the reactor is of the order of milliseconds instead of tens of seconds. This fraction for ^{235}U, is $\beta = 0.78\%$; (unfortunately it is considerably smaller than this for both ^{233}U and ^{239}Pu) and is called « one dollar ». In terms of excess criticality one has a deposit of « one dollar » in the bank. If one overdraws, he is in serious trouble).

To take into account the delayed neutrons, we write down the kinetic equation for the total neutron population. Recall that the total criticality constant can be written as $C = \eta P_0$ (see Sect. 3 of Chapter I). The contributions to this by the i-th group of delayed neutrons is:

$$C_i = \eta \beta_i P_0 , \tag{II.108}$$

where β_i is the fraction of the total neutrons which are delayed and re-emitted by the radioactive parents of mean life τ_i. The excess reactivity, due to the prompt neutrons, is then:

$$\text{excess prompt neutron reactivity} = C - 1 - \sum_i C_i . \tag{II.109}$$

The kinetic equation for neutron population N, is then:

$$\frac{dN}{dt} = \frac{C - 1 - \Sigma_i C_i}{l} N + \sum_i \frac{\xi_i}{\tau_i} , \tag{II.110}$$

where ξ_i are the populations of the delayed neutron precursors among the fission fragments. The population of each precursor will be given by the rate

at which they are formed minus the rate at which they decay, i.e.:

$$\frac{\mathrm{d}\xi_i}{\mathrm{d}t} = \frac{CN\beta_i}{l} - \frac{\xi_i}{\tau_i} = \frac{C_i N}{l} - \frac{\xi_i}{\tau_i} . \tag{II.111}$$

This pair, (II.110) and (II.111) of linear differential coupled equations have solutions of the form:

$$N(t) = \sum_{n=1}^{\mu} A_n \exp\left[t/T_n\right] , \tag{II.112}$$

where μ is the number of equations of system (II.110)–(II.111).

Working out the expression between the reactivity and the T_n one gets:

$$\frac{C-1}{C} = \frac{l}{CT_p} + \sum_i \beta_i \frac{\tau_i}{\tau_i + T_p} , \tag{II.113}$$

where T_p is the period of the reactor. Equation (II.113) is sometimes called the « in-hour equation ». An « in-hour » is defined as the reactivity $(C-1)/C$ obtained from $T_p = 1$ hour, in equation (II.113). In practice, reactors are started up with a period of 5 to 10 seconds. To solve equation (II.113) for T_p

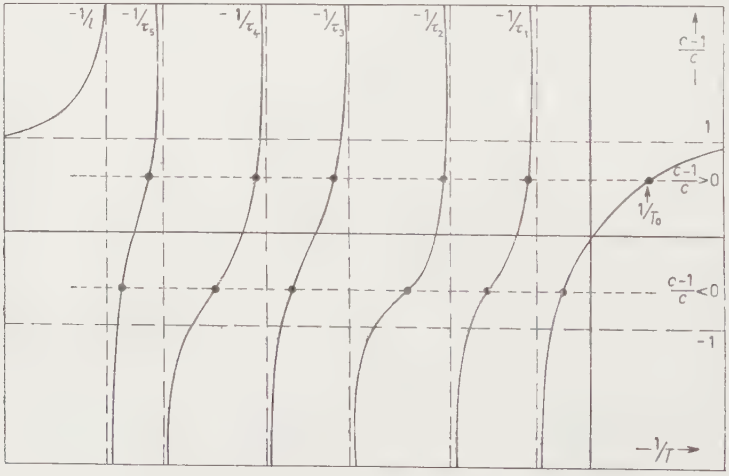

Fig. 7. – Graphs for solving the « in-hour » equation.

one plots the two sides of (II.113) on the same graph as function of T and finds the intersection. Thus one can read off the sustained period of the reactor.

If $(C-1)/C > 0$ (starting up a reactor), one has a number of negative periods (one for each delayed neutron family) which die off exponentially and one is left with a positive period given by the rightmost intersection in the

figure. If $(C-1)/C < 0$, one has the negative periods due to the delayed neutrons and then one is left with a long negative period given by the left-most intersection for the dying away of the chain reaction.

It is also of interest to mention the behavior of a reactor, when a control rod is pulled out slightly. There is first a jump in the neutron population of fractional amount $(C-1)/C\ (\beta - (C-1)/C)$ due to the prompt neutrons, increasing like an exponential with a period of the order of milliseconds. Then the period of the delayed neutrons takes over and the exponential rise is with a period of the order of several second, as shown in the Fig. 8. If the control rod is removed sufficiently far, so that reactivity exceeds the delayed neutron fraction, the increase continues with the millisecond period.

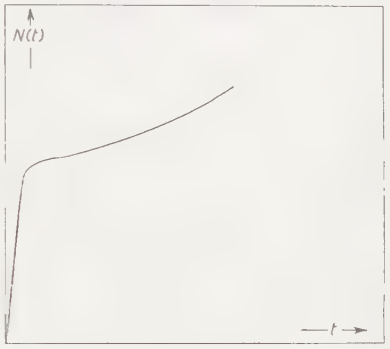

Fig. 8. – Time behaviour of the neutron population in a reactor for a sudden increase of reactivity by an amount less than the delayed neutron fraction.

Finally it should be mentioned that as reactors of higher specific power and temperature are developed, the non-linear kinetics of the reactor become more important than the linear kinetics described here.

BIBLIOGRAPHY

General:

S. Glasstone and M. Edlund: *Elements of Nuclear Reactor Theory* (New York, 1952).

Cross-Sections:

E. P. Wigner: *Am. Journ. Phys.*, **17**, 99 (1949); *Proceeding of Geneva Conference* vol. 2 and vol. 5.

Reactor Theory:

A. M. Weinberg: *Am. Journ. Phys.*, **20**, 401 (1952).

Research Reactors:

M. Benedict: *Chem. Eng. Progr.*, **51**, 53 (1955).

Power Reactors:

A. M. Weinberg: *Scientific American*, **191**, 33 (1954).

The *Proceedings of the Geneva Conference* (August, 1955) constitute a first rate reference library for reaction technology and science.

SUPPLEMENTO AL VOLUME IV, SERIE X
DEL NUOVO CIMENTO

N. 3, 1956
2° Semestre

« Zephyr » – Zero Energy Fast Reactor.

T. M. FRY

Atomic Energy Research Establishment - Harwell (England)

Zephyr is a small low-power fast reactor with a plutonium core surrounded by a uranium envelope. The core is a cylinder 15 cm in diameter and 15 cm in length. The plutonium is contained in nickel tubes about 5 mm in diameter and rather more than 15 cm long. Several hundreds of these are packed in a hexagonal lattice inside the core. The space between the tubes can be left empty or can be filled with a solid « matrix », such as uranium or steel. The nature of the matrix material affects the energy distribution of neutrons in the core.

At present, the composition of the core by volume is roughly: ^{239}Pu 50%, Nickel 10%, Void 10%, Matrix (which may be void, natural uranium or steel) 30%.

To reduce the leakage of neutrons, and hence to reduce the amount of plutonium required for criticality, a reflector is employed. The reflector comprises a hollow cylinder of natural uranium fitting round the core and is surrounded by 8 tons of natural uranium rods. Solid uranium blocks are also placed up against the ends of the core. The whole acts both as reflector and as a blanket to absorb escaping neutrons.

Control is effected in three ways. Firstly, there are six uranium rods which penetrate into the uranium reflector and which may be moved vertically. This produces a variation in reactivity of 0.01% per cm per rod. Secondly, the bottom reflector operates as a safety device, and can be moved down to produce a reduction of 2% in reactivity. Thirdly, the plutonium inside the nickel tubes is held at the top and consists of two sections soldered together. If the temperature rises appreciably, the solder will melt, the sections will separate and the reactivity will decrease. The top reflector has to be removed for loading. This produces a large reduction in reactivity and enables the loading to be performed with safety.

The heat generated in Zephyr is very small, — about 2 w from fission. It is therefore unnecessary to provide forced cooling. The fast flux is 10^9 neutrons per cm^2 per s.

The purpose of the « Zephyr » reactor is to investigate neutron physics in fast reactors. From a practical point of view the most attractive feature of fast reactors is the possibility of breeding. Because there is very little radiative capture in ^{239}Pu at these energies, almost all the neutrons produced in fission are available for the production of plutonium. The conversion factor — plutonium atoms produced per plutonium atoms fissioned — is determined by measuring fission rates and ^{239}U activity throughout the core and blanket.

Another field of investigation is the value of the nuclear constants to be used in the theory of fast reactors. In such a small core diffusion theory is not applicable because the neutron mean free path is comparable with the dimensions of the reactor. Transport theory is therefore required. Variation of cross-sections with energy should be taken into account but, so far, theory has been based on a « one-group » hypothesis. The neutron parameters employed are thus averages with respect to energy. They are determined by perturbation experiments.

Perturbation experiments also throw light on inelastic scattering processes, which are difficult to investigate with particle accelerators. With the reactor, measurements are easy to obtain, although not very easy to interpret physically.

The first problem is to calibrate the control system — to find by how much the reactivity is affected by the control rods. This is done by observing the instantaneous change in neutron flux produced by a sudden displacement of the rods. When it is sub-critical, the rate of fission in a reactor is given by:

$$R = -cS/\varrho \,,$$

where c is a constant not far from unity, S is the number of neutrons emitted per second by the source, ϱ is the reactivity of the system defined as $\Delta k/k$.

In normal steady operation $R \simeq S$ and ϱ is negative but not significantly different from zero.

With regard to prompt neutrons the reactor is still sub-critical; $\varrho_p = -\beta$, where β is the delayed neutron fraction. The prompt multiplication is then about 140. Now, consider the effect of a sudden change in the prompt reactivity from a value $-\beta$ to $-\beta + \delta$.

The multiplication goes from $1/\beta$ to $1/(\beta - \delta)$ and the neutron flux changes in the ratio $\beta'/(\beta - \delta)$. For β' it is necessary to substitute an effective value because the different delayed neutron groups have different energies and the more energetic neutrons are worth more than the others. δ is therefore determined in terms of β.

After the sudden change, the flux will increase exponentially with period

T given by:

$$\frac{\delta}{\beta} = \sum_i \frac{\mu_i}{1 + \lambda_i T}.$$

where μ_i is the fraction of delayed neutrons in the i^{th} group, λ_i is the time constant of the group, T is the period of the reactor. Measurement of T provides a second check on δ/β.

One may similarly investigate the effect of a sudden shut-down and from the two experiments obtain information on the half lives of the various groups (Table I).

TABLE I.

Half life of group	μ_i (relative yield)
(55.8 ± .5) s	.025 ± .004
(21.9 ± .4) s	.229 ± .005
(4.22 ± .15) s	.341 ± .019
(1.07 ± .06) s	.405 ± .036

In practice, a mixed bag of delayed neutrons is found because there is fission not only of ^{239}Pu but also of ^{238}U and ^{235}U.

For the determination of the distribution of neutron flux or fission rate through the system as a function of energy, three types of detector are employed. The first type is known as a « flat-response » detector and employs the fission of ^{239}Pu (ionisation fission chamber). The second type is preferentially sensitive to the slower neutrons and uses the activation of gold (n, γ). The third type is designed to detect the more energetic neutrons and employs a threshold reaction e.g. ^{238}U fission with threshold of 0.9 MeV. Other more direct methods can be tried such as proton recoils on photographic plates but such work is difficult because of lack of space in the core. The results for neutron flux density are shown in Fig. 1. Outside the core, the distribution becomes spherical taking the form given by the theory: $\Phi = 1/r \sinh((r_0 - r)/L)$. Here L is a diffusion length = 12 cm.

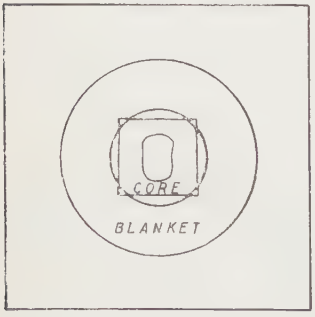

Fig. 1. – Neutron flux distribution in « Zephyr ». The innermost contour is at 90% of the maximum value and the second at 45%.

Conversion Factor.

To assess breeding, one wants to have information on the ^{238}U (n, γ) reaction. However, ^{238}U undergoes fission at the same time. There is therefore a background of fission product activity against which the decay of ^{239}U to neptunium cannot be detected. It is therefore necessary to take samples of natural uranium exposed in the blanket and in the core, perform chemical separation of the uranium and measure its degree of activation. This must be done quickly because ^{239}U has a 23 min half-life.

By these methods it has been established that, for every fissile atom destroyed, two plutonium atoms are produced; that is to say, we have a conversion ratio of two. This shows that it is possible in principle to utilize ^{238}U completely as a fuel in a fast reactor. These results should be compared with those for a thermal reactor, when the highest conversion factor is about 0.8 to 0.85.

Perturbation Measurements.

We observe the effect of introducing various small samples of material into the core. For samples placed at the centre, a reduction in reactivity may be due to capture or to inelastic scattering or both. The reduction produced by the latter process occurs because the neutron energy is degraded to a value below the threshold for ^{238}U fission and because η for Pu falls with energy. This effect is not found to be very dependant on atomic weight.

If a sample is placed at the edge of the core, one may observe an increase in reactivity due to elastic scattering.

In transport theory, one can define two constants α and β for each medium. α defines the number of neutrons lost per cm of neutron path.

$$\alpha = N(\sigma_s + \sigma_c + \sigma_f) ,$$

where N is the number of nuclei per cm^3 and σ_s, σ_c, σ_f are respectively the cross-sections for scattering, capture and fission. β defines the number of neutrons emitted per cm of path

$$\beta = N(\sigma_s + \nu\sigma_f) ,$$

where ν is the number of neutrons produced per fission.

For a sample at the point r, the change in reactivity is given by:

$$\Delta\varrho = \frac{(\beta - g(r)\cdot\alpha)\Phi^2(r)\,\delta V}{\iiint p(r')\Phi(r')\,dr'}$$

where $\Phi(r)$ is the neutron flux, $g(r)$ is the perturbation factor, $p(r)$ is the neutron production rate and δV is the element of volume occupied by the sample. The integral is taken over all regions of the reactor in which fission occurs.

N. B. – As one can see from considering the pure scatterer in which $\alpha = \beta$, $g = 1$ at $r = 0$ since $\Delta\varrho = 0$ — there is no change in reactivity for a scatterer placed at the centre. Elsewhere, g falls slightly with radius. It is of the order of 0.9 near the edge. From measurements of $\Delta\varrho$ as a function of r, α and β can be determined and hence σ_c. Observations have been made for 70 elements and the results are plotted in Fig. 2.

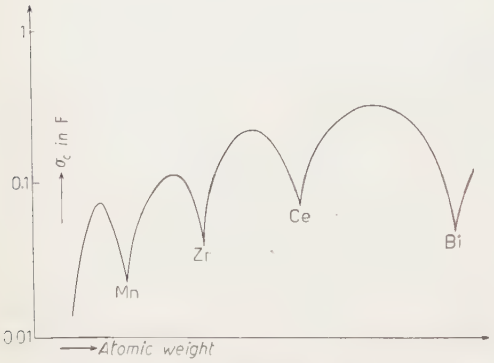

Fig. 2. – Effective capture cross-sections of the elements in « Zephyr ».

Very low cross sections are observed at magic nuclei (the experiments have not so far been performed with separated isotopes). It should be noted that σ_c is a composite quantity and includes both the effects of neutron capture and of the energy loss in inelastic collisions. The latter effect predominates at lower A values.

SUPPLEMENTO AL VOLUME IV, SERIE X
DEL NUOVO CIMENTO

N. 3, 1956
2° Semestre

The Displacement of Atoms in Solids by Radiation.

T. M. FRY

Atomic Energy Research Establishment - Harwell (England)

When the first nuclear reactors were being designed E. P. WIGNER pointed out that, in solids exposed to bombardment by high-energy nuclear particles, atoms would be displaced from their normal positions. The effects of these displacements were in fact known long before Wigner's conjecture. Minerals containing naturally radioactive substances — uranium and thorium — have the outward appearance of crystalline structure but reveal no such structure to X-ray analysis. The α-particles have disturbed the ordered arrangement of atoms in the crystal. Mineralogists refer to this as the « metamict state ». Such natural processes have occurred very slowly, but with the much greater fluxes of particles obtained in reactors, much more rapid results may be anticipated. In particular, fast neutrons can displace atoms from their positions in the crystal lattice, and this changes the physical properties of the material.

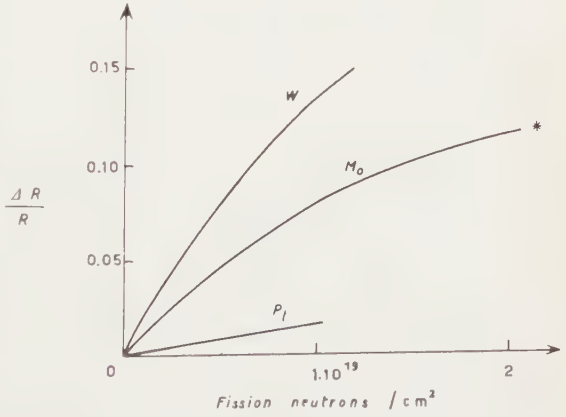

Fig. 1. – Fractional increase in resistivity of metals. * Lattice spacing of Mo had increased $1.5 \cdot 10^{-4}$ at this point.

Many experiments have been performed on metals to investigate the influence of irradiation on structure-sensitive properties. For instance, measurements have been made of the variation of electrical resistivity with irradiation. The results of such investigations are shown in Fig. 1.

The increasing resistivity is due to the introduction of imperfections into the lattice structure of the metal, which results in a reduction of the mean free path of the conduction electrons. In copper and aluminium no change was observed. This was because the temperature of the specimen in the reactor was sufficient to permit a recovery to the stable configuration. Both the increase of lattice spacing, observed for Mo, and the increase of resistivity are consistent with the production of interstitial atoms and vacant lattice points. Some other changes observed in structure — sensitive properties are also consistent with this mechanism.

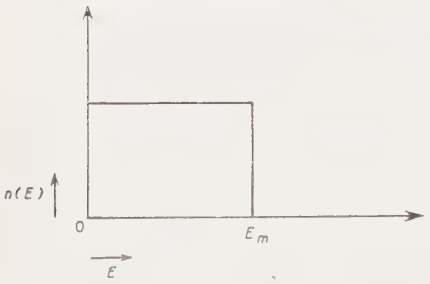

Fig. 2. – Energy distribution of atoms struck by mono-energetic neutrons.

Since scattering is approximately isotropic, we may treat the encounter of a fast neutron and a nucleus as a hard-sphere collision. The energy distribution of atoms which have been struck by neutrons of a certain energy therefore takes the form shown in Fig. 2.

E_m, the maximum energy, is related to the incident neutron energy by

$$E_m = \frac{4A}{(1+A)^2} E_n ,$$

where A is atomic weight of nucleus; E_n is energy of incident neutron.

Taking for example $E_n = 1$ MeV, the values of E_m in three cases are given in Table I.

TABLE I.

	Carbon	Copper	Tungsten
A	17	64	184
E_m	280 keV	61 keV	21 keV
L_e	15 keV	50 keV	100 keV
L_A	5 keV	200 keV	2 MeV
λ_A	$6.7 \cdot 10^{-7}$ cm	$27 \cdot 10^{-7}$ cm	

An ion, moving through a solid with sufficient velocity, loses energy by exciting orbital electrons. This process ceases, for a given particle, when its energy has been degraded to a value at which its velocity is considerably less

than that of the least strongly bound electrons. This is estimated to be

$$L_c = \frac{1}{16}\frac{M}{m}\varepsilon_0 ,$$

where ε_0 is a « maximum » kinetic energy of the electrons present in the solid and M and m are the masses of ion and electron respectively. Values for L_c are also given in Table I.

Energy loss to electrons does not disturb other atomic nuclei. However the moving ion occasionally approaches so close to another nucleus that it knocks it out of its path, thus producing a second displacement. If the collision is at sufficiently high energy, Rutherford scattering takes place, but, at lower energies, the ion carries a screen of orbital electrons with it and the collision resembles that of hard spheres. The minimum energy at which Rutherford scattering occurs has been given by BOHR:

$$L_1 = \sqrt{2}\cdot 4\cdot E_R Z^{\frac{7}{3}} ,$$

where E_R is the Rydberg energy (13.6 eV), Z the atomic number (assumed the same for moving and stationary atoms). At this energy the cross-section for scattering is given by $\sigma_s = \pi a^2$ where $a = a_0/\sqrt{2}Z^{\frac{1}{3}}$ and a_0 is the Bohr radius for hydrogen.

The mean free path is obtained as

$$\lambda_1 = 1/N\sigma_s ,$$

where N is the number of atoms per cm^3.

Values of L_A and λ_A are given in Table I.

At energies below L_A the mean free path is approximately proportional to energy. In the case of graphite, for example, a carbon nucleus struck by a 1 MeV neutron is first slowed from a possible maximum of 280 keV to 15 keV by energy loss to electrons. At 5 keV, where hard sphere scattering becomes important, the mean free path is 67 Å — about 40 times the distance between nearest carbon atoms. At the next collision the atom shares its energy, so that two atoms are now moving through the lattice. Their mean energy is 2.5 keV and their mean free path 20 atomic spacings. After the next collisions there will be four moving atoms and so on.

Eventually the moving atoms reach an energy, E_D, below which they cannot displace others, even in a head-on collision. This energy has been estimated by SEITZ to be ~ 25 eV. At some higher energy, of the order of $2E_D$, the atom will be able to produce 2 displacements. Thus, bearing in mind the distribution of energy for hard-sphere collisions, one can see that the total number

of displacements produced by a single neutron collision is $n_D \sim (E/2E_D)$ where E is the energy of the moving atom when electronic energy loss has ceased. The number of vacancies and interstitials produced by our carbon atom is therefore about 100. n_D can also be assessed from observation of resistivity changes, lattice expansion, production of electron traps and so on. Experimental figures show n_D to be only about $\frac{1}{3}$ or $\frac{1}{5}$ of the values calculated above. This is partly because no allowance has been made for the recovery process.

Recovery Process.

The lattice can recover its initial degree of perfection in two ways. On the one hand the vacancies and interstitials may diffuse to crystal boundaries. On the other hand they may combine together, the interstitials falling back into the vacancies.

In the first process the rate of recovery should be proportional to the numbers of defects remaining. If there are n vacancies $\mathrm{d}n/\mathrm{d}t = -An$, whence $n(t) = n(0)\exp[-At]$ and similarly for the interstitials.

In the second process the numbers of vacancies and interstitials must remain equal. The rate of recovery is proportional to the product of the number of each present.

$$\frac{\mathrm{d}n}{\mathrm{d}t} = -Bn^2 ,$$

$$n(t) = \frac{n(0)}{1 + n(0)Bt} .$$

In Fig. 3, we show these two cases as functions of time together with a typical experimental recovery curve, all fitted to the same value and derivative at $t = 0$. It will be seen that there is a large discrepancy. The experimental data can best be fitted by a 6th order reaction i.e. $\mathrm{d}n/\mathrm{d}t = -Cn^6$ for which

$$n = \frac{n(0)}{(1 + 5n^5(0)Ct)^{\frac{1}{5}}} .$$

That recovery requires the co-operation of 6 defects is improbable. However our supposition that the displaced atoms and vacancies are placed randomly with respect to each other is false. At least half the interstitials

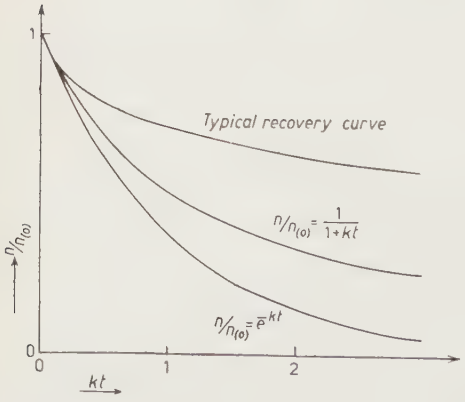

Fig. 3.

will have been displaced only a very short distance from their vacancies. In order to illustrate the effect of this correlation between the positions of pairs of displaced atoms and vacancies on the variation of recovery rate with time, we can consider the following model in 1 dimension (Fig. 4). In the model the interstitial jumps one place, either to right or left, with equal probability at regular intervals of time. In Table II the probable position of the interstitial is given for the first 8 jumps.

TABLE II.

Jump Number	*Position*								
	Vacancy	1	2	3	4	5	6	7	8	9
0	0	256								
1	128		128							
2	128	64		64						
3	160		64		32					
4	160	32		48		16				
5	176		40		32		8			
6	176	20		36		20		4		
7	186		28		28		12		2	
8	186	14		28		20		7		1

The probability of capture is at first very high, but falls off rapidly as the mean distance of the remaining interstitials from the vacancy increases. This is evidently the type of behaviour which will produce recovery curves similar to those observed.

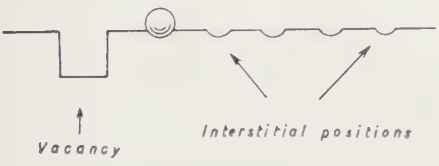

Fig. 4. – One dimensional model to illustrate recovery process

In this one dimensional case it is easy to show that the interstitial cannot evade capture indefinitely. The same follows for two dimensions, though capture is much longer delayed. In three dimensions, there is a finite probability of escape. The closeness of many of the displaced atoms to their vacant lattice points can thus account for the apparent high « order » of the annealing reaction.

The problem can also be tackled analytically using diffusion theory.

For the 3-dimensional case we obtain:

$$n(t) = n(0)\left\{1 - \frac{a}{b} + \frac{a}{b}\operatorname{erf}\left|\frac{b-a}{2(Dt)^{\frac{1}{2}}}\right|\right\},$$

where a is the radius at which recombination occurs;

b is the initial separation of interstitial and vacancy;

D is the diffusion coefficient;

note that

$$n(\infty) = n(0)\left\{1 - \frac{a}{b}\right\},$$

is the proportion escaping altogether. This simple picture has not, of course, taken into account capture at grain boundaries, mutual interaction between interstitial atoms and other complicating factors.

* * *

The student is referred to a comprehensive paper by G. H. Kinchin and R. S. Pease (*Reports on Progress in Physics*, **18**, 1 (1955)) from which the material for this lecture was largely taken.

SUPPLEMENTO AL VOLUME IV, SERIE X
DEL NUOVO CIMENTO

N. 3, 1956
2° Semestre

Différentes méthodes de mesure du libre parcours moyen de transport des neutrons thermiques.

J. HOROWITZ

Commissariat à l'Énergie Atomique - Centre d'Études Nucléaires de Saclay

1. – Introduction.

Le libre parcours moyen de transport λ_{tr} des neutrons thermiques est défini par la relation: $\lambda_{tr} = \lambda_s/(1 - \cos\theta)$ où λ_s est le libre parcours moyen de diffusion et $\cos\theta$ la valeur moyenne du cosinus de l'angle de diffusion. Si λ_s et $\cos\theta$ dépendent de l'énergie, des moyennes doivent être effectuées sur le spectre de Maxwell.

On a

$$\lambda_{tr} = 3D\,,$$

où D est la constante de diffusion et, dans un milieu faiblement capturant

$$L^2 = \tfrac{1}{3}\lambda_{tr} \times \lambda_a\,, \tag{1}$$

L étant la longueur de diffusion et λ_a le libre parcours moyen d'absorption correspondant à la vitesse moyenne du spectre maxwellien.

La connaissance précise de λ_{tr} pour des matériaux utilisés comme modérateurs ou réflecteurs de réacteurs thermiques (H_2O, D_2O, C, Be, BeO) est importante pour deux raisons principales.

1) Les fuites de neutrons thermiques dépendent directement de λ_{tr}.

2) Sauf H_2O ces matériaux ont une section efficace de capture σ_a très faible et sauf dans le cas du deuteron ces sections efficaces ne peuvent être mesurées par activation. En mesurant à la fois la longueur de diffusion L et le libre parcours moyen de transport λ_{tr} on détermine λ_a donc σ_a.

2. – Différentes méthodes de mesure de λ_{tr}.

2·1. *Méthode de la longueur d'extrapolation.* – Considérons un milieu semi-infini non absorbant limité par le vide ou par un plan absorbant et possédant

des sources à l'infini dans la direction z perpendiculaire au plan limite. A partir d'une distance du plan limite de l'ordre de quelques λ_{tr} le flux neutronique est une fonction linéaire de z comme le prédit la théorie élémentaire de la diffusion. Au voisinage du plan limite il faut utiliser la théorie du transport qui indique en particulier que le flux linéaire asymptotique s'extrapole à zéro à une distance d du plan et que $d = 0.71\ \lambda_{tr}$.

En mesurant le flux neutronique à des distances de l'ordre de quelques λ_{tr} du plan, on peut donc déterminer d et en déduire λ_{tr}. La méthode s'applique encore si le milieu est absorbant et fini pourvu que L et les dimensions soient assez grandes pour que la longueur de relaxation dans la direction des z soit nettement supérieure à λ_{tr}.

Cette méthode a été utilisée par Auger, Munn et Pontecorvo [1] pour la détermination du λ_{tr} de D_2O. Après corrections tenant compte de la présence d'une petite quantité de H_2O, la valeur obtenue pour le λ_{tr} de l'eau lourde pure, à une température d'environ 20 °C était $\lambda_{tr} = (2.63 \pm 0.12)$ cm.

Les mêmes auteurs ont obtenu pour le graphite (ramené à la densité 1.6) la valeur: $\lambda_{tr} = (2.5 \pm 0.1)$ cm.

Plusieurs autres mesures ont été effectuées par cette méthode dans le cas du graphite. La valeur $\lambda_{tr} = 2.74$ cm citée par D. J. Hughes [2] semble aussi avoir été obtenue par cette méthode.

L'utilisation de cette méthode présente d'assez grandes difficultés si l'on veut obtenir une bonne précision. Les mesures s'effectuent dans une région où le flux neutronique est faible et les corrections dues à la dépression du flux causée par les détecteurs peuvent être importantes.

2·2. *Méthodes d'empoisonnement.* – La relation (1) peut encore s'écrire

$$\frac{1}{L^2} = 3\,\Sigma_{tr}\,\Sigma_a\,. \tag{2}$$

L'addition d'une petite quantité d'un absorbeur de neutrons particulièrement fort tel que le bore affectera la section efficace macroscopique de capture Σ_a sans changer la section efficace macroscopique de transport Σ_{tr}. Un tel « empoisonnement » homogène n'est possible que dans le cas des liquides. Dans le cas de D_2O on pourra écrire:

$$\frac{1}{L^2} = 3\,\Sigma_{tr}\,\Sigma_a\,(D^2O) + 3\,\Sigma_{tr}\,\Sigma_a\,(B)\,,$$

$1/L^2$ est une fonction linéaire de la quantité de bore ajoutée et, de la pente, on déduit Σ_{tr}, l'ordonnée à l'origine donnant $\Sigma_a(D_2O)$. L'expérience a été

(1) P. Auger, A. M. Munn et B. Pontecorvo: *Can. Journ. Res.*, A **25**, 143 (1947).
(2) D. J. Hughes: *Pile Neutron Research* (Cambridge, Mass., 1953), p. 223.

effectuée par KASH et WOODS [3] en utilisant une cuve cylindrique (diamètre 1.5 m, hauteur $h = 1.8$ m) remplie d'eau lourde. La source était constituée par un piédestal de graphite contenant en son centre un « water boiler » et sur lequel reposait la cuve. Le flux neutronique dans la cuve est de la forme:

$$\Phi = AJ_0(\mu r)\sin\nu(h - z)$$

et on a

$$\frac{1}{L^2} = \nu^2 + \mu^2 .$$

La mesure de la constante de relaxation axiale ν en fonction de la quantité de bore ajoutée fournit Σ_{tr}. La valeur de $\Sigma_a(D_2O)$ donnée par l'ordonnée à l'origine permet de déterminer avec précision la quantité d'eau légère présente et d'effectuer les corrections correspondantes sur Σ_{tr}.

Ces mesures ont donné pour l'eau lourde pure la valeur

$$\lambda_{tr} = 2.52 \pm 0.03 \text{ cm}$$

d'où on déduit $\overline{\cos\theta} = 1.15 \pm 0.03$.

La méthode est très précise mais d'une part elle ne s'applique qu'aux liquides et d'autre part le résultat dépend de la valeur admise pour la section efficace de capture du bore (prise égale à 750 barn à 2 200 m/s dans l'expérience ci-dessus).

2·3. *Mesure par impulsion.*

a) Principe de la méthode. – L'évolution du flux neutronique $n(\boldsymbol{r}, t)$ est décrite d'après la théorie élémentaire de la diffusion par l'équation

$$\frac{\partial n(\boldsymbol{r}, t)}{\partial t} = -\frac{n(\boldsymbol{r}, t)}{\tau} + D\Delta n(\boldsymbol{r}, t) , \tag{3}$$

où τ est la vie moyenne des neutrons par rapport à la capture et D le coefficient de diffusion multiplié par la vitesse. Les solutions de l'équation (3) sont de la forme

$$n(\boldsymbol{r}, t) = \sum_\nu n_\nu(\boldsymbol{r}) \exp[-\alpha_\nu t] , \tag{4}$$

les $n_\nu(\boldsymbol{r})$ étant les solutions de l'équation $(\Delta + \mathcal{B}_\nu^2)(n_\nu(\boldsymbol{r})) = 0$ s'annulant aux limites extrapolées du milieu. Les constantes de temps α_ν dépendent à la fois

[3] S. W. KASH et D. C. WOODS: *Phys. Rev.*, **90**, 564 (1953).

de la capture et des fuites; on a

$$\alpha_\nu = \frac{1}{\tau} + D\mathcal{H}_\nu^2 .$$

La valeur la plus faible α_0 correspond au plus petit laplacien $\mathcal{H}_0^2$, c'est-à-dire au mode fondamental $u_0(\boldsymbol{r})$. Dans le cas d'un cylindre (rayon extrapolé R', hauteur extrapolée H')

$$\mathcal{H}_0^2 = \left(\frac{2.405}{R'}\right)^2 + \left(\frac{\pi}{H'}\right)^2 .$$

On a

$$\alpha_0 = \frac{1}{\tau} + D\mathcal{H}_0^2 , \tag{5}$$

en mesurant α_0 en fonction de $\mathcal{H}_0^2$, on détermine donc à la fois D et τ.

Le calcul ci-dessus a été fait en attribuant aux neutrons une seule vitesse: la vitesse moyenne du spectre de Maxwell. En réalité le spectre neutronique se modifie au cours du temps, les neutrons les plus rapides s'échappant les premiers et cela d'autant plus que le volume est plus petit c'est-à-dire que le laplacien $\mathcal{H}_0^2$ est plus grand. La relation (5) est à remplacer par

$$\alpha_0 = \frac{1}{\tau} + D\mathcal{H}_0^2(1 - E\mathcal{H}_0^2) , \tag{6}$$

où le terme correctif $E\mathcal{H}_0^2$ tient compte de l'effet considéré pour des valeurs pas trop grandes de $\mathcal{H}_0^2$.

Le principe de la mesure est donc le suivant. On envoie pendant un temps très court sur le corps à étudier un flux de neutrons. Le fait que ces neutrons puissent être rapides n'a pas d'importance si le temps de ralentissement est petit devant $1/\alpha_0$. On étudie la décroissance du flux neutronique en fonction du temps au moyen d'un détecteur qui peut être placé à l'extérieur du milieu étudié. Pour atteindre α_0, il faut attendre suffisamment longtemps pour que la contribution des harmoniques supérieurs soit devenue négligeable; une disposition convenable du détecteur permet d'ailleurs de diminuer l'importance des harmoniques les plus gênants. L'étude de la variation de α_0 en fonction du volume c'est-à-dire de $\mathcal{H}_0^2$ donne d'après la relation (6) les valeurs de D, τ et E.

Les principaux avantages de cette méthode sont les suivants:

1) Le volume nécessaire est plus petit que celui exigé par les autres méthodes. Pour cette raison la méthode par impulsion se prête bien à la mesure de la variation de λ_{tr} avec la température.

2) On ne se réfère pas à une section efficace supposée connue (celle du bore par exemple).

3) Le détecteur peut être placé en dehors du milieu ce qui est particulièrement important dans le cas de l'eau légère.

b) L'expérience a été effectuée dans le cas de H_2O par Von Dardel et Sjöstrand [4]. Les neutrons étaient produits par l'impact d'un faisceau pulsé de deutons de 150 keV sur une cible de glace lourde. Les mesures ont été faites sur deux cylindres d'eau (diamètres: 18 et 14.5 cm) le niveau d'eau variant de 3.5 à 15 cm. Le détecteur était placé sur le côté du cylindre.

Sans entrer davantage dans les détails expérimentaux voici les résultats de la mésure:

$$1/\tau = (4\,892 \pm 50)\ \mathrm{s}^{-1}$$

$$D = (36\,340 \pm 750)\ \mathrm{cm}^2/\mathrm{s}$$

$$E = (0.20 \pm 0.04)\ \mathrm{cm}^2$$

pour une température de 22 °C.

La même méthode a été utilisée en URSS [5] non seulement dans le cas de H_2O mais aussi pour la graphite et le beryllium. Dans les cas du graphite la densité 1.67 la valeur de D était $D = (1.98 \pm 0.03)\cdot 10^5$ ce qui, ramené à la densité 1.6, donne $\lambda_{tr} = 2.5$ cm.

Dans le cas dy béryllium (densité 1.78), on a: $D = 1.22 \pm 0.05$, c'est-à-dire $\lambda_{tr} = 1.47$ cm.

2·4. *Méthode de modulation* [6]. – Considérons un milieu diffusant et ralentisseur, et soit $f(\boldsymbol{r}, E, t)$ la distribution spatiale et énérgétique des neutrons un temps t après leur émission d'une source S, en l'absence de capture. Si le milieu a une capture en $1/v$ et si τ est la vie moyenne des neutrons, la distribution créée par la source stationnaire S est

$$g\left(\boldsymbol{r}, E, \frac{1}{\tau}\right) = \int_0^\infty f(\boldsymbol{r}, E, t) \exp\left[-\frac{t}{\tau}\right] \mathrm{d}t\,.$$

---

[4] G. Von Dardel rt N. G. Sjöstrand: *Phys. Rev.*, **96**, 1245 (1954).

[5] A. V. Antonow, A. I. Isakoff, I. D. Murin, B. A. Neupocoyev, I. M. Frank, F. L. Shapiro and I. V. Shtranich: *A Study of Neutron Diffusion in Beryllium, Graphite and Water by the Impulse Method*, Rapport P/661 de la Conférence de Genève (Août, 1955).

[6] V. Raievski et J. Horowitz: *Détermination du libre parcours moyen de transport des neutrons thermiques par la mesure d'une longueur de diffusion complexe*, Rapport P/360 de la Conférence de Genève (Août, 1955)

En remplaçant la source stationnaire S par une source $S \exp[i\omega t]$ modulée avec la fréquence $f = \omega/2\pi$ nous obtenons la distribution

$$\exp[i\omega t] g(\boldsymbol{r}, E, 1/\tau + i\omega)$$

où

$$g\left(\boldsymbol{r}, E, \frac{1}{\tau} + i\omega\right) = \int_0^\infty f(\boldsymbol{r}, E, t) \exp\left[-t\left(\frac{1}{\tau} + i\omega\right)\right] \mathrm{d}t \,.$$

Ces quelques considérations montrent qu'il est facile de transposer les résultats obtenus pour les problèmes stationnaires avec capture en $1/v$ au cas d'une source modulée.

Dans le cas des neutrons thermiques, si la capture est faible ($\Sigma_a \lambda_{tr} \ll 1$) et si la fréquence n'est pas trop élevée ($(\omega\lambda_{tr}/v) \ll 1$), on peut appliquer la théorie élémentaire de la diffusion qui, en milieu infini, pour une source ponctuelle placée à l'origine $S = S_0 + \delta S_0 e^{i\omega t}$ donne la distribution $n(\boldsymbol{r}, t) = n_0(\boldsymbol{r}) + \delta n_0(\boldsymbol{r}) \exp[i\omega t]$, avec

$$n_0 = \frac{S_0}{4\pi D r} \exp\left[-\frac{r}{L}\right],$$

$$\delta n_0 = \frac{\delta S_0}{4\pi D r} \exp\left[-\frac{r}{L\omega}\right],$$

où

$$L_\omega^{-2} = \frac{\omega}{D}\left(\frac{1}{\omega t} + i\right).$$

On voit que tandis que la partie stationnaire n_0 est caractérisée par la longueur de diffusion L habituelle, la quantité variable δn_0 dépend d'une longueur de diffusion complexe L_ω.

Si $\omega\tau \gg 1$ on peut effectuer un développement en puissances de $1/\omega\tau$, ce qui donne

$$\frac{1}{L\omega} = \sqrt{\frac{\omega}{2D}}\left\{\left(1 + \frac{1}{2\omega\tau} + \ldots\right) + i\left(1 - \frac{1}{2\omega\tau} + \ldots\right)\right\}.$$

En mesurant les parties du taux de modulation

$$M = \frac{\delta n_0}{n_0} = \varphi(r) \exp\left[-\frac{\tau}{L\omega}\right],$$

respectivement en phase et en quadrature avec la source on obtient d'une part le module

$$|M| = \varphi(r) \exp\left[-r\sqrt{\frac{\omega}{2D}}\left(1 + \frac{1}{2\omega\tau}\right)\right],$$

d'autre part la phase

$$\text{Arg } M = -r\sqrt{\frac{\omega}{2D}}\left(1 - \frac{1}{2\omega\tau}\right).$$

On voit que $\log|M|$ et Arg M sont des fonctions linéaires de $\sqrt{\omega}(1 \pm 1/2\omega\tau)$, les pentes des droites étant égales à $-r/\sqrt{2D}$. En principe, la variation en fonction de ω soit de $\log|M|$ soit de Arg M en un point donné, fournit donc le coefficient D d'où l'on déduit le libre parcours moyen de transport λ_{tr}. En pratique pour ne faire intervenir que des distances relatives, ce qui est plus précis, on fait les mesures en plusieurs points.

Remarquons que cette méthode comme la méthode par impulsion fournit une mesure absolue ne se référant pas à una section efficace supposée connue. De plus les dimensions du milieu expérimental doivent seulement être grandes par rapport à L_ω qui, à fréquence suffisamment élevée est nettement plus faible que la longueur de diffusion L.

Les expériences ont été effectuée à Saclay par V. Raievski dans le cas de l'eau lourde et du graphite.

Pour l'eau lourde la mesure a été faite dans la pile de Saclay entourée de son réflecteur, les barres d'uranium ayant été enlevées. La source était constituée par une tige de radioantimoine placée suivant l'axe de deux secteurs de béryllium d'ouverture de 90° et diamétralement opposés. Un écran constitué par un matériau de densité élevée (uranium) permet de moduler l'intensité du rayonnement γ reçu par la cible. On a ainsi obtenu pour de l'eau lourde pure à 17 °C la valeur $\lambda_{tr} = (2.45 \pm 0.07)$ cm. Une première expérience a donné pour le graphite de densité 1.6 la valeur $\lambda_{tr} = (2.55 \pm 0.09)$ cm.

Dans le cas du graphite la source est constituée par un faisceau de neutrons issu de la pile, modulé par un disque de cadmium. Le faisceau est ensuite diffusé par une cible placée dans l'axe d'un empilement de graphite (parallélépipède $160 \times 160 \times 180$ cm^3). Le flux est mesuré suivant l'axe à l'aide d'une chambre à impulsions, les directions du faisceau et de l'axe formant entre elles un angle de 90°.

Étant donné l'importance pour les projets de réacteurs d'une connaissance exacte du λ_{tr} des modérateurs, des expériences précises sont nécessaires, en particulier pour déterminer la variation de λ_{tr} avec la température du modérateur. L'intérêt respectif des trois dernières méthodes dépendra probablement des conditions particulières des mesures.

PROPRIETÀ LETTERARIA RISERVATA

Direttore responsabile: G. POLVANI

Tipografia Compositori - Bologna

Questo fascicolo del *Supplemento* è stato licenziato dai torchi il 15-XII-1956